NAVAL POSTGRADUATE SCHOOL

Monterey, California

THESIS

A FLOW VISUALIZATION STUDY OF
LEX GENERATED VORTICES ON A SCALE MODEL
OF A F/A-18 FIGHTER AIRCRAFT AT HIGH
ANGLES OF ATTACK

by

Odilon V. Cavazos Jr.

June 1990

Thesis Advisor: S. K. Hebbar
Co-Advisor: M. F. Platzer

SECURITY CLASSIFICATION OF THIS PAGE

REPORT DOCUMENTATION PAGE

1a REPORT SECURITY CLASSIFICATION UNCLASSIFIED	1b. RESTRICTIVE MARKINGS
2a SECURITY CLASSIFICATION AUTHORITY	3 DISTRIBUTION / AVAILABILITY OF REPORT Approved for public release; distribution is unlimited
2b DECLASSIFICATION / DOWNGRADING SCHEDULE	
4 PERFORMING ORGANIZATION REPORT NUMBER(S)	5 MONITORING ORGANIZATION REPORT NUMBER(S)
6a. NAME OF PERFORMING ORGANIZATION Naval Postgraduate School 6b OFFICE SYMBOL (If applicable) AA/67	7a. NAME OF MONITORING ORGANIZATION Naval Postgraduate School
6c. ADDRESS (City, State, and ZIP Code) Monterey, CA 93943-5000	7b. ADDRESS (City, State, and ZIP Code) Monterey, CA 93943-5000
8a NAME OF FUNDING / SPONSORING ORGANIZATION 8b OFFICE SYMBOL (If applicable)	9. PROCUREMENT INSTRUMENT IDENTIFICATION NUMBER
8c ADDRESS (City, State, and ZIP Code)	10 SOURCE OF FUNDING NUMBERS PROGRAM ELEMENT NO / PROJECT NO / TASK NO / WORK UNIT ACCESSION NO

11 TITLE (Include Security Classification)
A FLOW VISUALIZATION STUDY OF LEX GENERATED VORTICES ON A SCALE MODEL OF A F/A-18 FIGHTER AIRCRAFT AT HIGH ANGLES OF ATTACK

12 PERSONAL AUTHOR(S)
Cavazos, Odilon V. Jr.

13a TYPE OF REPORT	13b TIME COVERED	14 DATE OF REPORT (Year, Month, Day)	15 PAGE COUNT
Master's Thesis	FROM _____ TO _____	June 1990	164

16 SUPPLEMENTARY NOTATION
The views expressed in this thesis are those of the author and do not reflect the official policy or position of the Department of Defense of the U.S. Government

17 COSATI CODES		
FIELD	GROUP	SUB-GROUP

18 SUBJECT TERMS (Continue on reverse if necessary and identify by block number)
High angle of attack aerodynamics, effect of pitch rate and yaw, vortex development and bursting, flow visualization by dye injection, water tunnel studies, F/A-18 fighter aircraft

19 ABSTRACT (Continue on reverse if necessary and identify by block number)

A water tunnel flow visualization investigation was performed into the high angle of attach aerodynamics of a 2% scale model of the F/A-18 fighter aircraft. The main focus of this study was the effect of pitch rate on the development and bursting of vortices generated from the leading edge extensions in the high angle of attack range with and without yaw. Results of this investigation indicate that that the vortex bursting point (relative to the static case) moves rearward with increasing pitch-up motion and forward with increasing pitch-down motion. For the same pitch rate, vortex bursting was found to occur earlier for the pitch-down motion than for the pitch-up motion, implying aerodynamic hysteresis effects. Yawing the model generated significant vortex asymmetries due to the delayed vortex breakdown on the leeward side for yaw angles of less than 10°. The presence of these asymmetric vortices led to undesirable side forces and yawing moments.

20 DISTRIBUTION / AVAILABILITY OF ABSTRACT	21 ABSTRACT SECURITY CLASSIFICATION
☒ UNCLASSIFIED/UNLIMITED ☐ SAME AS RPT ☐ DTIC USERS	UNCLASSIFIED
22a NAME OF RESPONSIBLE INDIVIDUAL S.K. Hebbar	22b TELEPHONE (Include Area Code) (408) 646-2997
	22c OFFICE SYMBOL AA/Hb

DD FORM 1473, 84 MAR 83 APR edition may be used until exhausted
All other editions are obsolete

SECURITY CLASSIFICATION OF THIS PAGE

Approved for public release; distribution is unlimited.

A Flow Visualization Study of LEX Generated Vortices on a Scale Model
of a F/A-18 Fighter Aircraft at High Angles of Attack

by

Odilon V. Cavazos Jr.
Lieutenant, United States Navy
B.S., California Polytechnic State University, San Luis Obispo,1980

Submitted in partial fulfillment
of the requirements for the degree of

MASTER OF SCIENCE IN AERONAUTICAL ENGINEERING

from the

NAVAL POSTGRADUATE SCHOOL
June 1990

Author: Odilon V. Cavazos Jr.

Odilon V. Cavazos Jr.

Approved by:

S.K. Hebbar, Thesis Advisor

M.F. Platzer, Co-Advisor

E. Roberts Wood, Chairman,
Department of Aeronautics and Astronautics

ABSTRACT

A water tunnel flow visualization investigation was performed into the high angle of attack aerodynamics of a 2% scale model of the F/A-18 fighter aircraft. The main focus of this study was the effect of pitch rate on the development and bursting of vortices generated from the leading edge extensions in the high angle of attack range with and without yaw. Results of this investigation indicate that the vortex bursting point (relative to the static case) moves rearward with increasing pitch-up motion and forward with increasing pitch-down motion. For the same pitch rate, vortex bursting was found to occur earlier for the pitch-down motion than for the pitch-up motion, implying aerodynamic hysteresis effects. Yawing the model generated significant vortex asymmetries due to the delayed vortex breakdown on the leeward side for yaw angles of less than 10°. The presence of these asymmetric vortices led to undesirable side forces and yawing moments.

TABLE OF CONTENTS

ACKNOWLEDGEMENT

This thesis was sponsored by the Naval Air System Command and the Naval Postgraduate School in support of on going high angle of attack research effort.

My gratitude goes to my thesis advisor, Professor S.K. Hebbar, and co-advisor Professor M.F. Platzer, for their guidance, encouragement and patience throughout the course of this project.

I would also like to thank the many people at the Naval Postgraduate School who provided the services and expertise necessary for this research. In particular:

Mr. Al McGuire, Aeronautics Lab

Mr. Mitch Nichols and Mr. Andy Sarakon, Photo Lab

Mr. Tony Cricelli, Aeronautics System and Network Manager

Mr. John Molten, Aeronautics Metal Shop

Mr. Ron Ramaker, Aeronautics Wood Shop

Mr. Jack King, Aeronautics Lab

Finally I would like to take this opportunity to express my deepest gratitude to my wife Vicki for her encouragement and self sacrifice in support of my efforts.

I. INTRODUCTION

The development of current and future short and medium range air-to-air weapons requires today's aircraft to be highly maneuverable while operating at high angles of attack. The all aspect capability of short range weapons leads to a dominance of head-on engagement and thus to potential advantages of instantaneous maneuver capability over the classical sustained performance.

These concepts have lead to a new term: supermaneuverability. This term combines both post stall trajectory (PST) and direct force mode (DFM) capabilities. PST represents the ability of the aircraft to perform controllable tactical maneuvers beyond maximum lift at angles of attack up to at least 70 degrees; DFM represents the ability of the aircraft to yaw and pitch independently of the flight or to maneuver at constant fuselage attitude.

PST capability will be primarily used for maneuvering the aircraft into a position of advantage. Any limitations of the angle of attack capability and/or its controllability at high incidence constitutes a limitation of its offensive and defensive air combat capability. DFM capabilities in air combat will be primarily used for aiming the fuselage for longer and more precise firing solutions independent of the flight path.[Ref. 1 and 2]

Supermaneuverability has the potential for increasing the tactical and survivability effectiveness of aircrafts. Significant advantages in air combat can be gained with the ability to perform rapid, transient maneuvers at high angles of attack (AOA) [Ref. 3]. Several countries are currently placing a high priority on research in this field; in

particular, the United States and the Soviet Union. The 1989 Paris air show showcased the Soviet's development in the area of high AOA aerodynamics with the demonstration of the "Pougachev's Cobra" [Ref. 4 and 5]. This maneuver was performed with a Sukhoi Su-27 long range interceptor. During the maneuver the pilot pitched the Su-27 from forward level flight (Figure 1) to 120° above the horizontal (Figures 2 and 3). He then pitched forward to a level attitude but without any appreciable gain or loss of altitude (Figure 4). The tactical advantage of this maneuver was demonstrated by a simulator comparison of a standard F-16, and an F-16 modified to use more of its aerodynamic potential (Figure 5). The enhanced F-16 uses the Pougachev's cobra maneuver to rapidly decelerate. The standard F-16 is also slowing down, but not as quickly by performing the maximum pull-up allowed by the electronic flight control system. It goes beyond the more rapidly decelerating modified aircraft and becomes a target. Lines between the aircraft are drawn at one second intervals. It must be pointed out however that this is only a simulated comparison. To-date, there is no current U.S. military aircraft capable of performing Pougachev's Cobra.

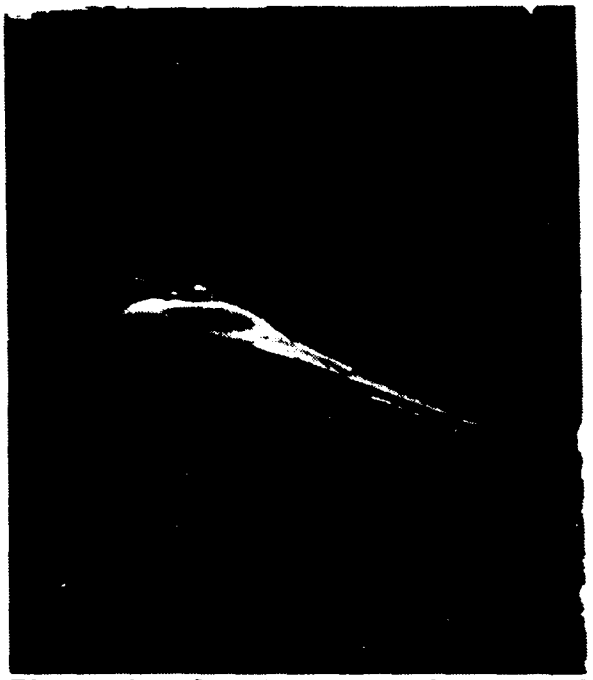

Figure 1. Su-27 Approaching at 240 Knots, Level Flight

Figure 2. Su-27 Pitching Nose Up at Initiation of "Cobra" Maneuver

Figure 3. Maximum Pitch Attitude of 120° Above the Horizon

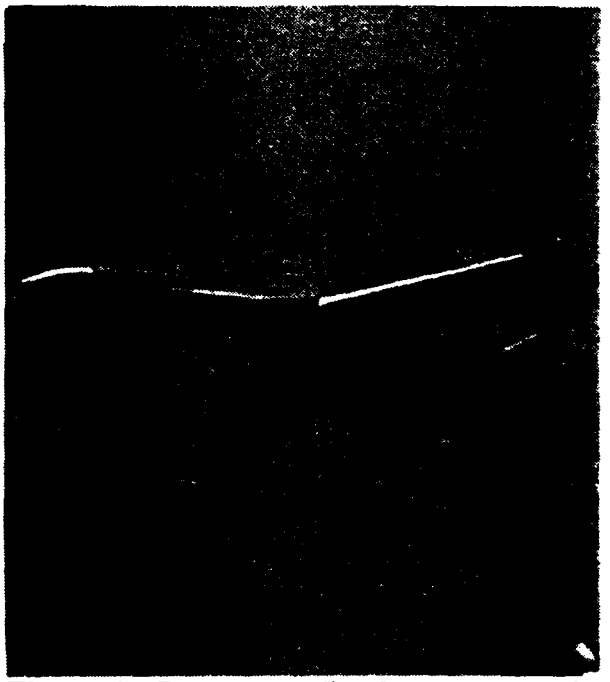

Figure 4. Recovery With Nose Level, 60 Knots Airspeed

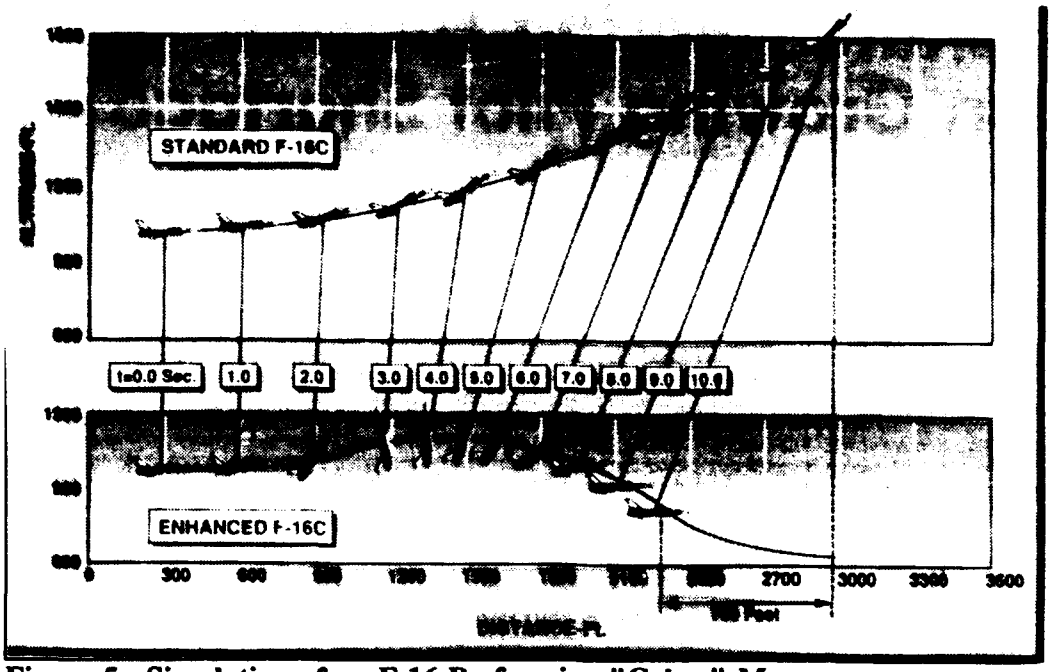

Figure 5. Simulation of an F-16 Performing "Cobra" Maneuver

The U.S. current studies on high angle of attack research are being conducted by NASA. The NASA research program integrates F/A-18 flight test and wind tunnel data with computational fluid dynamics (CFD) predictions in providing a new understanding concerning the behavior of modern fighters at high angles of attack [Ref. 6].

The F/A-18, though not designed for supermaneuverabilty, has achieved improved high angle of attack performance by incorporating innovative aerodynamic design features. The F/A-18 designers incorporated a hybrid wing planform in direct response to the challenge of achieving maximum lift and angle of attack while maintaining positive stability and control. The hybrid wing planform results from combining a conventional wing with a wing root leading edge extension (LEX) [Ref. 7]. Figure 6 illustrates these

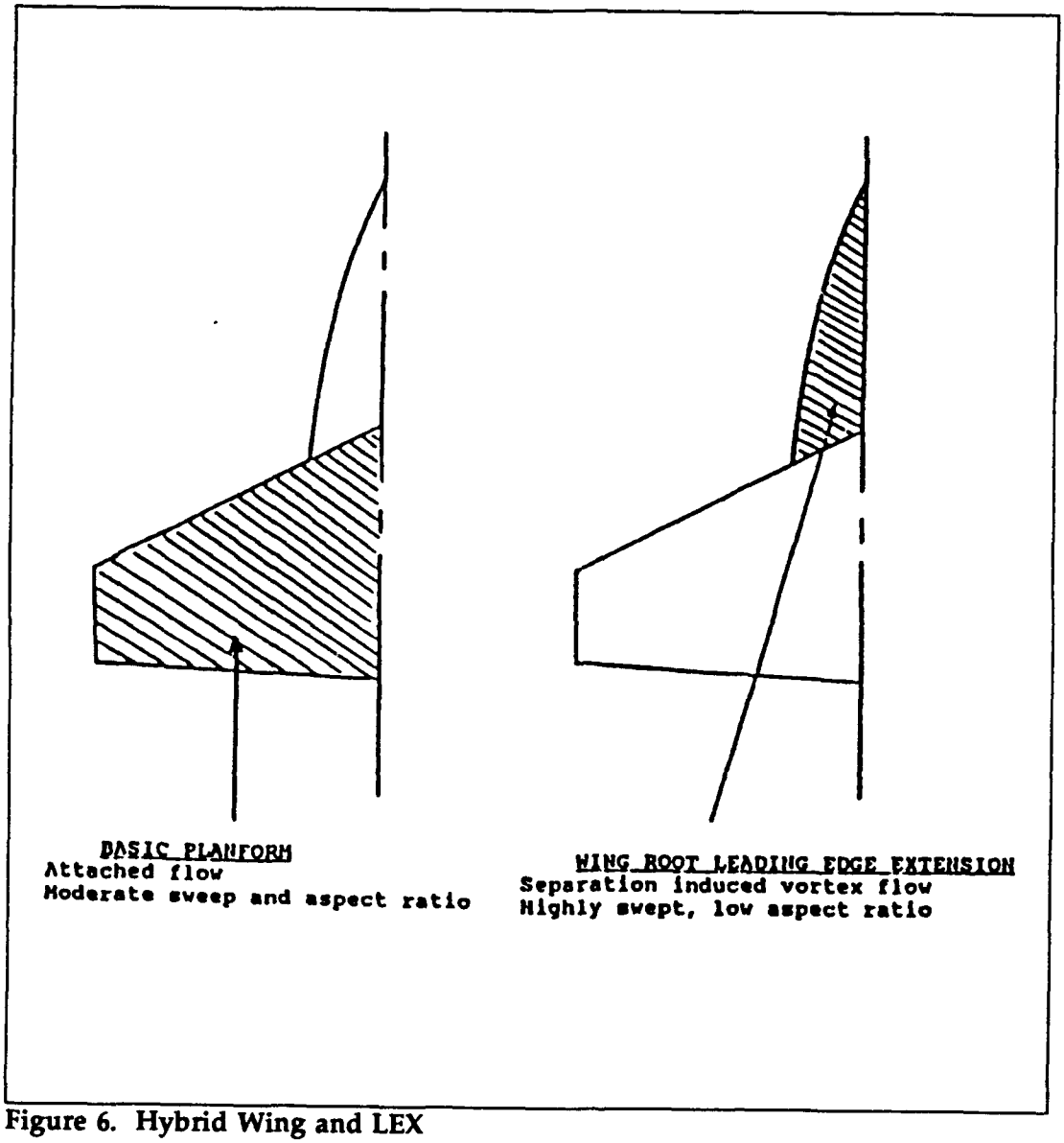

Figure 6. Hybrid Wing and LEX

two concepts in their combined form. The advantage of the hybrid planform over the conventional wing is due to the LEX induced vortex flow which increases in strength with increasing angle of attack. The stable vortex flow creates an area of high negative pressure on the wing upper surface which increases lift and delays separation of laminar flow in the basic planform.

Prediction of separation characteristics over wings and airfoils in steady flow at high AOA has been the subject matter of various researchers for the past several years. As the angle of attack is increased, lift also increases; but soon the upper surface flow starts to separate near the trailing edge. Further increase in the angle of attack causes the separation point to move forward toward the leading edge, eventually resulting in stall. The lift producing mechanism of a hybrid planform wing at lower angles of attack is similar to a conventional wing but is accompanied by flow separation from the LEX and the formation of counter rotating vortices called LEX vortices [Ref. 8]. External flow is drawn over these vortices and is accelerated downward causing the flow to reattach resulting in additional lift, commonly called the vor. lift. At high angles of attack the flow separates, but flow separation is not the sole cause of stall. Instead, lift is lost due to a breakdown (bursting) of the vortices. This vortex breakdown on stationary wings has been investigated extensively by Wedemeyer [Ref. 9].

As previously stated expanding flight envelopes of current and future fighter aircraft often require that the aircraft be highly maneuverable while operating at high angles of attack. Since the aerodynamics of this high angle of attack flight regime can be dominated by vortical flows the design of future fighter aircraft will require an

increased understanding of these types of flows. The ability to predict the locations, strength and bursting characteristics of these vortices and then manage these flows is critical.

Vortex formation involves the shear layer shed from the leading edge of a swept wing which, at moderate angles of attack, rolls up to form a rotational vortex core. Under certain conditions, this tightly wound vortex structure rapidly breaks down into a more diffused vortical flow field with much milder flow gradients. The point where the vortex undergoes this sudden transformation is called vortex breakdown or burst. This vortex bursting phenomenon is of particular importance in aircraft design due to the unexpected loads it can produce on the aircraft.[Ref. 10] These large undesirable forces and moments may lead to departure from controlled flight. Therefore, attention must be paid to high rate pitch up problems, lateral and directional instability problems, and roll and yaw control problems.

At high angles of attack, these unsteady aerodynamic effects have a major impact on the maneuverability and controllability of an aircraft. For reasons stated previously, the current emphasis on aggressive maneuvering capability near or beyond the stall angle has renewed the interest in the lift enhancement caused by dynamic effects.

Experimental studies related to vortex breakdown on pitching wings/aircraft have been somewhat limited to-date. Recently Magness, et al. examined the response of vortex bursting on a pitching delta wing for various classes of ramp motion [Ref. 11]. Included in these studies were pitch-up, pitch-down, continuous pitch-up and pitch-down motions; and combinations of ramp pitching rates. The unsteady response of leading edge vortex

flows over a delta wing was discussed for high angle of attack conditions by Reynolds and Abtahi [Ref. 12]. The focus of their investigation considered the response of vortex development and bursting due to large amplitude transient pitching motions on a sharp edged delta wing. Brandon and Shah [Ref. 13] report the results of large amplitude pitching motions at high angles of attack on the aerodynamic characteristics of a modern fighter aircraft configuration. The unsteady aerodynamic effects were seen to be dependent on pitch rate and motion-time history. Another significant finding was the substantial increase in measured lift, drag, and pitching moment due to unsteady effects for the rapid large amplitude pitch motion.

An investigation by Park [Ref. 14] was performed in a water tunnel to visualize the vortex bursting phenomenon on a 2% scale of the F-18 fighter aircraft. The investigation focussed on the effect of pitch rate and yawing on burst locations of vortices shed from the forebody and the LEX. A close scrutiny of the results reported in this investigation showed that the data on the bursting location of the LEX generated vortices during pitch-up motion with zero yaw were not in agreement with previous studies for similar conditions. It is suspected that the procedure employed during the data acquisition and reduction might have contributed to this disagreement.

Therefore, this investigation was undertaken to study in detail the dynamic effects of pitch rate on the LEX vortex development and bursting on the 2% scale model of the F/A-18 fighter aircraft. The LEX vortex formation and bursting were investigated in the NPS water tunnel using dye-injection for flow visualization. This was accomplished for

both static and dynamic (simple pitch-up and pitch-down) conditions, through a range of angles of attack (0° to 50°) at yaw angles of 0°,+5°,+10° and +20°.

II. EXPERIMENTAL APPARATUS

A. NPS WATER TUNNEL

The investigations were carried out in the Naval Postgraduate School flow visualization water tunnel facility [Ref 15]. The water tunnel was designed by Eidetics International, Inc., Torrance, California, and installed at NPS in late 1988. Figure 7 depicts the layout of the water tunnel.

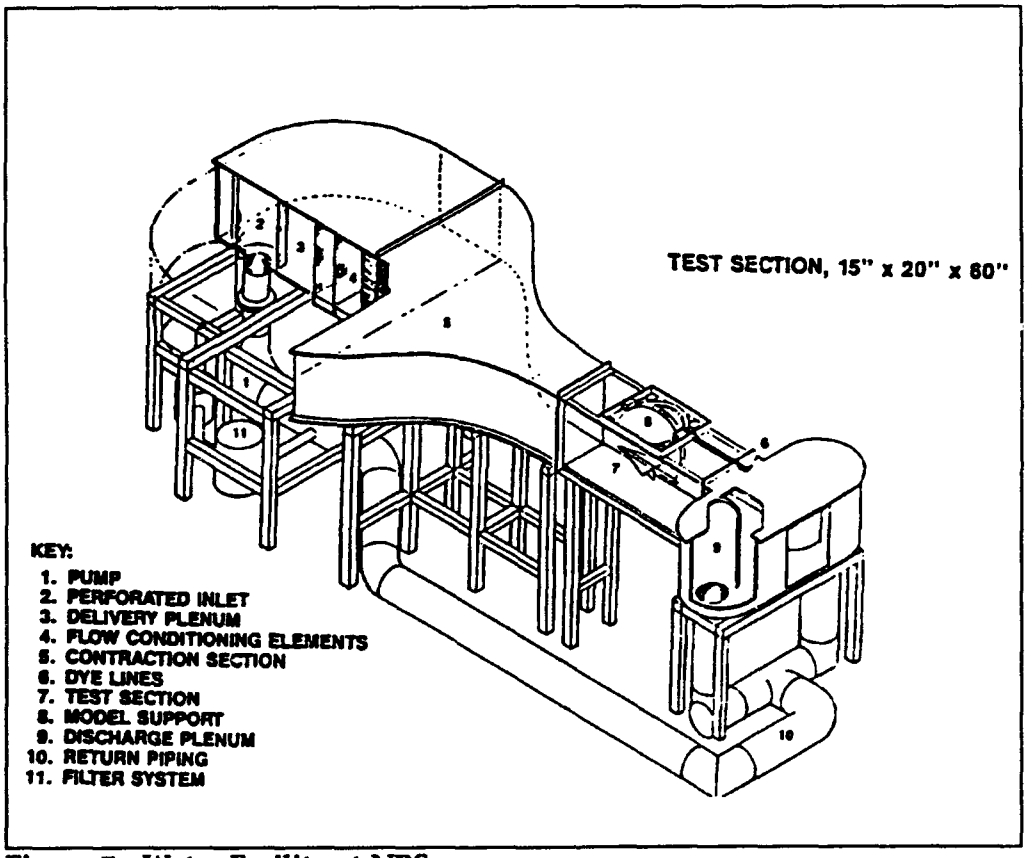

Figure 7. Water Facility at NPS

The water tunnel is a closed circuit facility for studying a wide range of aerodynamic and fluid dynamic phenomena. Its key design features are high flow quality and horizontal orientation. The horizontal orientation facilitates model access, and enables models to be readily changed without emptying the water tunnel. The facility is operated as a continuous flow channel. The water level is usually adjusted to be 1"-2" below the top of the test section, thus, negating the need for a sealed cover; this provides simpler access to the model while the water tunnel is operating.

The test section is 15 inches wide, 20 inches high, and 60 inches long. The sidewalls of the test section slightly diverge to compensate for boundary layer growth and maintain uniform flow velocity. It is constructed primarily of glass to permit maximum viewing of the model. The test and discharge plenum are configured to allow simultaneous viewing of a model from the bottom[1], both sides and from the rear.

The level of the flow quality (measured outside the boundary layer) over the test section is as follows:

Mean flow angularity : $< \pm 1.0°$ in both pitch and yaw angle

Velocity uniformity : $< \pm 2\%$

Turbulence intensity level : $< 1.0\%$ RMS

Six pressurized canisters containing water soluble food coloring were used for flow visualization. Each canister was connected to the model port through an individually routed line. Pressurization for the dye canisters was provided by a small compressor and a pressure regulator used to control the pressure level.

[1]The model is usually mounted upside down in the test section.

The model support system utilized a C-strut arrangement to vary the pitch angle and a turntable to change the yaw angle. Varying the attitude of the model was accomplished with two remotely driven motors. Each motor had a high/low rate switch. The high rate and low rate corresponded to 4.75 deg/sec and 2.00 deg/sec, respectively.

B. F/A-18 MODEL

A 2% scale model of the McDonnel Douglas F/A-18 fighter aircraft was used in this investigation (Figure 8).

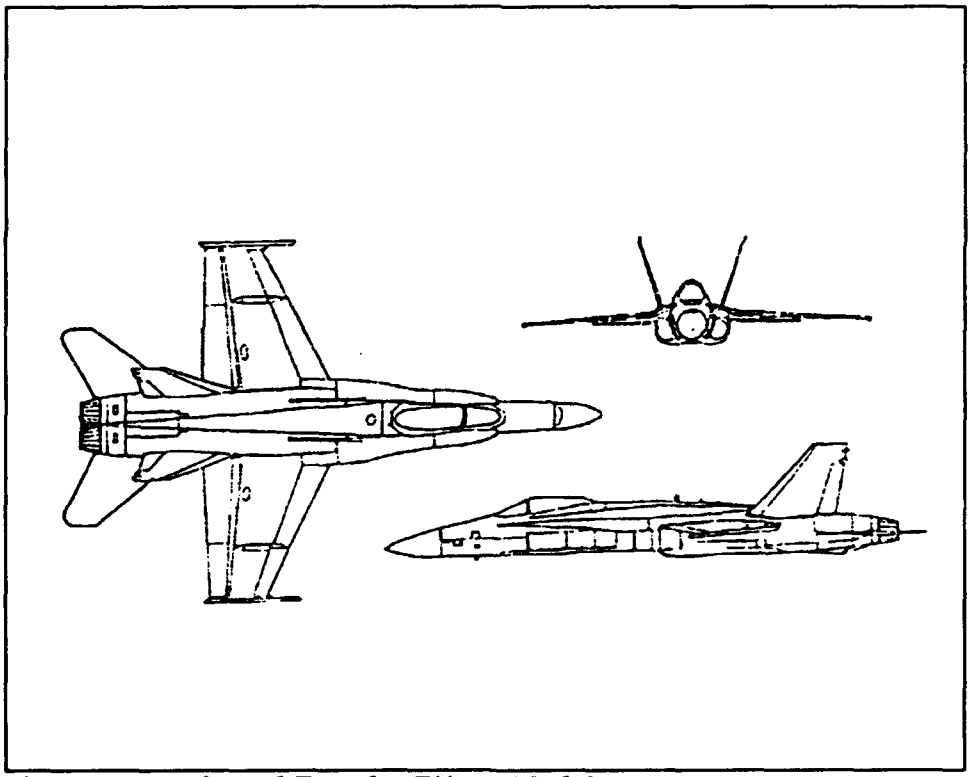

Figure 8. Mcdonnel Douglas F/A-18 Model

This model was equipped with several dye injection ports. Figure 9 illustrates the location of these ports. For flow visualization the dyes are drawn from the pressurized dye supply system described earlier and injected through the ports of the model. Table 1 lists the different colors and their injection locations. In this investigation, the focus was on the development and bursting of vortices shed from the leading edge extensions; therefore, only LEX ports were used. Key dimensions of the model are listed below:

1. Total length = 13.68 in
2. Wing span = 9.375 in
3. Wing chord = 3.5 in(root), 1.5 in(tip)
4. Wing Area = 24.97 in^2
5. Wing mean aerodynamic chord = 2.89 in

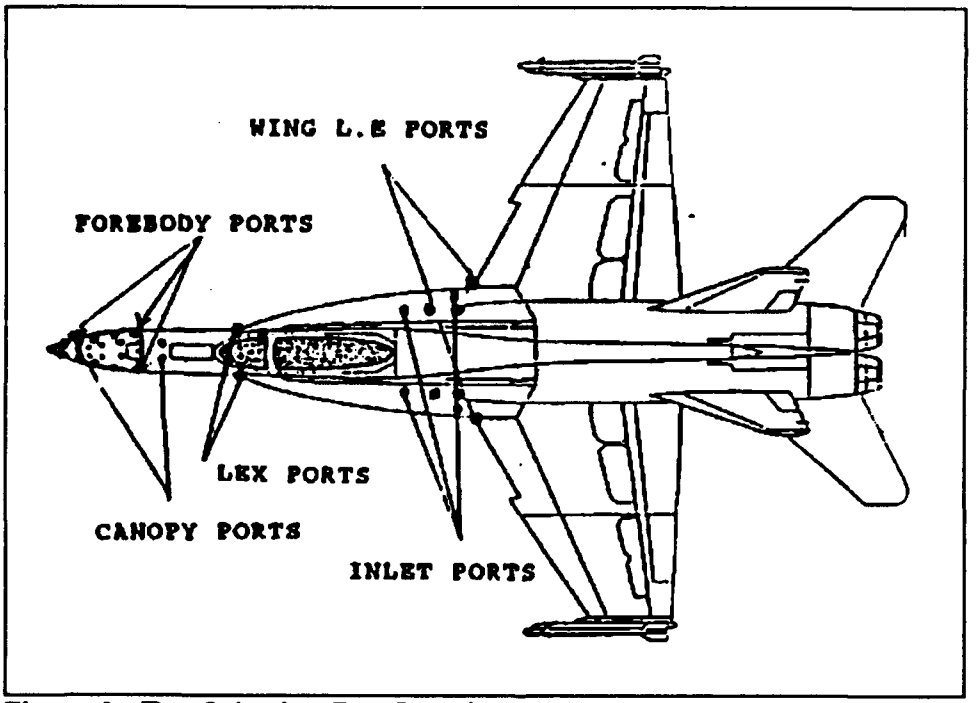

Figure 9. Dye Injection Port Locations

TABLE 1. DYE COLORS AND THEIR INJECTION LOCATION

LOCATION	COLOR(S)
Forebody	Red,Blue
Canopy	Pink
Leading Edge Extension	Black
Wing Leading Edge	Green
Inlet flow	Yellow

C. MODEL MOUNTING

It is very important to insure that the model is mounted horizontally in the water tunnel with zero pitch, zero yaw, and zero roll. The installation of the model in the test section was accomplished in two steps. In the first step, the model and the sting were attached to the sting holder on the model support with the model support base resting in its vertical position out of the water. In the second step, the model was introduced into the test section by rotating the model support base to its horizontal position and properly aligning it with the tunnel walls in both the vertical and horizontal planes. First the centerline of the model (fuselage) is aligned with the freestream (tunnel centerline). To assure zero yaw the model nose and the tail were set at equal distance from either sidewall of the test section. To assure zero roll angle the left and right wing tips of the model were located at the same height from the bottom of the test section. The pitch angle was calibrated by choosing a reference line on the model (say fuselage centerline). The axis of rotation for the pitch and yaw motions were located at 7.2 inches aft of the nose.

III. EXPERIMENTAL PROCEDURES

A. EXPERIMENTS

As previously stated, the goal of this investigation was to study the dynamic effects of pitch rate on the development and bursting location of vortices shed from the leading edge extensions (LEX) of a F/A-18 aircraft model. The experiment consisted of flow visualization on the F/A-18 model for static conditions and for two pitch rates, with angle of attack varying from 0° to 50° (simple pitch-up motion) and 50° to 0° (simple pitch-down motion). The model yaw angle was varied from 0°to +20°. Both still-picture photography and videotape recordings were used for documentation of the flow field of the model. The flow velocity in the water tunnel was kept nearly constant at 0.25 ft/sec which corresponds to a nominal Reynolds Number of 23000/ft or 5500 based on the mean aerodynamic chord. Table 2 illustrates the different test conditions.

TABLE 2. LEX VORTEX FLOW VISULIZATION

AOA(Degrees)	YAW(degrees)	CONDITION	PITCH RATE	REMARKS
0° to 50° at 10° increments	0,+5,+10,+20	Static	----	Sideview Planform view, Photos, Viedotape recording
		Dynamic	Low pitch rate down	
			Low pitch rate up	
			High pitch rate up	
			High pitch rate down	

B. REDUCED FREQUENCY SIMULATION

In the low Reynolds number aerodynamics, all experiments and design methods have been based upon steady-state flow conditions. In actuality, however, aircrafts encounter unsteadiness under all operating conditions whether due to inputs of dynamic motion (i.e. pitch-up, pitch-down), or of a natural origin (i.e. wind shear, gusts). In the case of helicopter rotors the unsteadiness is a combination of both. The rotating blades can be modeled as oscillating in pitch and translation while operating in their own wake. They are also subjected to natural disturbances such as wind shear and gusting. From the preceding discussion it follows that, to understand the stability of an aircraft operating in these environments, a knowledge of its response to flow unsteadiness is essential.

The guiding non-dimensional parameter for a recurrent unsteady flow is the reduced frequency, k, given by the formula

$$k=\frac{\omega c}{2U_{\infty}}$$

where,

k : reduced frequency

w : rotational frequency, rad/sec

c : characteristic length of the body, ft

U_{∞} : free stream velocity, ft/sec

The reduced frequency is the ratio of the characteristic length of the body to the wavelength of the imposed unsteadiness. When k is equal to unity, the imposed unsteadiness has a wavelength equal to the characteristic length of the body. For a pitching wing, the reduced frequency represents non-dimensional pitch rate. In the case of a wing pitching about its mid-chord location, it may be interpreted as the ratio of the vertical motion of the leading edge to its longitudinal motion.

Using this formula the reduced frequency can be estimated for various conditions. The reduced frequency for the F/A-18 aircraft (Full Scale) was calculated and compared with the values for the water tunnel model. Table 3 lists these values and indicates that the water tunnel facility is capable of simulating the full scale values of the reduced frequency for the F/A-18 aircraft.

Table 3. REDUCED FREQUENCY

PITCH RATE *	w(rad/sec)	Length(ft)	$U_{\infty(ft/sec)}$	k(reduced frequency)
Low pitch rate model	.0356	1.14	.25	.0812
High pitch rate model	.0831	1.14	.25	.1895
Full scale F/A-18 aircraft	1.0472	56	608	.04823

* The model pitch - axis is located 7.2 inches aft of the nose.

C. DATA ACQUISITION

Data collection consisted of photographs taken with two 35mm cameras providing a simultaneous side and planform view of the vortical flow field originating off the LEX of the F/A-18 model. Section E describes the lighting and camera settings utilized for this investigation. A video camera was also used to record the flow phenomena for static and dynamic conditions.

D. DATA REDUCTION

Data reduction essentially consisted of measuring the burst location of the vortex shed off the LEX and plotting it against the angle of attack. When a yaw angle is imposed on an aircraft the side opposite the yaw input is termed the windward side. The side in the same direction as the yaw input is referred to as the leeward side. For this investigation all measurements were taken on the leeward side of the aircraft model using the nose as the reference point. The bursting locations were visually determined from these photographs with the utmost care and consistency, and scaled for nondimensionalization using the fuselage length of the model. Some degree of imprecision may be still present in the reduced data due to the difficulty in locating the vortex bursting location particularly at lower angles of attack and at high pitch rates (see discussion in Chapter IV). It should be pointed out here that during the static segment of the experiment, the vortex bursting location at any angle of attack was found to fluctuate up to ±0.5 inches. The photographs corresponding to the static conditions were timed to correspond roughly

to the mean location of the vortex burst. Figures 10 and 11 depict the side and planform views of the model, where

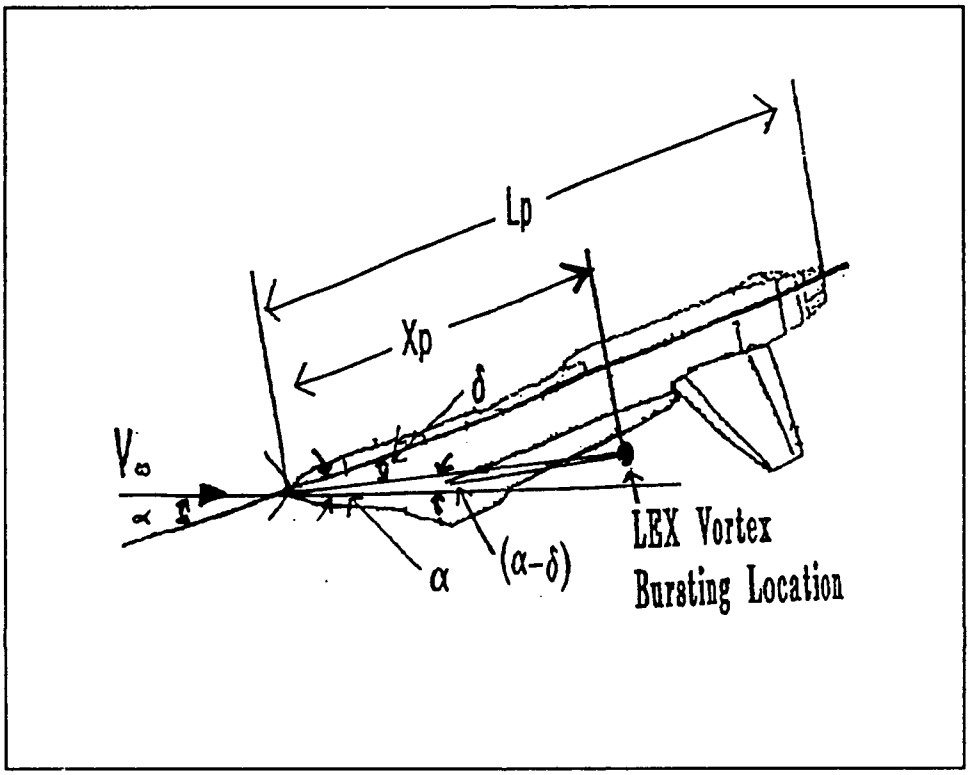

Figure 10. Side View F/A-18 Model

X = longitudinal distance of bursting location

L = overall length of model

α = pitch angle (angle of attack)

β = sideslip angle (angle of yaw)

δ = angle the line joining the vortex burst point to the nose makes with the centerline of the model as seen in the side view (Fig 10)

γ = angle the line joining the vortex burst point to the nose makes with the centerline of the model as seen in the planform view (Fig 11)

L_i = longitudinal distance from the nose to the engine inlet.

Subscripts

a = actual (on model)

p = picture (photographs)

i = inlet

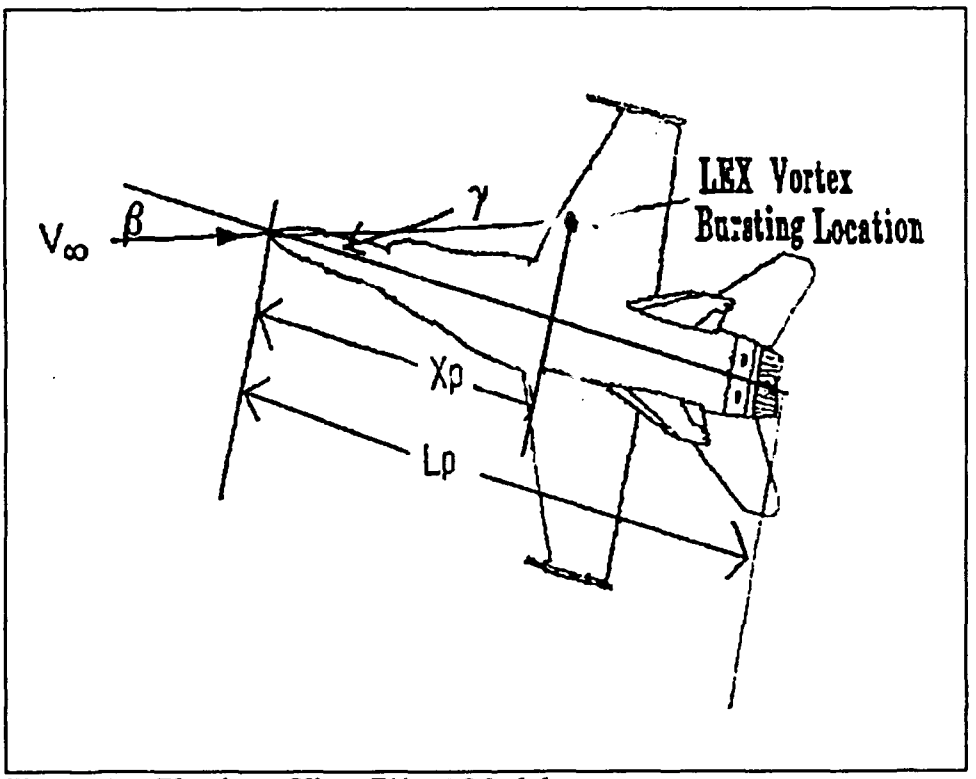

Figure 11. Planform View F/A-18 Model

Simultaneous measurements from both views are required to calculate bursting locations (unless δ and γ are very small). The following equations can be easily derived for the non-dimensional location of the vortex burst:

$$\frac{X_a}{L_a}=\left(\frac{X_p}{L_p}\right)\frac{\cos\beta}{\cos(\beta-\gamma)}$$

(1), for any α in the side view photograph.

$$\frac{X_a}{L_a}=\left(\frac{X_p}{L_{ip}}\right)\frac{\cos\beta}{\cos(\beta-\gamma)}\left(\frac{L_{ia}}{L_a}\right)$$

(2), for any α in the side view photograph.

$$\frac{X_a}{L_a}=\left(\frac{X_p}{L_p}\right)\left(\frac{\cos\alpha\times\cos\delta}{\cos(\alpha-\delta)}\right)$$

(3), for any β in the planform view photograph.

Equation (1) can be used if the entire model appears in the side view photograph; equation (2) is useful when only a portion of the model appears.

E. METHOD OF PHOTOGRAPHY

The equipment used for the photographic session consisted of two 35mm cameras, three Smith-Victor 400 watt photographic lights, and a floodlight fixed below the test section. For the side view photographs two of the lights were placed at a distance of three feet and at a 45 degree angle from the test section. The third photographic light was placed below the test section. This in conjunction with the fixed floodlight provided enough lighting for the planform photographs. Figure 12 shows the lighting setup for both the side view and planform photographs. The same lighting arrangement was used for video taping of the flow field on the model.

The type of film used for all the photographs was 35mm black and white ASA 400. During the exposure of the film, it was pushed to 1600 ASA in order to obtain a better contrast of the model flow field. The shutter speed and f-stop that produced the best photographic results for the side view were 250/16. The planform photographs were taken at a shutter speed and f-stop of 125/16 (see Table 4).

The side view photographs required the use of only one camera placed directly in front of the model. The angle of attack scale fixed to the rear side wall of the tunnel shows up in these photographs and helps in reading the instantaneous pitch angle. To know the pitch angle in the planform view photographs it was necessary to take both the side view and planform view photographs simultaneously. This was accomplished by placing a second camera below the test section and synchronizing the two cameras for simultaneous exposure.

Figure 12. Camera and Lighting Set-Up for Photographs

TABLE 4. PHOTOGRAPHIC SETTINGS

View	Speed/F-stop settings	Film
Side	250/16	ASA 400 Black and White Film. (pushed to ASA 1600 during exposure)
Planform (from tunnel bottom)	125/16	

IV. RESULTS AND DISCUSSION

The results of this investigation will be presented and discussed in a series of 4 numbered photographic sequences and bursting location plots. Several rolls of 35mm black and white film were exposed and several hours of videotape recorded during the investigation. The results of the 35mm photography are presented in Appendix A (Figure 15 through 115). Each figure shows two views of the flow field, one in the side view and the other in the planform view (taken from the bottom of the tunnel). The bursting location data derived from these photographs is included in Appendix B (Figures 116 through 121). However, before discussing these results, some general comments will be made on the F/A-18 flow field and the LEX generated vortex system (Figure 13), and the present bursting data for the static conditions will be compared with those of other investigations (Figure 14). Then the flow visualization photographs will be examined in sufficient detail to highlight the flow field characteristics in different model orientations. Some problems related to burst location determination associated with certain combinations of AOA/pitch rate/yaw will also be discussed. Finally, with the aid of burst location plots, the effects of pitch rate and yaw on the development/bursting of LEX vortices will be discussed.

A. DESCRIPTION OF F/A-18 FLOW FIELD

The prominent features of the F/A-18 model flow field are distinguished very explicitly in Figures 15 and 16. In the AOA range of 0° to 10° the flow over the LEX remains particularly smooth and stable. As the angle of attack is increased the sharp leading edge of the LEX generates a vortex core (Figure 18). The LEX vortex core is tightly wound and extends aft until undergoing vortex breakdown. The vortex bursting is unquestionably signified by the stagnation of the core and abrupt expansion in its diameter.

B. LEADING EDGE EXTENSION VORTICES

A schematic illustration of the LEX vortex system is shown in Figure 13. At high angles of attack the normal component of the flow velocity (Vn) is attached to the bottom surface of the LEX. The flow remains attached until reaching the leading edge of the LEX (S_1) where separation occurs and a vortex sheet is formed. Due to the presence of a pressure gradient the vortex sheet rolls up and moves inward towards the fuselage. As flow continues over the LEX vortex it is pulled down and reattaches at R_1. The interaction between the adverse pressure gradient located inboard of the LEX leading edge and the outboard moving boundary layer causes a weaker secondary counter-rotating vortex flow to develop at S_2. Similarly, a tertiary vortex is generated.[Ref. 8]

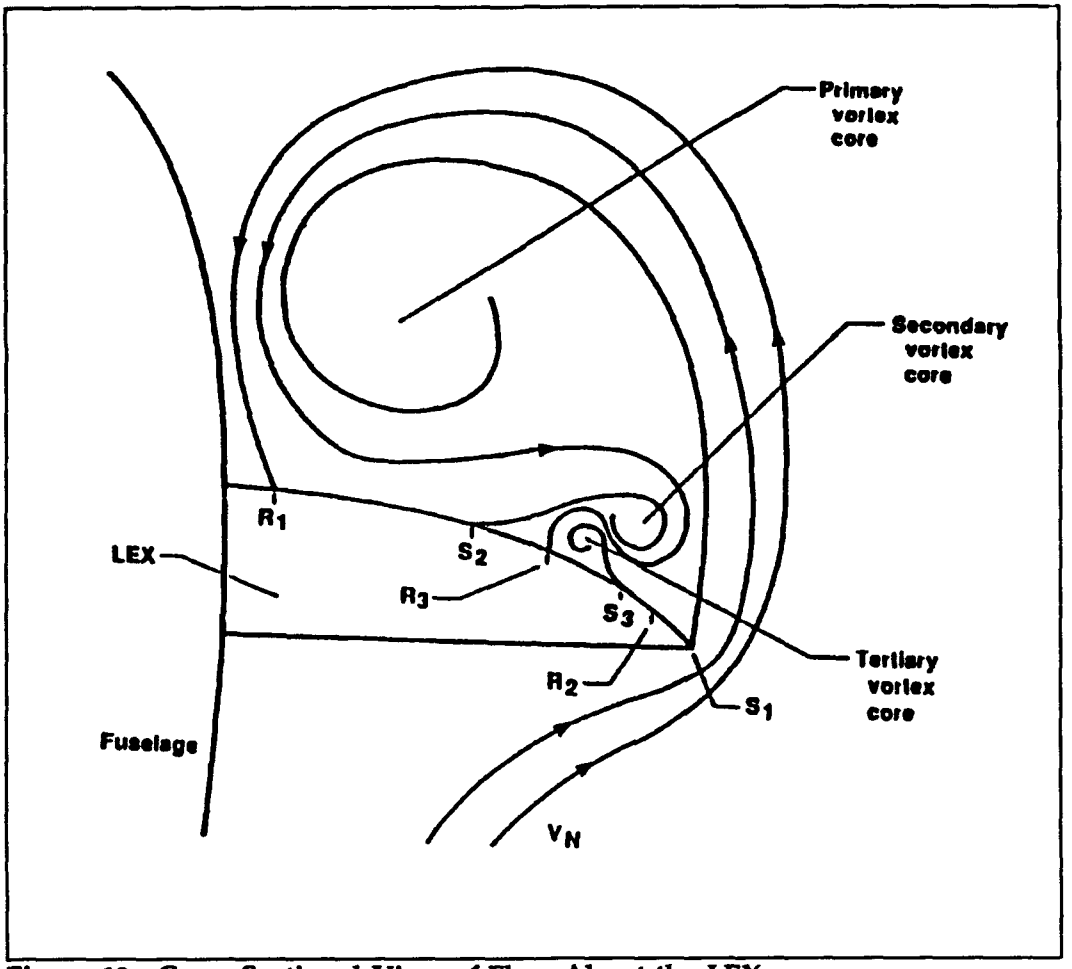

Figure 13. Cross-Sectional View of Flow About the LEX

C. ANGLE OF ATTACK EFFECTS ON LEX VORTEX CORE BURSTING

1. Static Conditions

Sequence Number 1, Figures 15 through 20. As stated previously at the lower angles of attack (<10°) the flow remains particularly smooth. At $\alpha = 20°$ (Figure 17) the LEX vortex is already well developed and moving outboard and breaking down near the wing trailing edge. As AOA is increased from 29° to 38° (Figures 18 and 19) the LEX vortex core bursting location moves forward from the intersection of the LEX and the

wing leading edge to the aft end of the canopy. At $\alpha = 49°$ (Figure 20) the LEX vortex bursting location has moved further forward close to the LEX apex. This sequence of photographs therefore clearly illustrates that as the angle of attack increases, the LEX vortex core bursting point moves toward the LEX apex. Figure 14 shows the longitudinal LEX vortex bursting locations plotted as a function of angle of attack. Also shown here for comparison is the vortex bursting location data from flight and ground tests. It can be seen that the data collected is in good agreement with previous investigations. Allowing for the experimental uncertainty in various data, the good agreement lends confidence in and credibility to the data reduction method utilized.

2. Dynamic Conditions

Sequence number 2, Figures 21 through 40. These photographs were taken at approximately 10° interval during simple pitch-up and pitch-down motions at two reduced frequencies with the model at zero yaw.

Figures 21 through 30 show the model flow field during simple pitch up and pitch down motion at $k = 0.0812$. At $\alpha = 10°$ (Figure 21) a symmetric pair of LEX vortices have already developed and burst outboard of the two vertical tails. As the AOA increases from 20° to 50° (Figures 22 - 25) the vortex core rolls up tighter denoting an increase in strength. Figures 26 through 30 show the pitch down motion with AOA decreasing from 50° to 9°. With decreasing AOA the vortex core appears to be growing and moving outboard. A rough indication of the relative size of the vortex during model motion can be seen by comparing Figure 23 ($\alpha = 30°$ pitch-up) and Figure 28 ($\alpha=28°$, pitch-down). During pitch-up motion the LEX vortex appears to be smaller indicating a

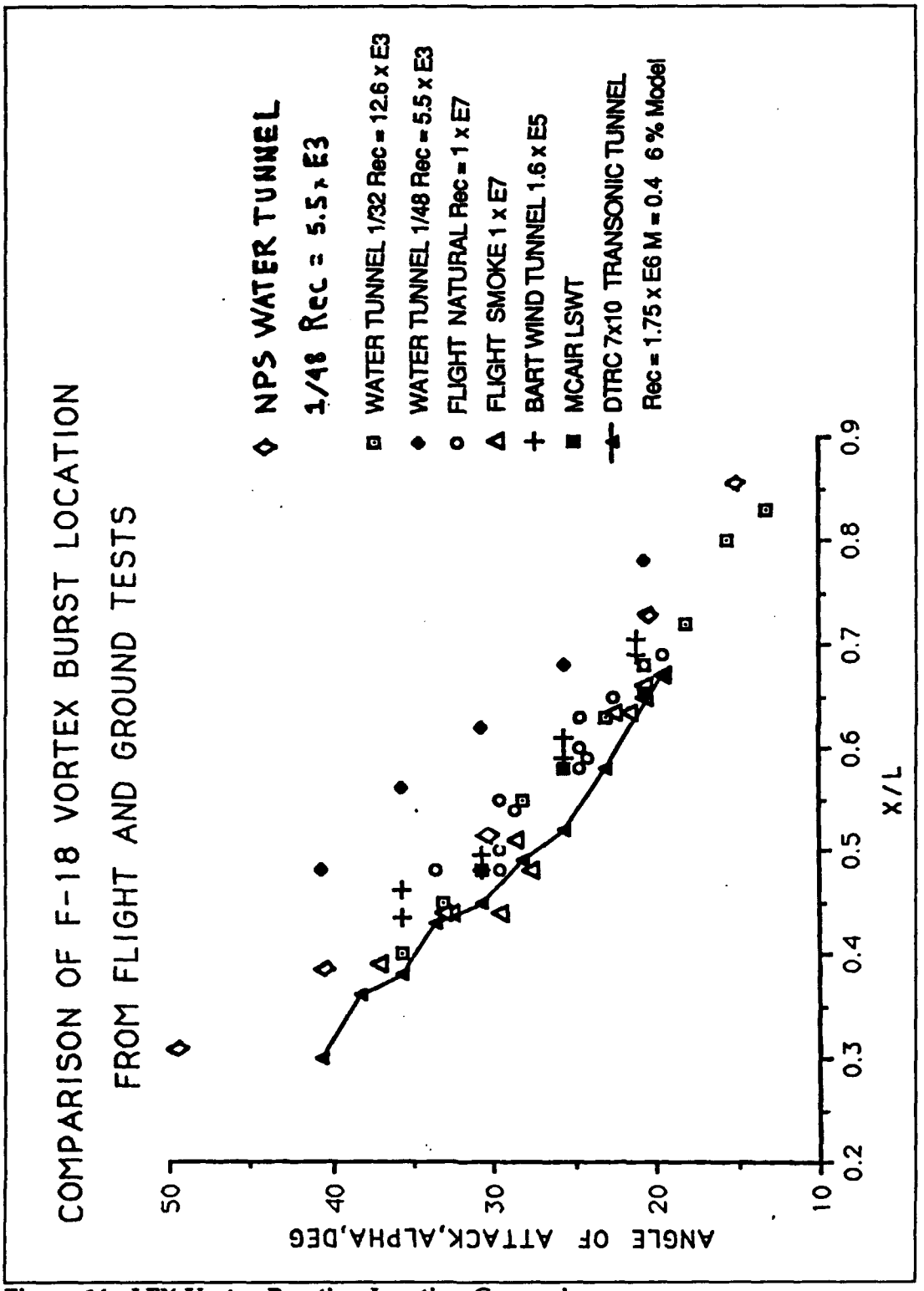

Figure 14. LEX Vortex Bursting Location Comparison

more stable vortex; this effect leads to a lag in vortex bursting. This indicates that during pitch-up motion, bursting occurs at a point further downstream than would occur for static conditions, resulting in a vortex system which is equivalent to a static system at a reduced angle of attack. During the pitch down-motion the LEX vortex is larger indicating a less stable vortex. Hence, the vortex bursting occurs earlier relative to the pitch up motion and static conditions. These characteristics are qualitatively very similar to those observed by Brandon and Shaw in their investigation of unsteady aerodynamics characteristics of a fighter model [Ref. 13].

Figures 31 through 40 display the model flow field during dynamic motion at k = 0.1895. Figures 31 - 35 show the model in a pitch up motion, with trends similar to those for the case of the lower reduced frequency pitch up motion (discussed previously) but amplified much more by the higher reduced frequency. There was one difference in that there was some delay in the tight vortex spiral forming until the AOA reached 30°. Figures 36 - 40 show the model flowfied during pitch-down motion. They clearly indicate that the vortex burst location occurs earlier relative to the corresponding low pitch-down motion. This can be seen very clearly in burst location plots to be discussed in a subsequent section.

From a careful study of the flow visualization photographs it was determined that the pitch up motion caused the vortex bursting point to lag the static condition point at the same AOA. The delay in the vortex bursting increased as the pitch rate increased (for

angles > 25°). For the pitch-down motion, it was concluded that the bursting occurred earlier than that of the static condition and moved further forward with increase in the pitch rate.

D. YAW EFFECTS ON LEX VORTEX CORE BURSTING

1. *Static Conditions*

Sequence number 3 (Figures 41 through 55) shows the model flow field for static conditions with the AOA ranging from 0° to 50° and for yaw angles of +5°, +10°, +20°.

Figure 41, $\alpha = 10°$, $\beta = 5°$, shows the leeward side LEX vortex flow divided in two segments initially. The first segment flows over the LEX, while the second starts out under the LEX and comes up and joins the first. The combination of these two forms a spiral vortex which moves outward as it travels downstream before it finally bursts outboard of the vertical tail. The windward LEX vortex forms into a tight vortex, moves outboard and bursts at the leading edge of the vertical tail. The photograph clearly shows a pair of asymmetrical LEX vortices with the leeward vortex bursting point lagging the windward vortex bursting point. As the AOA is increased from 20° to 30°, (Figure 42 and 43) both the leeward and the windward vortex bursting locations move inboard and forward, with the leeward bursting location still lagging the windward bursting location. At $\alpha = 39°$ and 50° (Figures 44 and 45) the bursting location moves further inboard and along the canopy. Also, the pair of vortices is now almost symmetrical and bursts at approximately the same location on both the leeward and the windward side.

Figures 46 through 50 show the LEX vortices for the same range of AOA but with the yaw angle increased to 10°. Figure 46, $\alpha = 10°$, $\beta = 10°$, shows the flow splitting on the leeward side. The segment of the vortex above the LEX comes up over the canopy and starts to cross over to the windward side but is pulled back and continues along the center line of the fuselage before bursting at some location off the model. The vortex segment moving along the bottom portion of the LEX strikes the wing leading edge. This photograph clearly highlights the difficulty in determining the bursting location at this model orientation. The windward side vortex moved along and outboard of the fuselage and finally burst at the vertical tail. As the AOA was increased to 20° (Figure 47) the leeward vortex traveled a short distance underneath the LEX before crossing over to the LEX upper surface. The vortex then traveled rearward and outboard along the fuselage where it burst along the wing trailing edge. On the other hand, the windward side vortex developed immediately at the apex of the LEX and traveled aft along the fuselage and burst near the wing leading edge. Once again, the leeward side vortex bursting location lagged that of the windward side. As the AOA was increased from 30° to 50° (Figures 48 - 50) the leeward side vortex burst location moved forward and inboard while still lagging the windward side vortex bursting point. Throughout the entire range of AOA evaluated the vortices remained asymmetric.

Figures 51 through 55 show the LEX vortices for the same range of the AOA but with the yaw angle increased to 20°. Figure 51, $\alpha = 10°$, $\beta = 20°$, shows the flow splitting and following similar trends to those for the case of 10° yaw angle (Figure 46). As the AOA was increased from 20°to 50° (Figures 52 - 55), the photographs show the

flow striking the LEX and developing into a big rolling vortex that moved forward with increasing AOA, but still lagged the windward side. The windward side LEX vortex bursting location continued to move forward with increasing AOA until it reached the apex of the LEX at $\alpha = 50°$.

To summarize the yaw effects for static conditions, at a small yaw angle (5°) an asymmetric LEX vortex pair was seen to develop with the leeward side vortex bursting location lagging that on the windward side for AOA < 30°. As the AOA was increased the vortices became symmetric and burst at approximately the same location for both the leeward and the windward side. As the yaw angle increased to +10°, the leeward side bursting location consistently lagged the windward side throughout the range of AOA investigated. At a yaw angle of +20° (for AOA > 20°) a big rolling vortex was observed to develop on the leeward side and caused the bursting location to move both outward and upward, as can be clearly seen in the photographs (Figures 52 - 55). Similar trends were observed by Del Frate and Zungia in their investigation of sideslip effects on LEX Vortex core breakdown [Ref. 8].

2. Dynamic Conditions

Sequence number 4 (Figures 56 through 115) shows the model flow field during simple pitch-up and pitch-down motions at two reduced frequencies and for yaw angles of +5°, +10°, and +20°.

In Figures 56 through 60 the model is being pitched up at a value of k = 0.0812 and at $\beta = 5°$. Figure 56, $\alpha = 10°$, $\beta = 5°$, shows the leeward side vortex already developed with bursting taking place at about the midpoint of the wing. The windward side flow

has split into two segments of which neither one has developed into a vortex. At α = 20°, ß = 5°, (Figure 57) both the leeward side and windward side vortices have developed and are bursting at approximately the same location. As the AOA is increased to 30° (Figure 58) the leeward side vortex diameter has decreased but the bursting location has moved outboard and still occurs at about mid-wing. The windward side vortex diameter has also decreased, with the bursting location moving inward and occurring earlier than the leeward side. As the AOA was increased to 40° (Figure 59) the leeward side bursting location moved inboard and forward and lagged the windward side burst location. At α = 50° (Figure 60) the leeward side vortex appears to be bursting slightly earlier than the windward side vortex.

Figures 61 through 65 display the model flow field during a pitch-down motion with k = 0.0812 and β = 5°. Figure 61, α = 49°, ß = 5°, shows the leeward side vortex bursting occurring slightly earlier than the windward side similar to the pitch-up motion. As the AOA is reduced from 40° to 28° (Figures 62 and 63) the leeward side vortex travels downstream along the fuselage and bursts later than the windward side. As the AOA is reduced further from 17° to 7° (Figures 64 and 65) both the leeward and windward side vortices move rearward and outboard burst near the vertical tail.

Figures 66 through 70 show the model flow field during a pitch-up motion with k = 0.0812 and β = 10°. Figures 66 and 67, α = 11° and 21°, ß = 10°, show the flow on the leeward side separating into two segments, similar to that in the static condition (Figures 46 and 47). It can be seen from the photographs that no vortex actually develops. On the windward side at α = 21° the vortex develops and moves rearward and

outboard and bursts at about the mid-wing. At α = 30° (Figure 68) the leeward side vortex develops and bursts near the trailing edge of the wing. The windward side vortex has moved inboard and bursts earlier relative to the leeward side. As the AOA is increased to 40° and 50° (Figures 69 and 70) the leeward side vortex moves inboard and the bursting location moves forward while still lagging the windward side vortex bursting location.

Figures 71 through 75 display the model flowfield during a pitch down motion with k = 0.0812 and β = 10°. As the AOA decreases from 49° to 17° (Figures 71 - 74) the leeward side vortex bursting location moves rearward and along the fuselage. The windward side vortex bursting location also moves aft but with bursting occurring earlier than on the leeward side. At α = 7°, ß = 10° (Figure 75) the flow did not split and the features were similar to those for the corresponding pitch-up motion (Figure 66).

Figures 76 through 80 show the model flow field during a pitch-up motion with k = 0.0812 and β = 20°. Figure 76, α = 10°, ß = 20°, shows the leeward side flow separating into two segments. The first segment develops into a vortex that moves up and rearward along the fuselage where it bursts outboard of the vertical tail. The second segment stays attached along the upper surface of the LEX and the side of the fuselage. The windward side vortex bursts near the leading edge of the wing. As the AOA is increased to 20° (Figure 77) the leeward side flow remains attached to the lower surface of the LEX. It doesn't cross over to the upper surface and therefore no vortex is developed. At α=30° (Figure 78) a vortex develops on the leeward side, travels rearward and outboard and finally bursts at about mid-wing. The windward LEX vortex bursting

occurs much earlier than the leeward side. Figures 79 and 80 show the flow field at 41° and 52° AOA respectively. In both photographs the leeward side LEX vortex traveled forward and upward as the AOA increased.

Figures 81 through 85 display the flow field during a pitch-down motion with k = 0.0812 and $\beta = 20°$. The vortex bursting location for the leeward side moved rearward and outboard with decreasing AOA. The windward side vortex bursting location also moved rearward with bursting consistently occurring earlier than on the leeward side.

Figures 86 through 115 show the model flow field during pitch-up and pitch-down motions with k = 0.1895. Figures 86 through 90 show the flow field during a simple pitch-up motion with $\beta = 5°$. From Figure 86, $\alpha = 11°$, $\beta = 5°$, the flow on the leeward side can be observed to split similar to that for the lower reduced frequency case with $\beta = 10°$ (Figure 66). As the AOA reaches 22° a pair of asymmetric vortices develops with the leeward side vortex bursting earlier than the windward side vortex (Figure 87). Figures 88 through 90 show the leeward side vortex bursting location moving forward and inboard with increasing AOA. Compared to the windward side vortex burst location, the vortex burst occurred later on the leeward side at the higher AOA.

Figures 91 through 95 show the model flow field during a pitch-down motion with k = 0.1895 and $\beta = 5°$. From the photographs the leeward side vortex bursting location can be observed moving rearward and outboard with decreasing AOA. Similarly for the windward side the bursting location traveled rearward and outboard. It should be noted that during this pitch-down motion the bursting of the LEX vortex occurred earlier on the leeward side than on the windward side throughout the AOA range.

Figures 96 through 100 correspond to the flow field during a pitch-up motion with $k = 0.1895$ and $\beta = 10°$. The leeward side flow split into two segments at a AOA of 11° (Figure 96). One segment of the flow came up over the canopy and traveled along the centerline of the fuselage between the two vertical tails. The second segment of the flow started out below the LEX and crossed over to the upper surface and joined the first segment of the flow. The windward side of the flow crossed underneath the model fuselage to the leeward side where it continued rearward along the bottom surface of the wing. As the AOA reached 22° (Figure 97) the leeward side flow remained separated with the second segment moving rearward along the upper surface of the LEX and bursting at mid-wing. A windward side vortex also developed but its bursting location lagged that of the leeward side vortex. Figures 98 through 100 show the development of asymmetric vortices. The leeward side vortex breakdown moved forward, upward and inboard as the AOA increased from 31° to 52°. Another noticeable characteristic was that the vortex breakdown on the leeward side at $\alpha = 52°$ traveled only as far forward as the junction of the LEX and the wing leading edge. The windward side vortex burst location also moved forward and inboard with increasing AOA. The vortex bursting on the windward side occurred consistently earlier than on the leeward side vortex.

Figures 101 through 105 display the model flowfield during a pitch down-motion with $k = 0.1895$ and $\beta = 10°$. Throughout the range of decreasing AOA the leeward side vortex bursting location traveled rearward and outward. The bursting location on the leeward side occurred earlier during the pitch-down motion than during the corresponding pitch-up motion for the same range of AOA. The windward side LEX vortex bursting

location also traveled rearward but did not move as far outward as the leeward side vortex. Once again the windward side vortex bursting location occurred earlier relative the leeward side bursting location.

Figures 106 through 110 correspond to the model flow field during pitch-up motion with $k = 0.1895$ and $\beta = 20°$. Throughout the entire range of the AOA the windward side flow split into two segments. The first segment crossed over the canopy and merged with the leeward side flow. The merged flows developed into a large diameter vortex core and traveled rearward and outboard on the leeward side of the model. Like the earlier trends observed during pitch-up motion, the vortex burst location traveled forward, upward and inboard with increasing AOA. The second segment of the windward side flow developed into a weak vortex until reaching a higher AOA ($\alpha > 30$) where the vortex core diameter decreased. This decreased vortex diameter core enhanced the vortex strength and pulled the first segment of the flow back toward the windward side. As with previous results the windward side vortex bursting location occurred earlier relative to the leeward side location.

Figures 111 through 115 illustrate the model flow field during a pitch-down motion with $k = 0.1895$ and $\beta = 20°$. With decreasing AOA the general trend of the leeward side vortex burst location was to travel rearward, outboard and down toward the surface of the LEX. The windward side vortex burst location followed the same trend until reaching the lower AOA ($\alpha < 20°$). At lower AOAs both segments of the windward side flow crossed over to the leeward side vortex. As can be seen from the photographs (Figures

114 and 115) the interaction of the leeward and windward side vortices made it difficult to locate the bursting location.

To summarize the effects of yaw for dynamic conditions, during pitch-up motion at low pitch rate and small yaw angle (5°) a symmetric pair of LEX vortices was seen to develop and burst at approximately the same location on both leeward and windward sides for AOA < 30°. For α > 40° the vortices became asymmetric with the leeward side vortex bursting location lagging the windward side. Increasing the pitch rate caused the leeward side vortex bursting location to occur earlier than the windward side for AOA < 20°. For AOA > 20° the leeward side bursting occurred later relative to the windward side. During the pitch-down motion at the low pitch rate the leeward side burst location occurred earlier for α = 50°. As the AOA decreased from 40 °to 10° the burst location for the leeward side lagged the windward side. However, at the high pitch rate the leeward side bursting location occurred earlier throughout the range of decreasing AOA. As the yaw angle was increased to 20°, the LEX vortex burst location on the leeward side was consistently observed to occur later relative to the windward side location. This trend was observed during both the pitch-up and pitch-down motions at both pitch rates throughout the AOA range.

E. BURSTING LOCATION PLOTS

The longitudinal LEX vortex core bursting locations for pitch-up and pitch-down motions are plotted as a function of angle of attack (AOA) in Figures 116 through 121

(see Appendix B). Note that in these figures bursting location refers to the bursting of the LEX vortex on the leeward side.

Figure 116 compares the pitch-up and pitch-down motions of the model to the static case for zero yaw angle. It can be seen clearly that during the pitch-down motion in the AOA range considered, the bursting location always occurred earlier relative to the static case. During the pitch up motion at high angles of attack (>25°), the bursting location occurred later relative to the static case. Thus the burst location curve consistently undershot the corresponding static curve during pitch-down motion and overshot during pitch-up motion at high AOA (>25°), this undershoot/overshoot increasing with the pitch rate. The vortex bursting response observed here for pitch-up and pitch-down motions is similar to the one observed by Magness, et al. [Ref. 11] in their experimental investigations of leading edge vortices on a pitching delta wing. The implications of these burst movement locations during pitch-up and pitch-down motions can be directly correlated with the results of force data reported by Branden and Shah [Ref. 13].

The effects of yaw on the bursting location of the LEX vortex for the static case is shown in Figure 117. It is clear from Figure 117 that for the static case the effect of small yaw up to 10° is to delay bursting at AOA greater than approximately 20°. For AOA less than 15° and $\beta > 10°$ the yaw input caused the flow to split making it difficult to accurately measure the bursting location. Figure 46, $\alpha = 10°$, $\beta = 10°$ distinctly shows the splitting and highlights the difficulty in determining the bursting location. Increasing the yaw angle to 20° caused a large rolling vortex to form which increased in size, with increasing AOA. This is very clearly seen in Figures 51 through 55 (see explanation on

pages 31 - 32). The increase in the vortex core diameter weakened the vortex causing the irregular curve as seen in Figure 117.

Figures 118 and 119 show bursting location plots highlighting the yaw effect during pitch-up motion at two reduced frequencies. At the lower pitch rate (Figure 118) the effects of yaw were similar to those observed for the static case. For AOA greater than 21° and yaw angles of up to 10° the bursting location was delayed relative to the low pitch rate motion at zero yaw. For AOA less than 21° the yaw effects once again caused flow splitting creating a weaker vortex and earlier bursting. Figures 66 and 67, α = 11° and 20°, β = 10° show the flow splitting and highlight the difficulty in determining the LEX vortex bursting location. Increasing the yaw angle to 20° resulted in similar trends to those observed for the static case for AOA less than 20° where the flow split into two segments. Figures 76 and 77, α = 10°and 20°, β = 20°, shows the flow splitting. The split flow made it difficult to accurately locate the LEX bursting location which led to the peculiar points on the graph for β = 20°. At AOA greater than 20° the yaw input caused an overshoot relative to the zero yaw curve up to 40° AOA. The effects of yaw during the higher pitch rate motion are shown in Figure 119. Throughout the range of AOA the yaw angle inputs (+5°,+ 10°,+ 20°) delayed vortex bursting relative to the high pitch rate motion at zero yaw. It should be noted that the two irregular points at α = 12°and 23°, β = 20° (Figures 106 and 107) were due to the windward flow splitting into two segments. One of the segments crossed over the canopy and merged with the leeward side flow increasing its vortex strength and further delaying LEX vortex bursting.

Figures 120 and 121 display the bursting location plots highlighting the yaw effect during pitch-down motion at two reduced frequencies. It can be clearly seen that during the lower pitch rate motion (Figure 120) yaw angles up to +10° cause a delay in vortex busting relative to the corresponding motion at zero yaw. Increasing the yaw angle to +20° caused a large rolling vortex to develop through the AOA range considered. This weaker vortex caused bursting to occur earlier relative to the curve for zero yaw. Figures 81 through 84 show these large rolling vortices developing at the lower reduced frequency. However, the higher pitch rate induced a delay in vortex bursting for AOA greater than 11° for β= +5° and +10° as can be seen in Figure 121. For β = +20° the delay in the bursting occurred at AOA greater than 16°. The undershoot at β = +20° for AOA less 16° was due to flow splitting leading to the development of a weaker vortex.

V. CONCLUSIONS AND RECOMMENDATIONS

A low speed flow visualization investigation was initiated into the high angle of attack aerodynamics of a 2% scale model of the F/A-18 fighter aircraft using dye injection in the Naval Postgraduate School water tunnel. The main focus of this study was the effect of pitch rate on the development and bursting of vortices generated from the leading edge extensions in the high angle of attack range with and without yaw. The following conclusions are drawn from the results of the experimental investigation:

1. Static Conditions: At lower angles of attack the LEX flow field was practically vortex free up to $\alpha \approx 10°$. As the angle of attack increased to 20° a symmetric pair of LEX generated vortices developed. As the angle of attack was increased further, the vortices grew and the bursting location moved forward indicating that the separated flow regime increased at higher angles of attack.
2. Pitch Rate Effects: During the pitch-down motion the bursting occurred earlier relative to the static case. During the pitch-up motion the bursting occurred later relative to the static case for AOA > 25°. These pitch rate effects increased with pitch rate.
3. Yaw Effects: Vortex core breakdown position is also a function of yaw angle. Yaw angle effects are pronounced at low AOA. At a constant angle of attack,

the windward LEX vortex bursting location was found to travel forward and inboard with yaw inputs and the leeward LEX vortex bursting location traveled aft and outboard. For yaw angles less than 10°, LEX vortex bursting occurred later on the leeward side than on the windward side. These effects were observed for both static and dynamic conditions at angles of attack greater than 20°. The presence of asymmetric vortices lead to undesirable side forces and yawing moments.

The following recommendation are made based on this investigation:

1. The flow visualization experiment should be extended to higher angles of attack beyond 50°.
2. The above study was carried out for the power-off condition. It is highly recommended that the investigation be extended to include power-on conditions.
3. The study of the interaction between forebody and LEX generated vortices at high angles of attack for power-on and power-off conditions should be undertaken.
4. An automated computer controlled system for carrying out flow visualization experiments and for data acquisition and analysis is highly recommended.

LIST OF REFERENCES

1. Herbst, W.B., *Future Fighter Technologies*, Journal of Aircraft, Vol. 17 Number 8, pp 561-566, August 1980.

2. Herbst, W.B., *Dynamics of Air Combat*, Journal of Aircraft, Vol. 20, Number 7, pp 594-598, March 1982.

3. Murri, D.G., and Rao, D.M., *Exploratory Studies of Actual Forebody Strakes for Yaw Control at High Angle of Attack*, AIAA paper pp 87-2557, 1987.

4. Fink, D.E., and others *Agile Sukhoi Su-27 Leads Strong Soviet Presentation*, Aviation Week and Space Technology, Vol. 130, pp 28-30, 19 June 1989.

5. Sommers, J.D., *An Experimental Investigation of Support Strut Interference on A Three-percent Fighter Model at High Angles of Attack*, Master's Thesis, Naval Postgraduate School, Monterey, California, September 1989.

6. Scott, W.B., *NASA Adds to Understanding of High Angle of Attack Regime*, Aviation Week and Space Technology, Vol. 130, pp 36-42, 22 May 1989.

7. Patierno, J., *Evolution of the Hybrid Wing YF-17/F/A-18 Type*, Proceedings of the Evolution of Aircraft Wing Design Symposium, pp 1-23, March 1988.

8. Del Frate, J.H. and Zuniga, F.A., *In-Flight Flow Field Analysis on the NASA F-18 High Alpha Research Vehicle with Comparison to Ground Facility Data*, AIAA paper 90-0231, 1990.

9. Wedemeyer, E., *Vortex Breakdown*, AGARD Lecture Series, No. 121, High Angle of Attack Aerodynamics, December 1982, pp. 9-1 to 9-17.

10. Hawk, J., Barnett, R., and O'Neil, P., *Investigation of High Angle of Attack Vortical Flow Over Delta Wing*, AIAA 90-0101, AIAA 28th Aerospace Sciences Meeting, January 8-11, 1990.

11. Magness, D., Robinson, O., and Rockwell, D., *Control of Leading Edge Vortices on a Delta Wing*, AIAA-89-0999, AIAA 2nd Shear Flow Conference, March 13-16, 1989.

12. Reynolds, G.A., and Abtahi, A.A., *Instabilities in Leading Edge Vortex Development*, AIAA-87-2424, AIAA Applied Aerodynamics Conference, August 17-19, 1987.

13. Brandon, J.M. and Shah, G.A., *Unsteady Aerodynamic Characteristics of a Fighter Model Undergoing Large - Amplitude Pitching Motions and High Angles of Attack*, AIAA-90-0309, AIAA 28th Aerospace Sciences Meeting, January 8-11, 1990.

14. Park, S., *Flow Visualization of the Effect of Pitch Rate on the Vortex Development on the Scale Model of a F-18 Fighter Aircraft*, Master's Thesis, Naval Postgraduate School, Monterey, California, June 1989.

15. User's Manual, *Flow Visualization Water Tunnel Operation Manual for Model 1520*, Eidelic International, Inc., Torrance, California, 1988. (Prepared for Naval Postgraduate School, Monterey, California).

APPENDIX A. EXPERIMENTAL RESULTS(PHOTOGRAPHS)

FIGURES 15 THROUGH 115

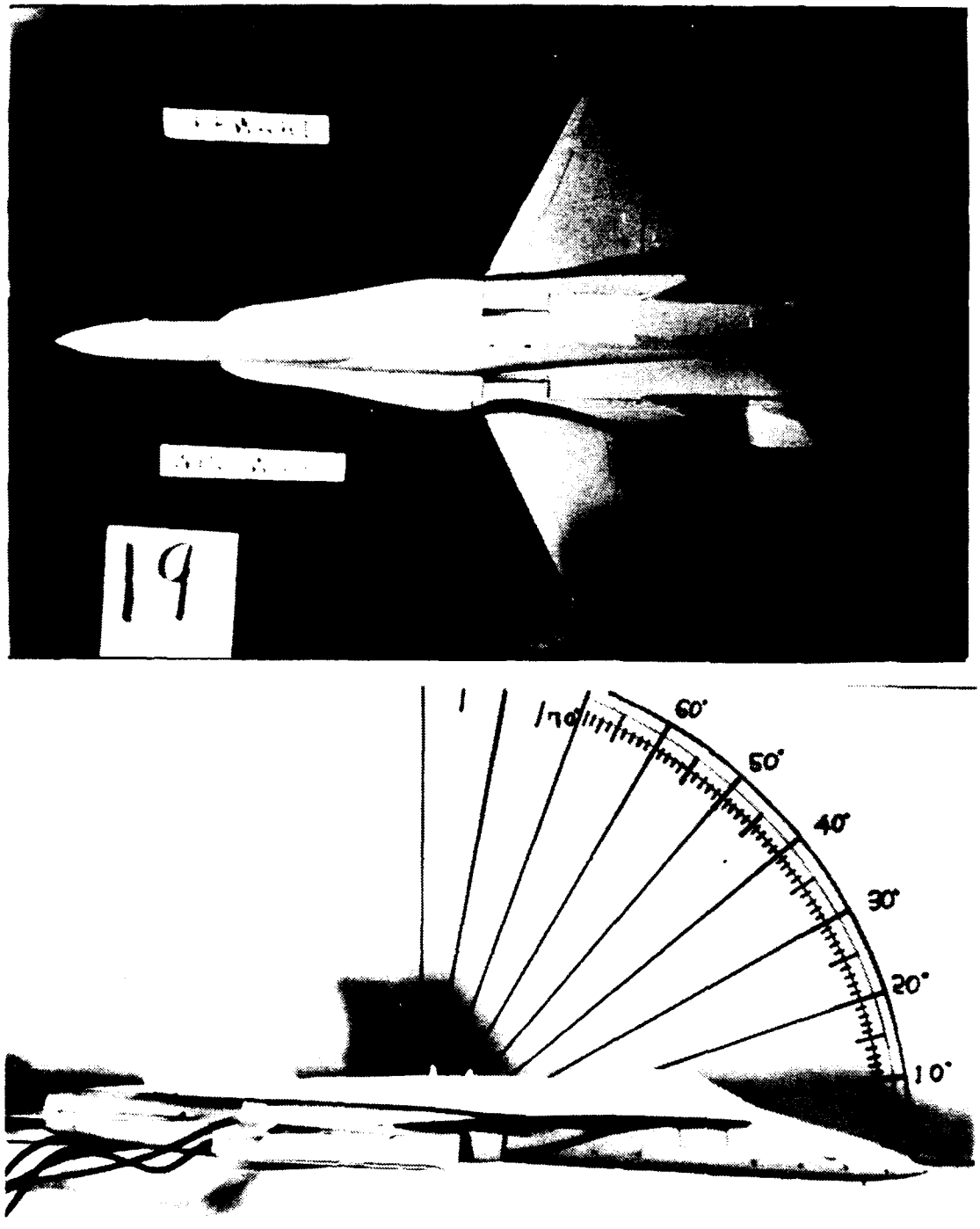

Figure 15. LEX Vortex, Static, $\alpha = 0°$, $\beta = 0°$

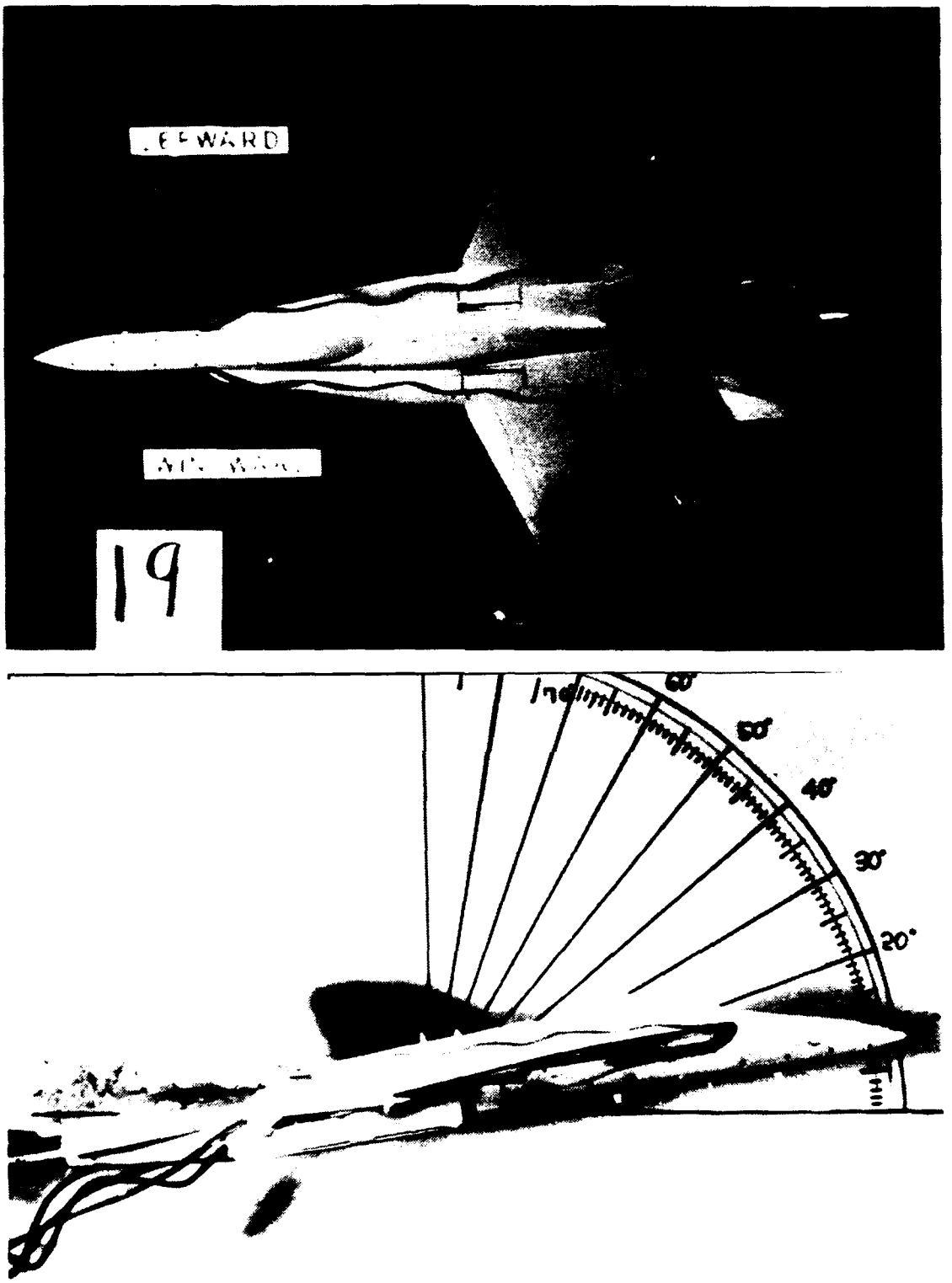

Figure 16. LEX Vortex, Static, α=10°, β=0°

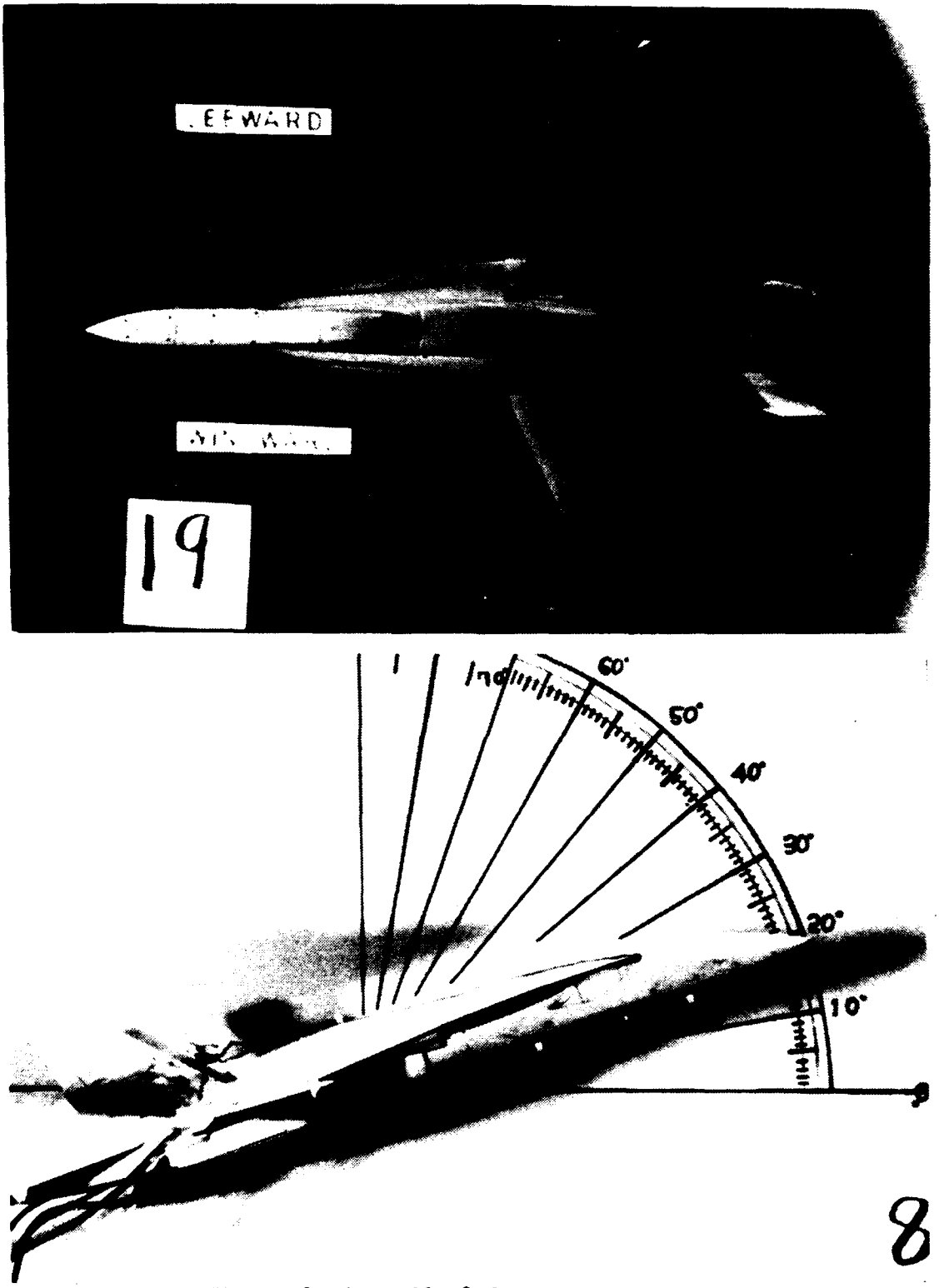

Figure 17. LEX Vortex, Static, α=20°, β=0°

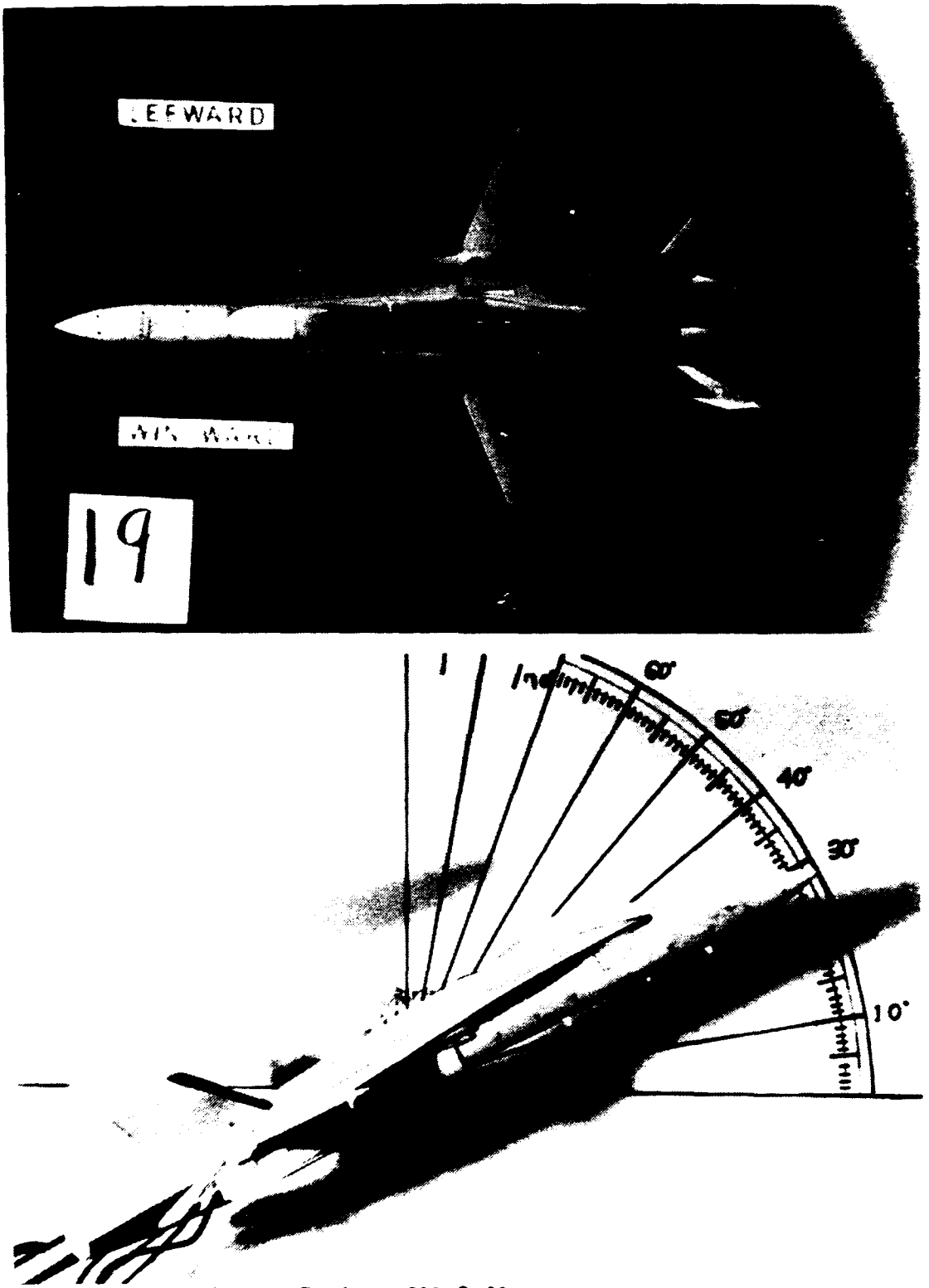

Figure 18. LEX Vortex, Static, α=29°, β=0°

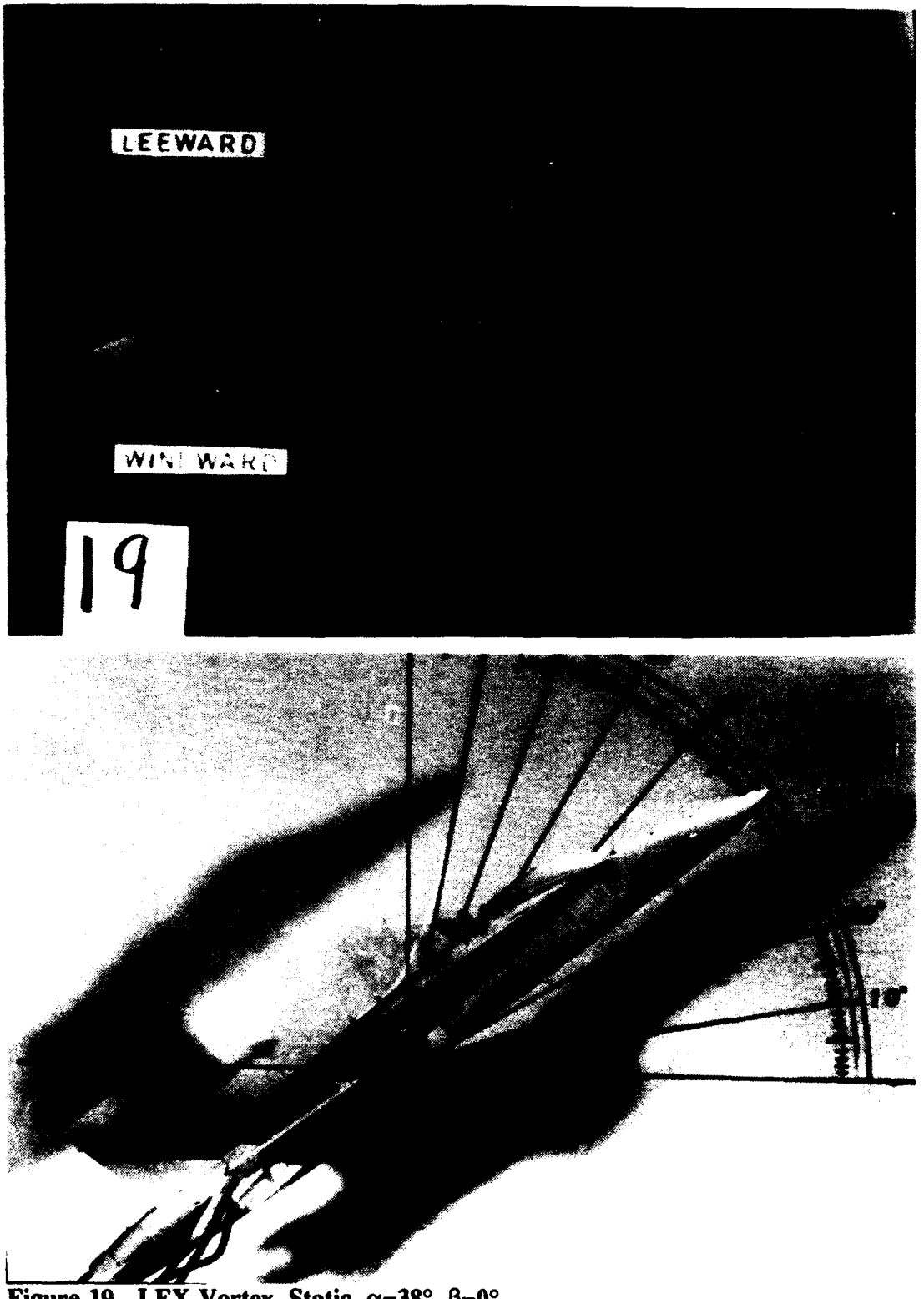

Figure 19. LEX Vortex, Static, α=38°, β=0°

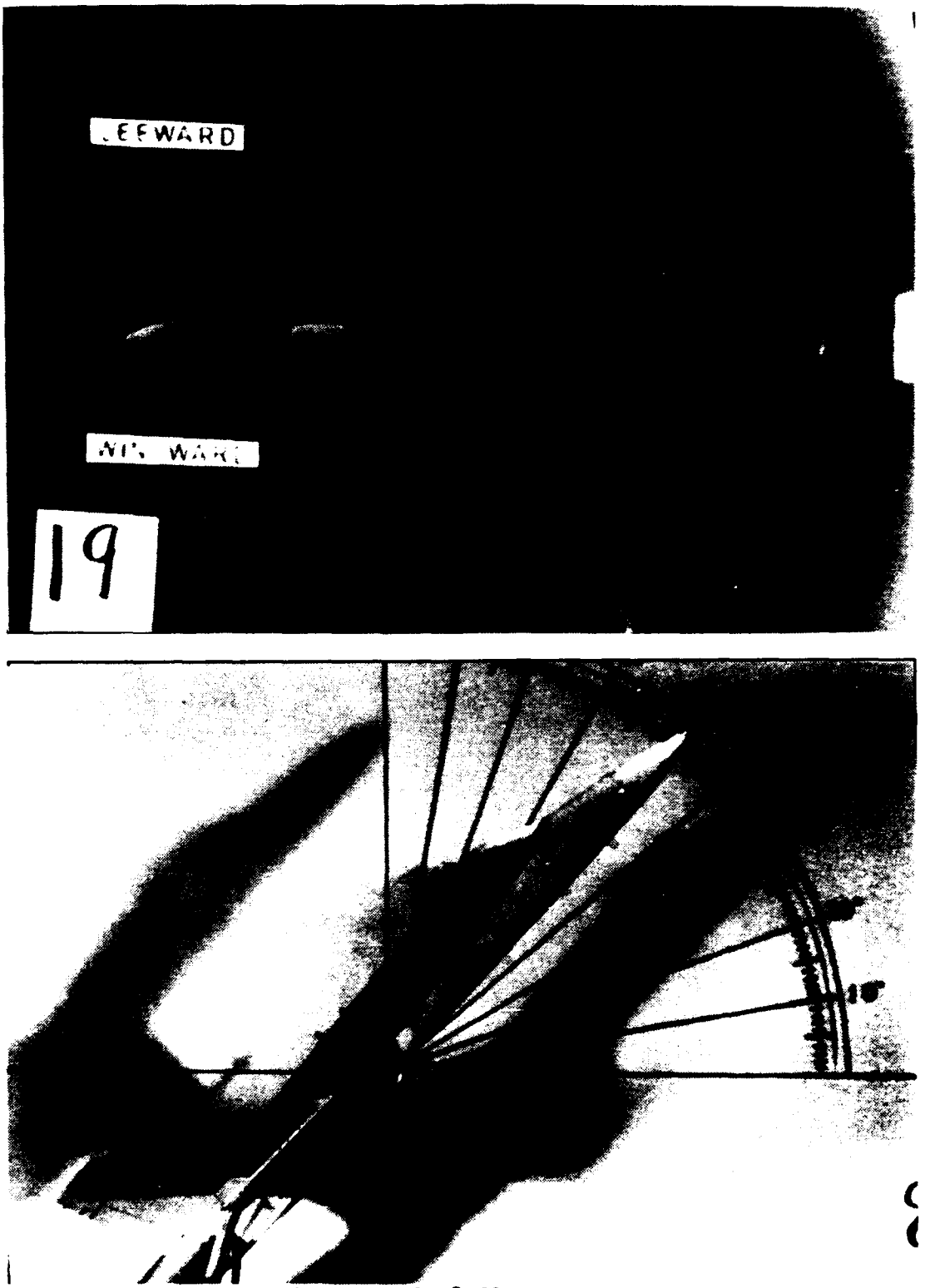

Figure 20. LEX Vortex, Static, α=49°, β=0°

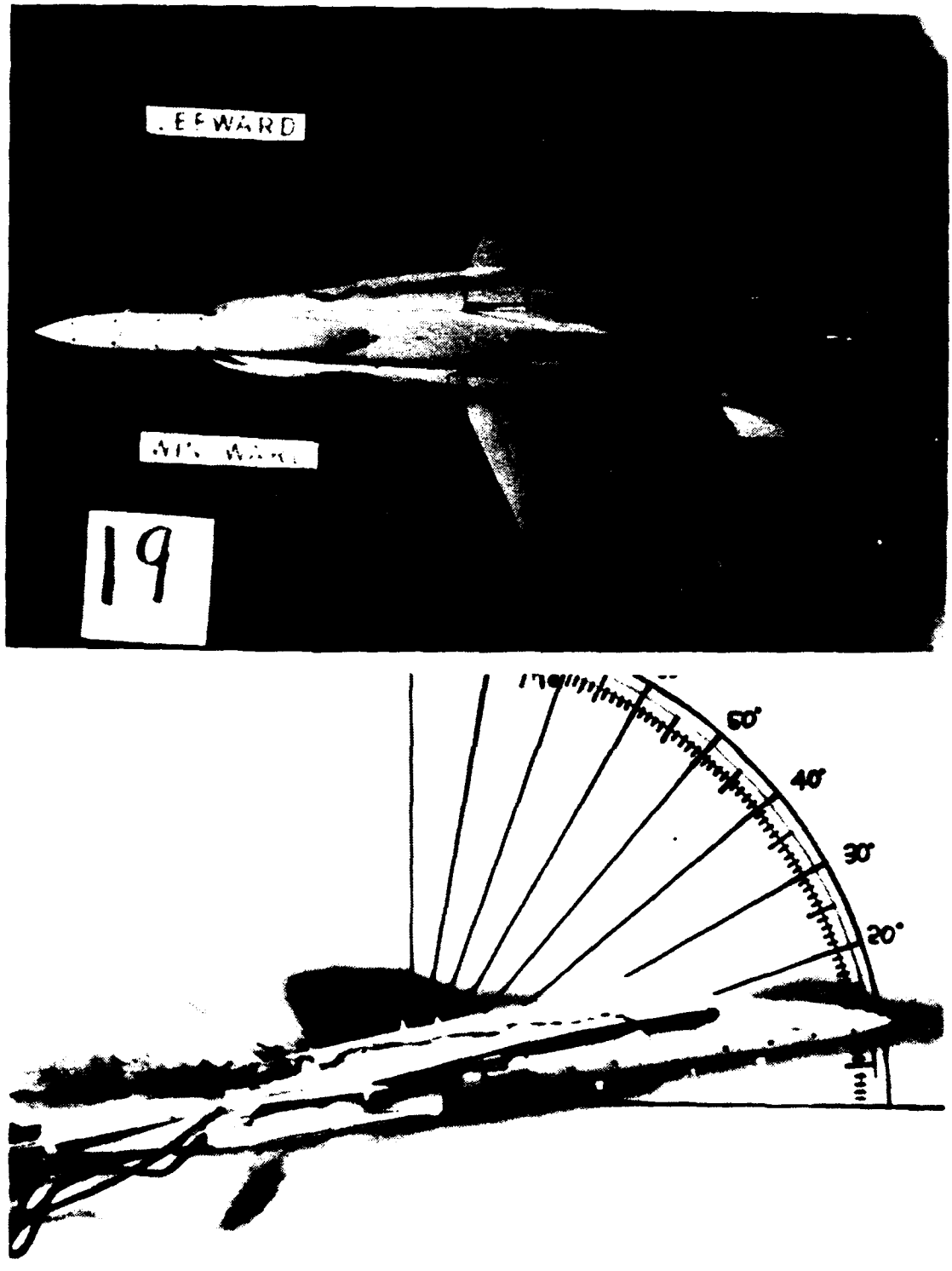

Figure 21. LEX Vortex, Low Pitch Rate Up, α=10°, β=0°

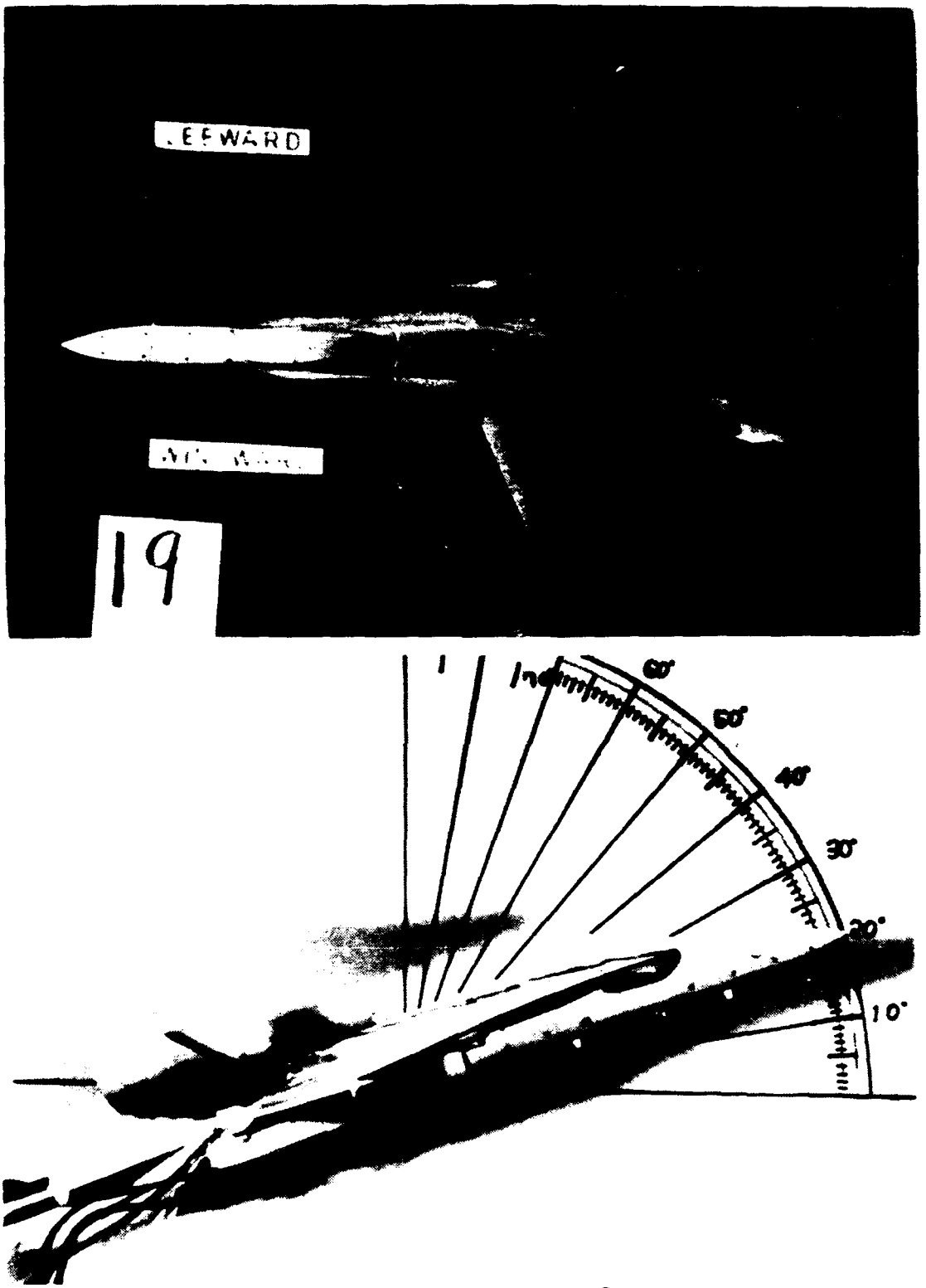

Figure 22. LEX Vortex, Low Pitch Rate Up, α=20°, β=0°

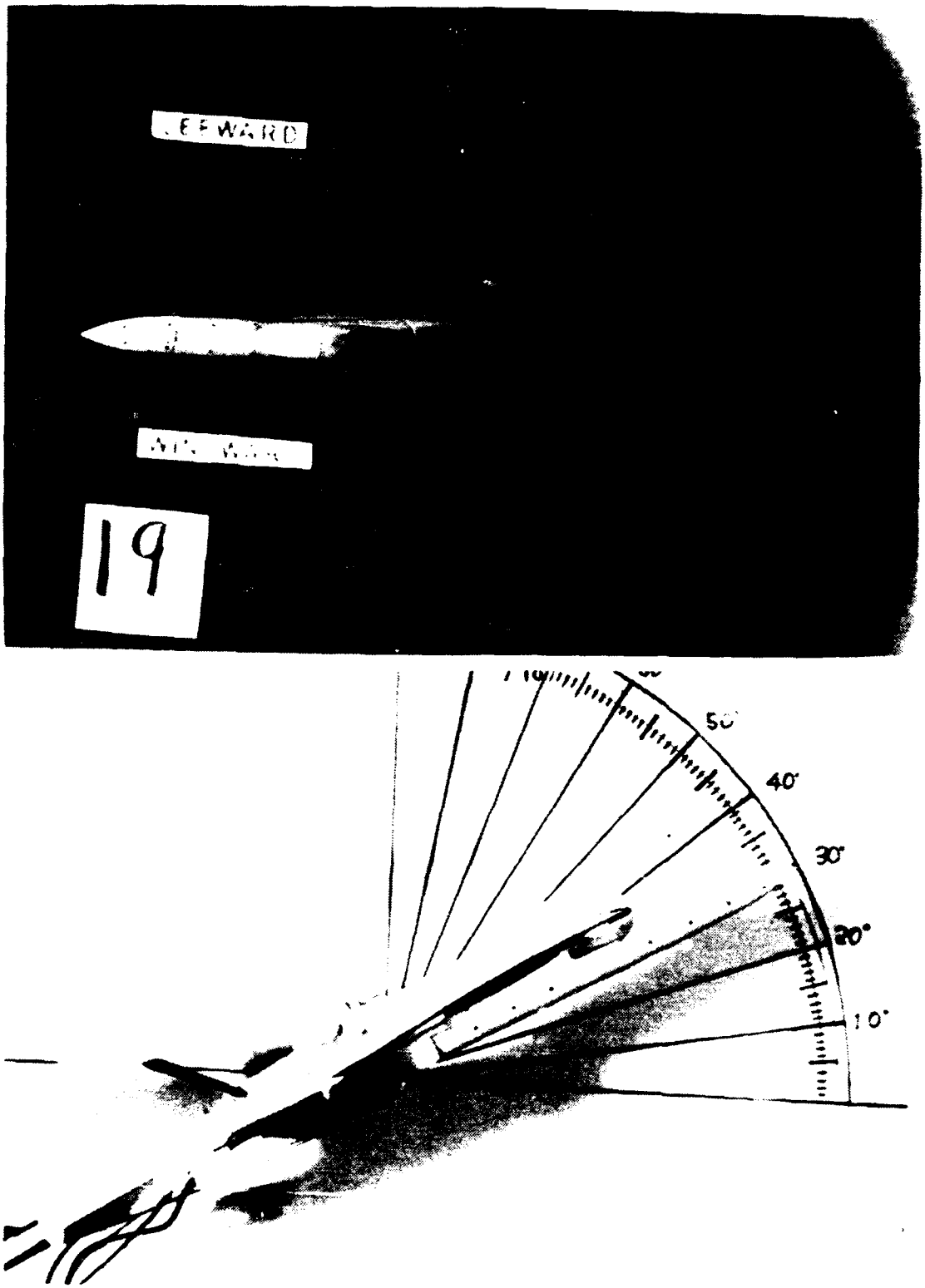

Figure 23. LEX Vortex, Low Pitch Rate Up, α=30°, β=0°

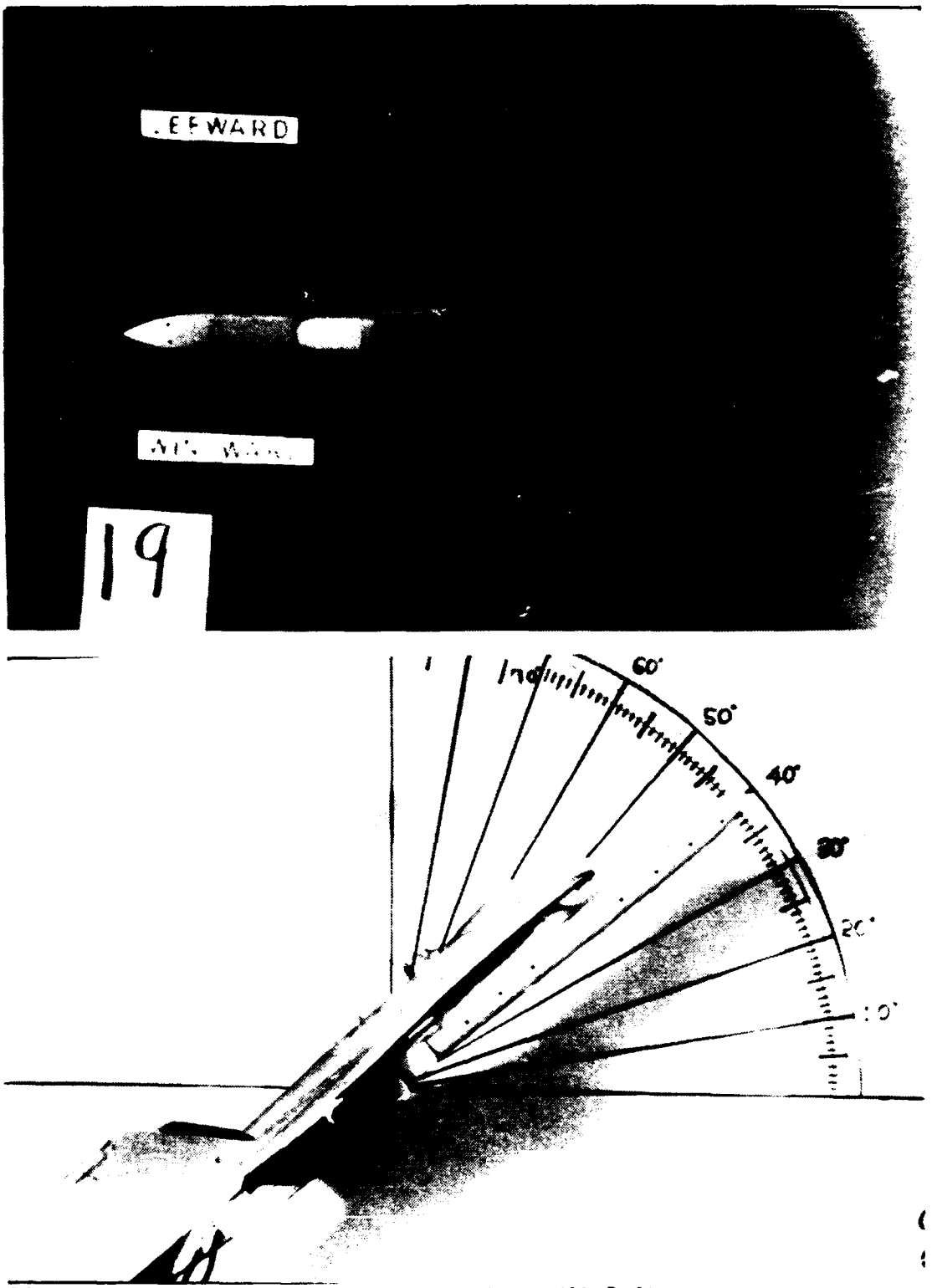

Figure 24. LEX Vortex, Low Pitch Rate Up, α=40°, β=0°

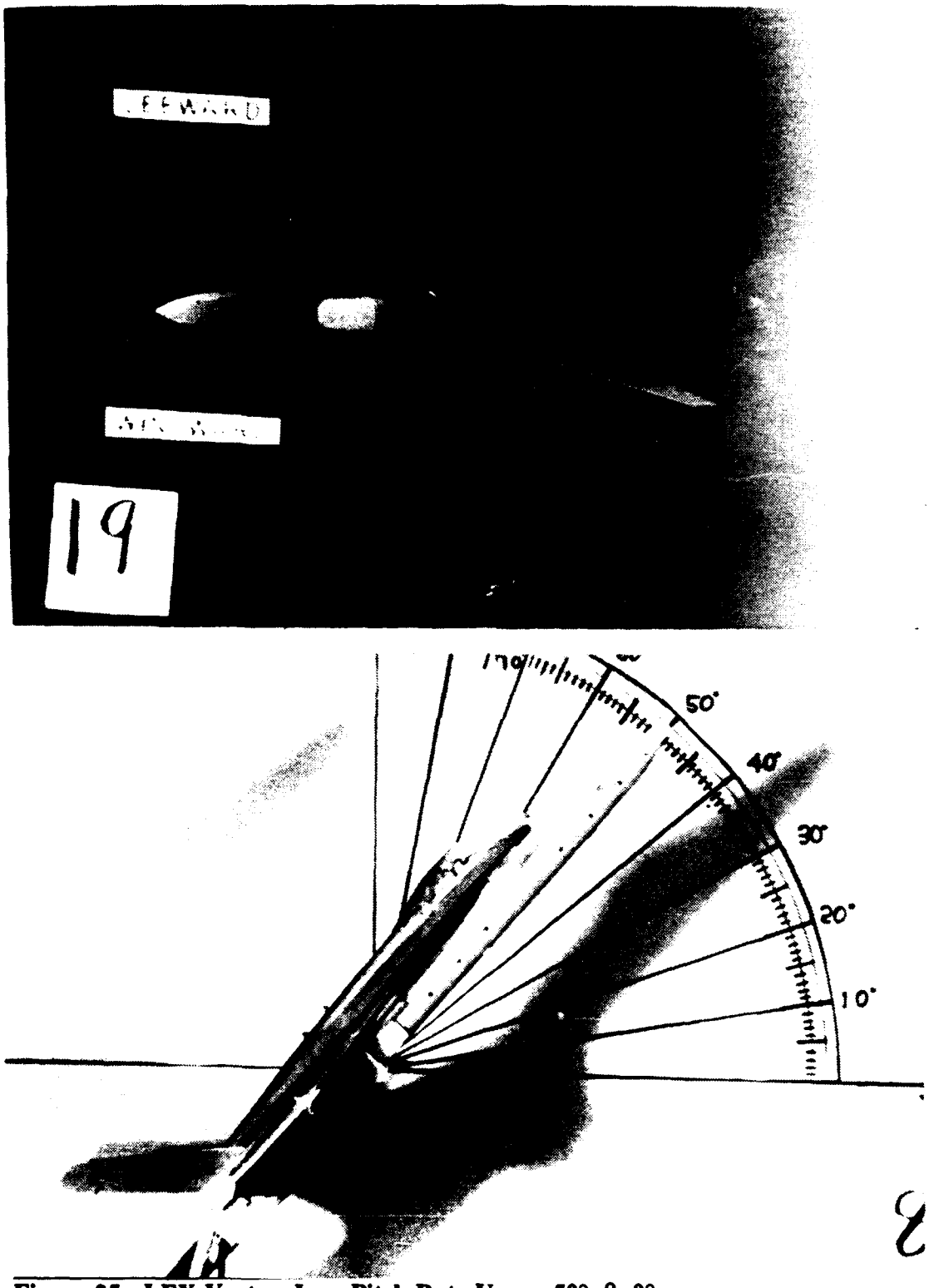

Figure 25. LEX Vortex, Low Pitch Rate Up, α=50°, β=0°

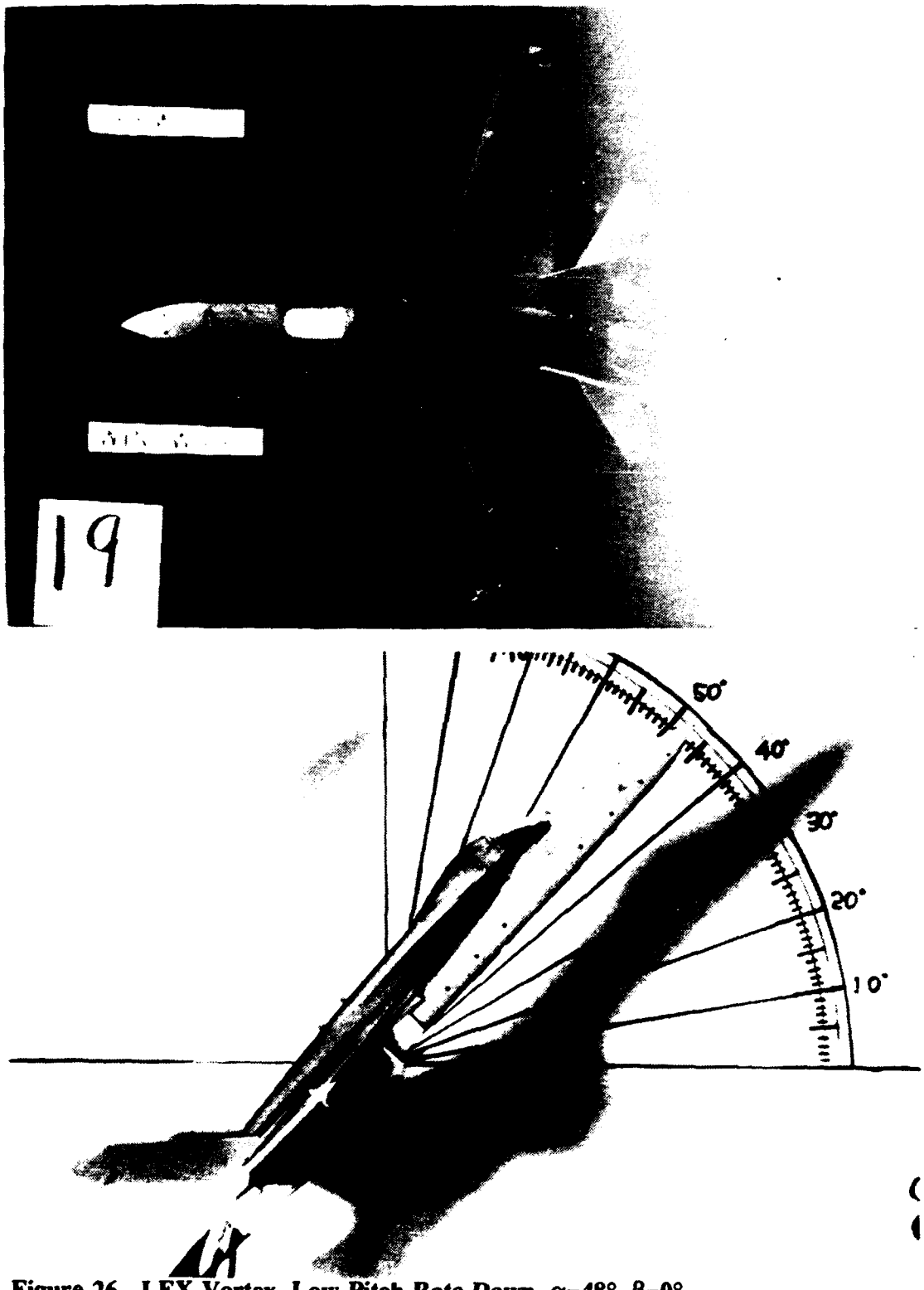

Figure 26. LEX Vortex, Low Pitch Rate Down, α=48°, β=0°

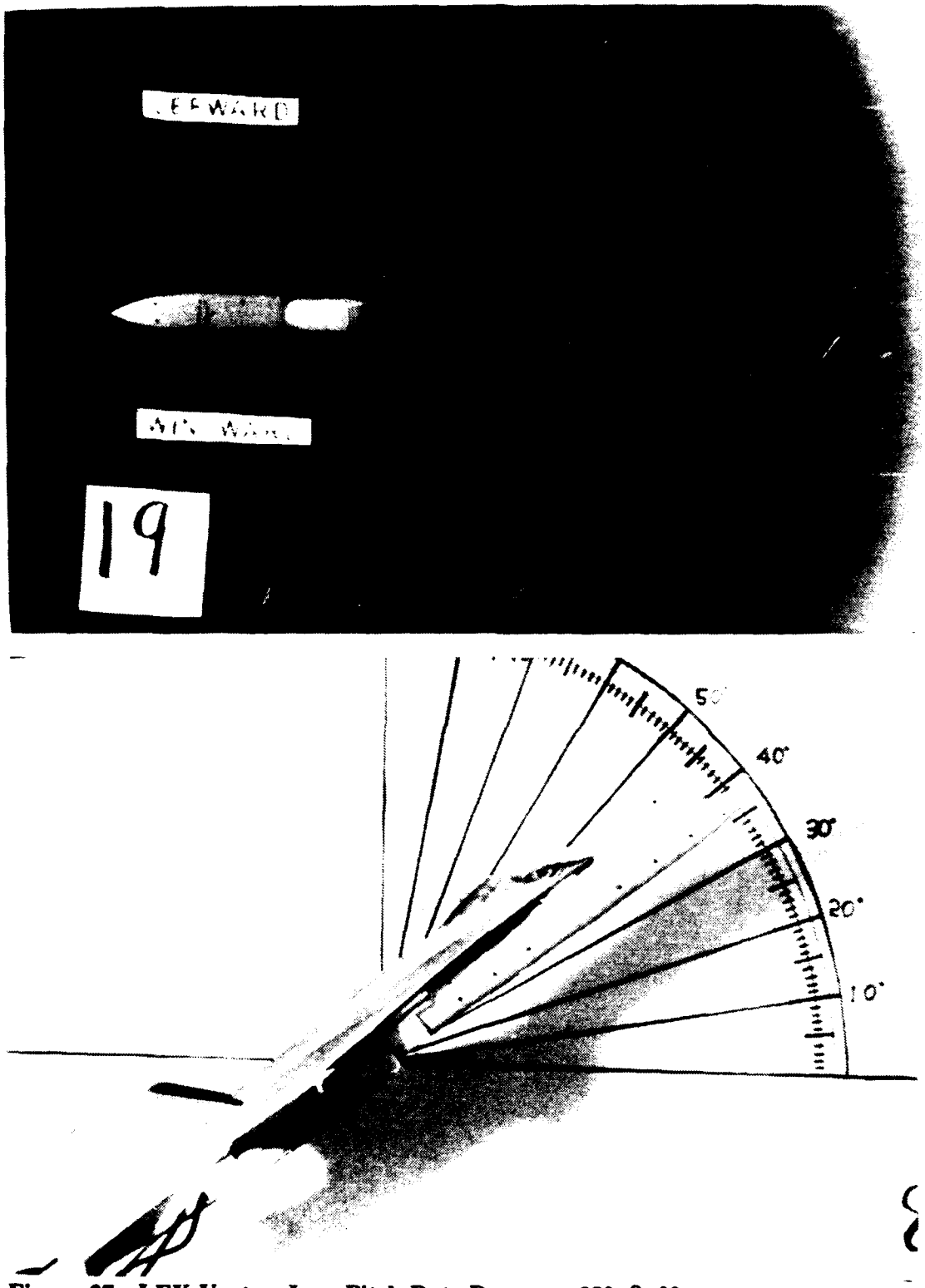

Figure 27. LEX Vortex, Low Pitch Rate Down, α=38°, β=0°

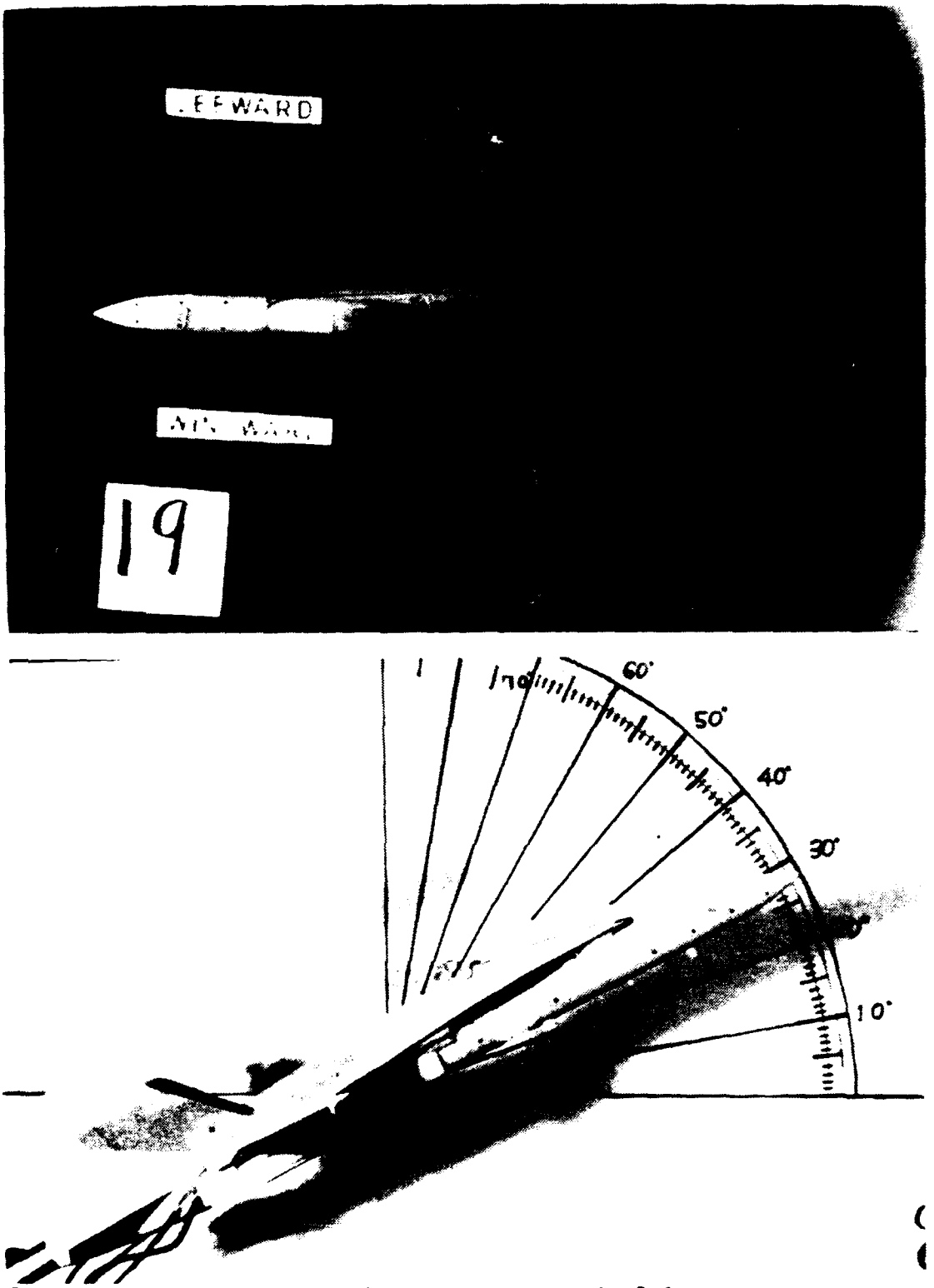

Figure 28. LEX Vortex, Low Pitch Rate Down, α=28°, β=0°

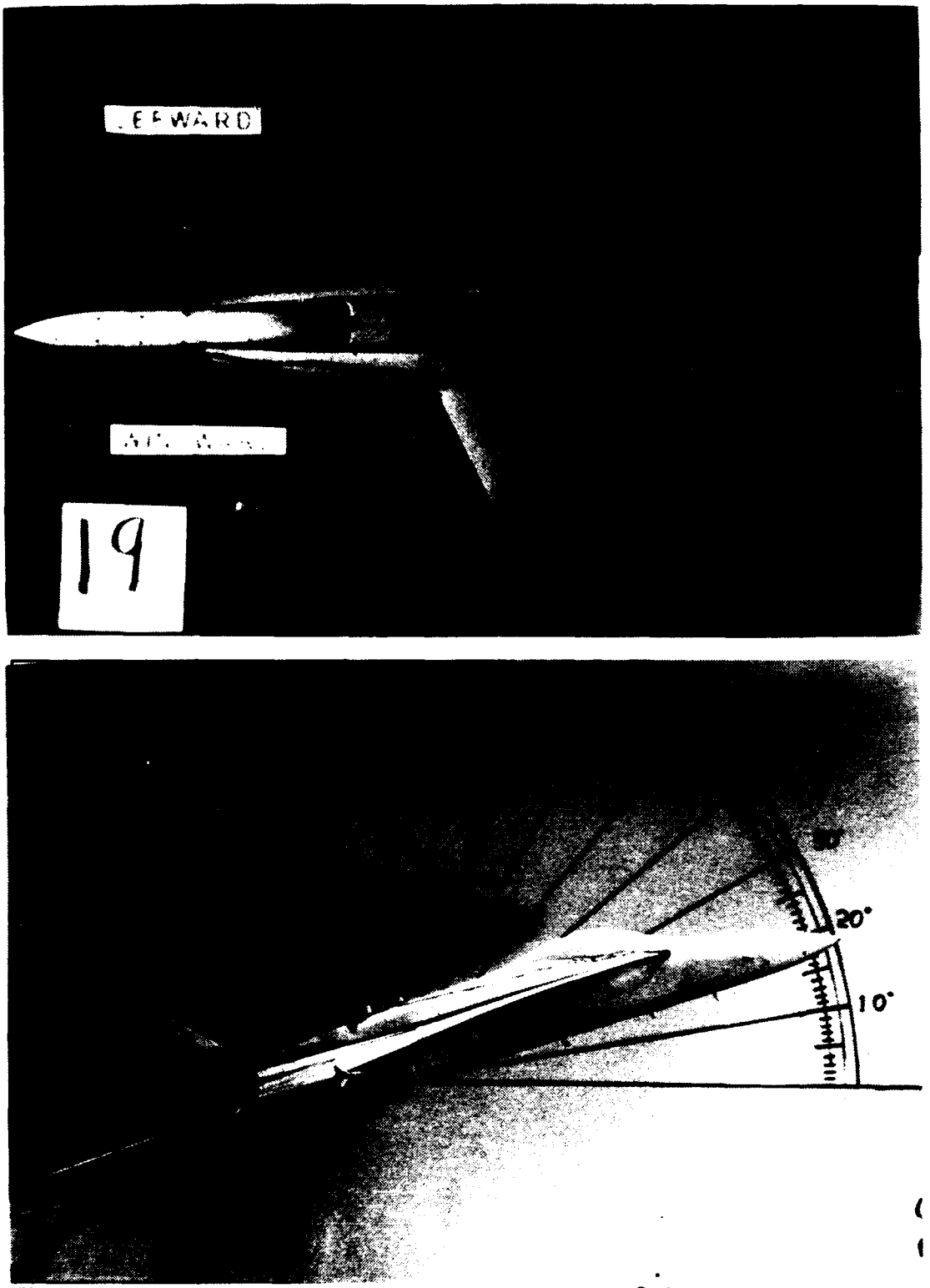

Figure 29. LEX Vortex, Low Pitch Rate Down, α=19°, β=0°

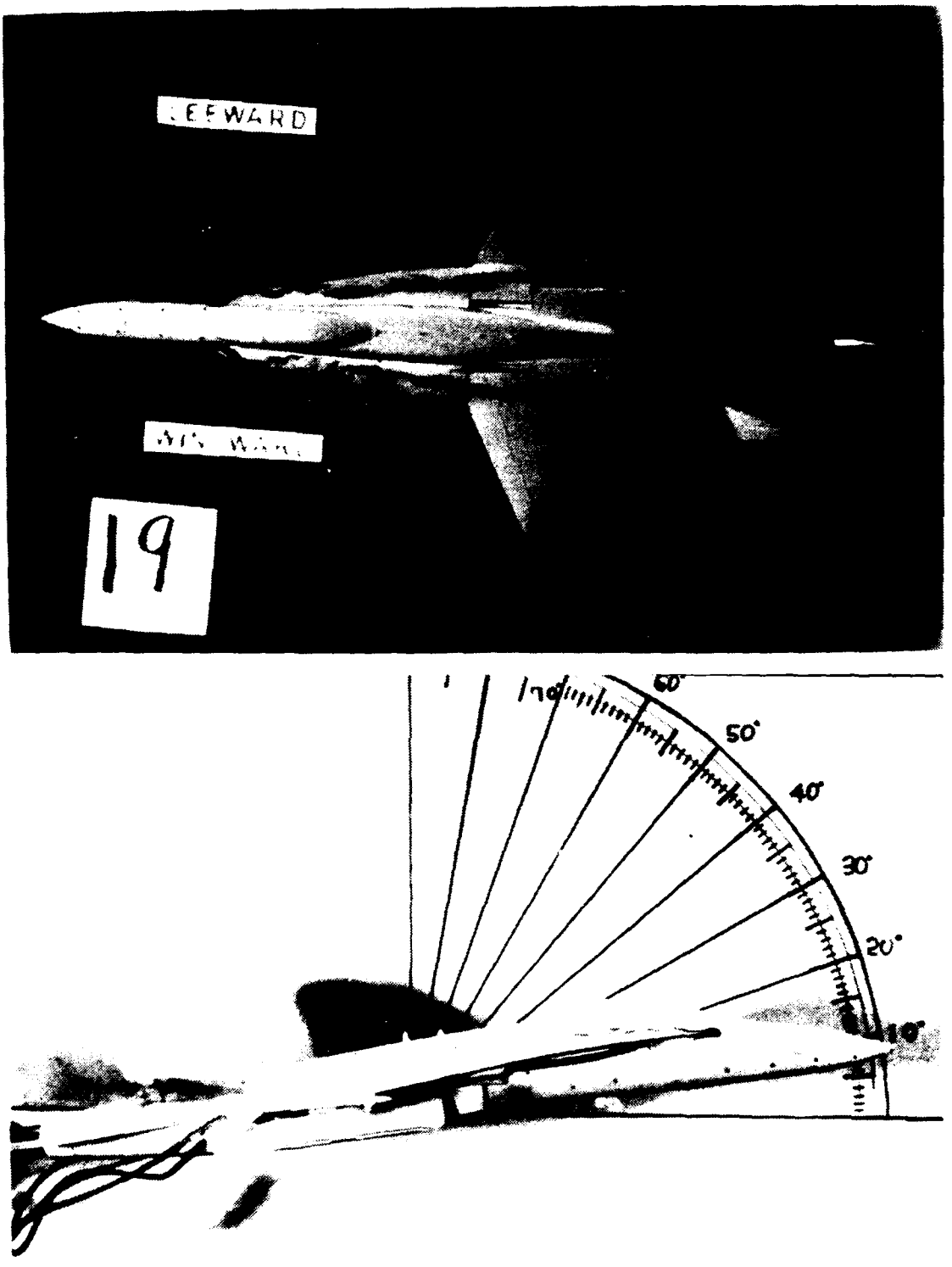

Figure 30. LEX Vortex, Low Pitch Rate Down, α=9°, β=0°

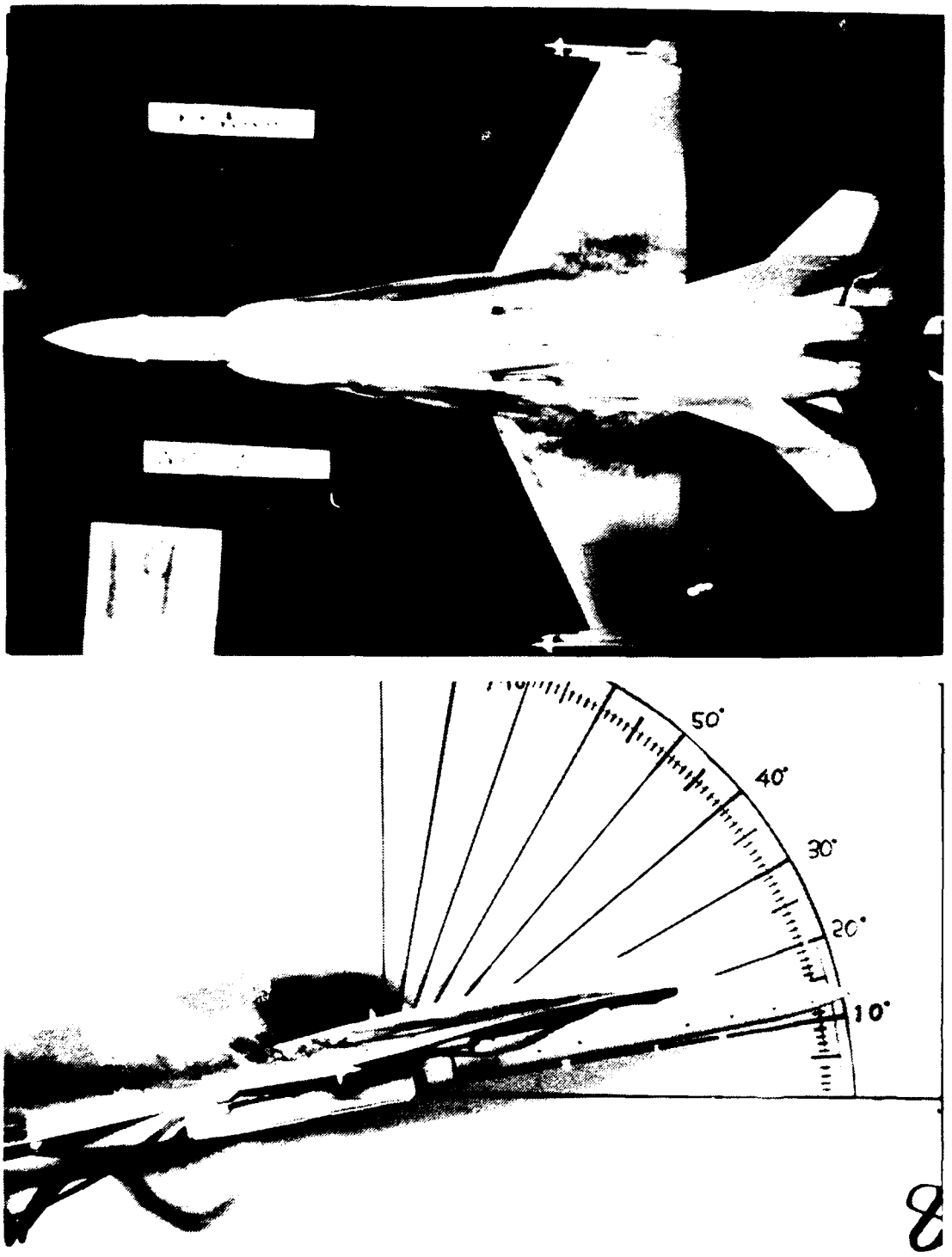

Figure 31. LEX Vortex, High Pitch Rate Up, α=12°, β=0°

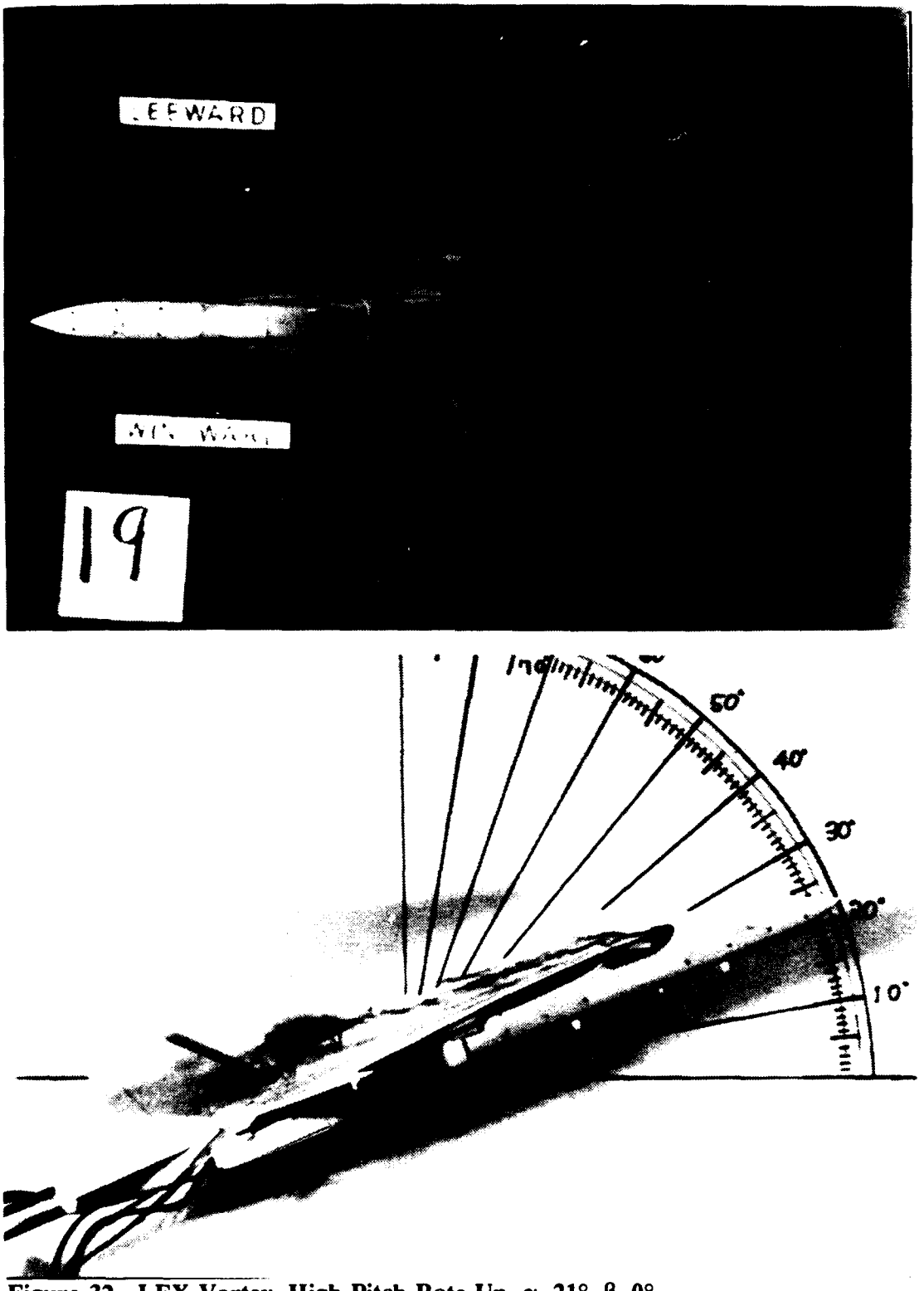

Figure 32. LEX Vortex, High Pitch Rate Up, α=21°, β=0°

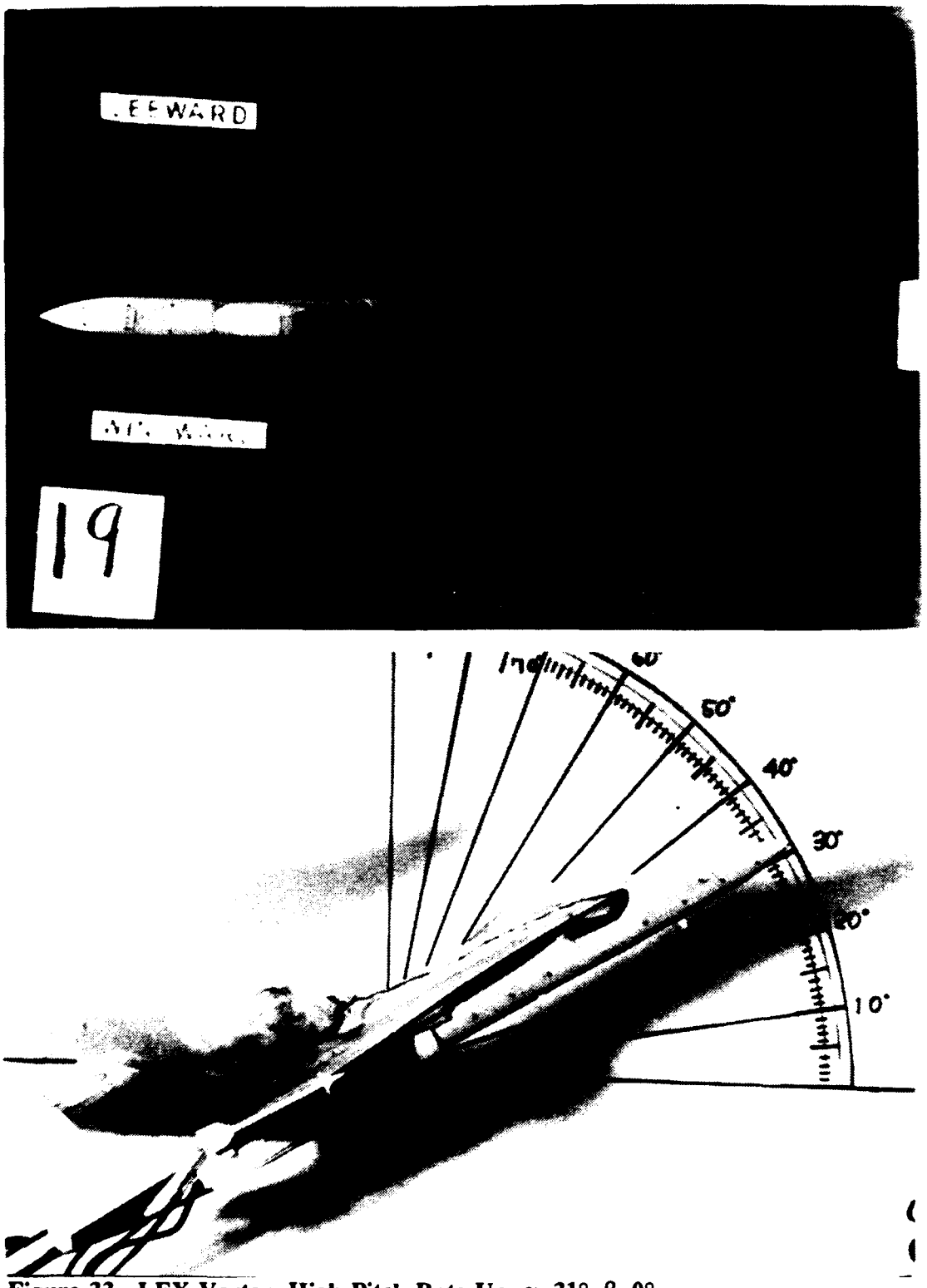

Figure 33. LEX Vortex, High Pitch Rate Up, α=31°, β=0°

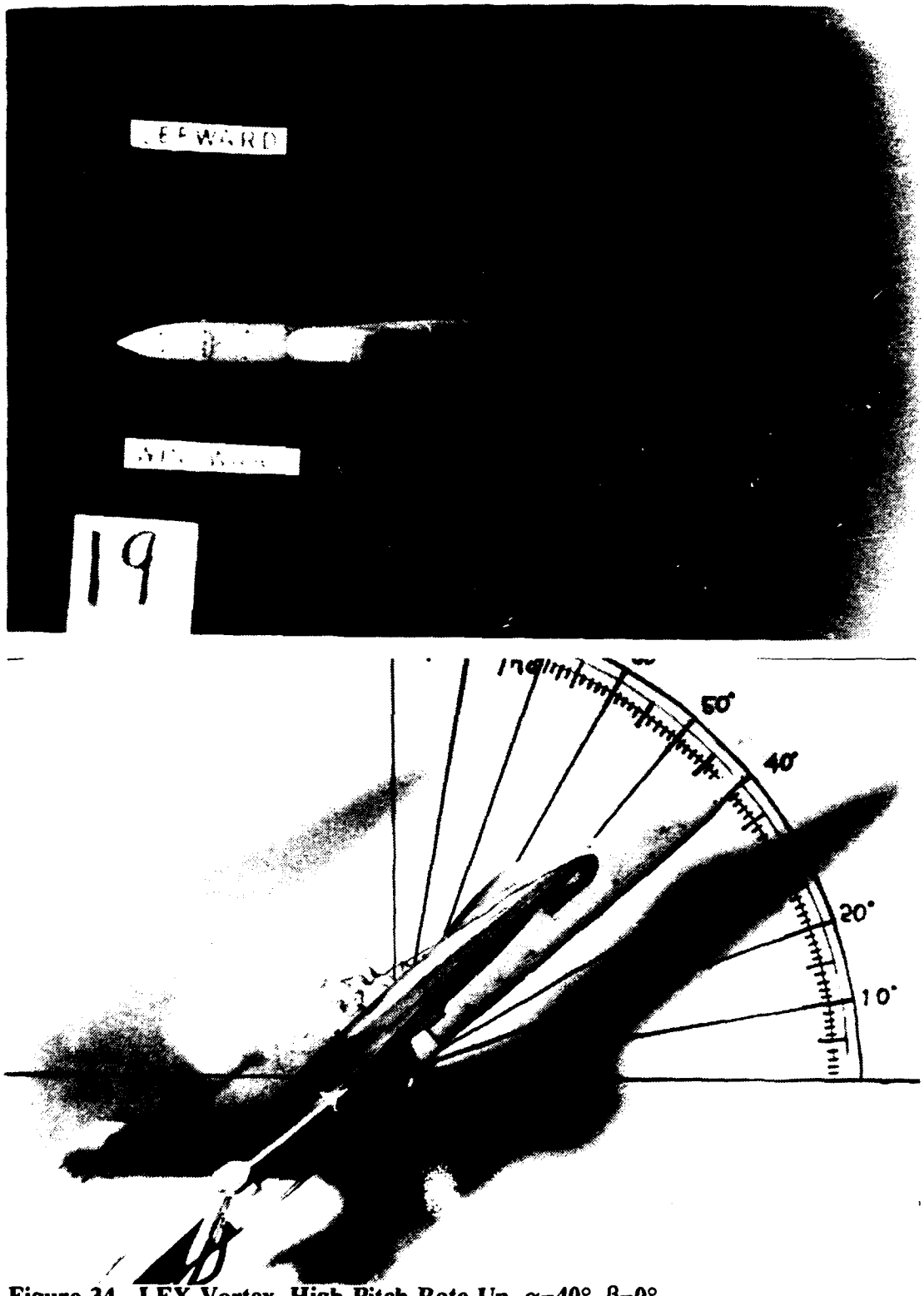

Figure 34. LEX Vortex, High Pitch Rate Up, α=40°, β=0°

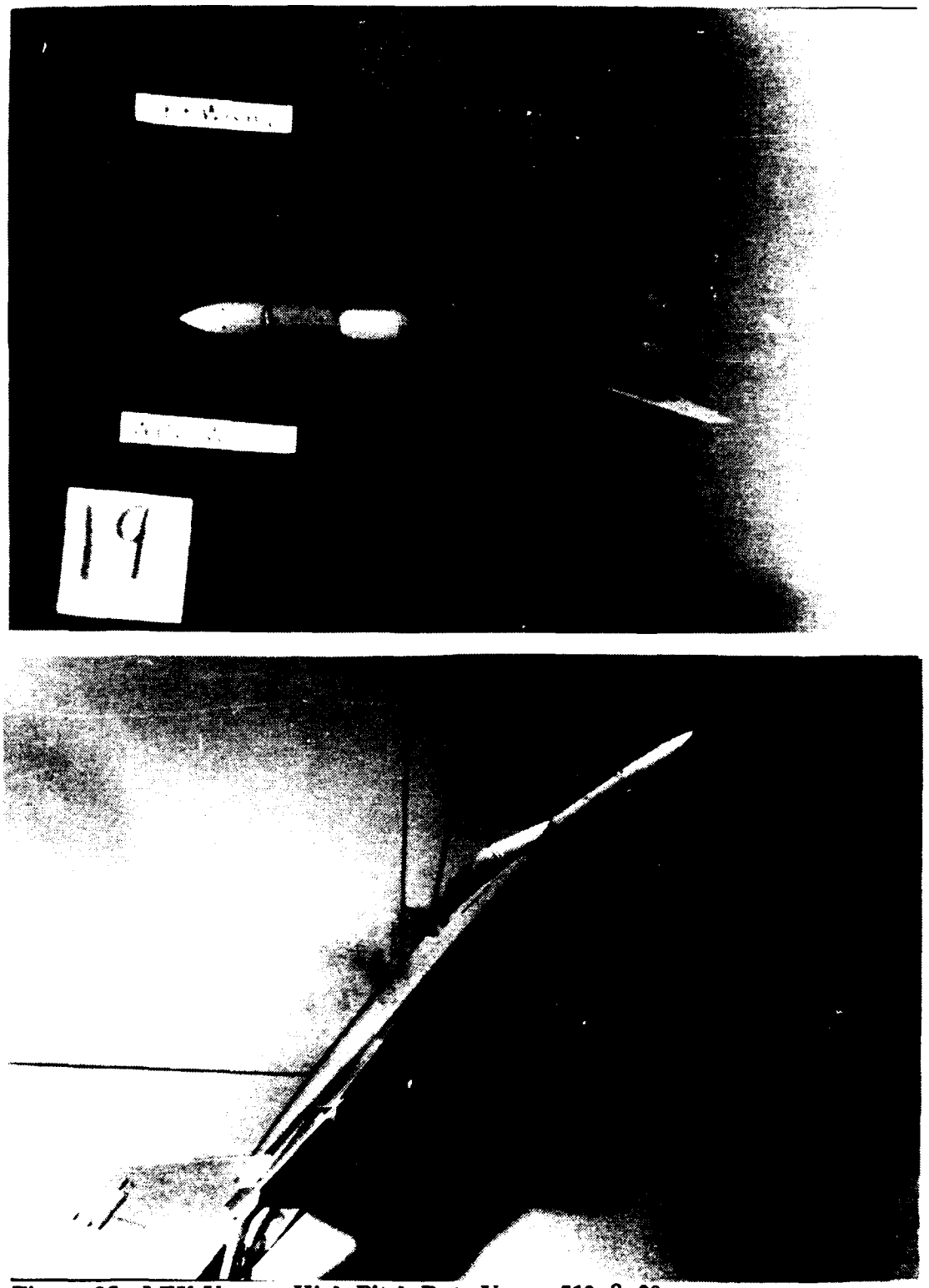

Figure 35. LEX Vortex, High Pitch Rate Up, α=51°, β=0°

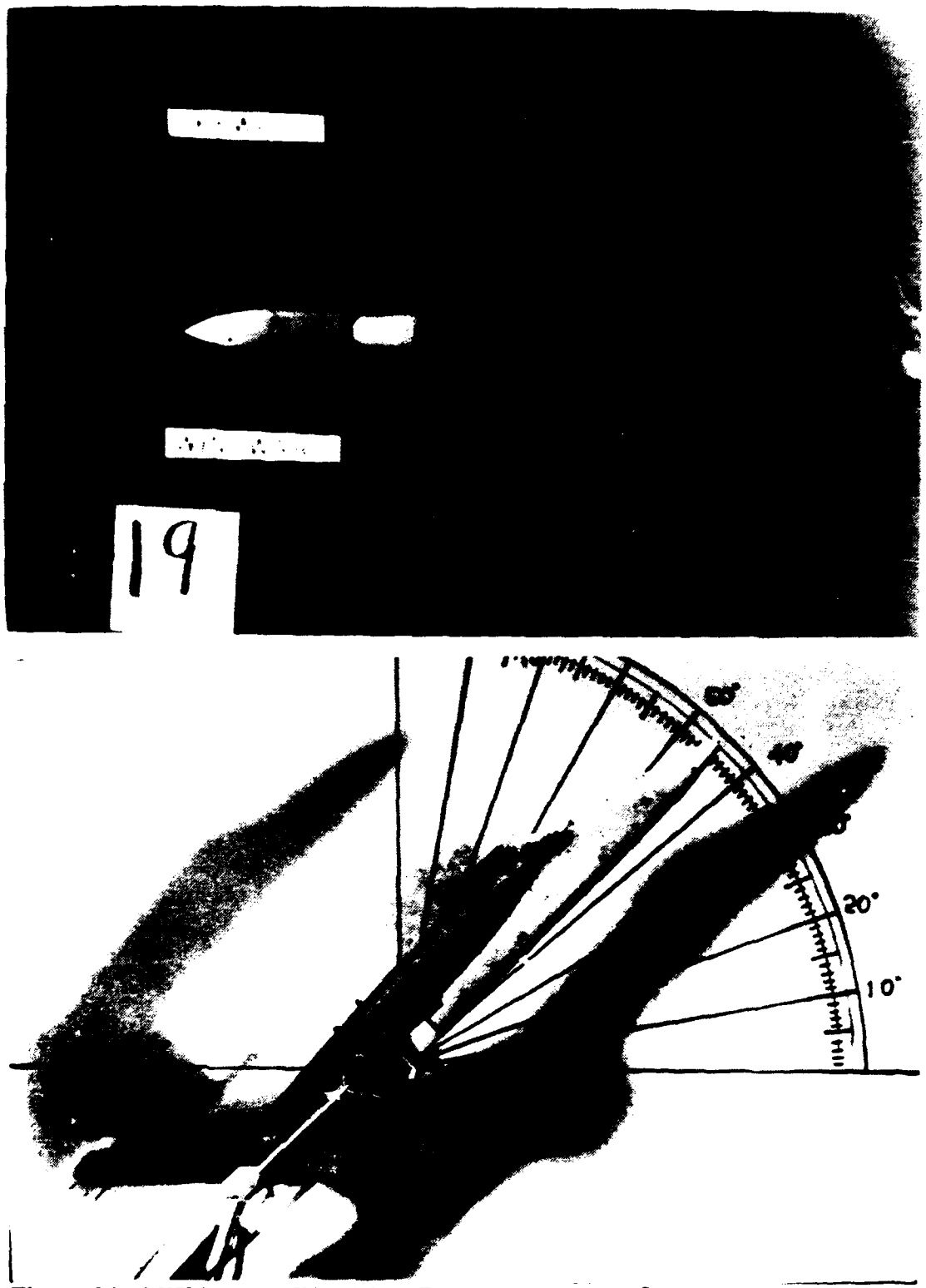

Figure 36. LEX Vortex, High Pitch Rate Down, α=46°, β=0°

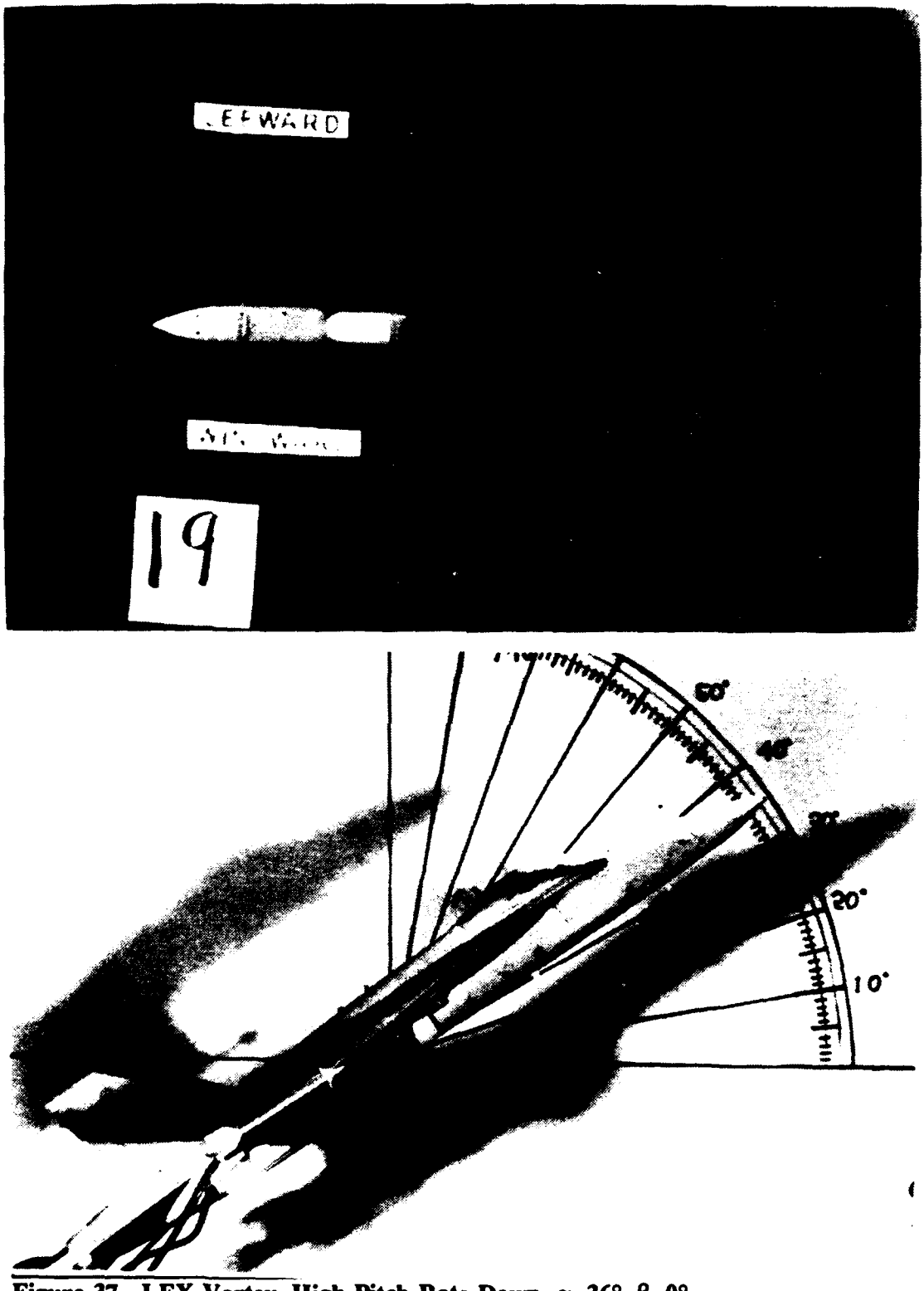

Figure 37. LEX Vortex, High Pitch Rate Down, α=36°, β=0°

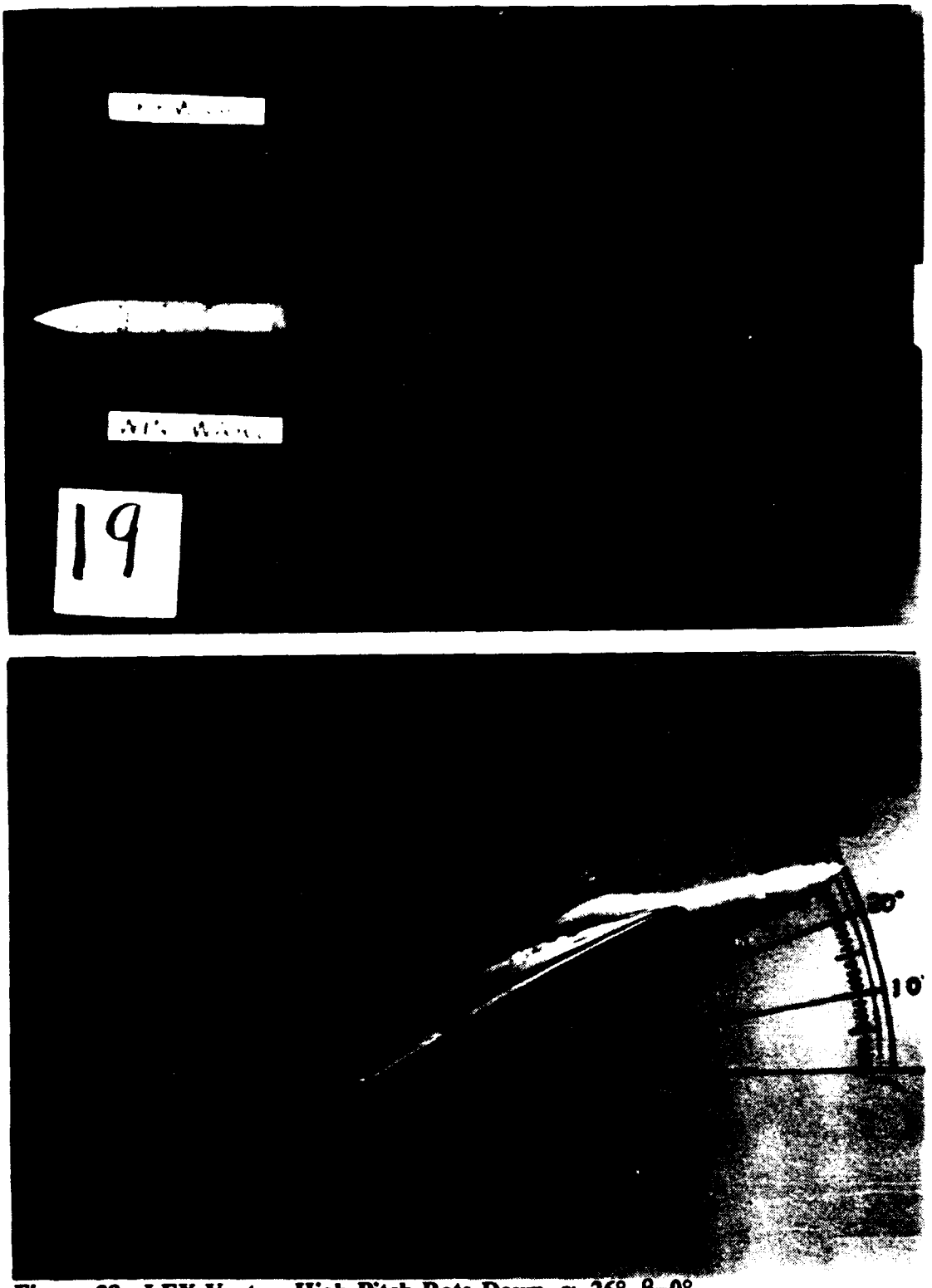

Figure 38. LEX Vortex, High Pitch Rate Down, α=26°, β=0°

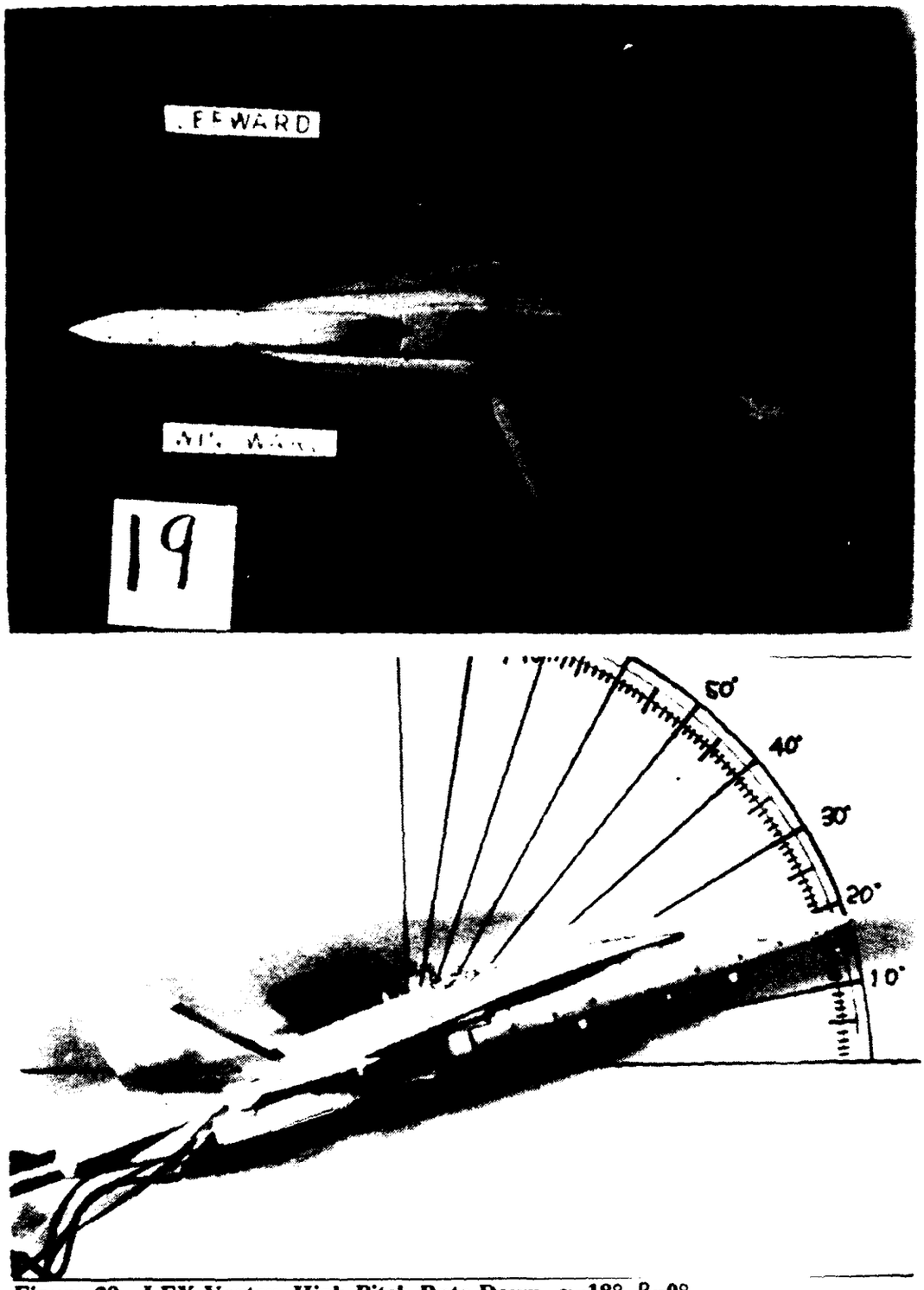

Figure 39. LEX Vortex, High Pitch Rate Down, α=18°, β=0°

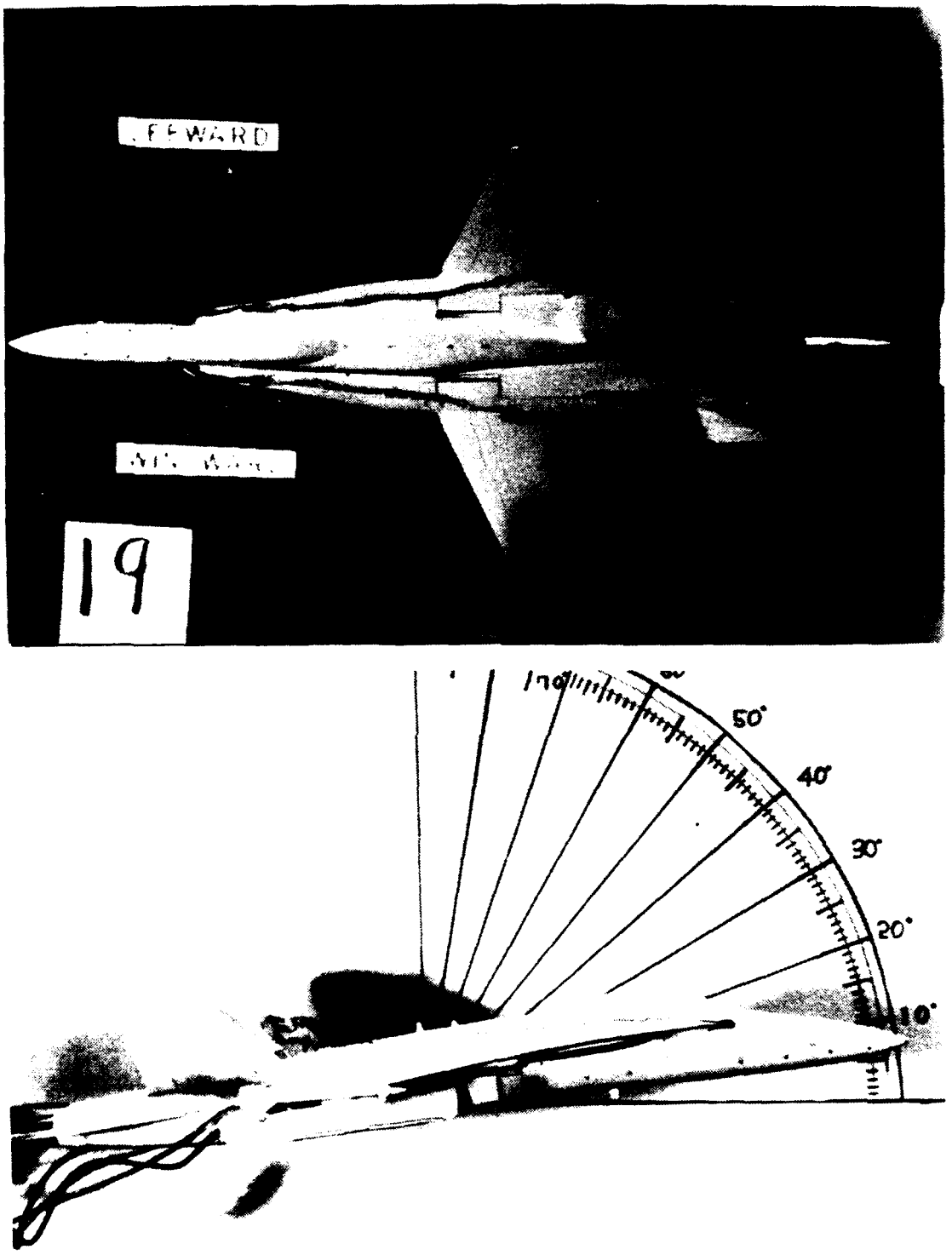

Figure 40. LEX Vortex, High Pitch Rate Down, α=7°, β=0°

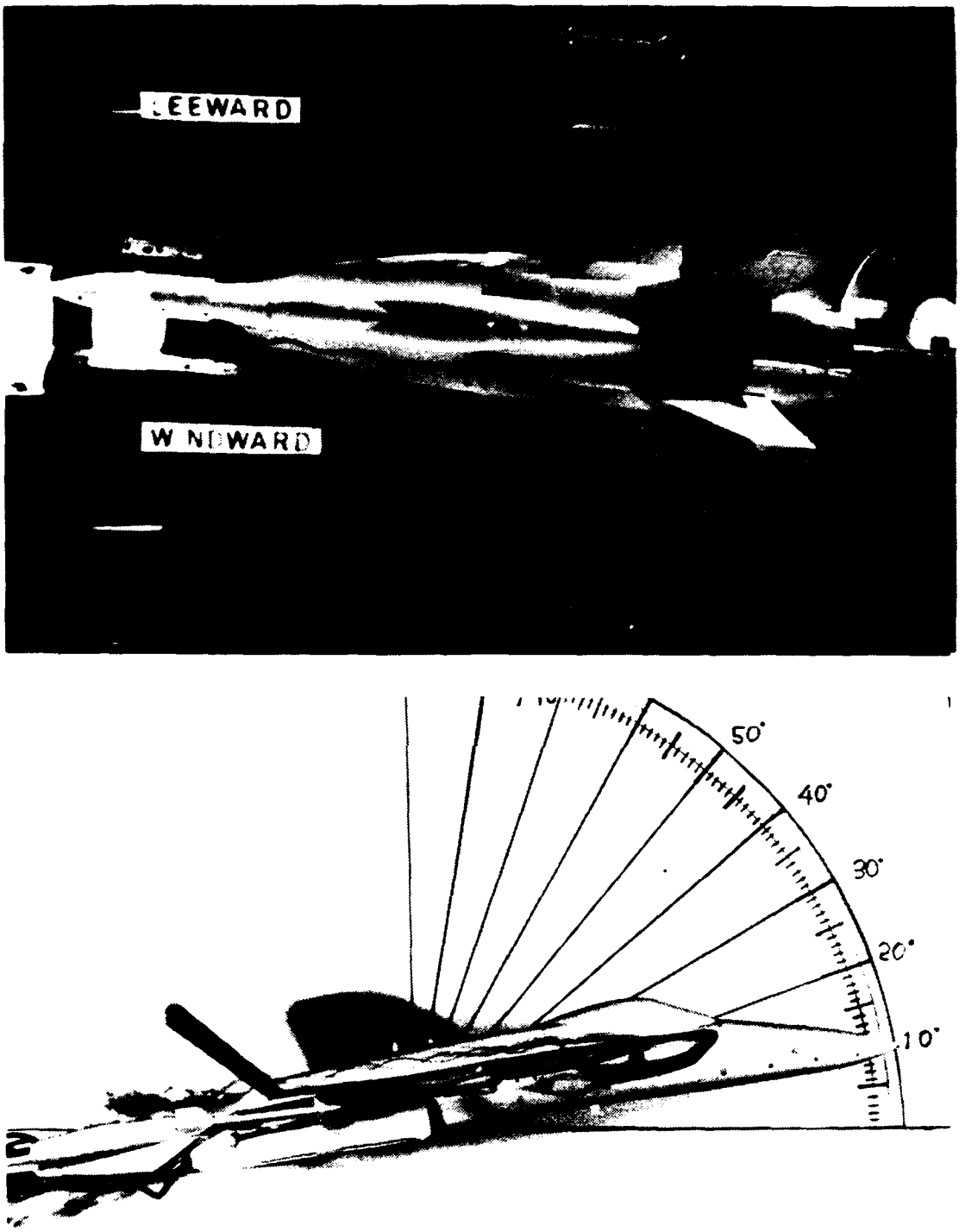

Figure 41. LEX Vortex, Static, α=10°, β=5°

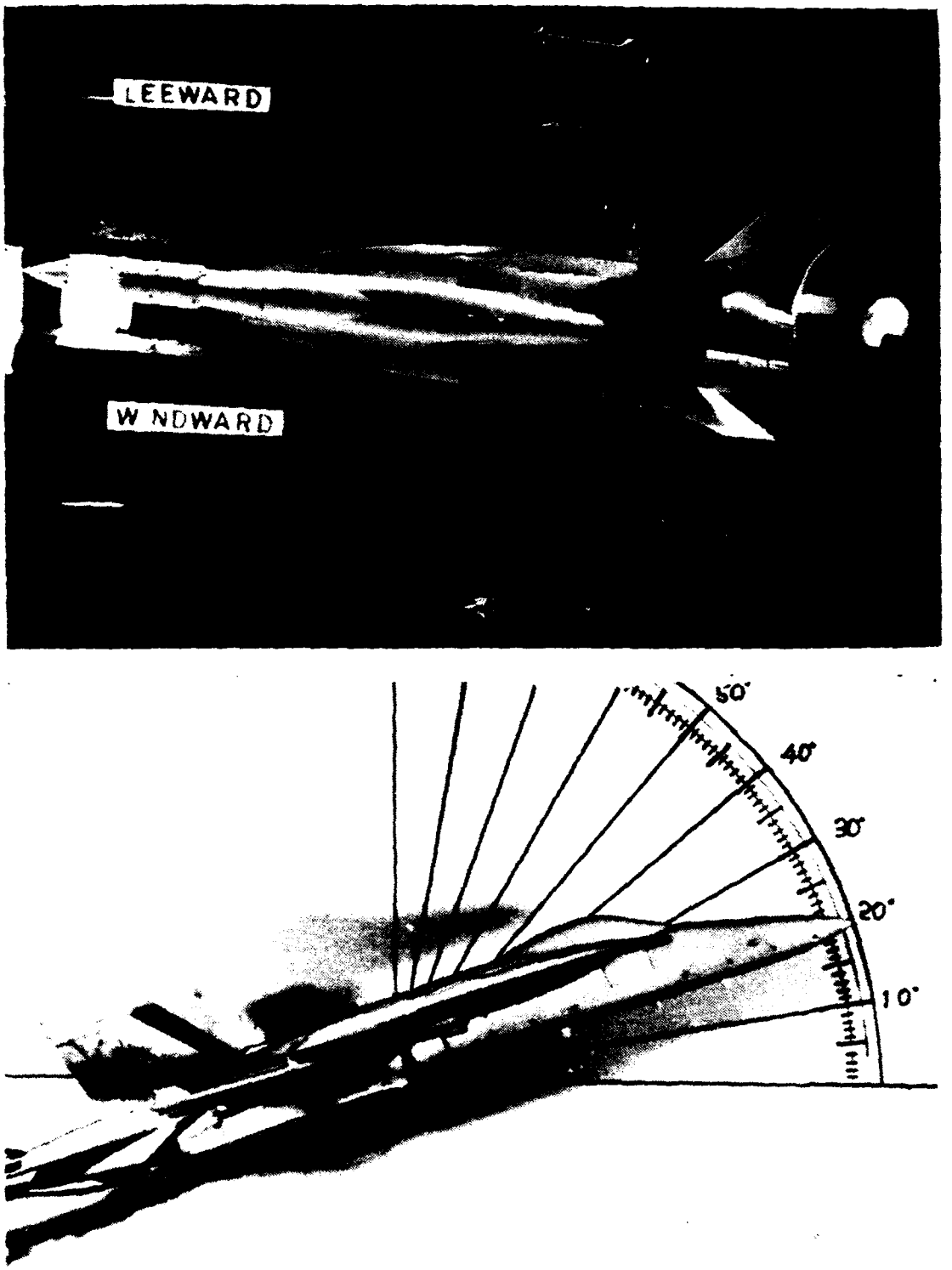

Figure 42. LEX Vortex, Static, α=20°, β=5°

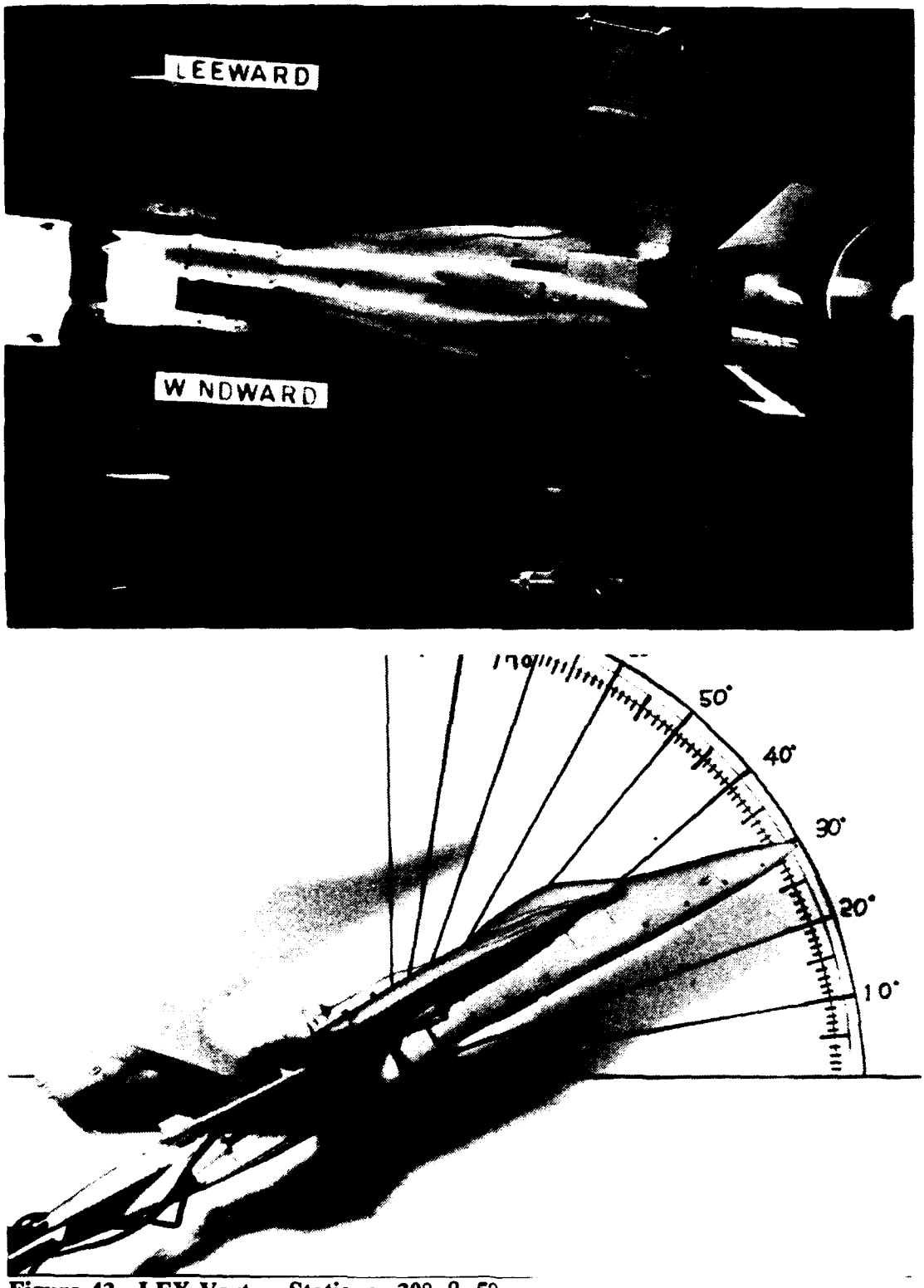

Figure 43. LEX Vortex, Static, α=30°, β=5°

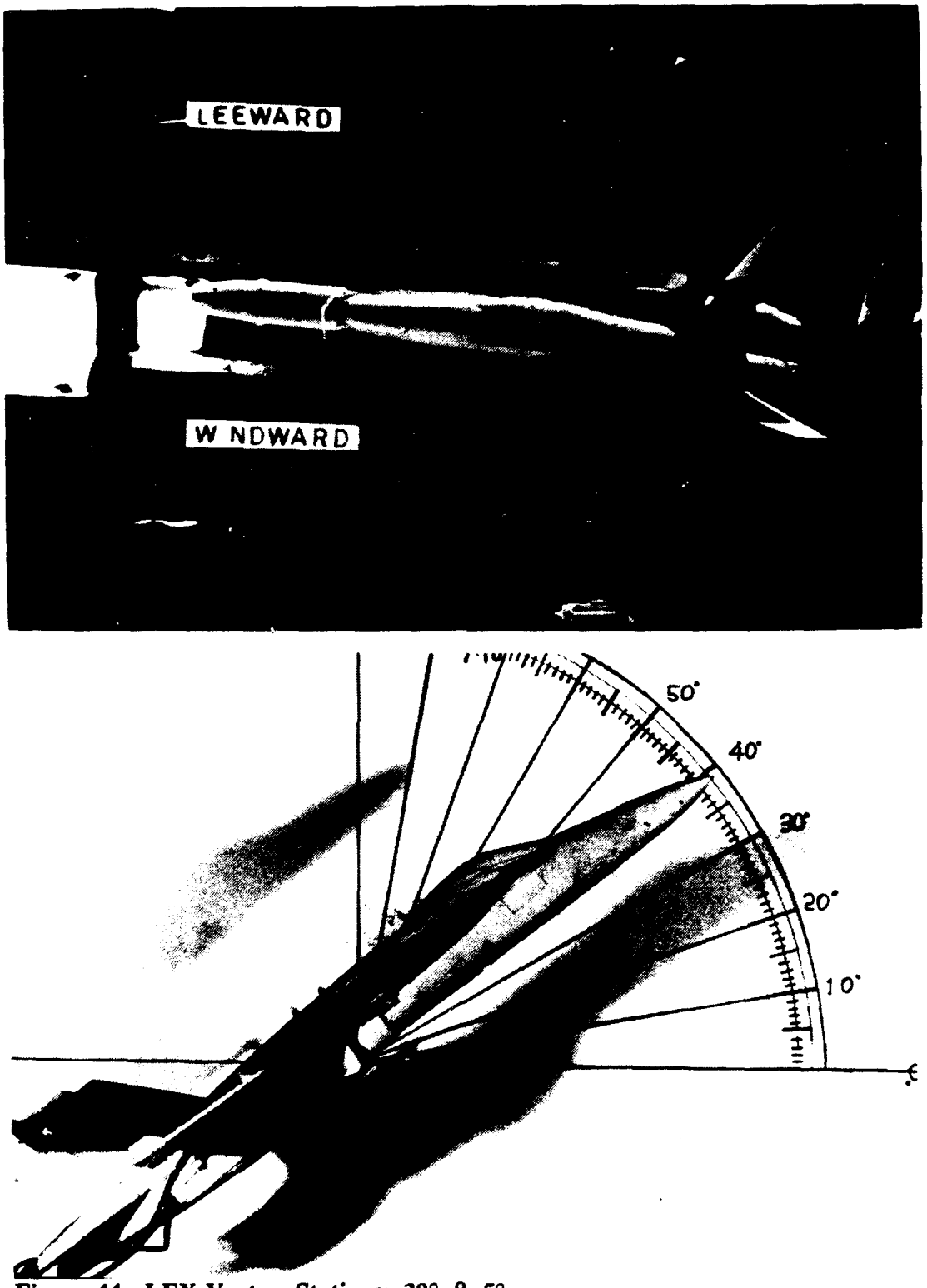

Figure 44. LEX Vortex, Static, α=39°, β=5°

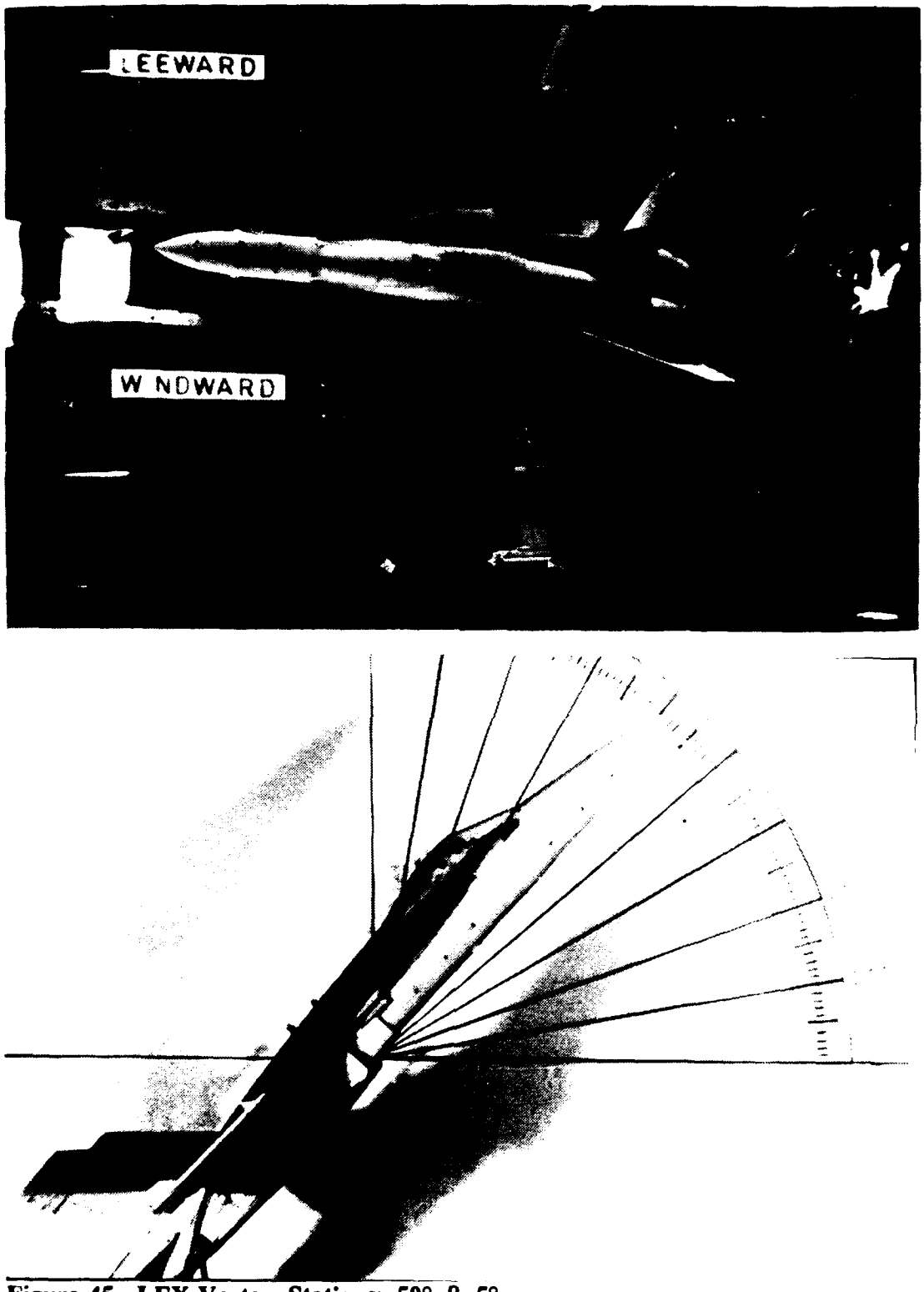

Figure 45. LEX Vortex, Static, α=50°, β=5°

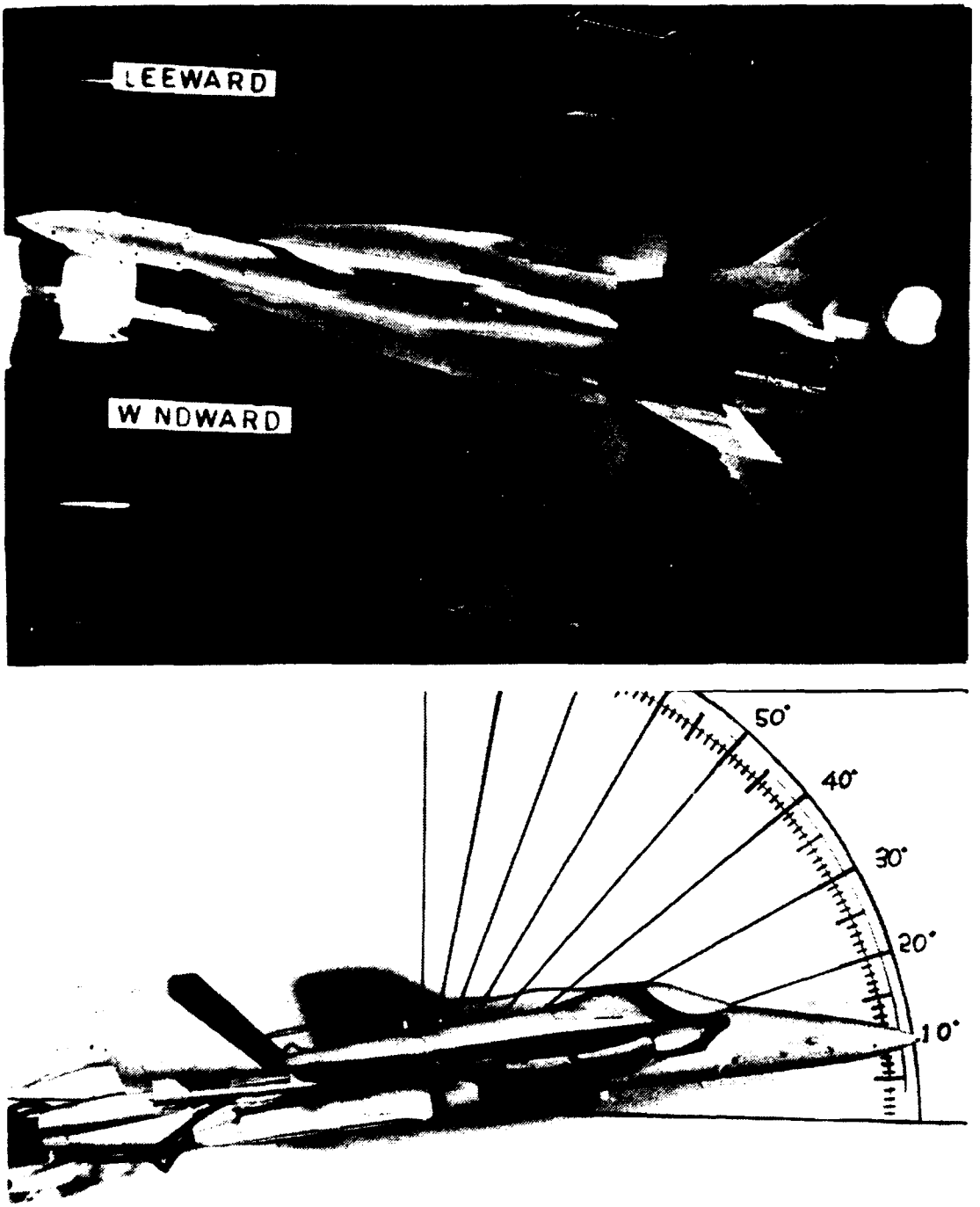

Figure 46. LEX Vortex, Static, α=10°, β=10°

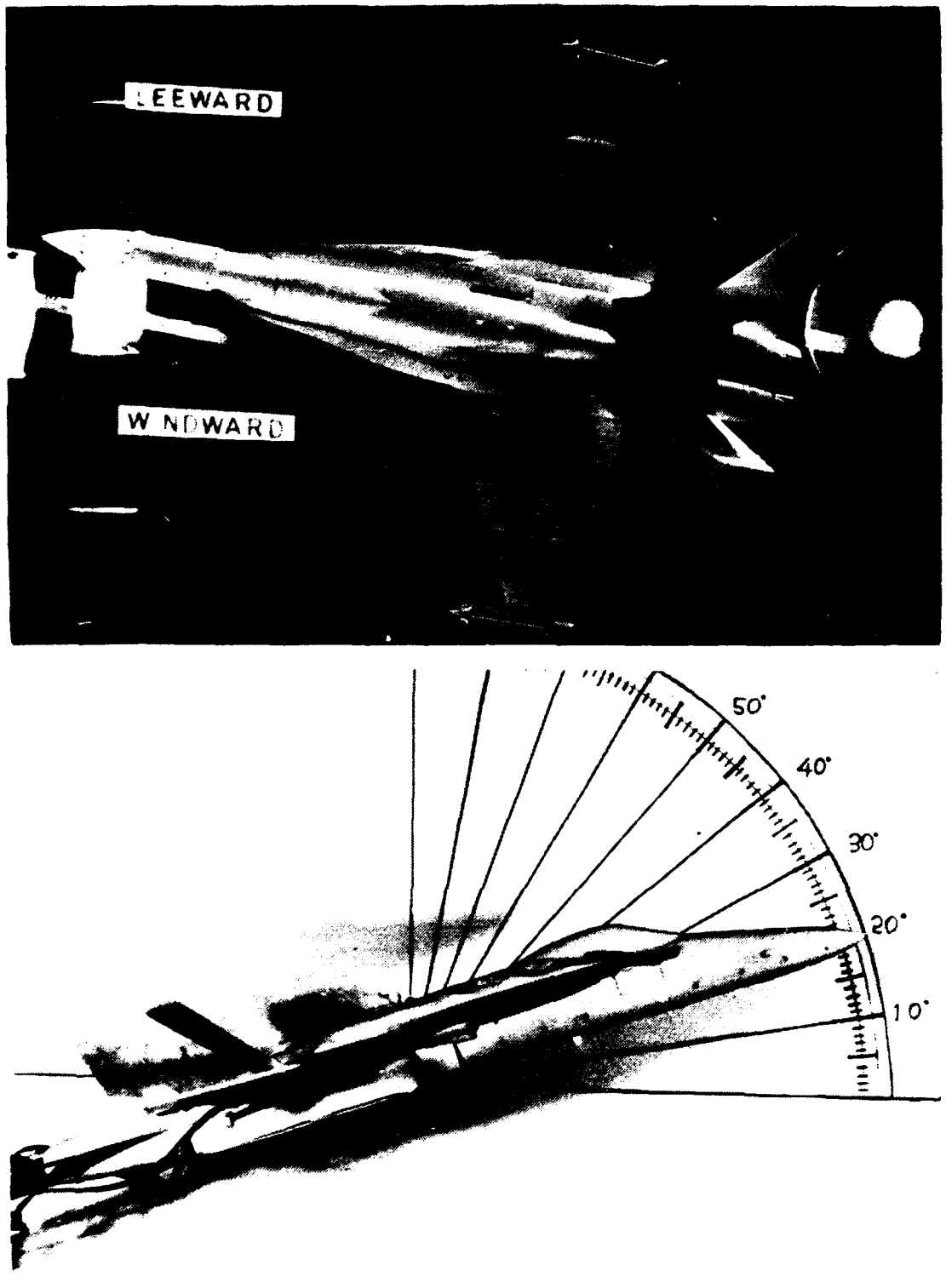

Figure 47. LEX Vortex, Static, α=20°, β=10°

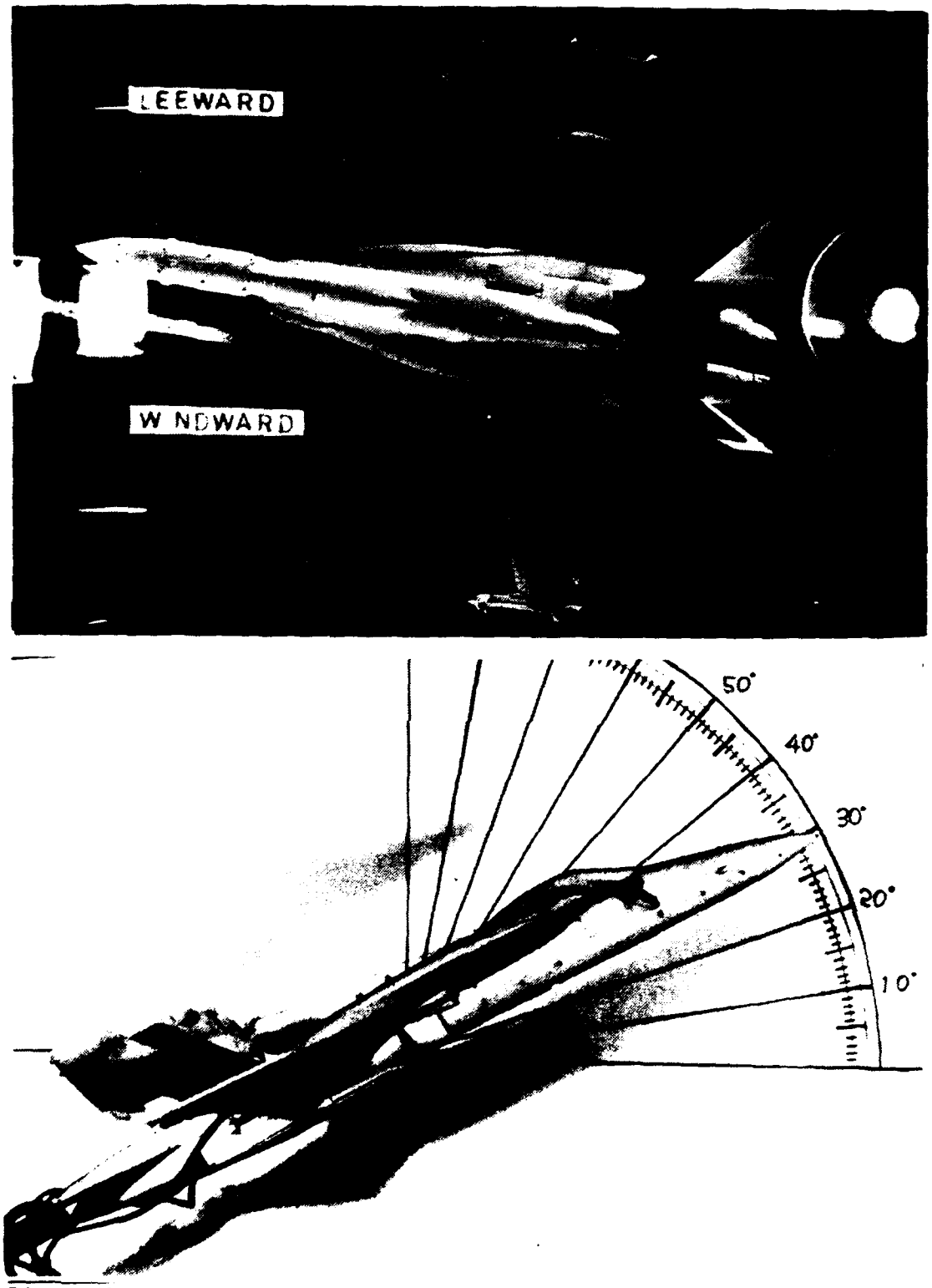

Figure 48. LEX Vortex, Static, α=30°, β=10°

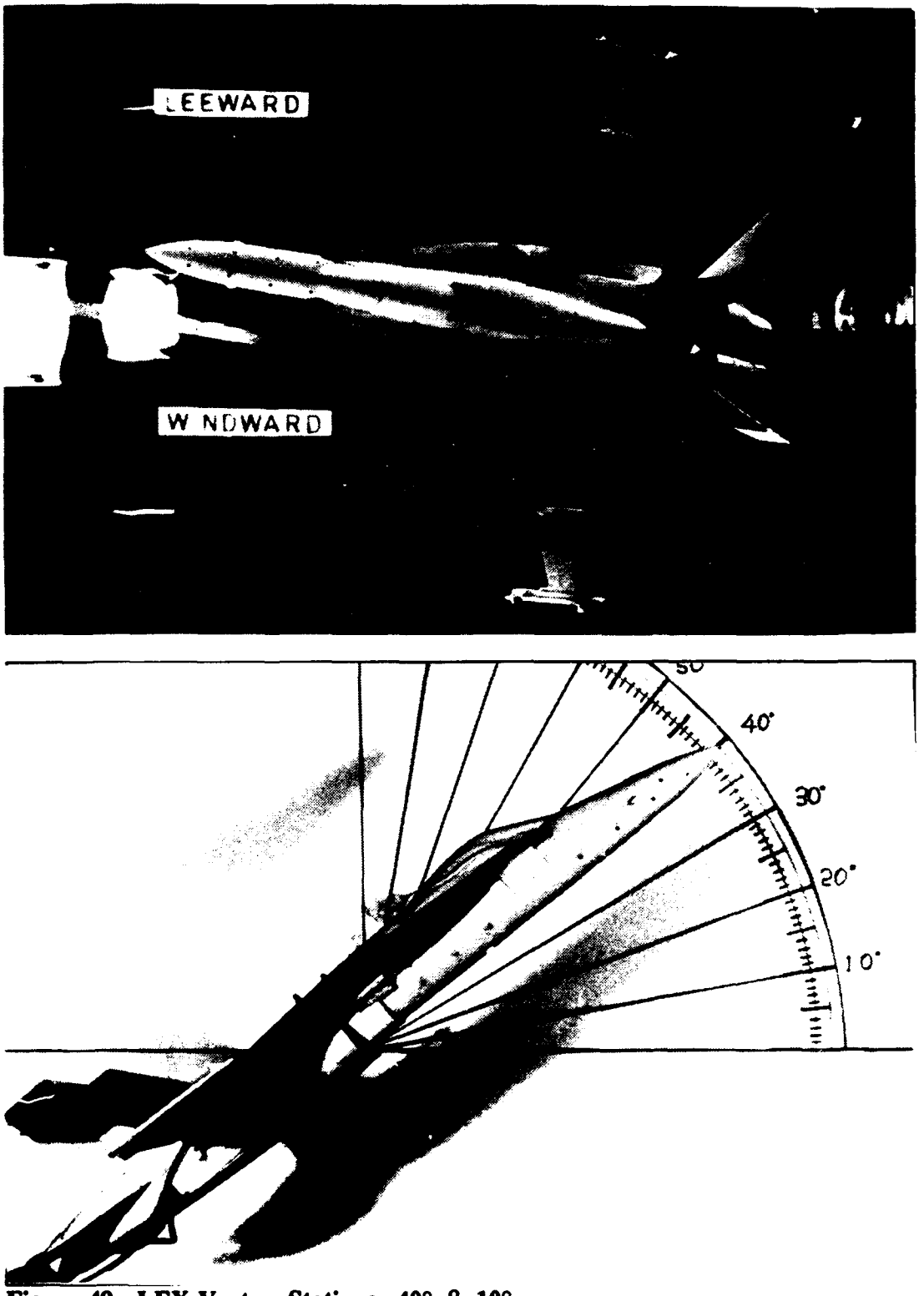

Figure 49. LEX Vortex, Static, α=40°, β=10°

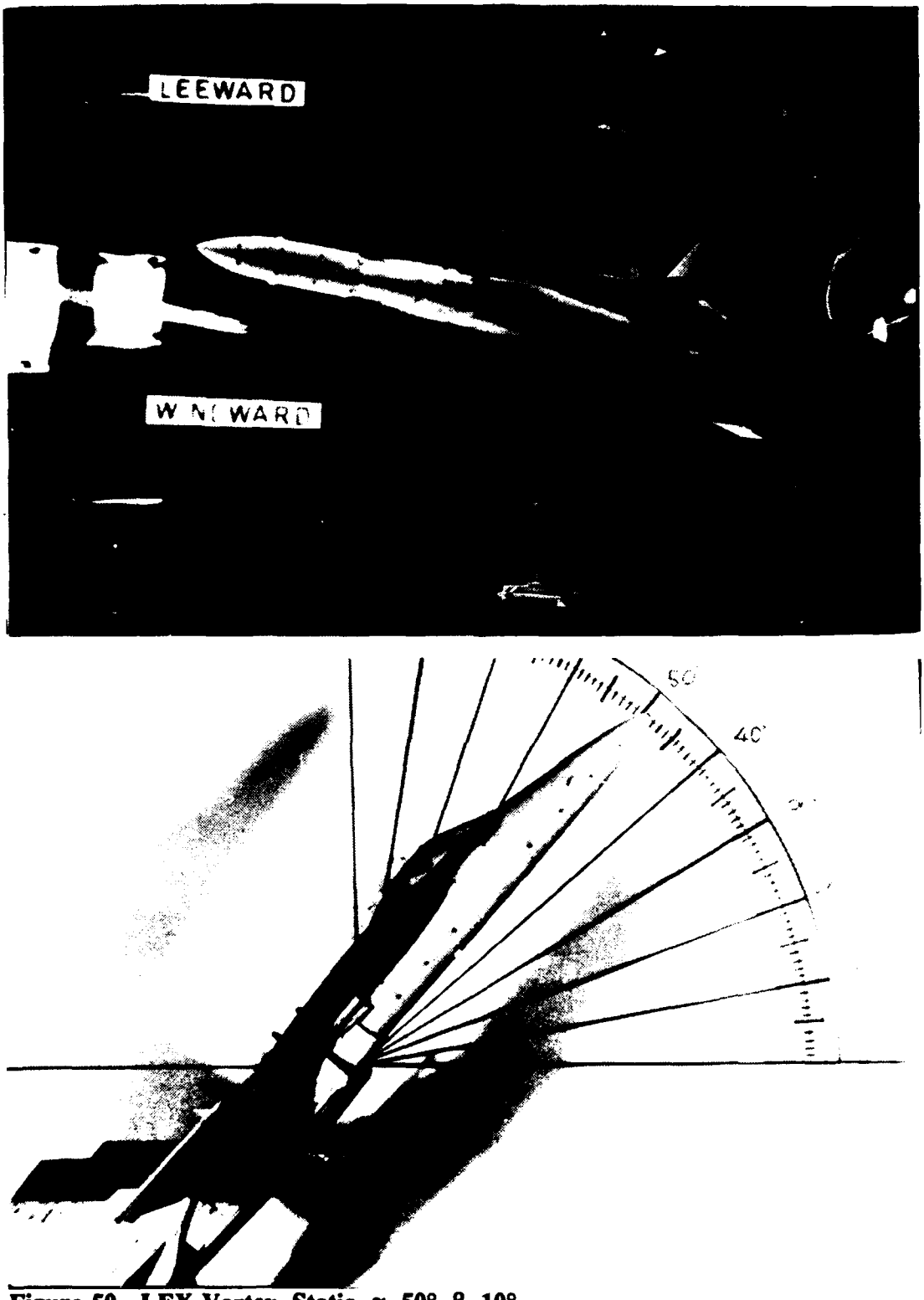

Figure 50. LEX Vortex, Static, α=50°, β=10°

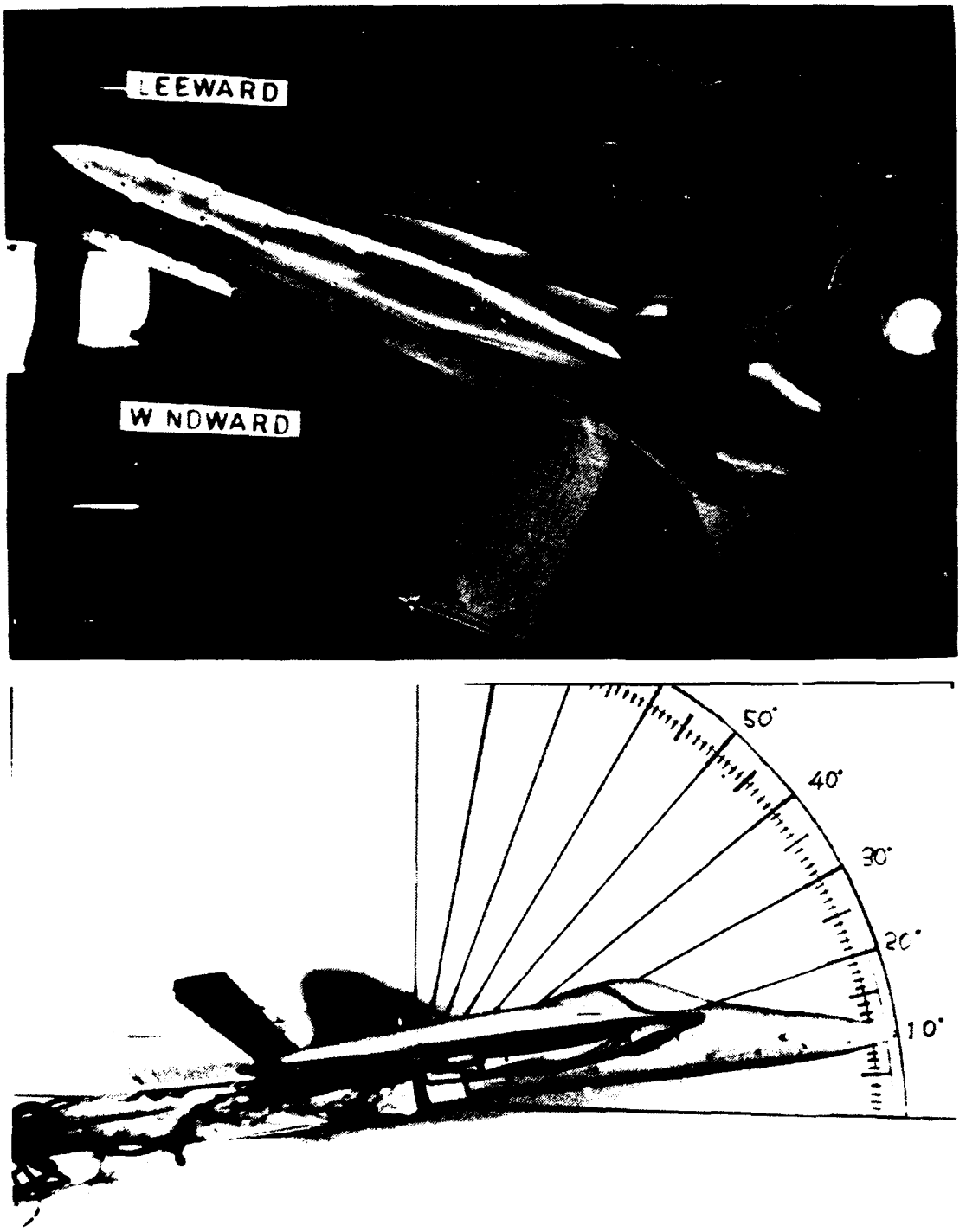

Figure 51. LEX Vortex, Static, α=10°, β=20°

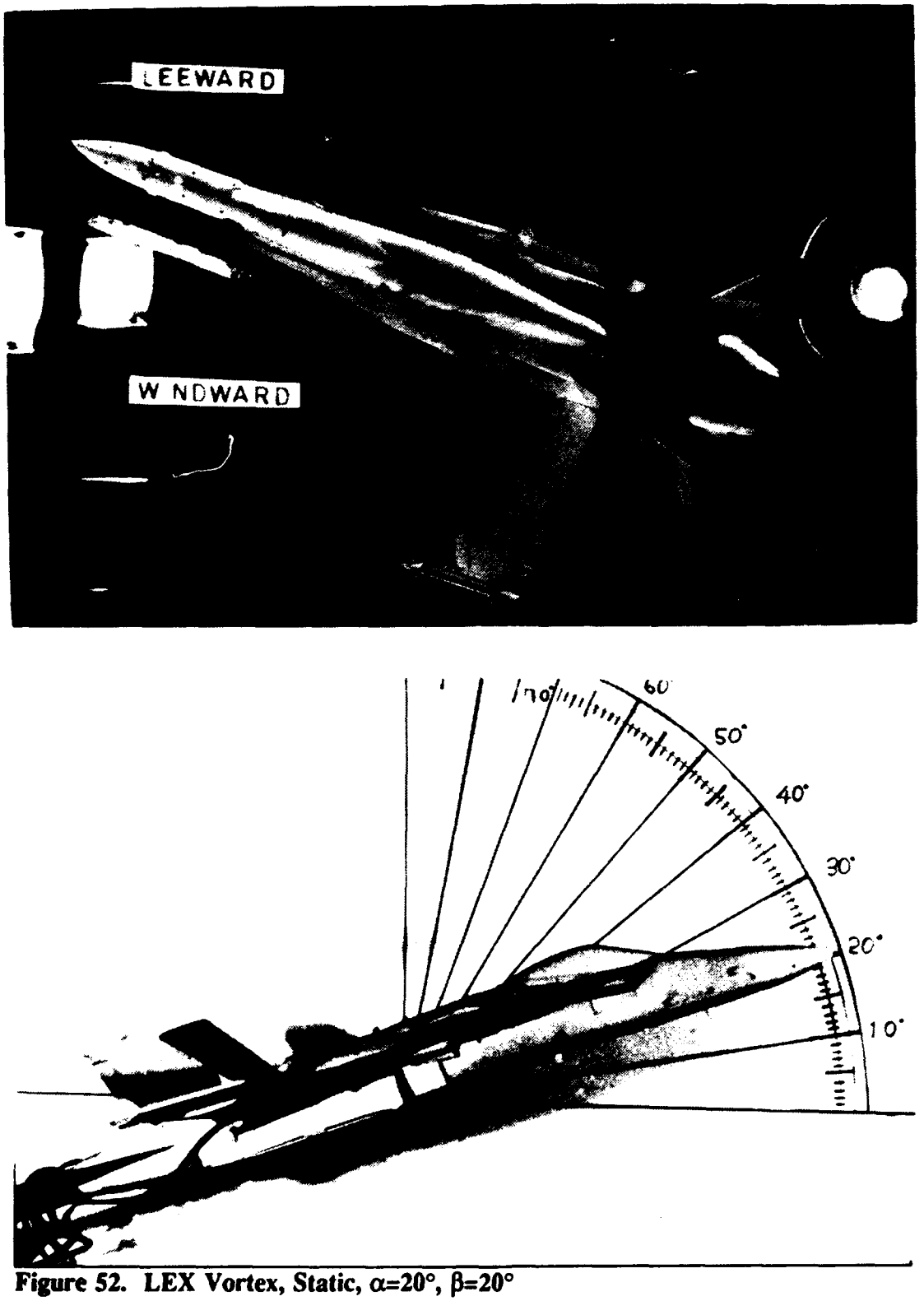

Figure 52. LEX Vortex, Static, α=20°, β=20°

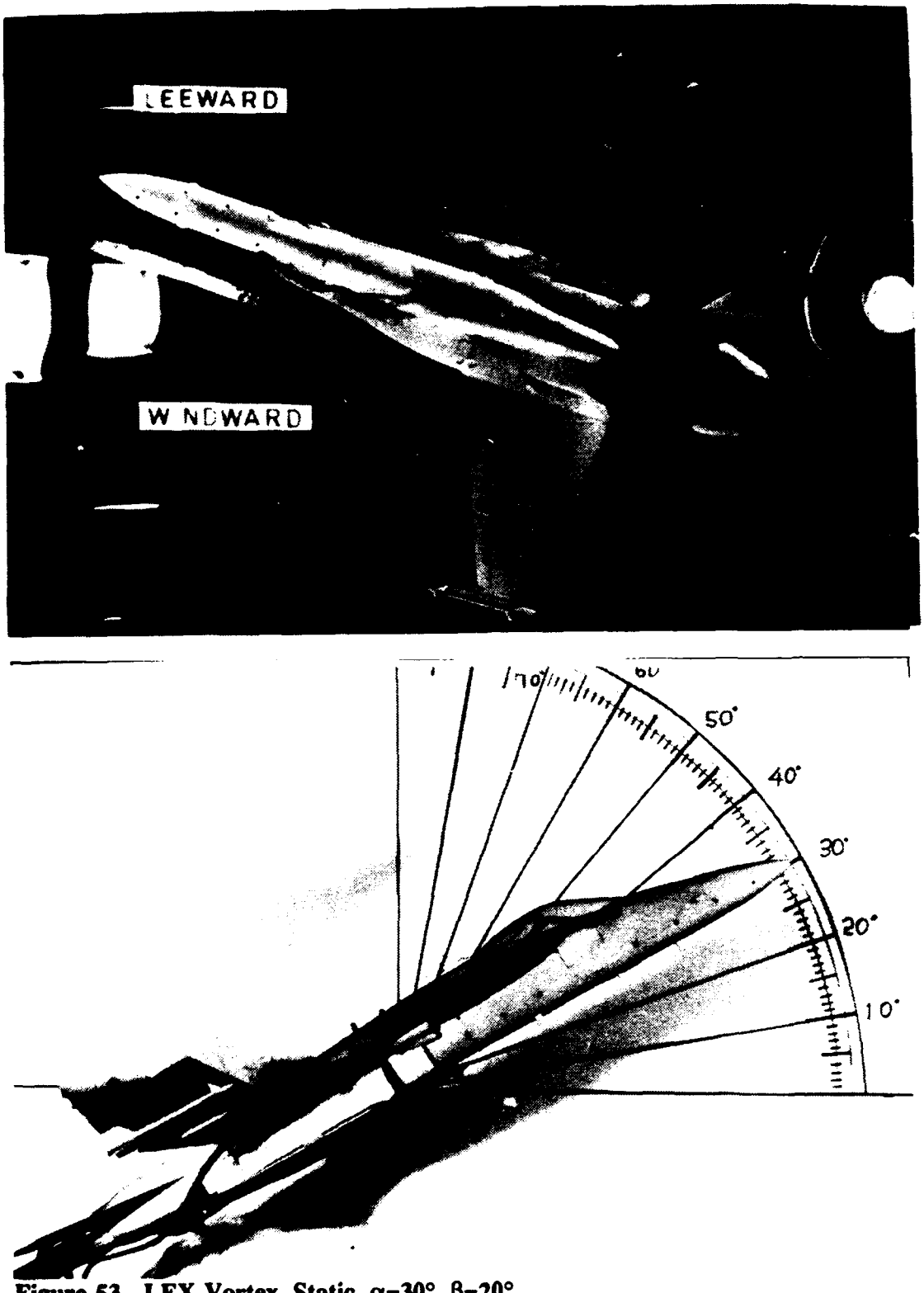

Figure 53. LEX Vortex, Static, α=30°, β=20°

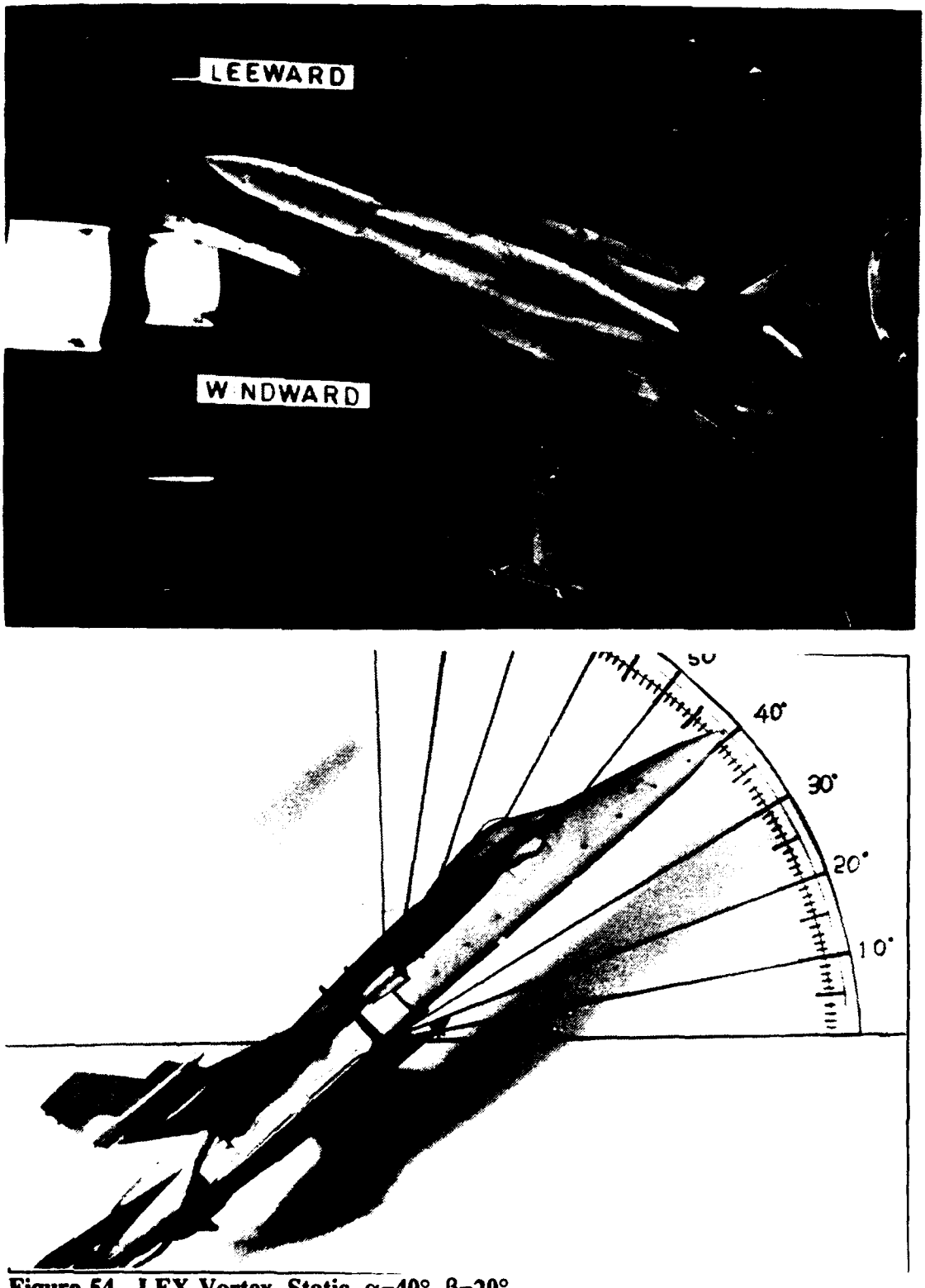

Figure 54. LEX Vortex, Static, α=40°, β=20°

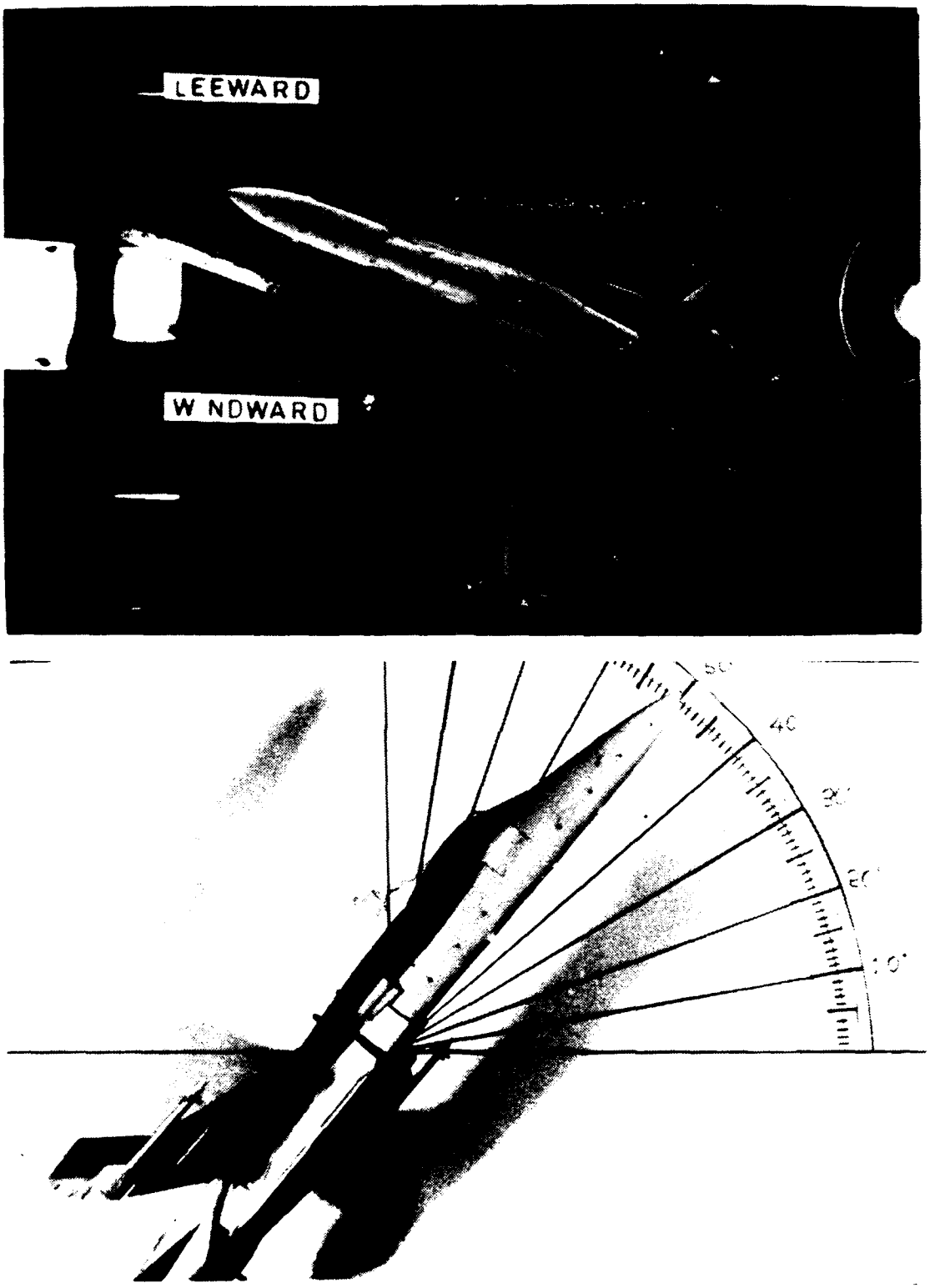

Figure 55. LEX Vortex, Static, α=50°, β=20°

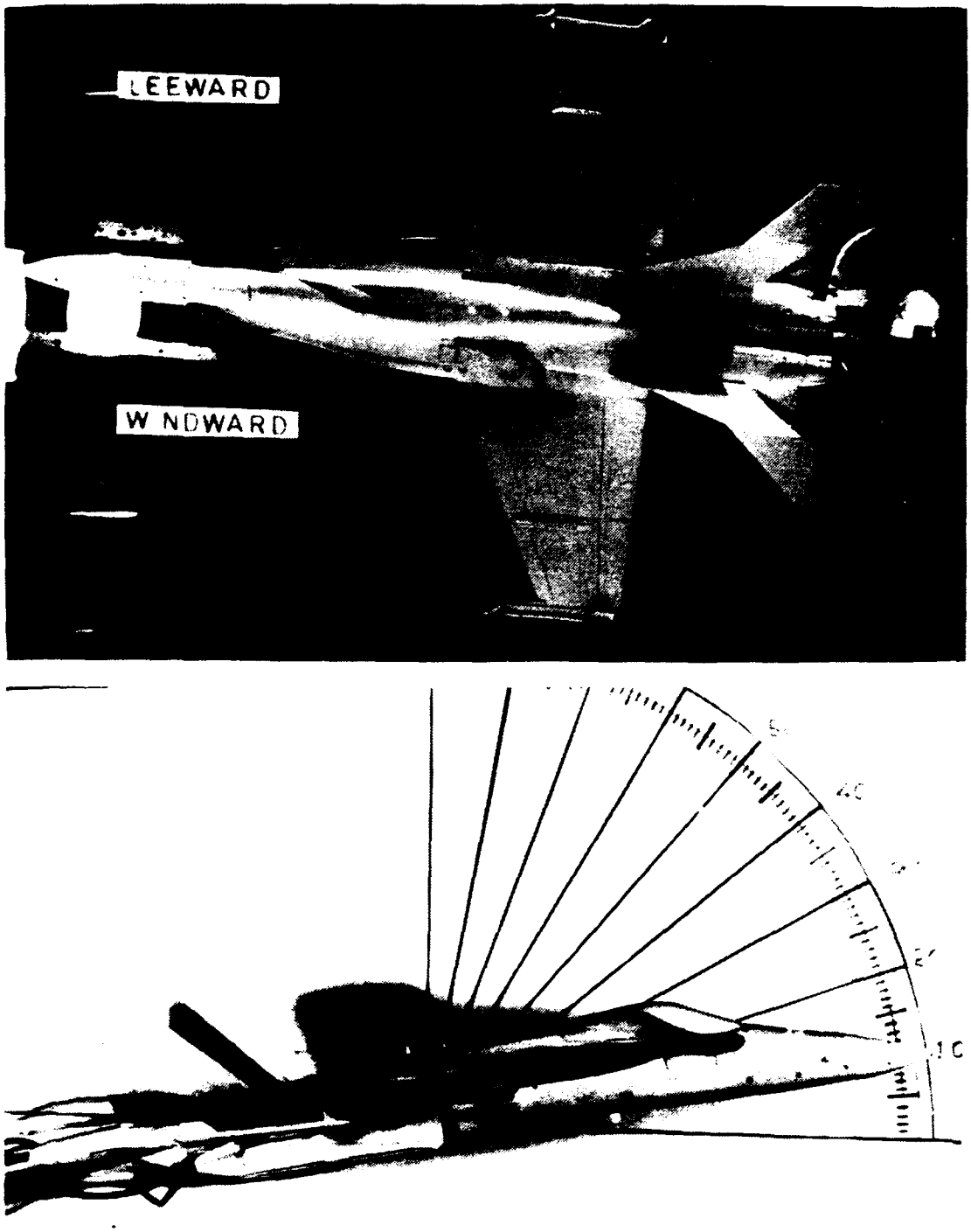

Figure 56. LEX Vortex, Low Pitch Rate Up, α=10°, β=5°

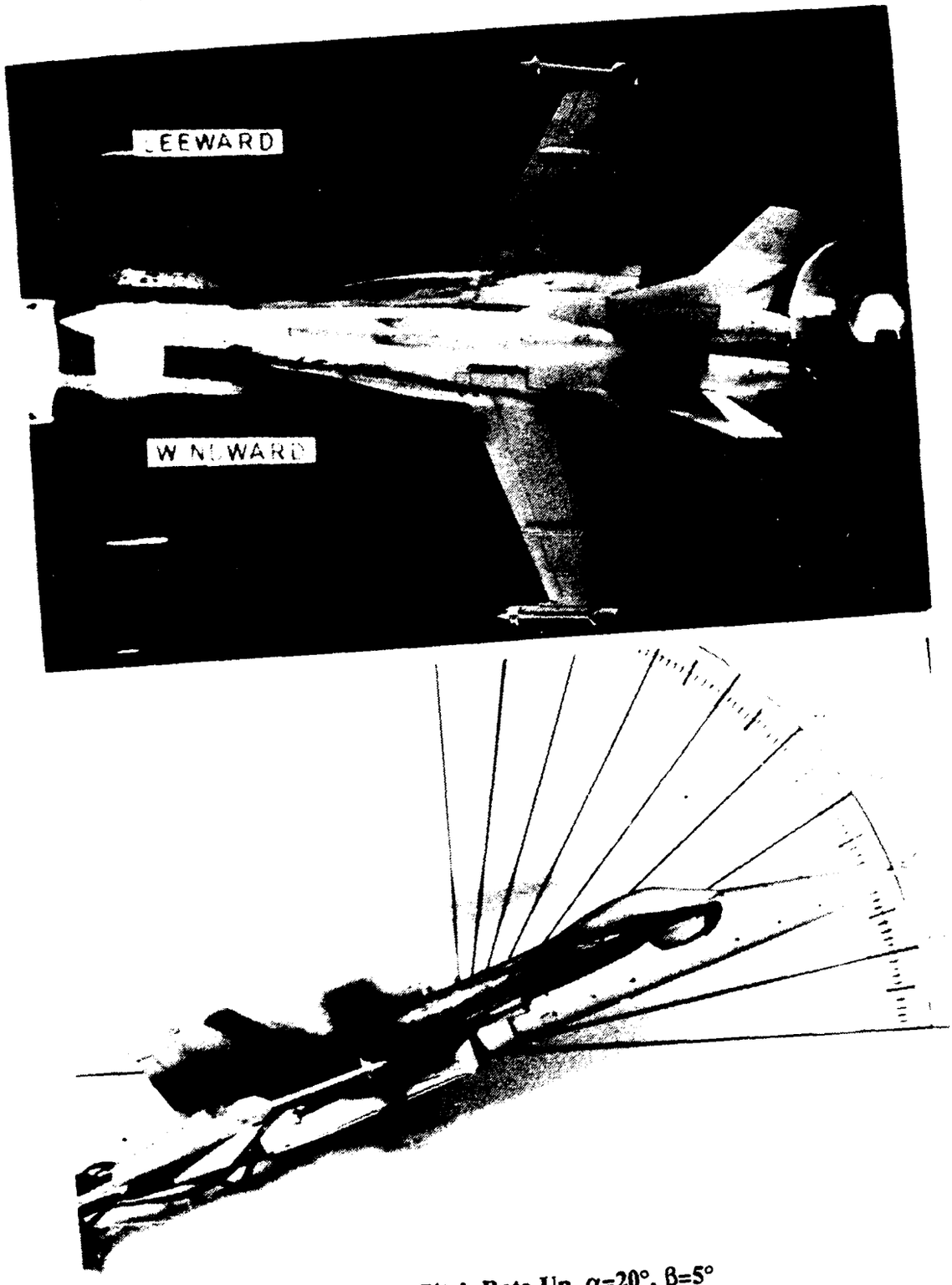

Figure 57. LEX Vortex, Low Pitch Rate Up, α=20°, β=5°

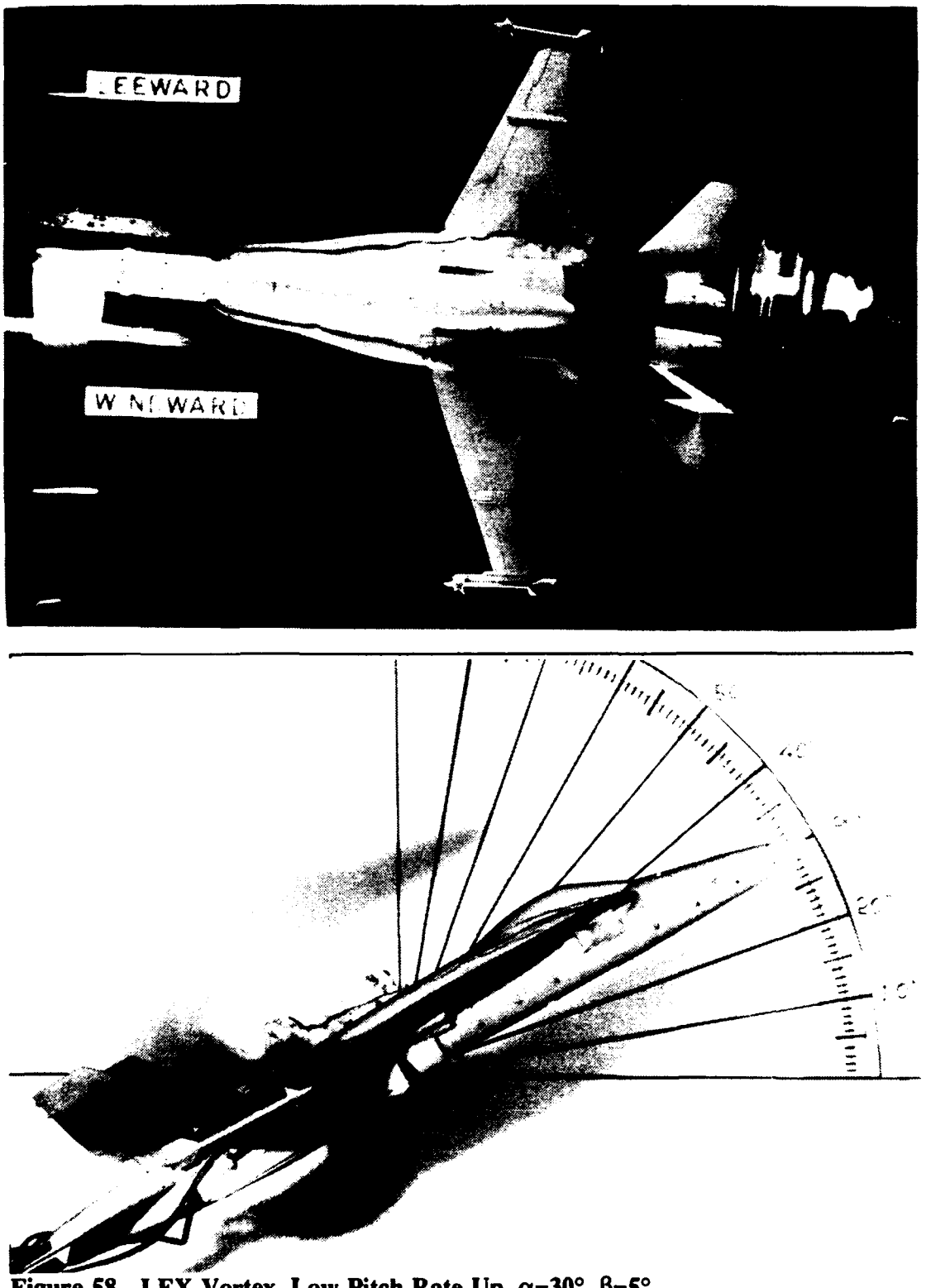

Figure 58. LEX Vortex, Low Pitch Rate Up, α=30°, β=5°

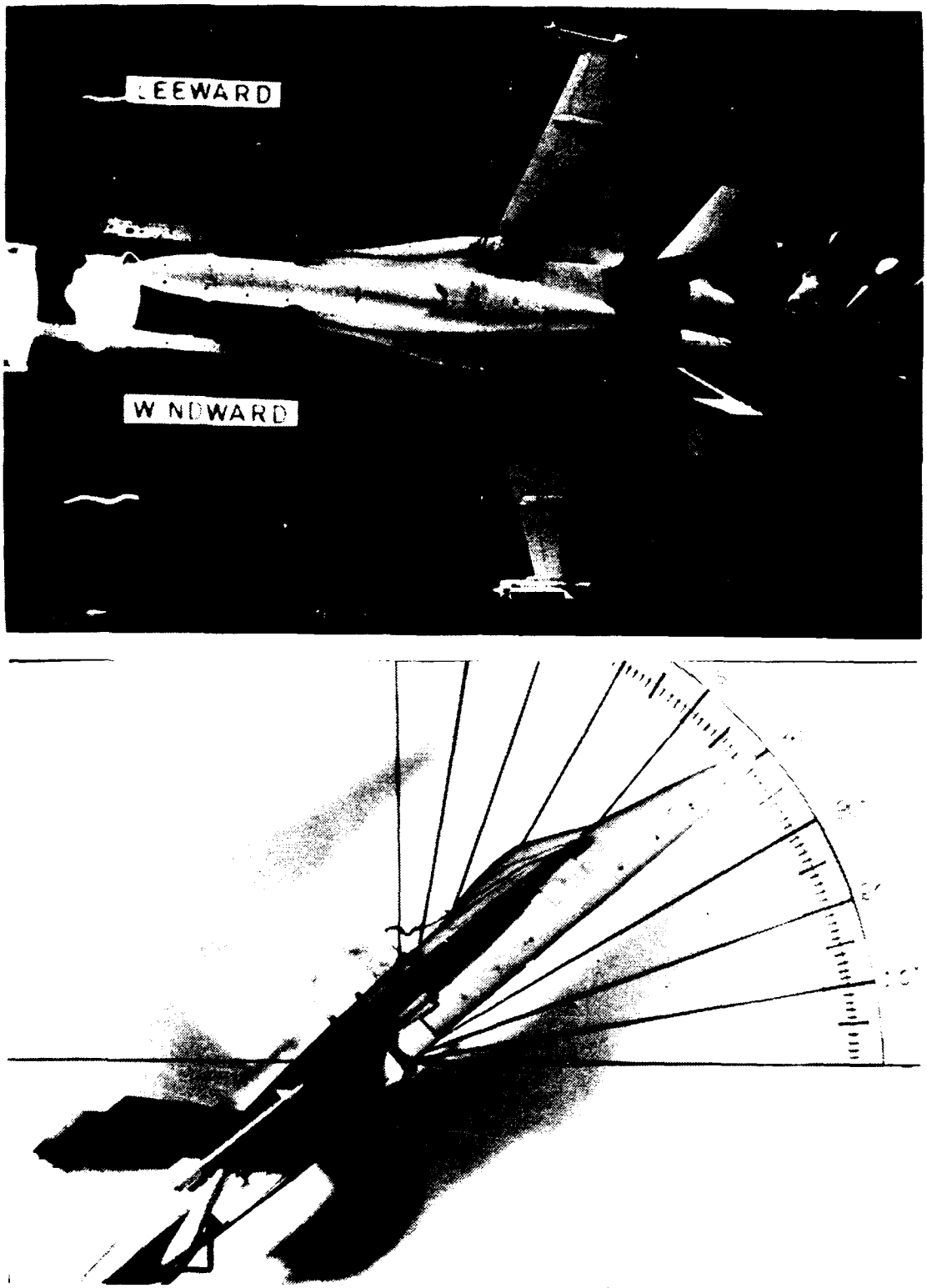

Figure 59. LEX Vortex, Low Pitch Rate Up, α=40°, β=5°

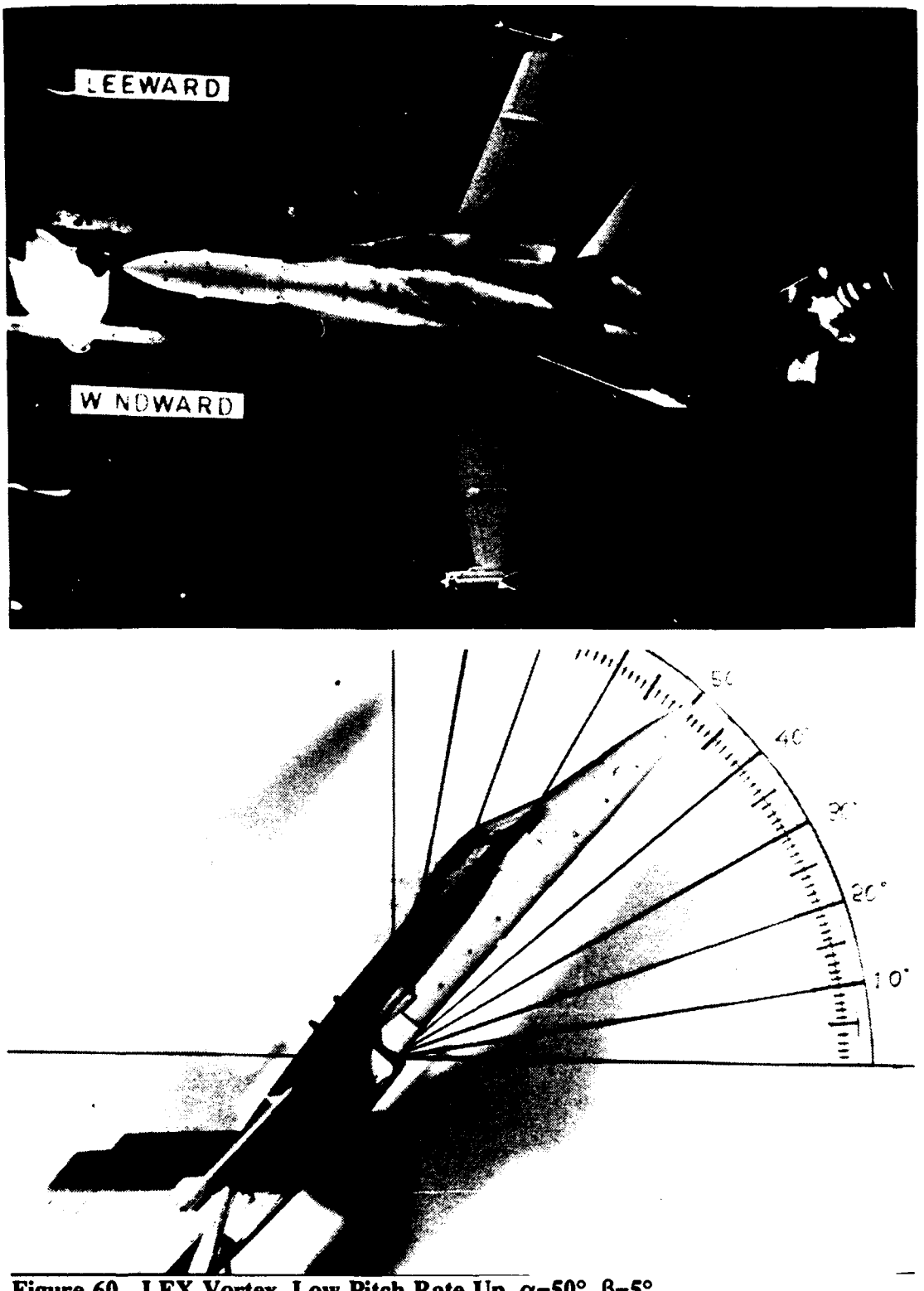

Figure 60. LEX Vortex, Low Pitch Rate Up, α=50°, β=5°

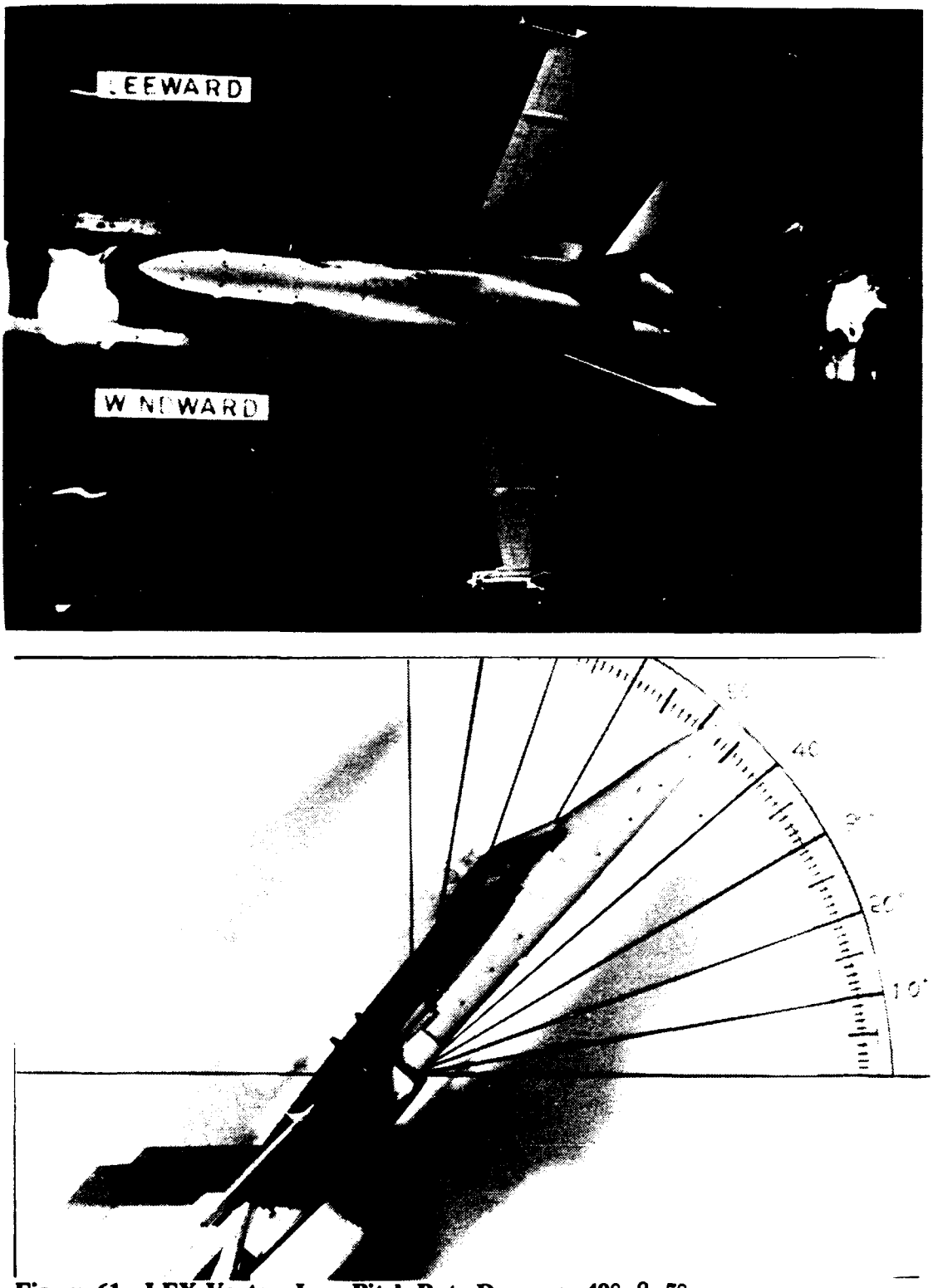

Figure 61. LEX Vortex, Low Pitch Rate Down, α=49°, β=5°

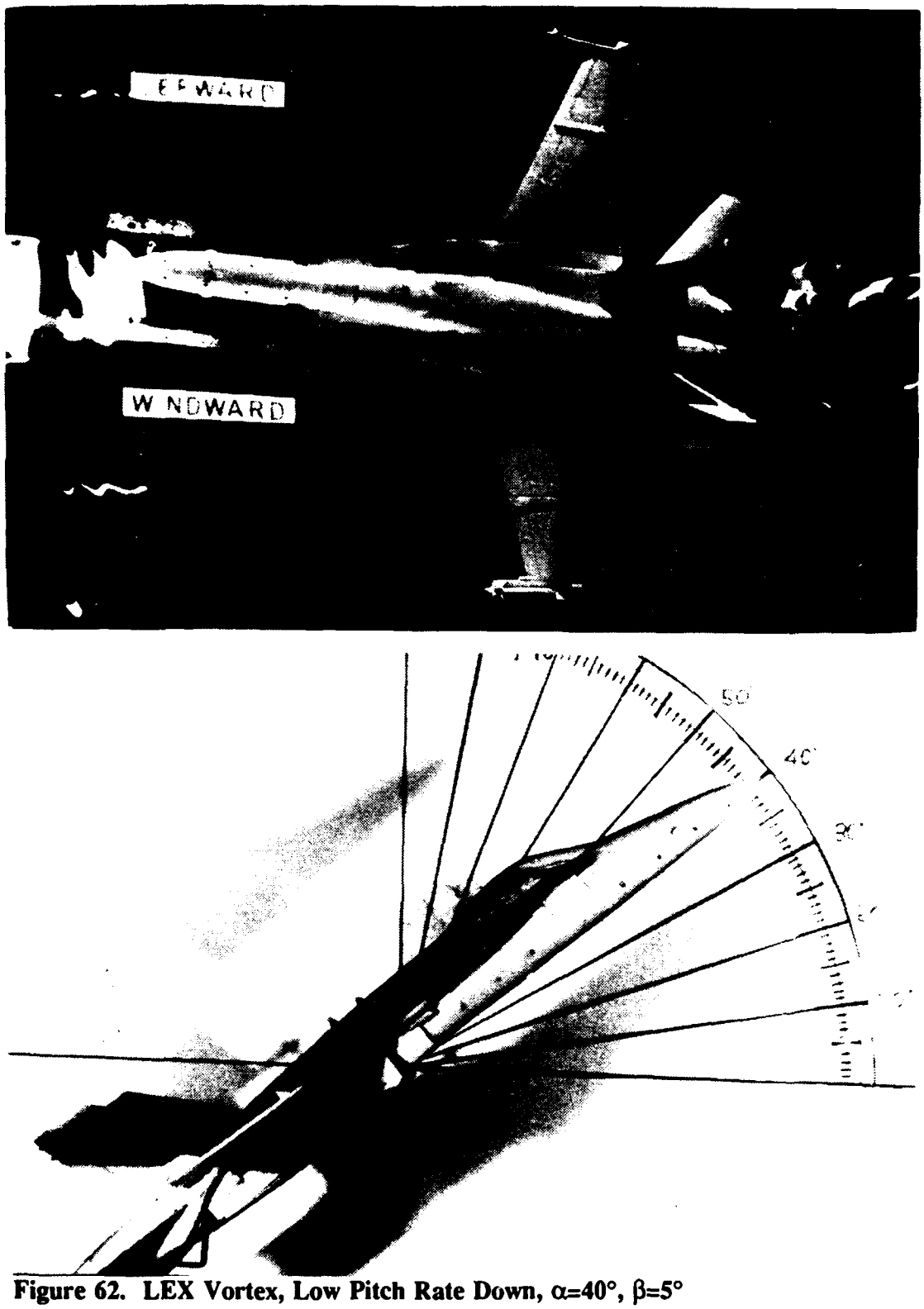

Figure 62. LEX Vortex, Low Pitch Rate Down, α=40°, β=5°

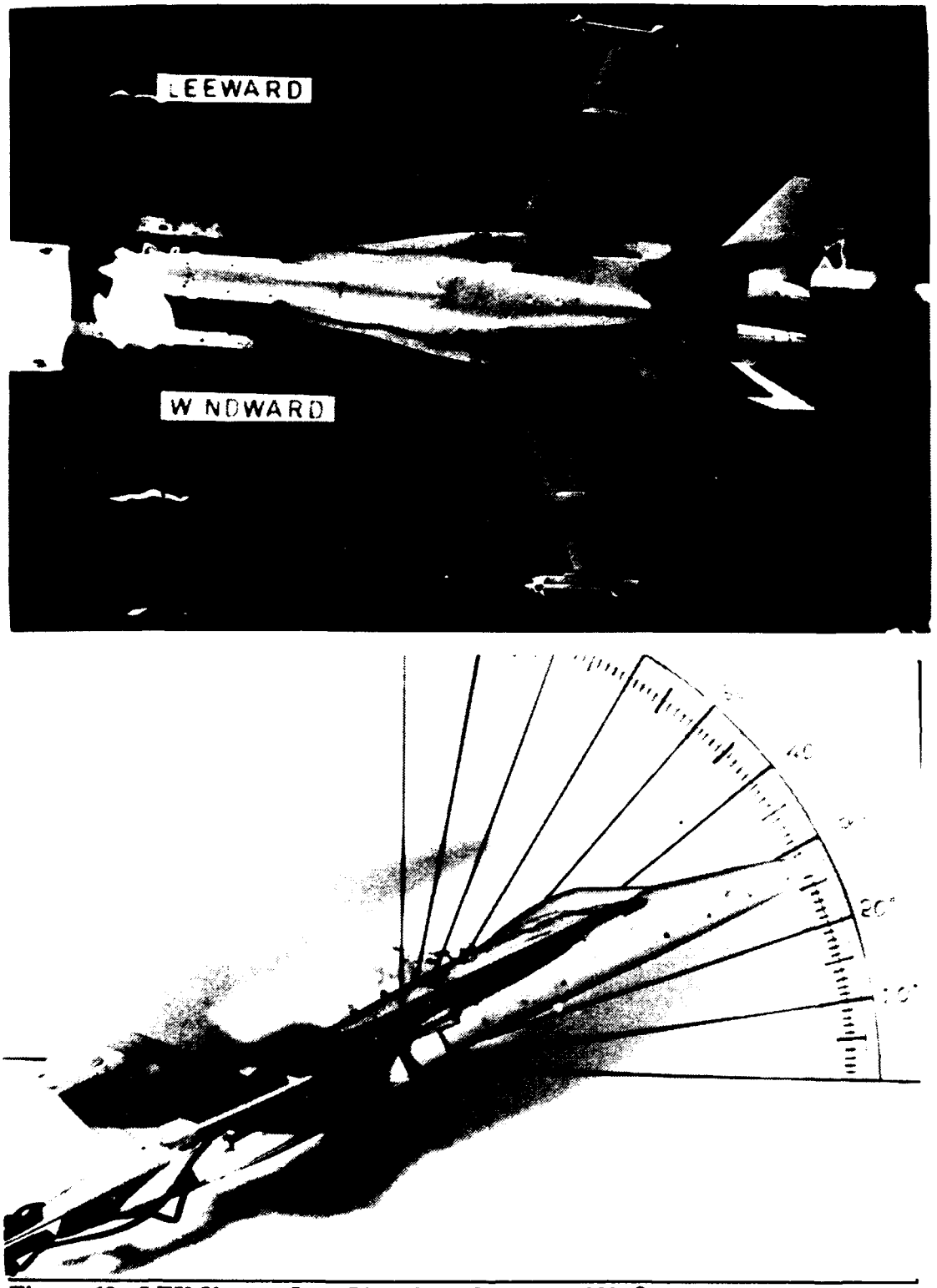

Figure 63. LEX Vortex, Low Pitch Rate Down, α=28°, β=5°

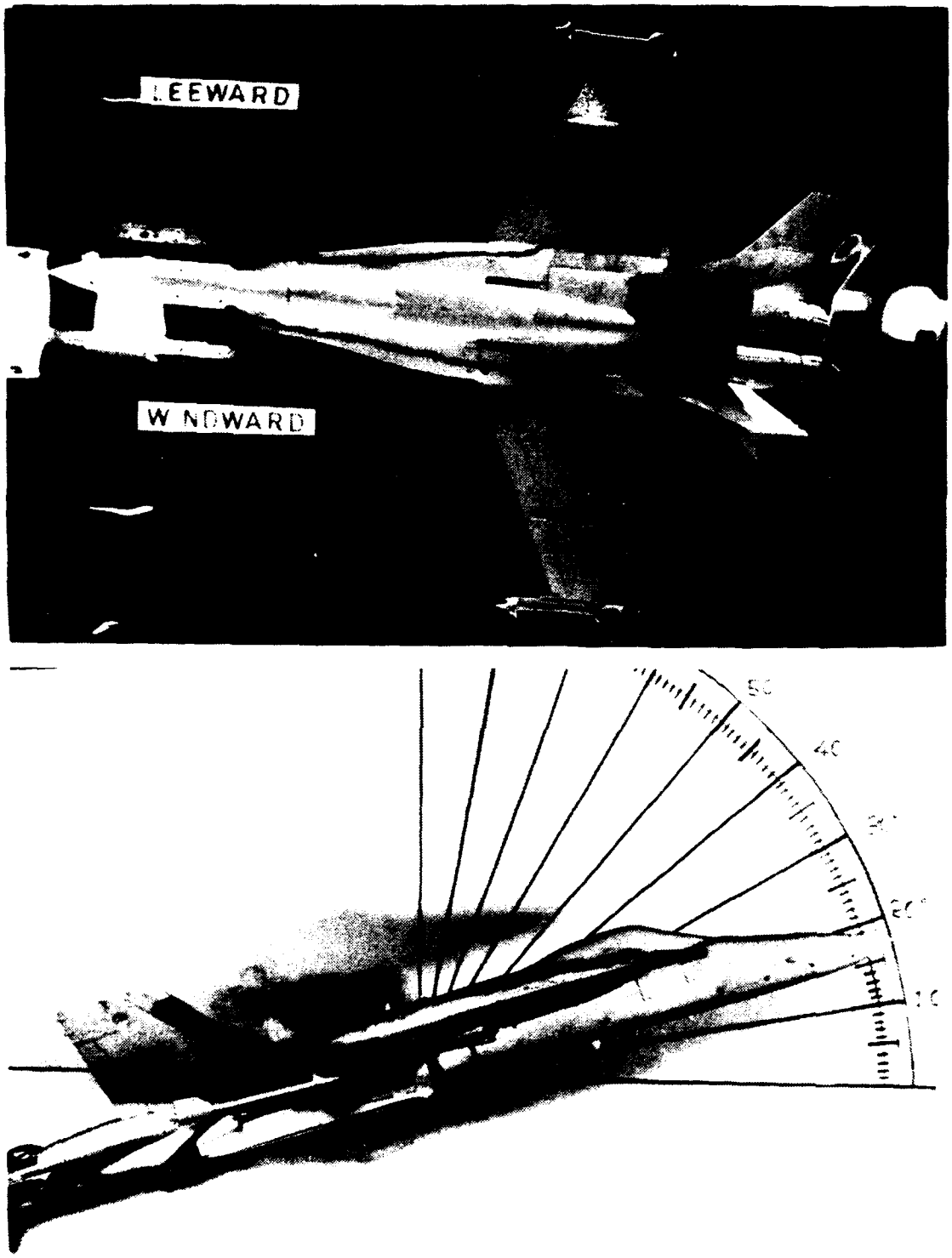

Figure 64. LEX Vortex, Low Pitch Rate Down, α=17°, β=5°

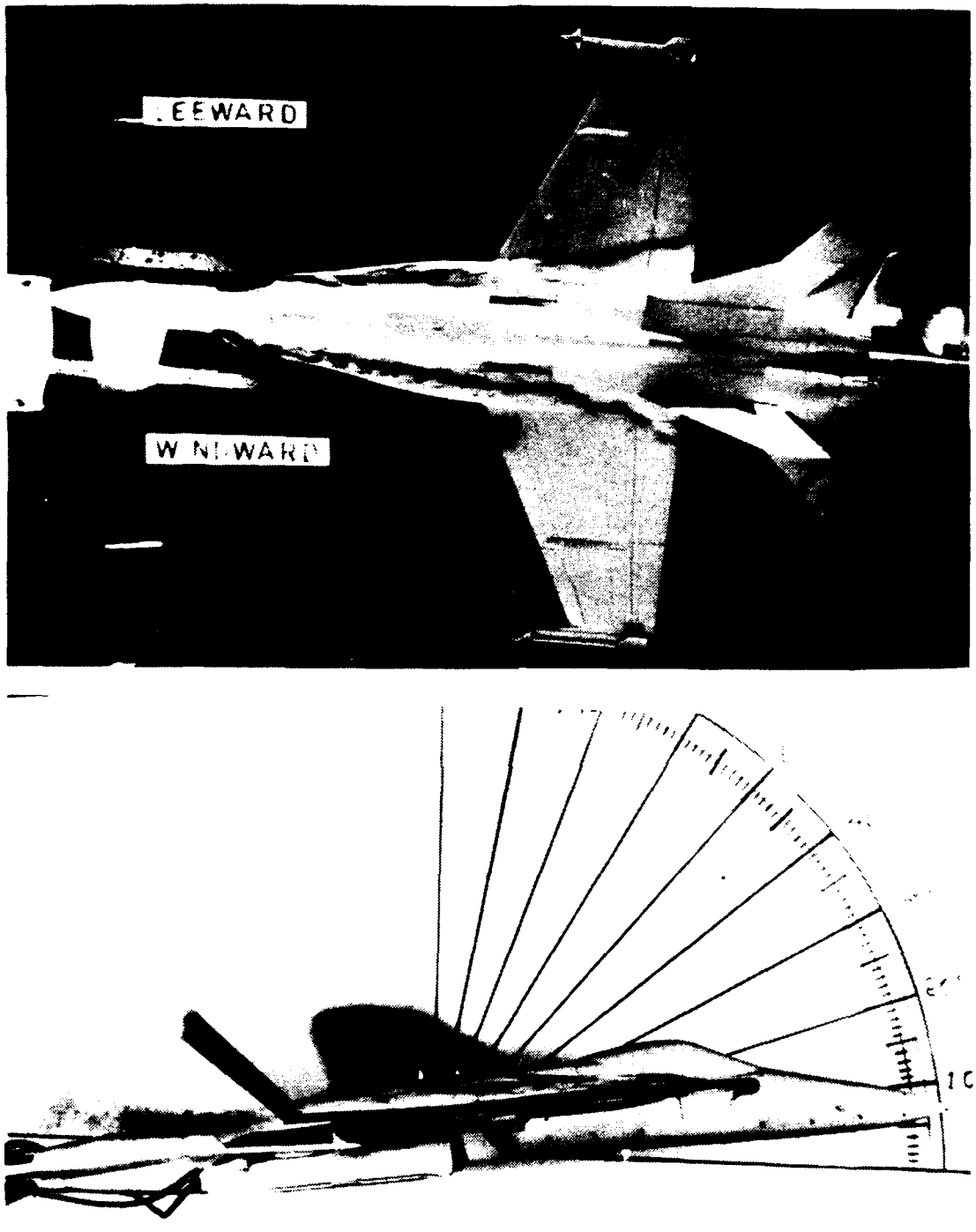

Figure 65. LEX Vortex, Low Pitch Rate Down, α=7°, β=5°

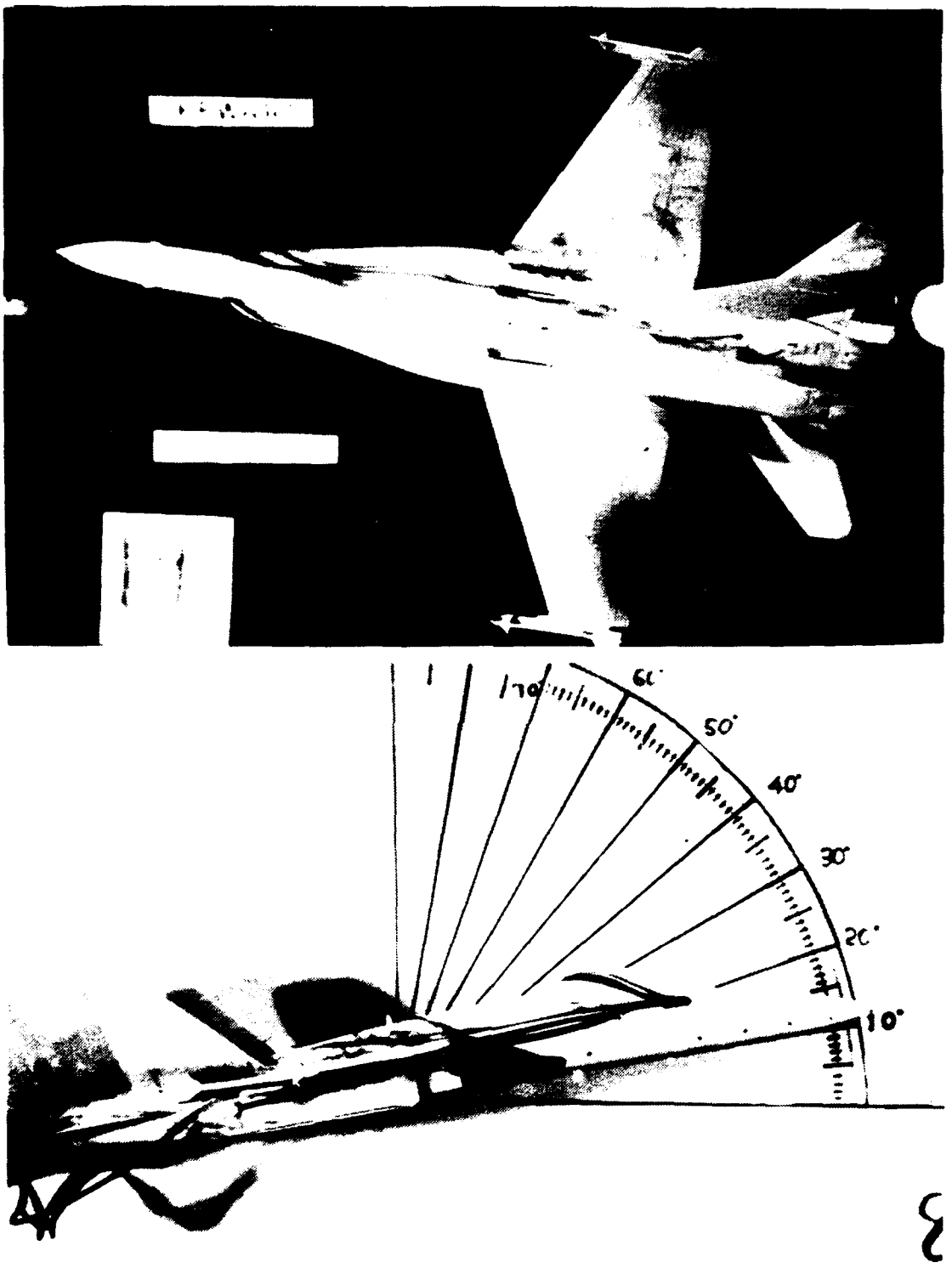

Figure 66. LEX Vortex, Low Pitch Rate Up, α=11°, β=10°

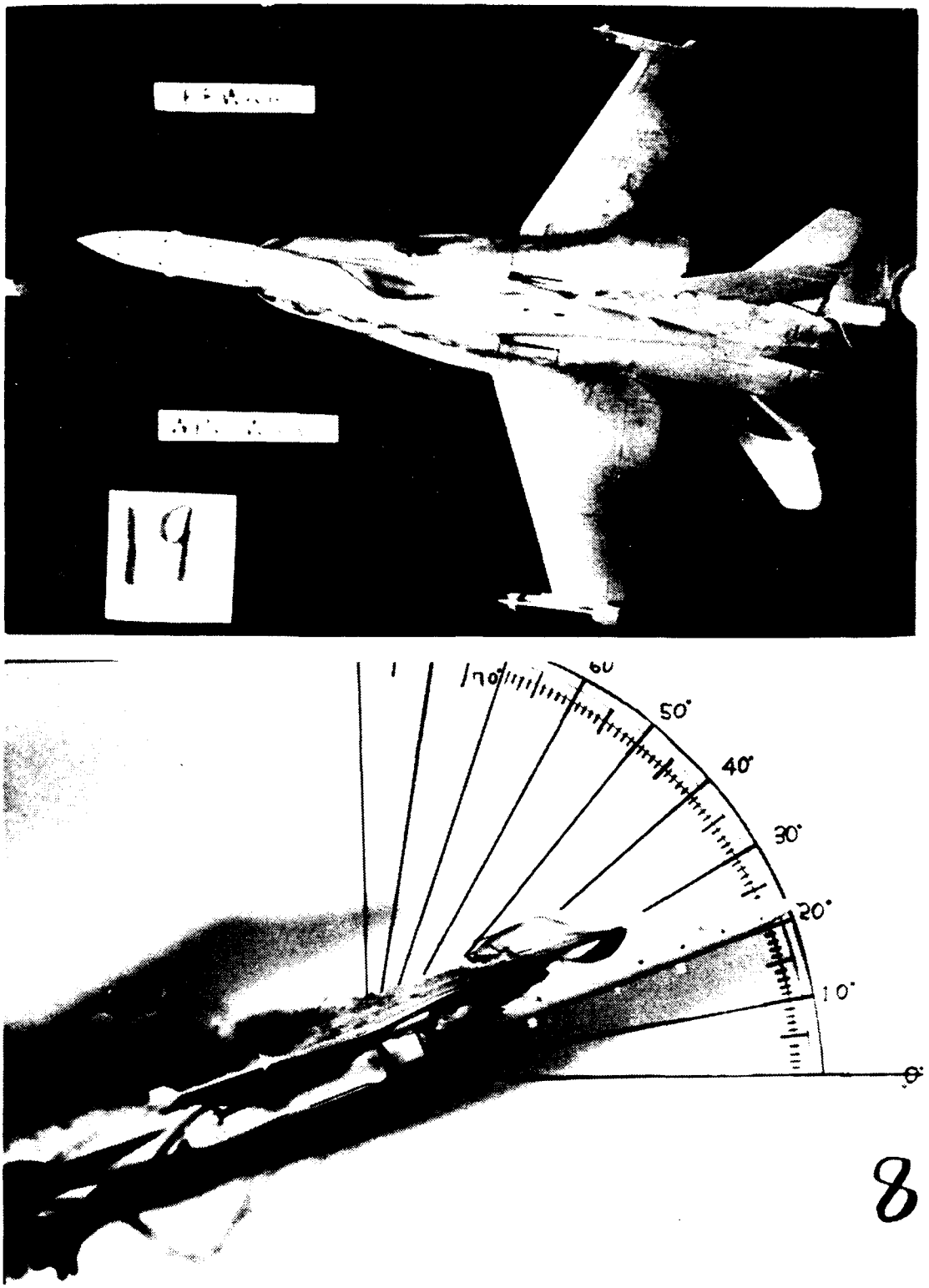

Figure 67. LEX Vortex, Low Pitch Rate Up, α=21°, β=10°

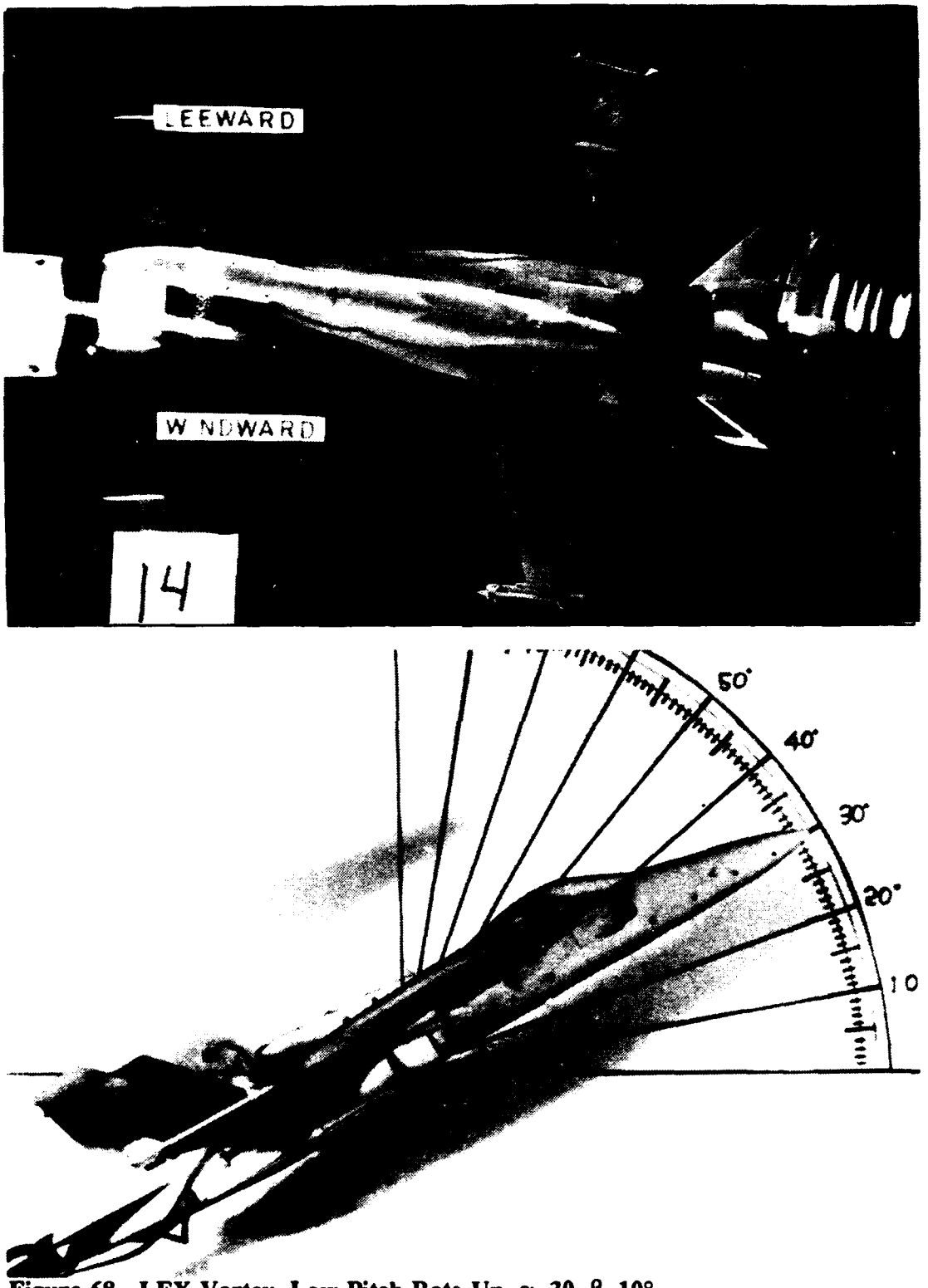

Figure 68. LEX Vortex, Low Pitch Rate Up, α=30, β=10°

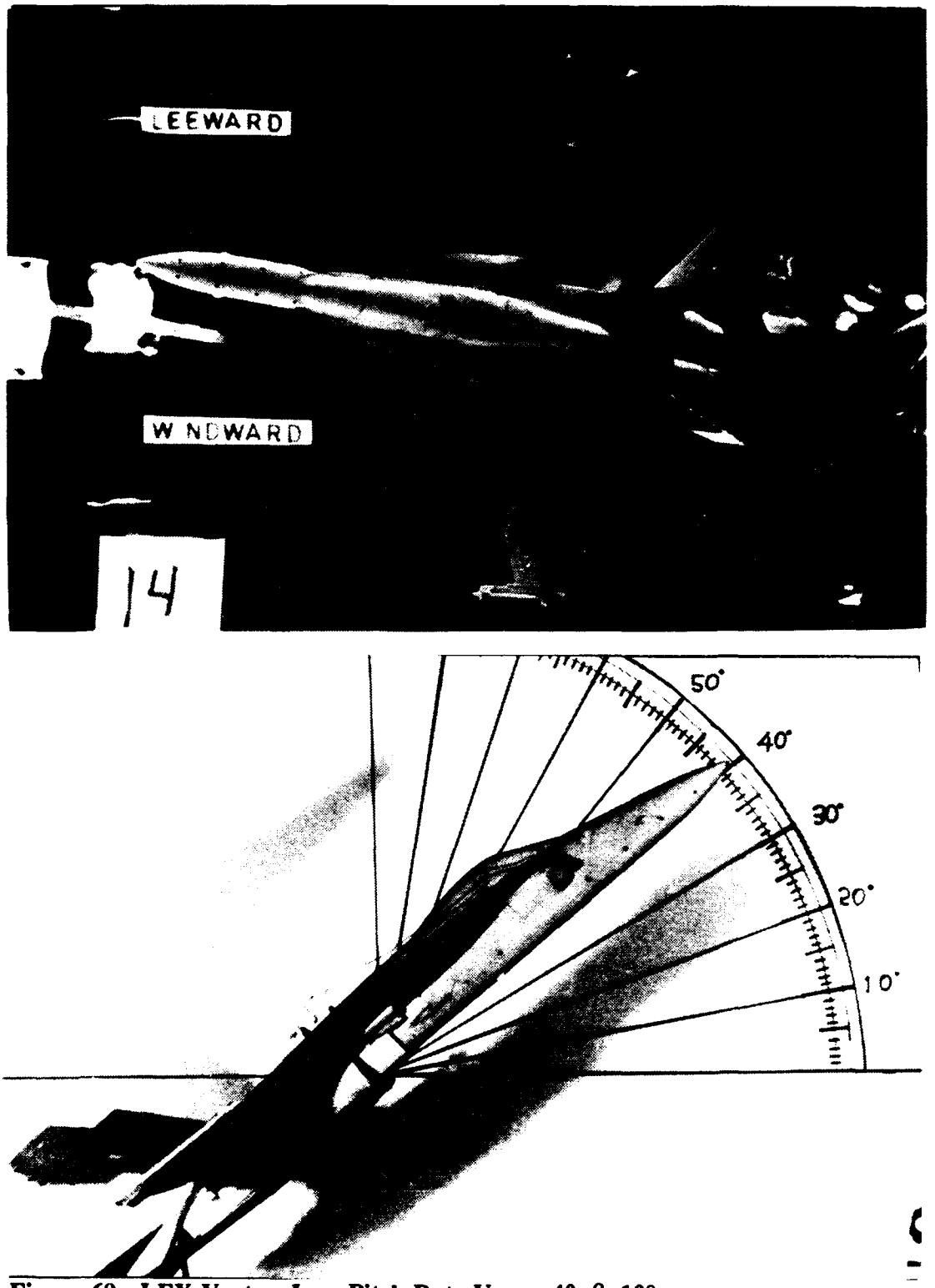

Figure 69. LEX Vortex, Low Pitch Rate Up, α=40, β=10°

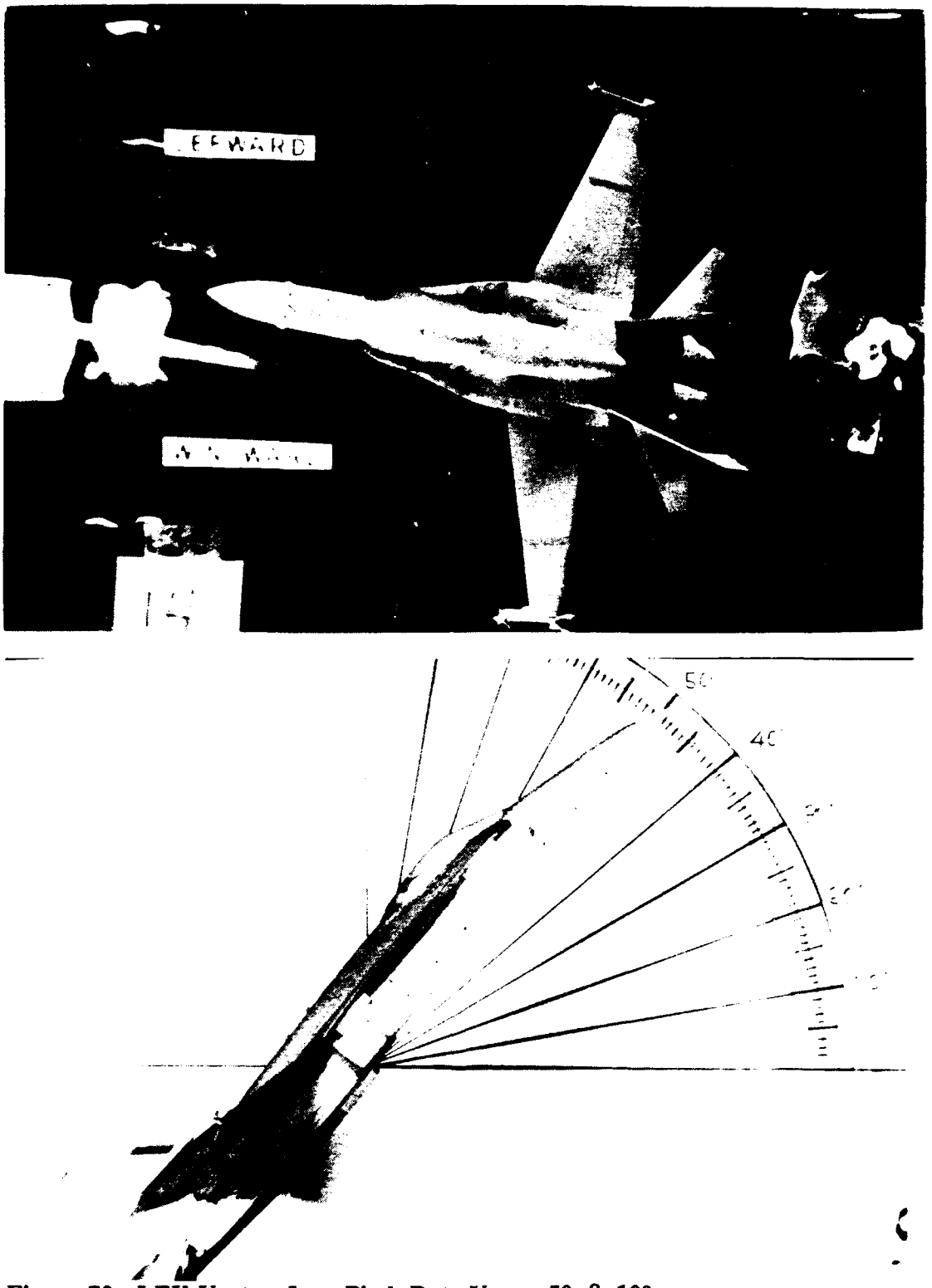

Figure 70. LEX Vortex, Low Pitch Rate Up, α=50, β=10°

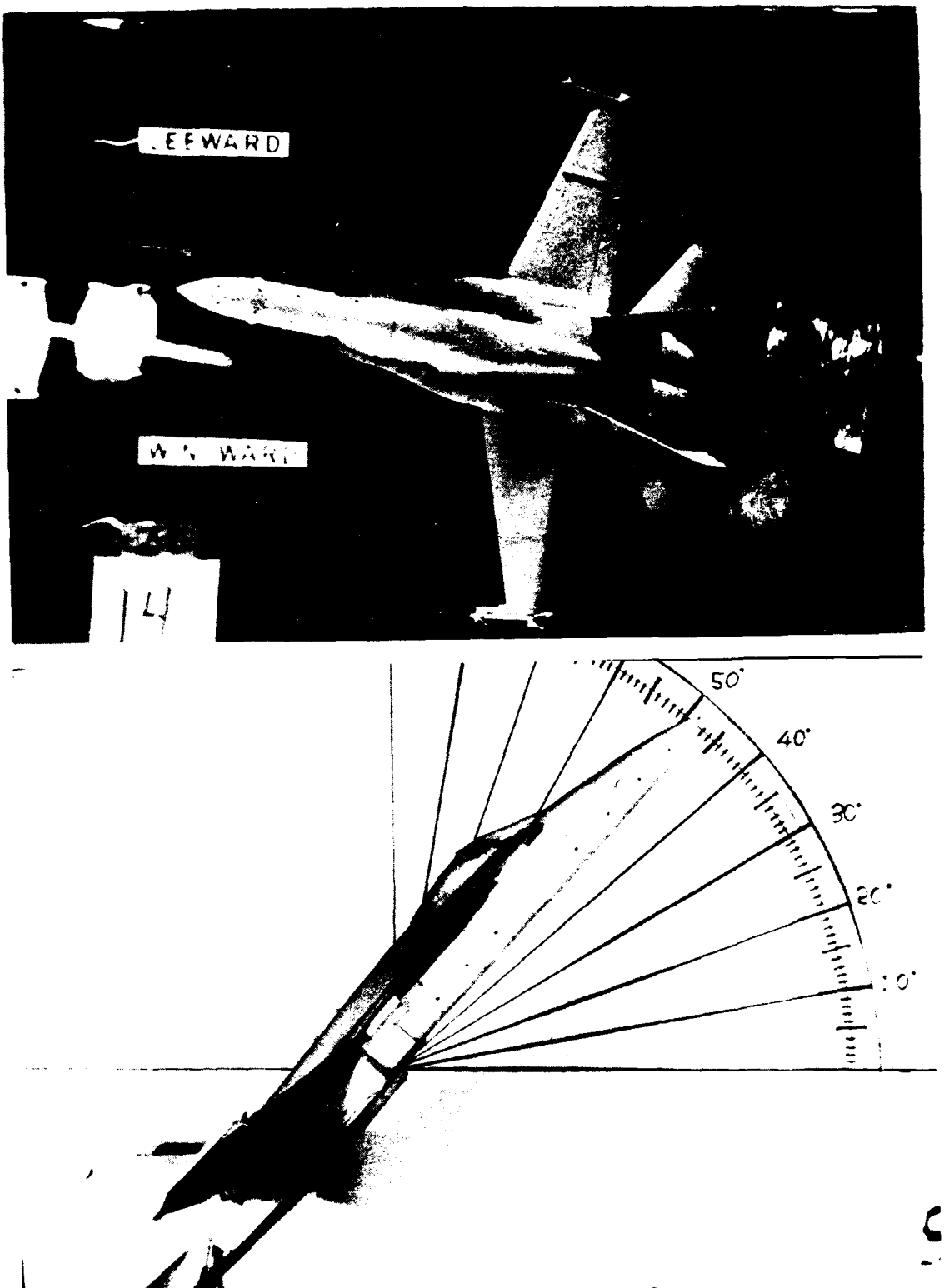

Figure 71. LEX Vortex, Low Pitch Rate Down, α=49°, β=10°

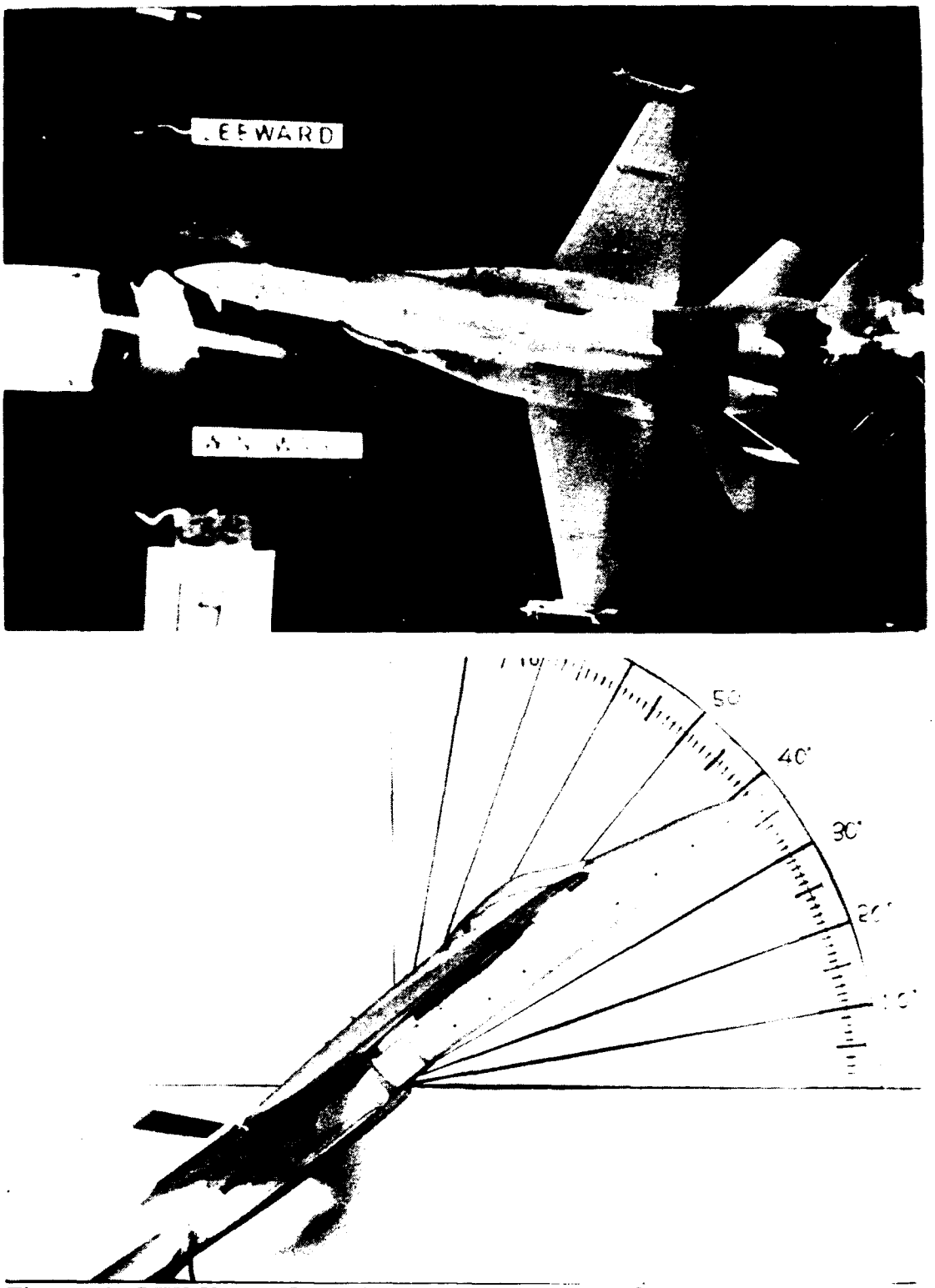

Figure 71. LEX Vortex, Low Pitch Rate Down, α=39°, β=10°

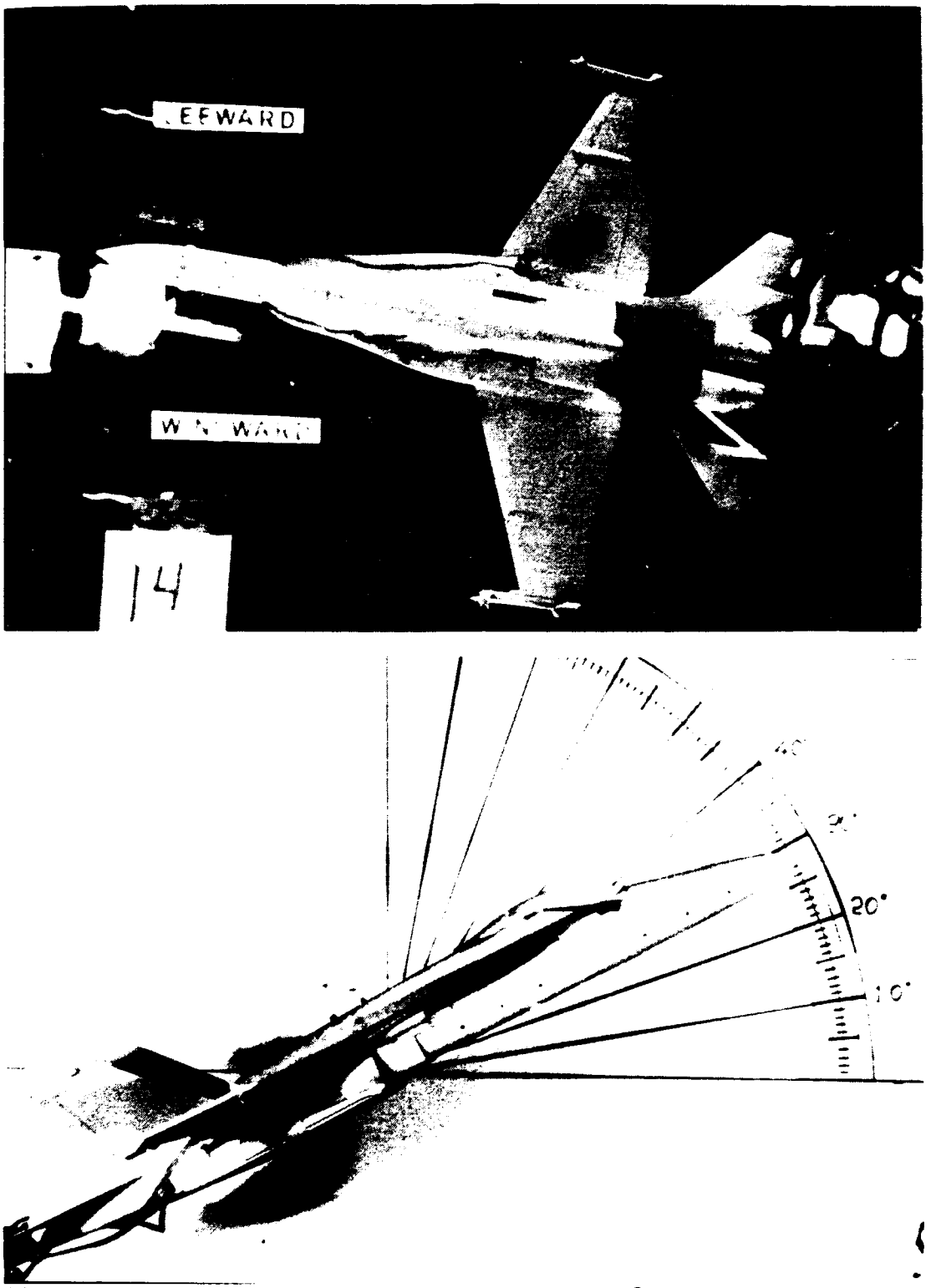

Figure 73. LEX Vortex, Low Pitch Rate Down, α=28°, β=10°

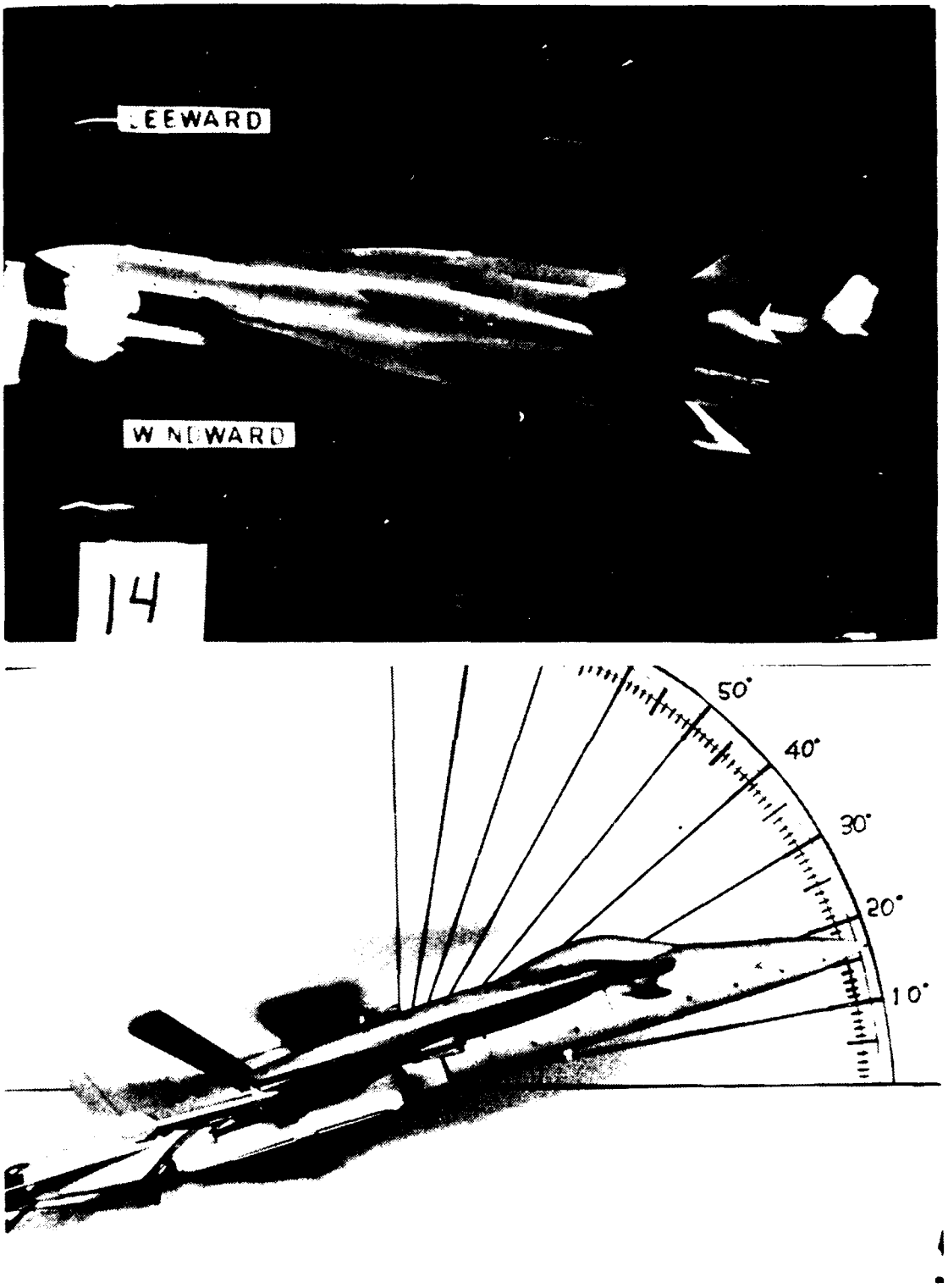

Figure 74. LEX Vortex, Low Pitch Rate Down, α=17°, β=10°

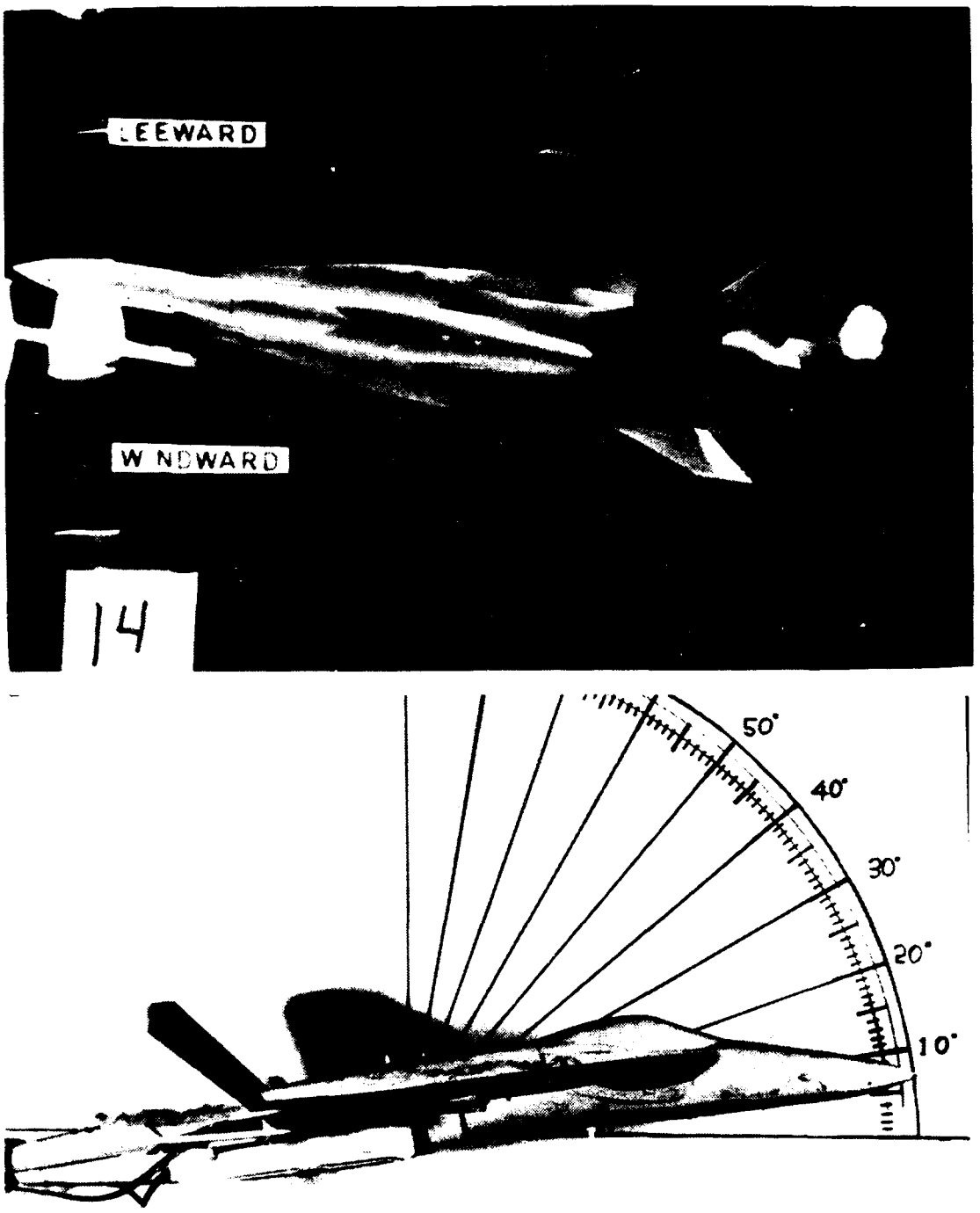

Figure 75. LEX Vortex, Low Pitch Rate Down, α=7°, β=10°

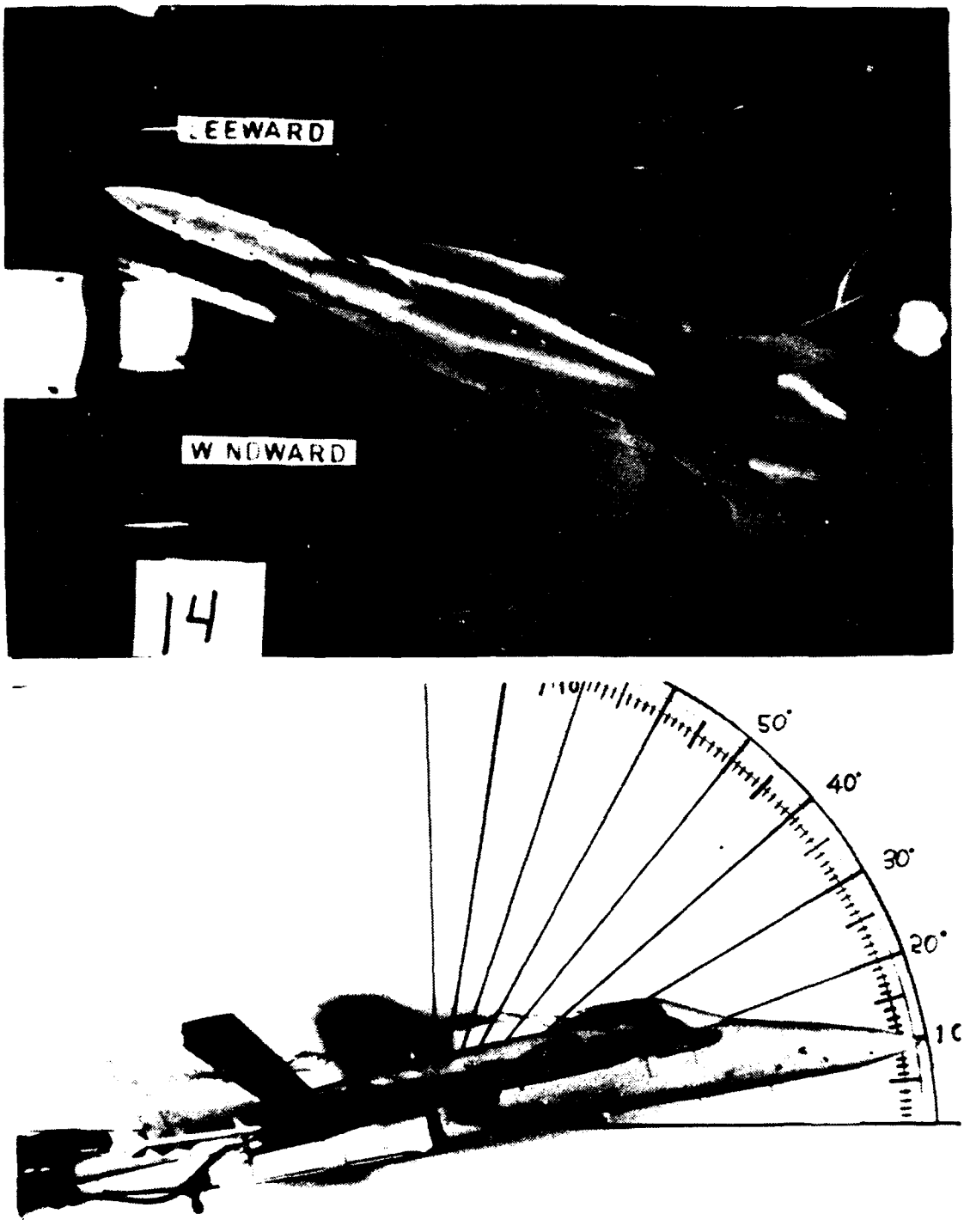

Figure 76. LEX Vortex, Low Pitch Rate Up, α=10°, β=20°

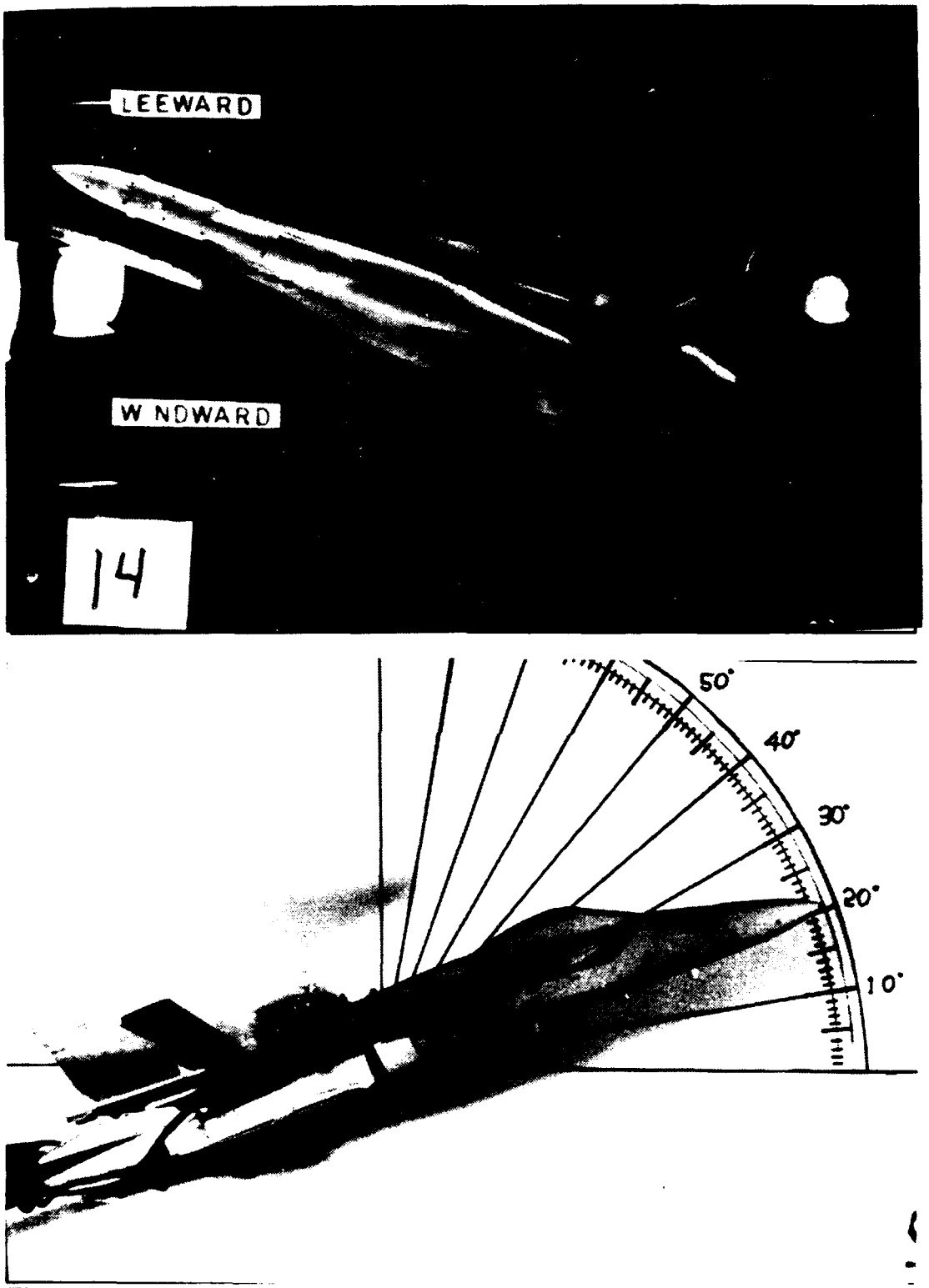

Figure 77. LEX Vortex, Low Pitch Rate Up, α=20°, β=20°

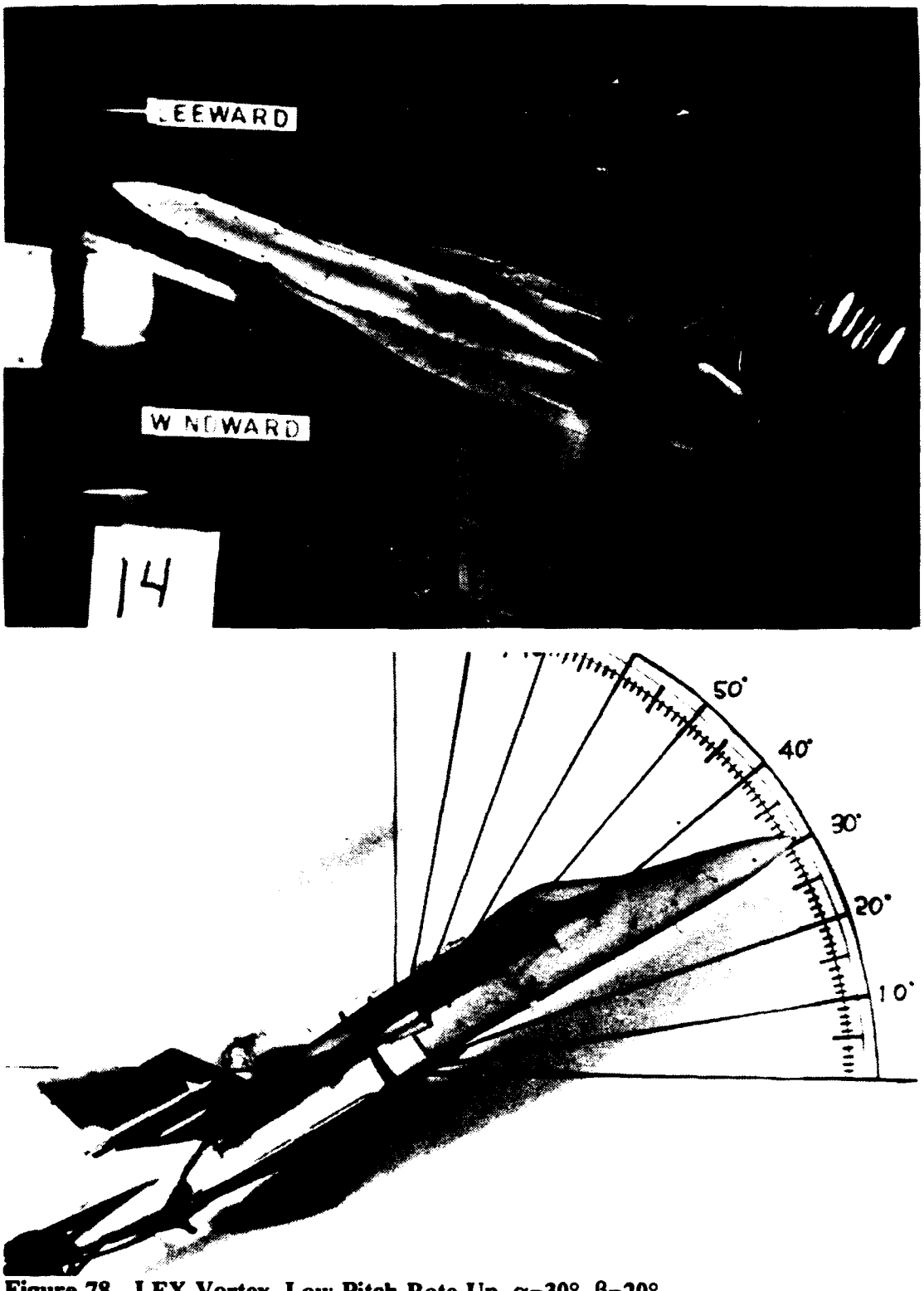

Figure 78. LEX Vortex, Low Pitch Rate Up, α=30°, β=20°

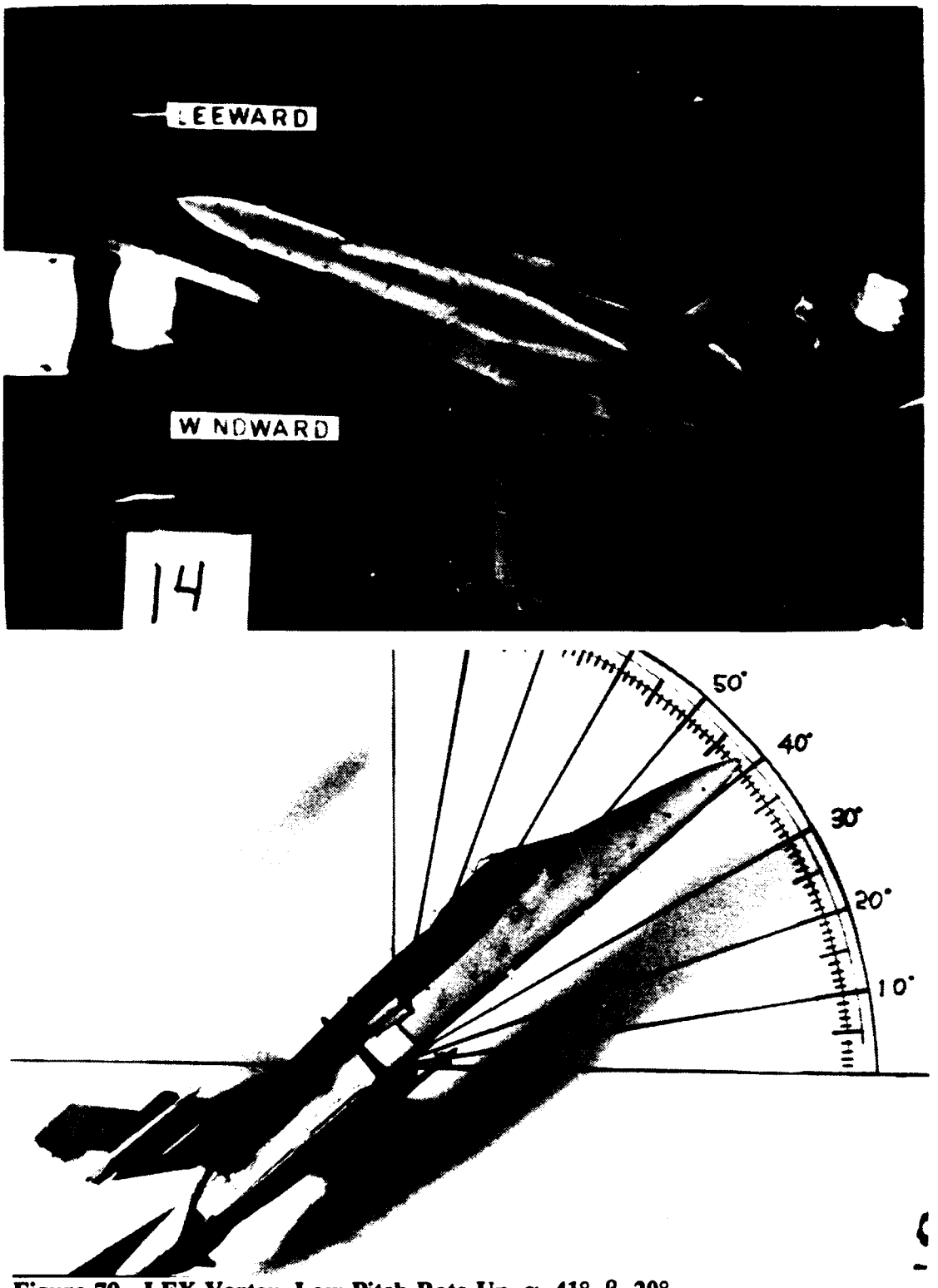

Figure 79. LEX Vortex, Low Pitch Rate Up, α=41°, β=20°

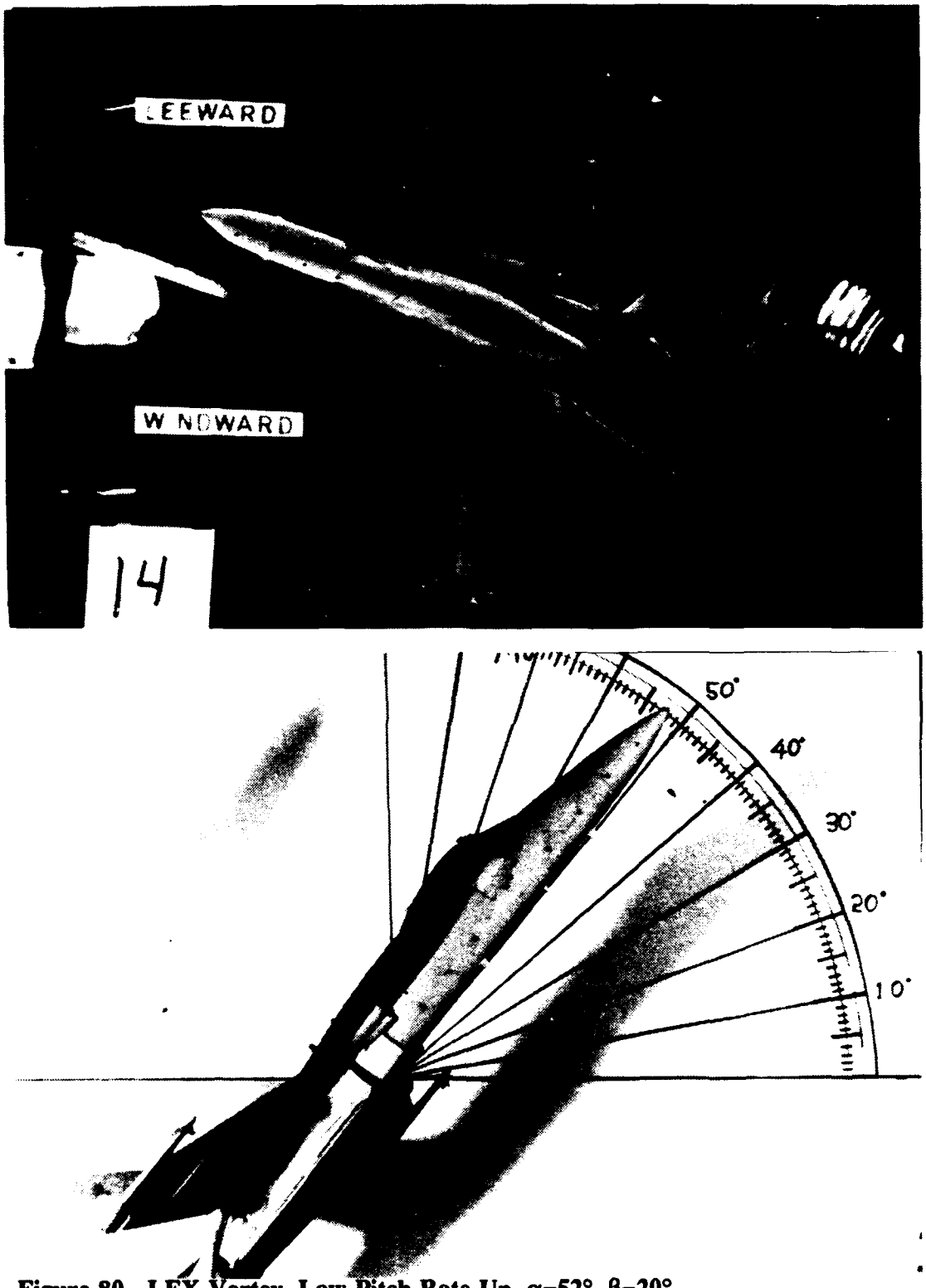

Figure 80. LEX Vortex, Low Pitch Rate Up, α=52°, β=20°

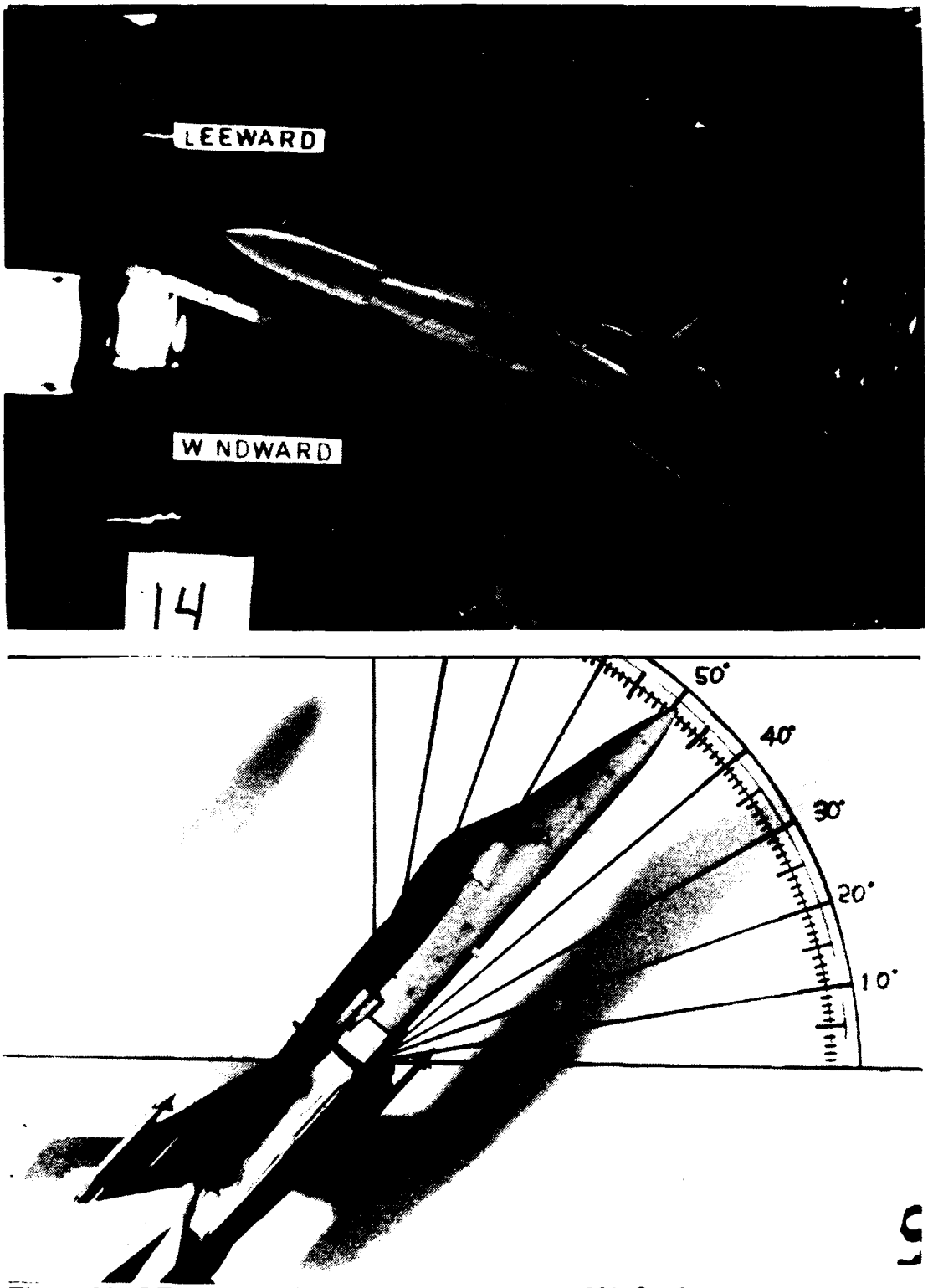

Figure 81. LEX Vortex, Low Pitch Rate Down, α=50°, β=20°

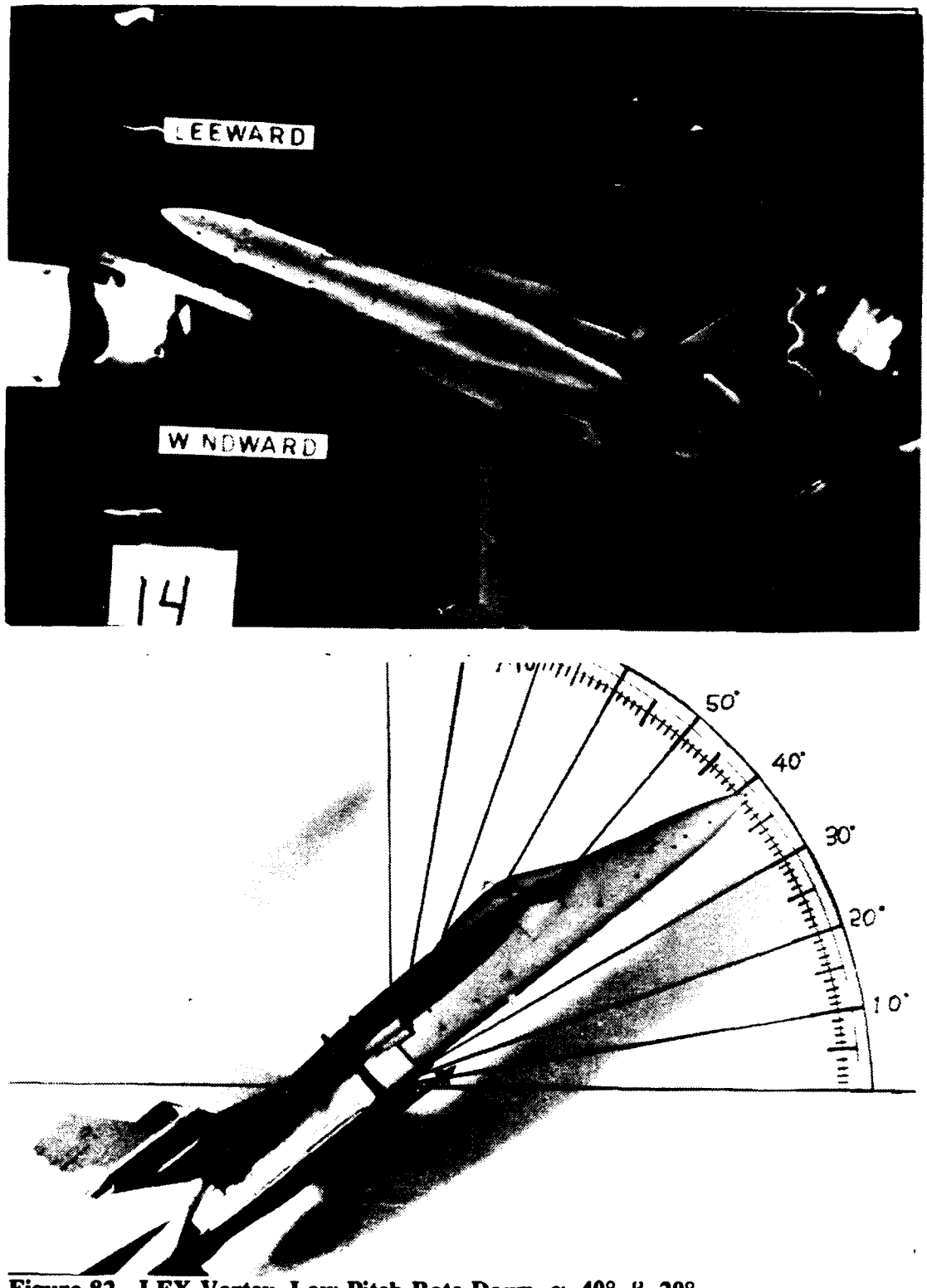

Figure 82. LEX Vortex, Low Pitch Rate Down, α=40°, β=20°

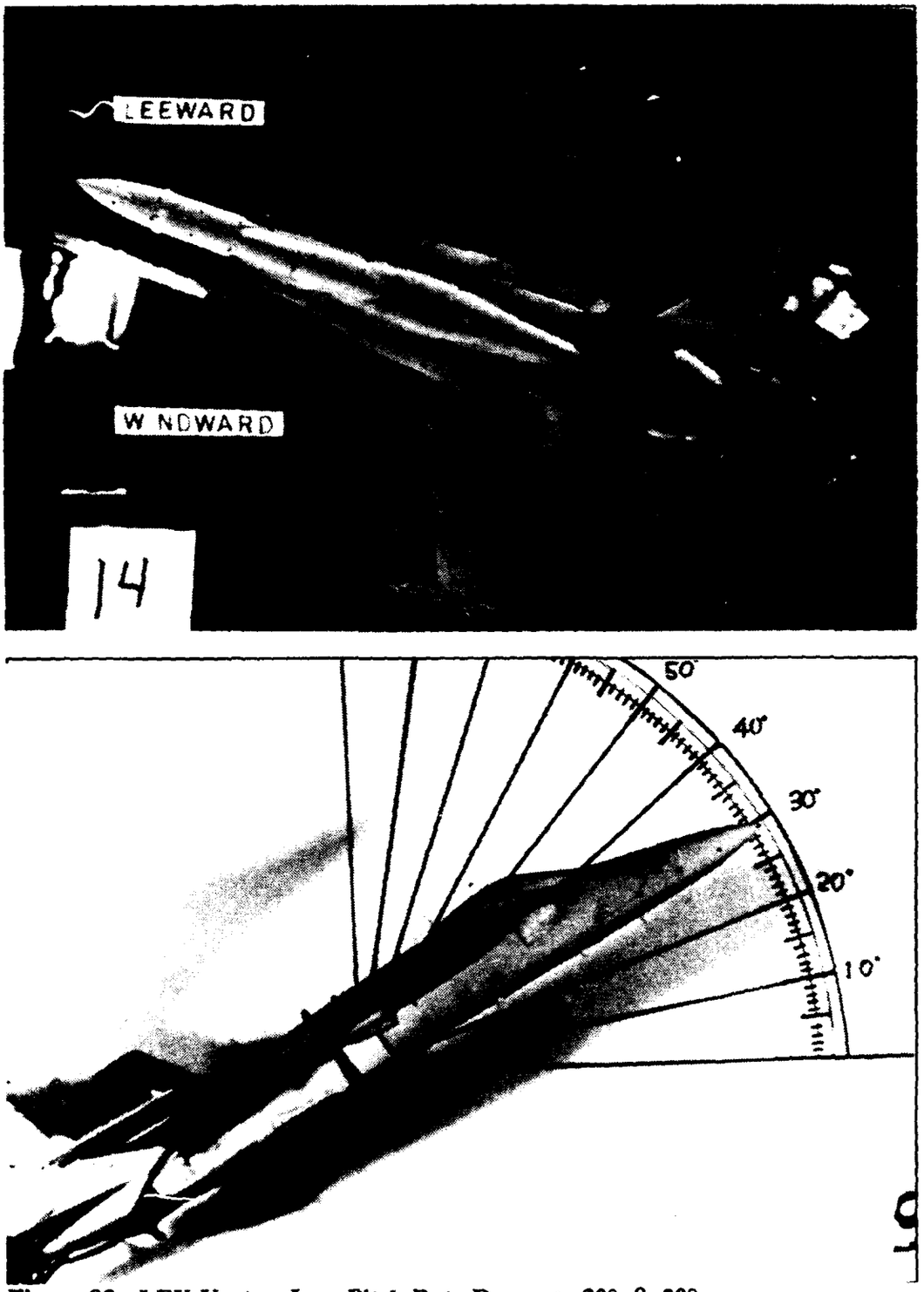

Figure 83. LEX Vortex, Low Pitch Rate Down, α=30°, β=20°

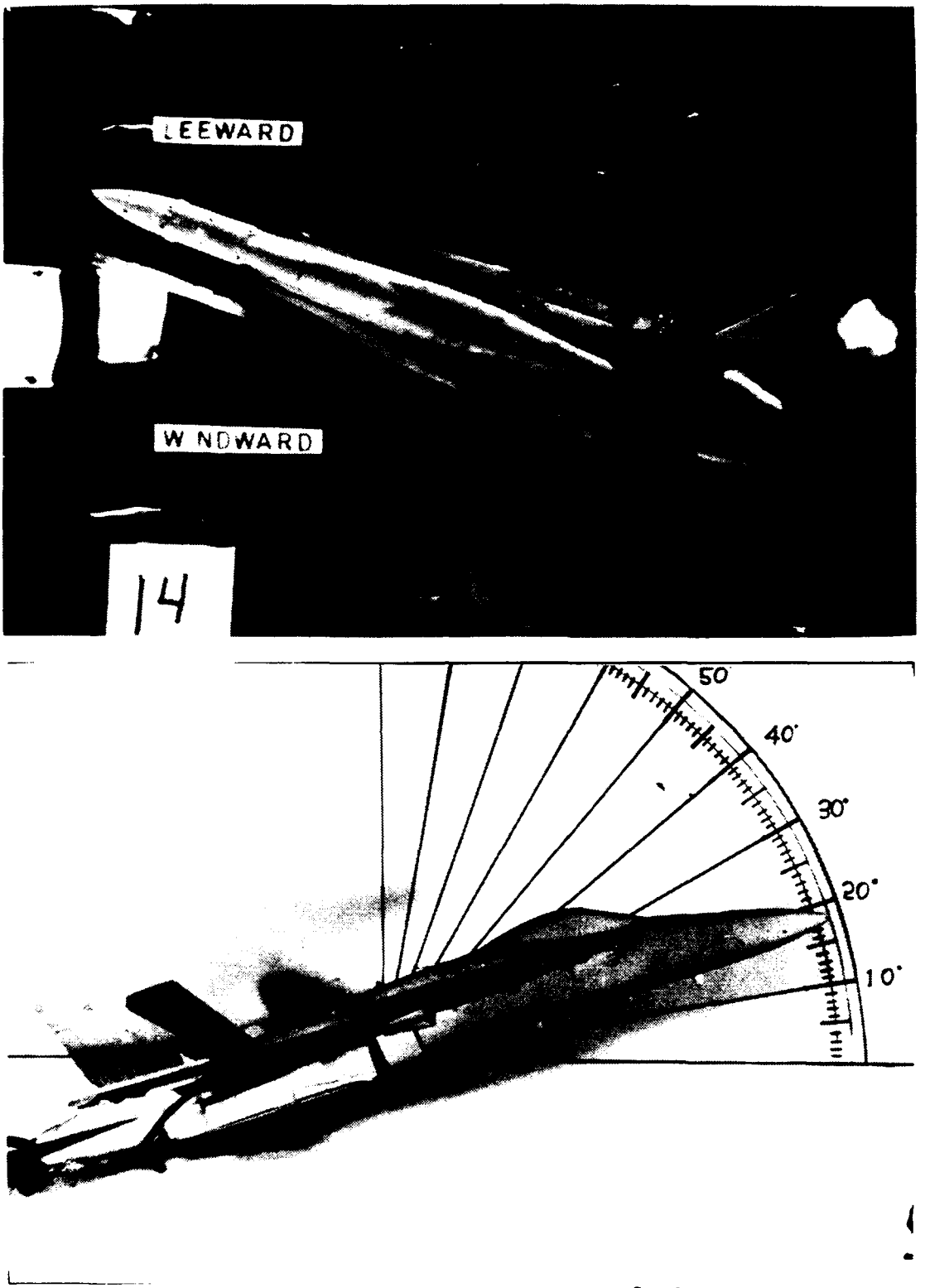

Figure 84. LEX Vortex, Low Pitch Rate Down, α=18°, β=20°

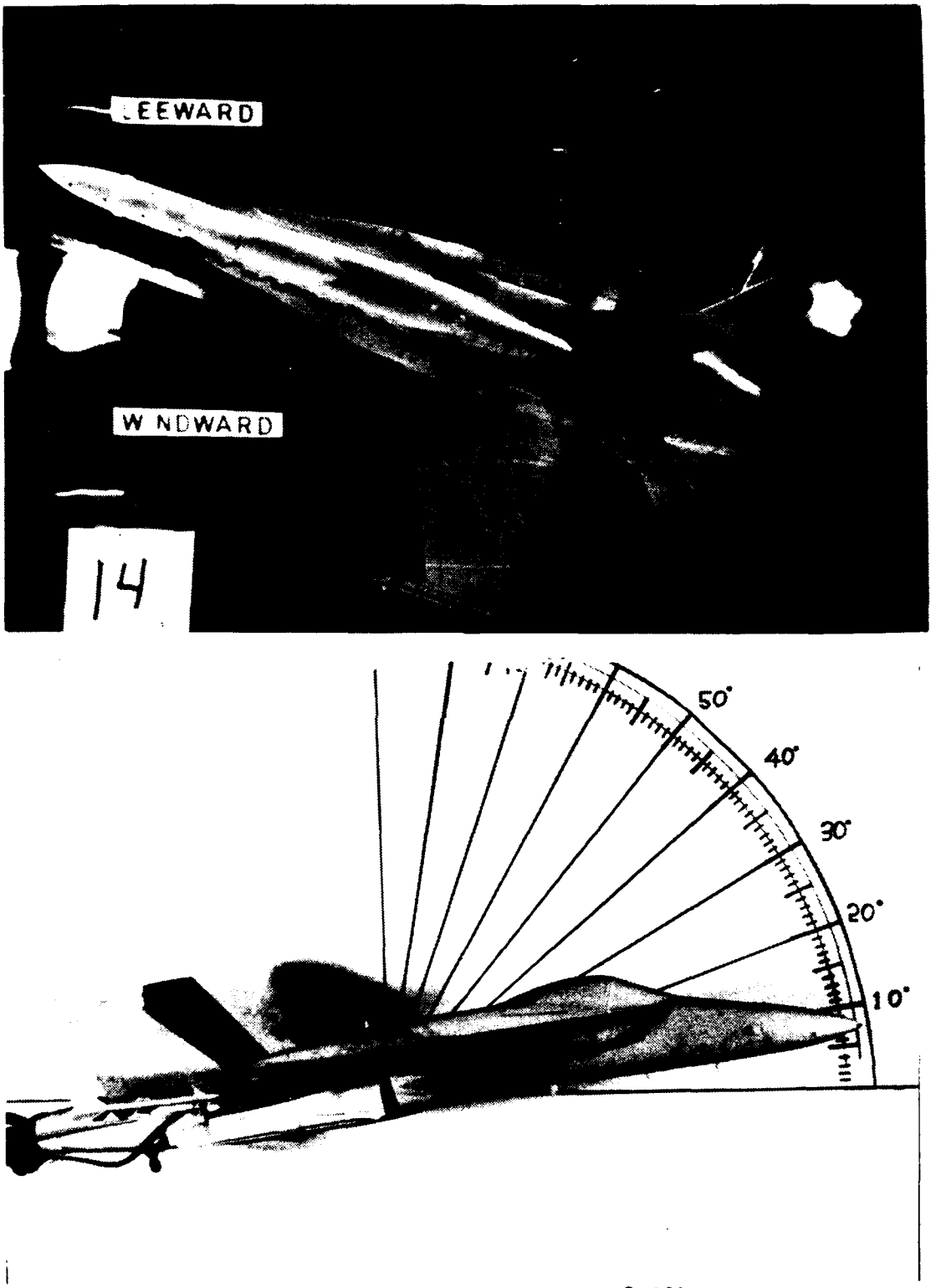

Figure 85. LEX Vortex, Low Pitch Rate Down, α=8°, β=20°

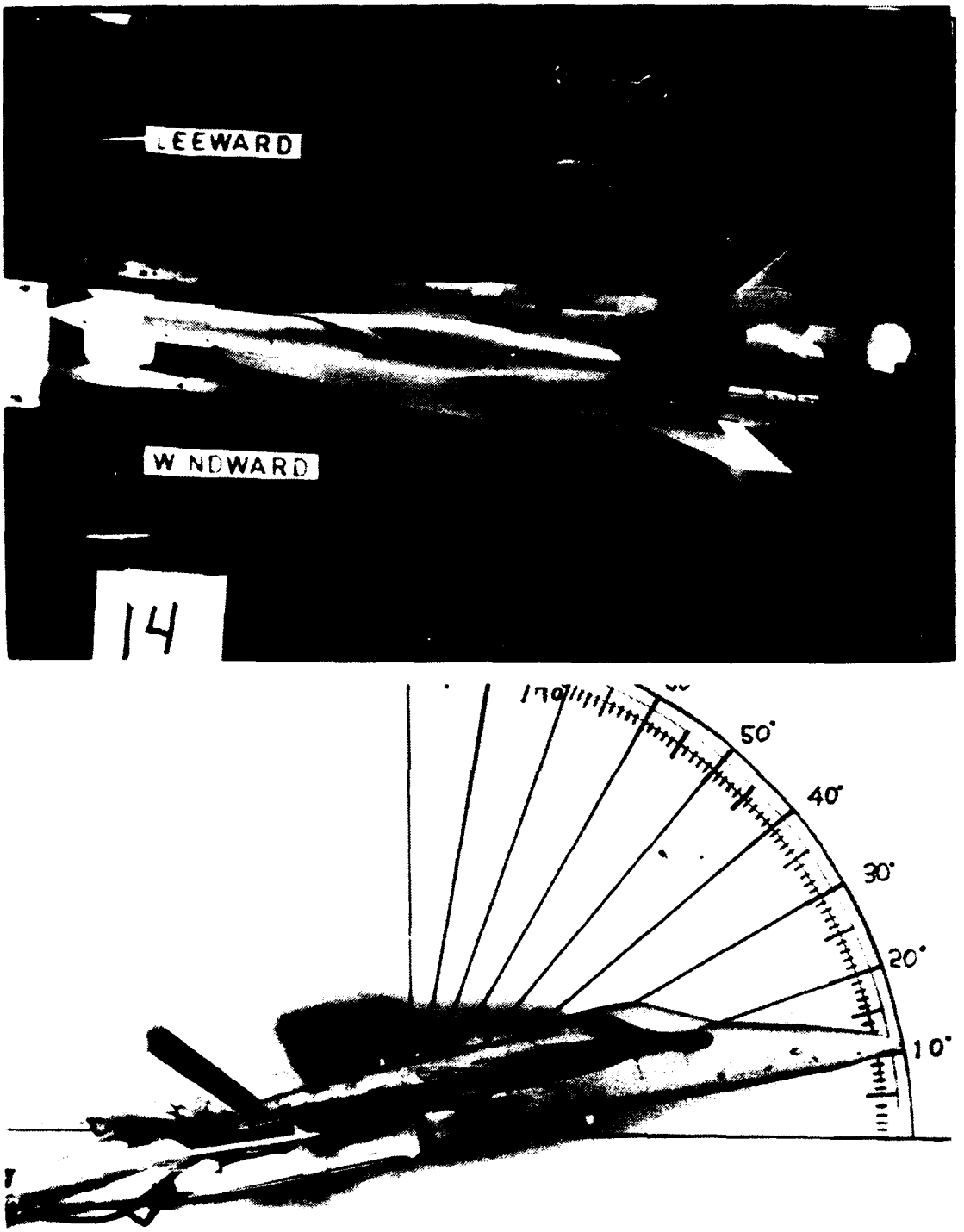

Figure 86. LEX Vortex, High Pitch Rate Up, α=11°, β=5°

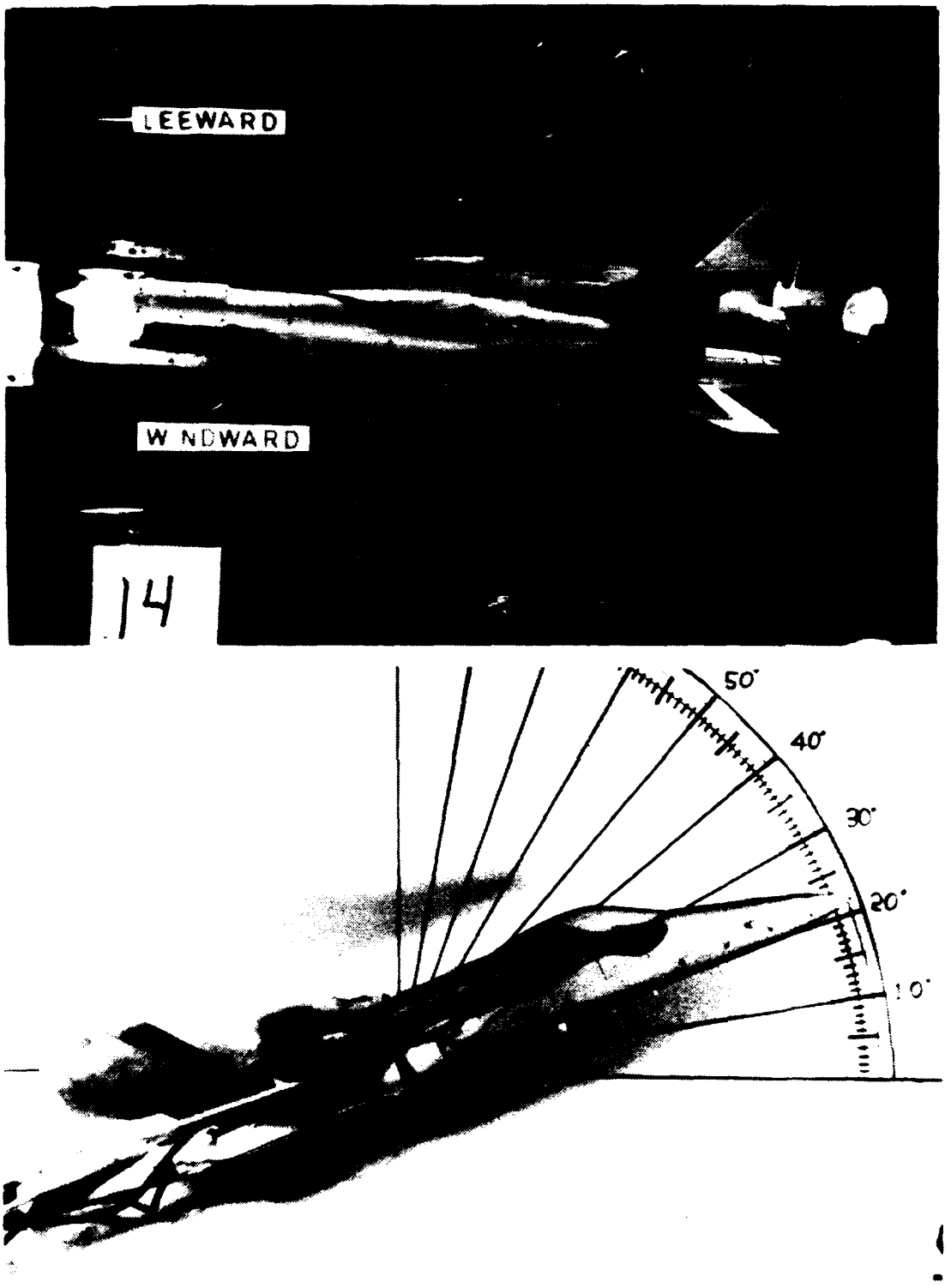

Figure 87. LEX Vortex, High Pitch Rate Up, α=22°, β=5°

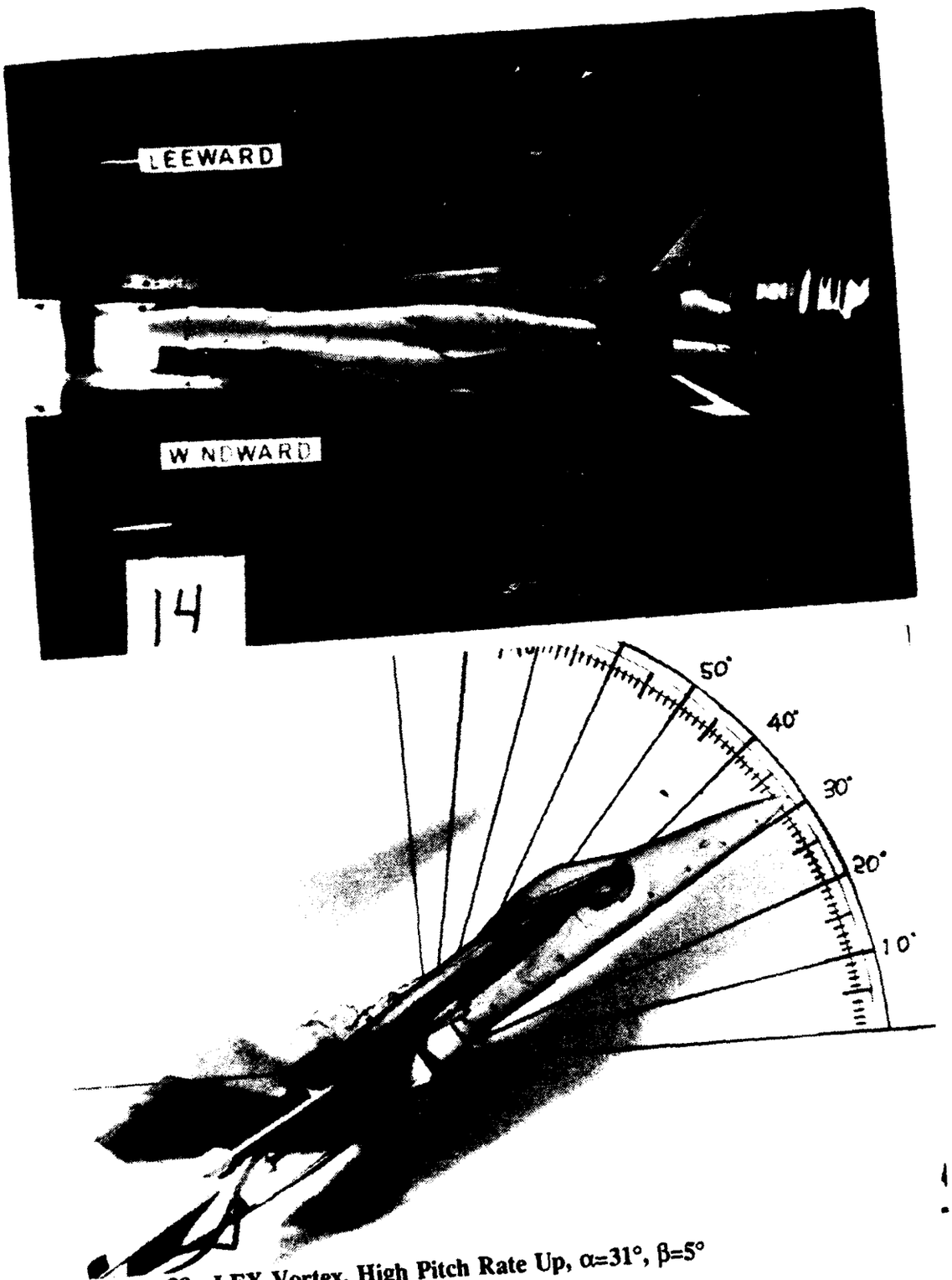

Figure 88. LEX Vortex, High Pitch Rate Up, α=31°, β=5°

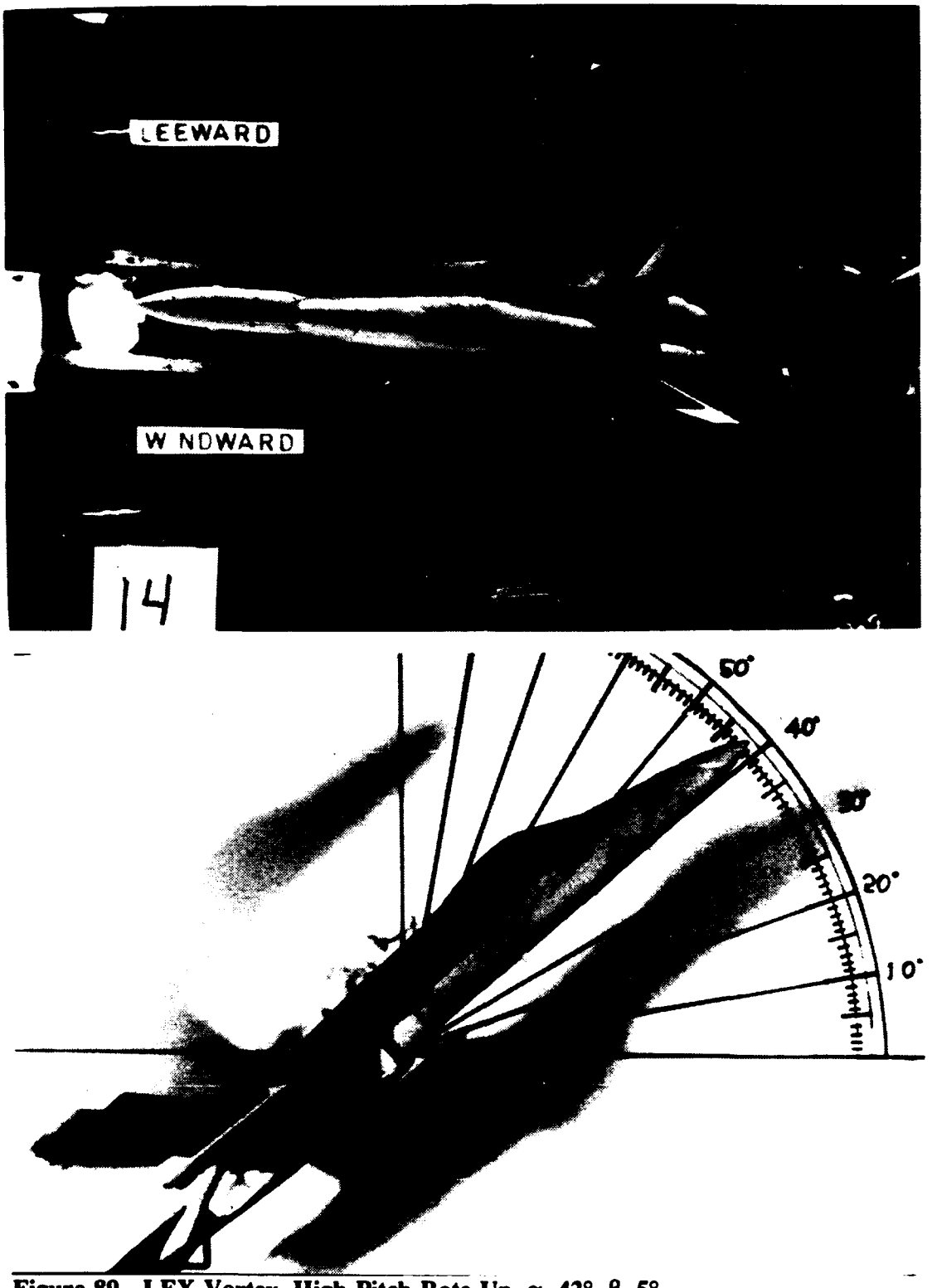

Figure 89. LEX Vortex, High Pitch Rate Up, α=42°, β=5°

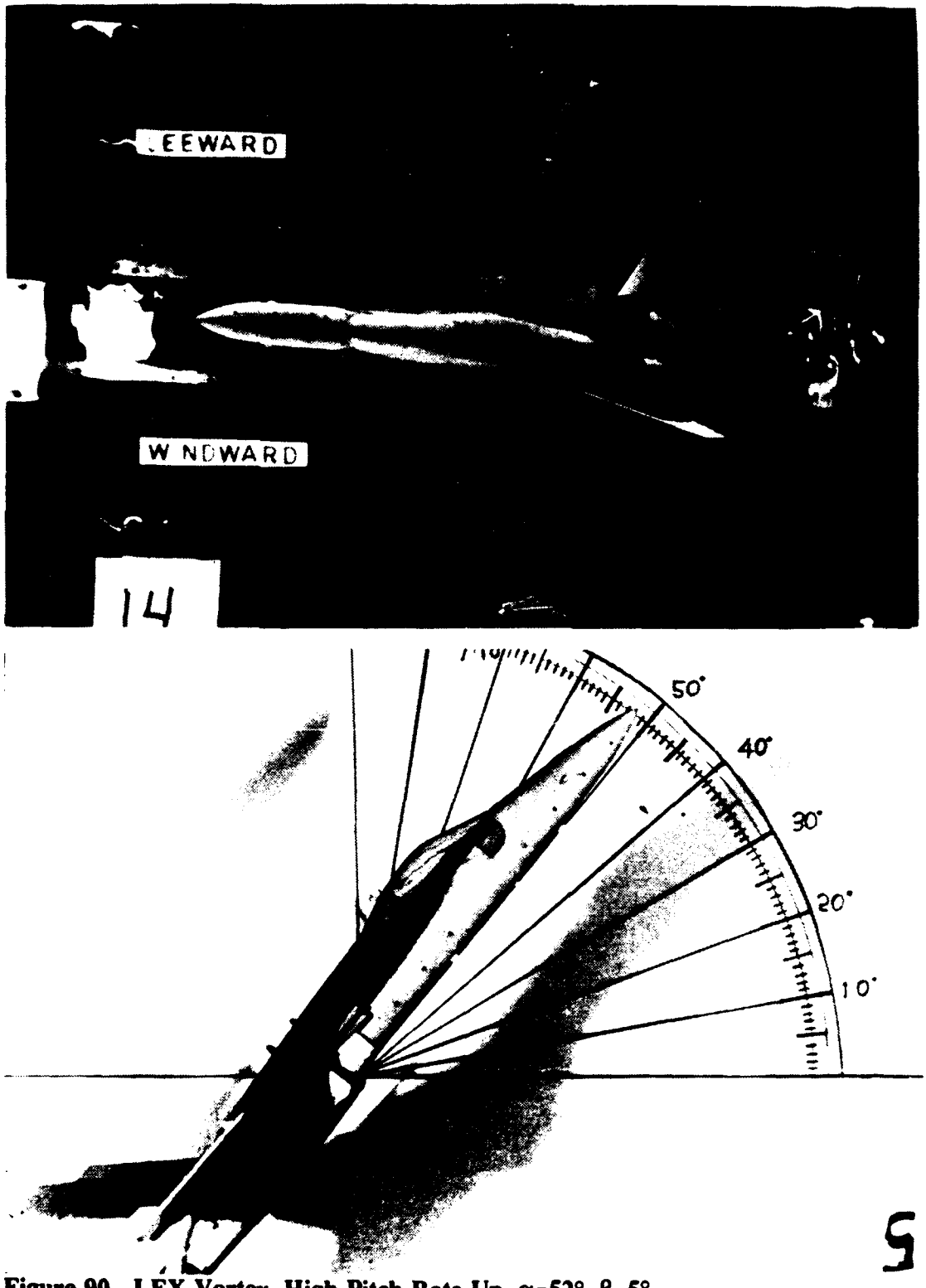

Figure 90. LEX Vortex, High Pitch Rate Up, α=52°, β=5°

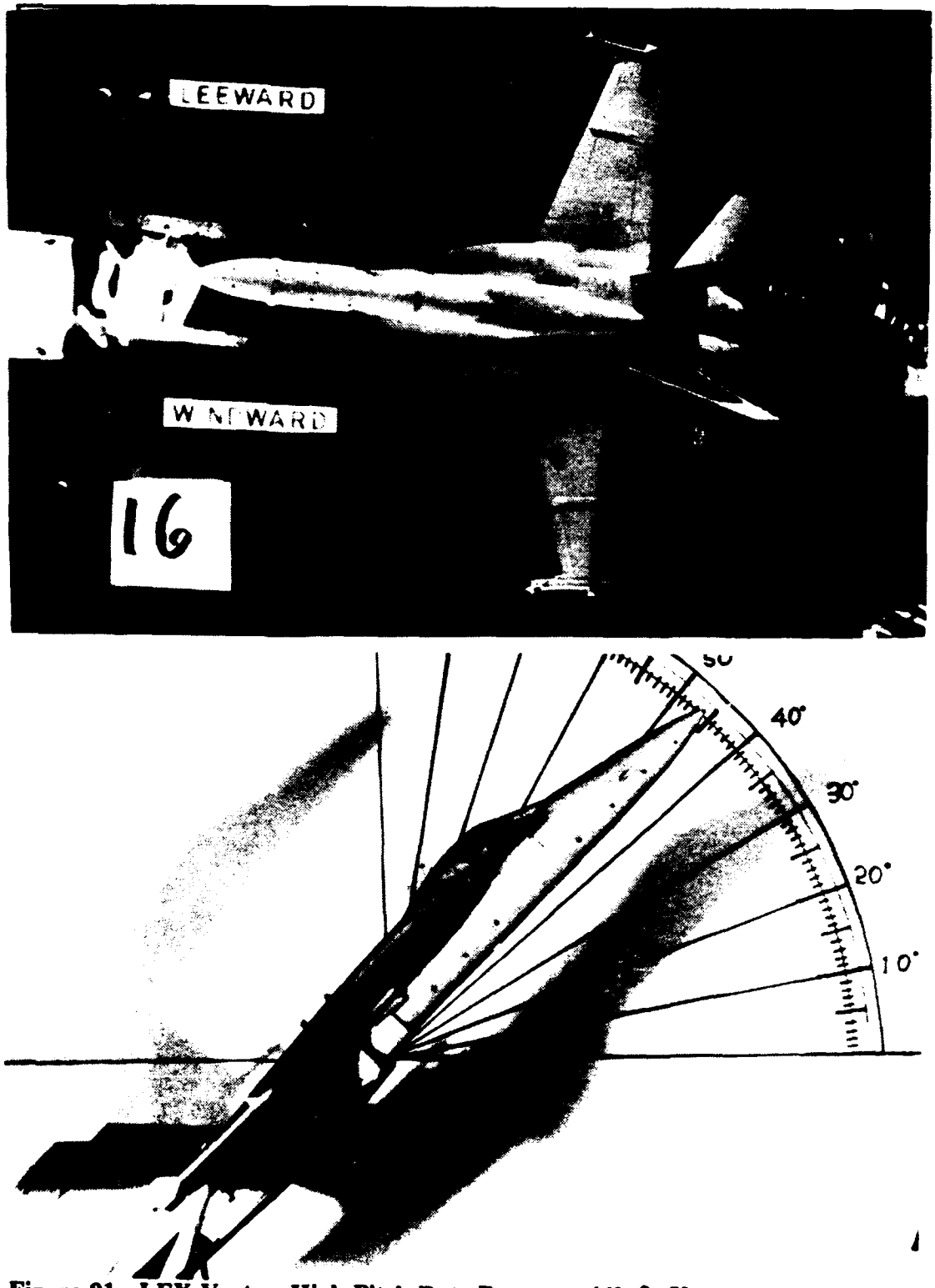

Figure 91. LEX Vortex, High Pitch Rate Down, α=46°, β=5°

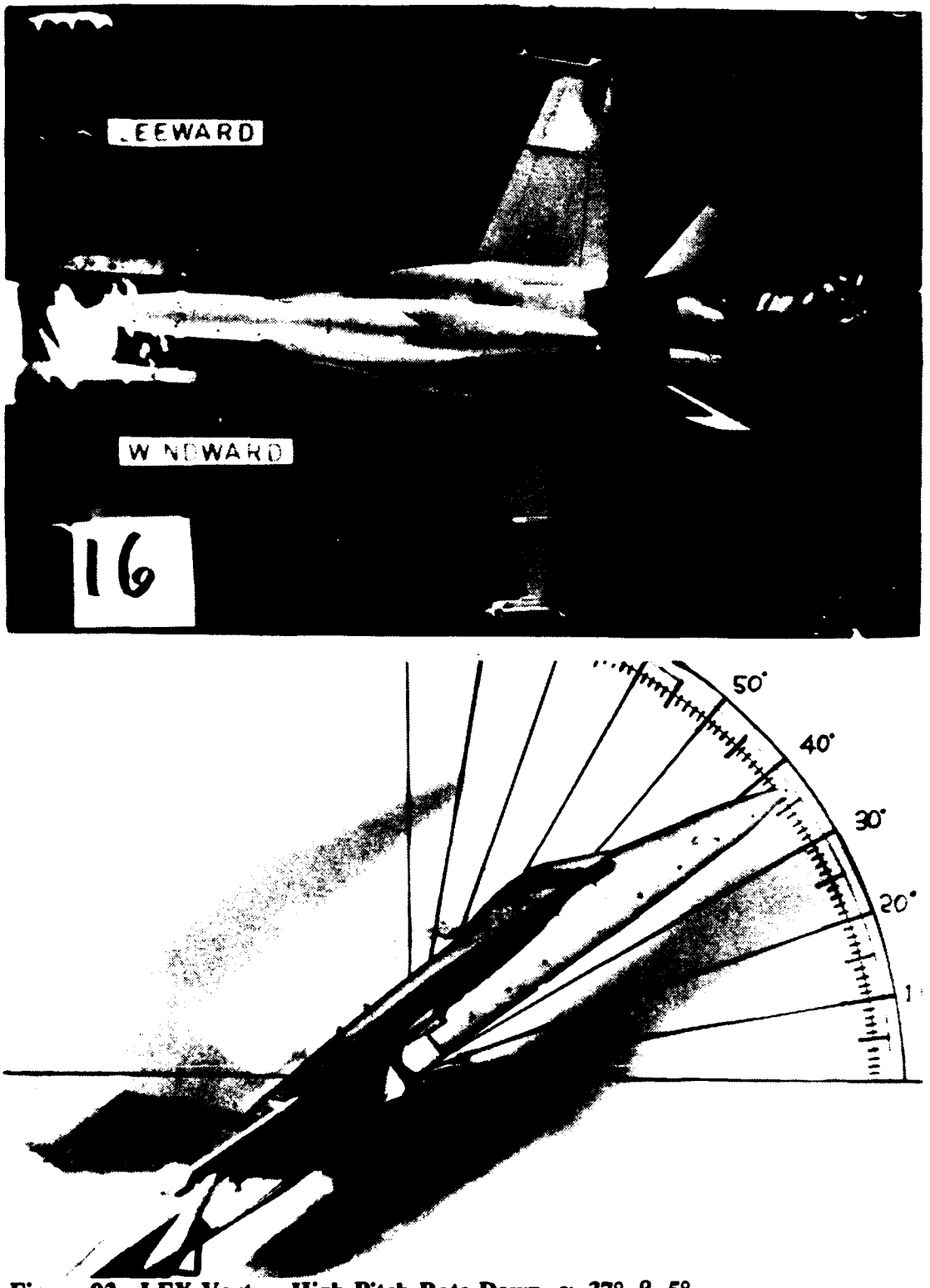

Figure 92. LEX Vortex, High Pitch Rate Down, α=37°, β=5°

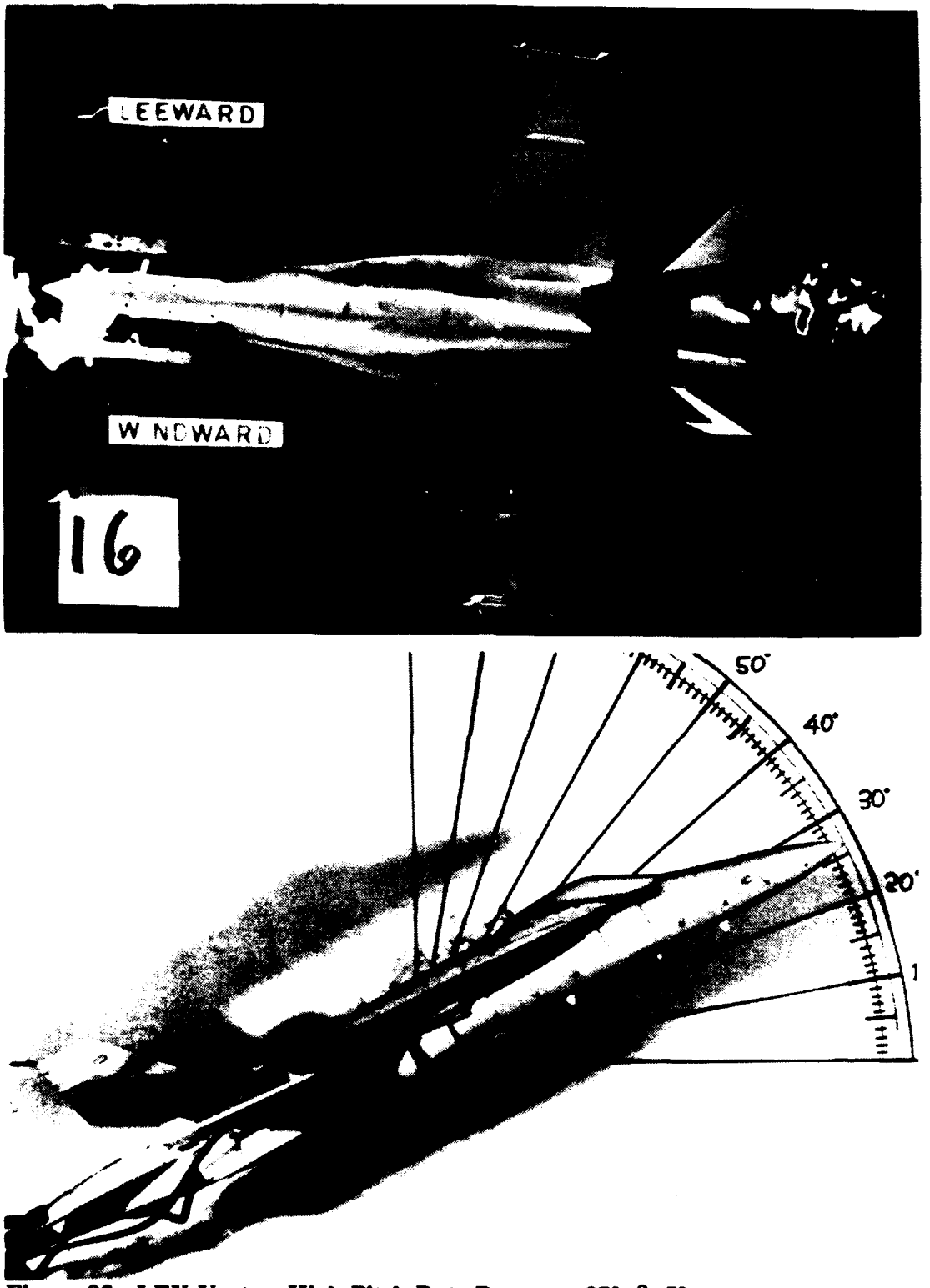

Figure 93. LEX Vortex, High Pitch Rate Down, α=27°, β=5°

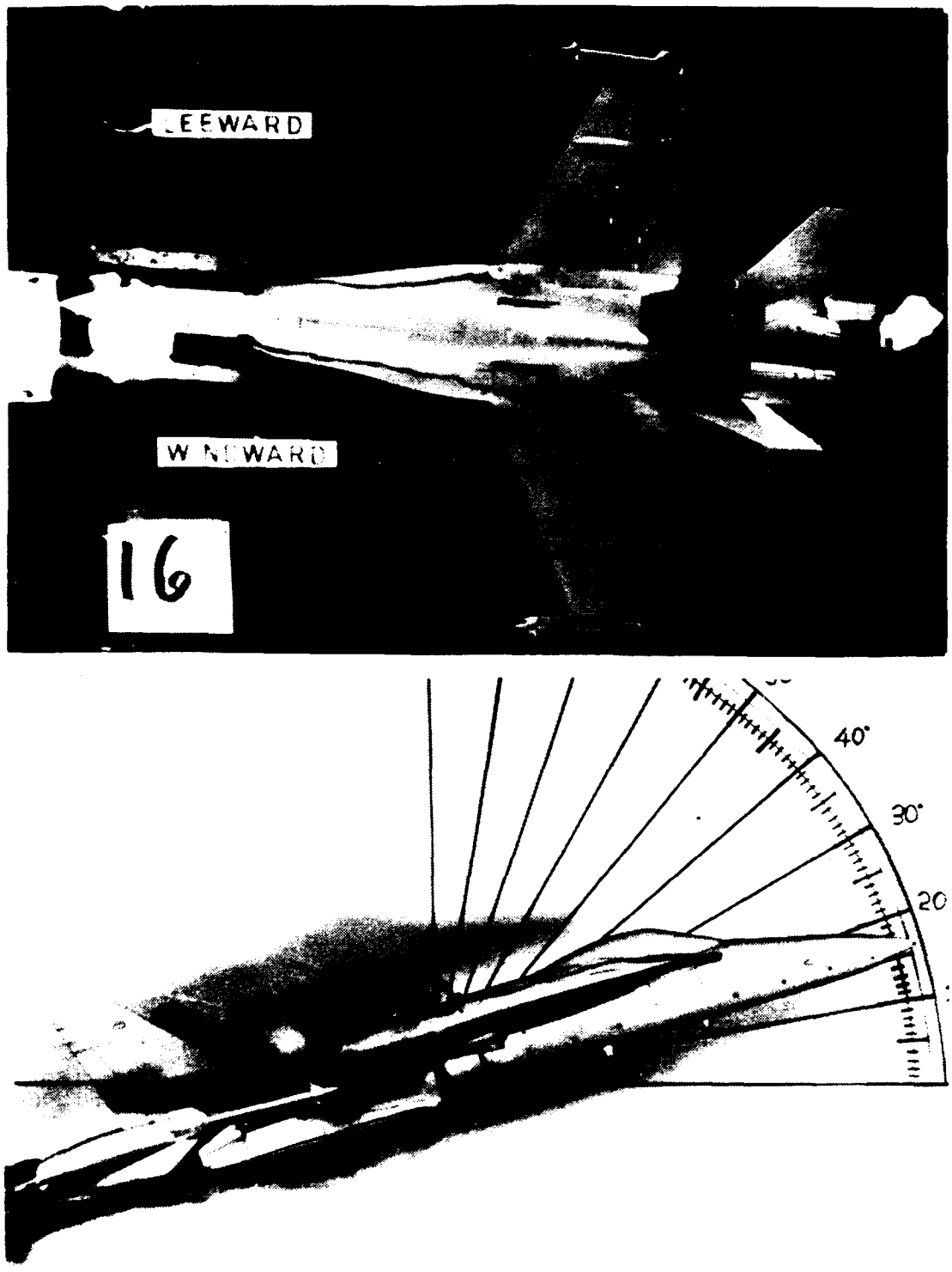

Figure 94. LEX Vortex, High Pitch Rate Down, α=17°, β=5°

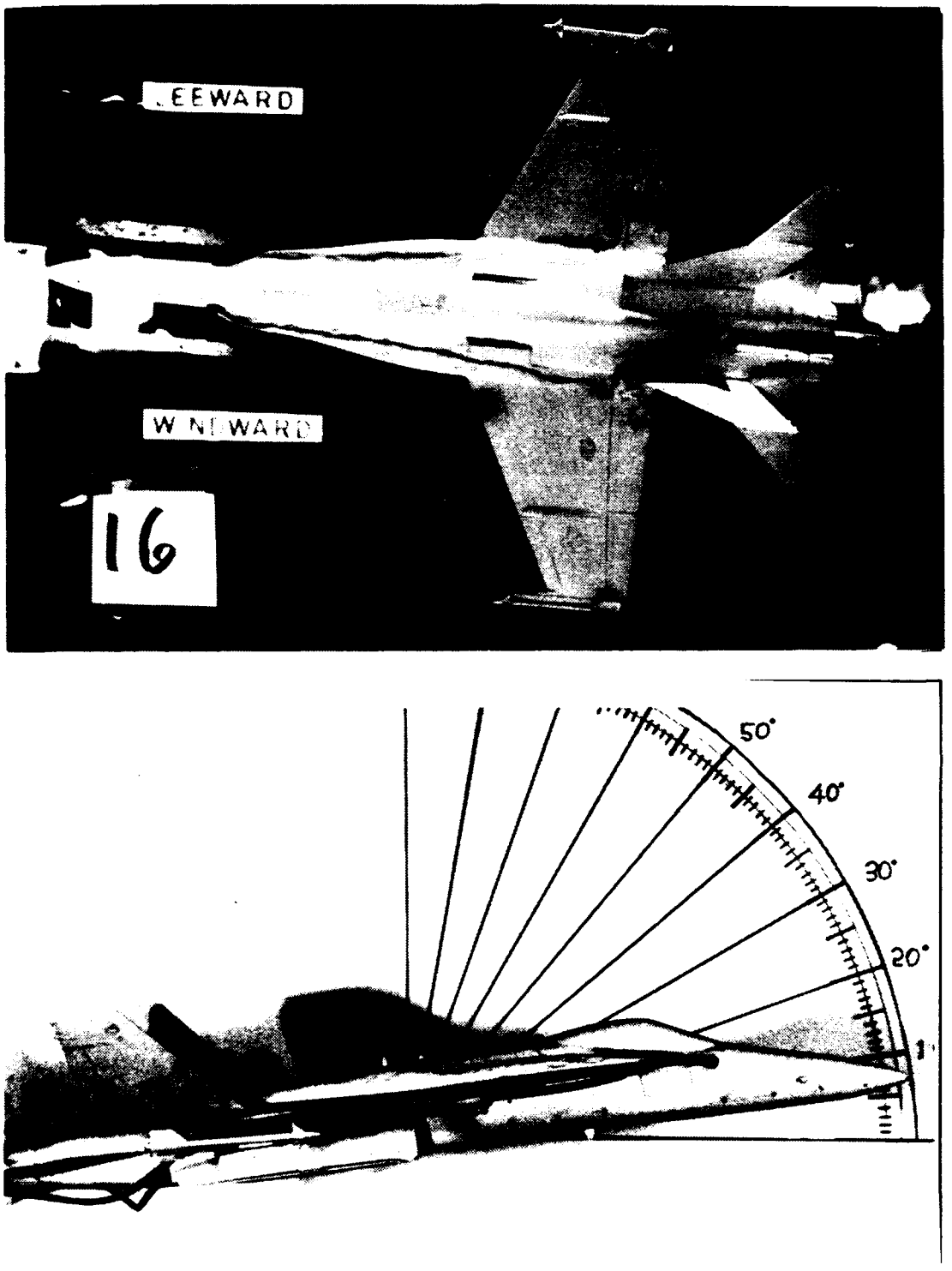

Figure 95. LEX Vortex, High Pitch Rate Down, α=8°, β=5°

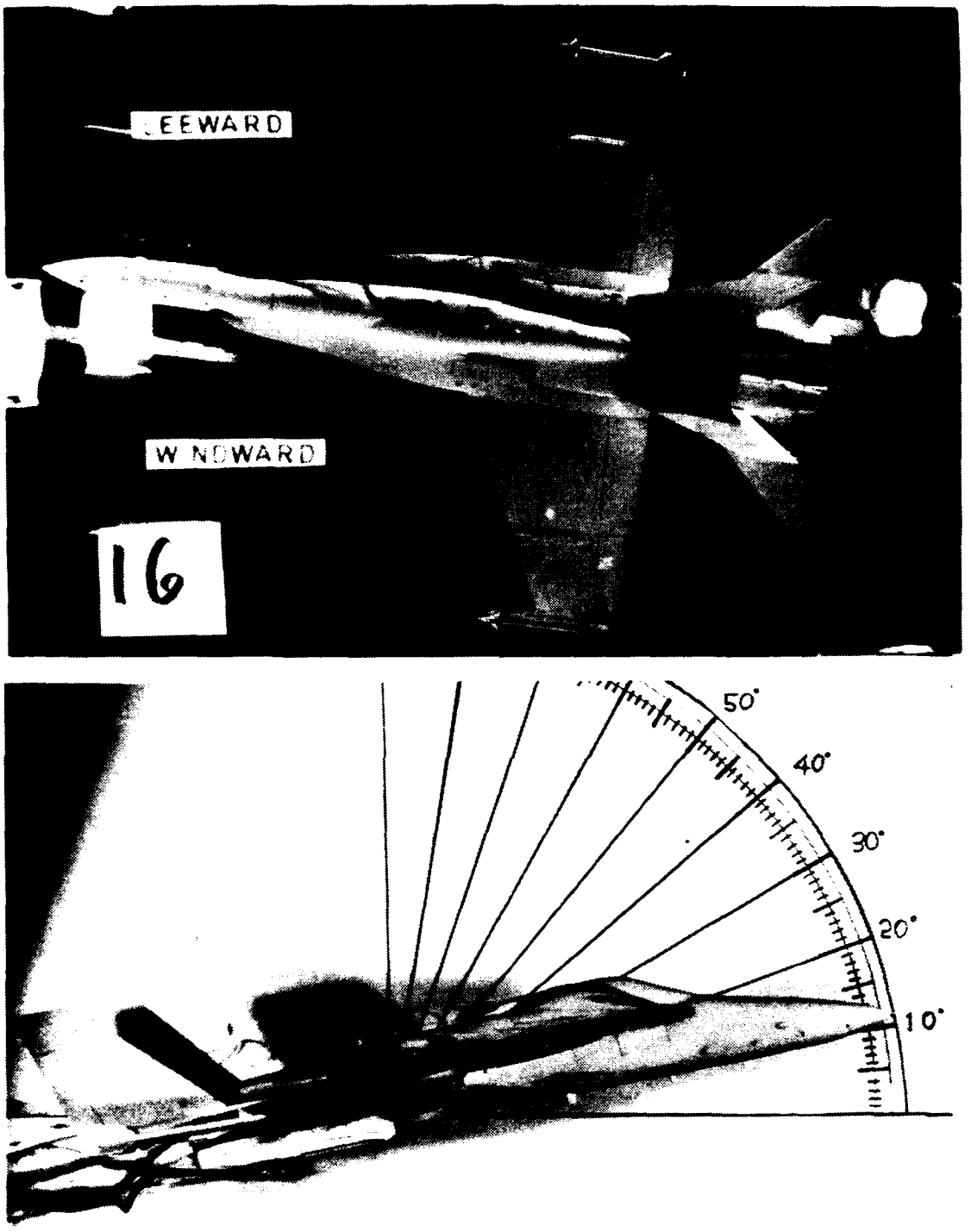

Figure 96. LEX Vortex, High Pitch Rate Up, α=11°, β=10°

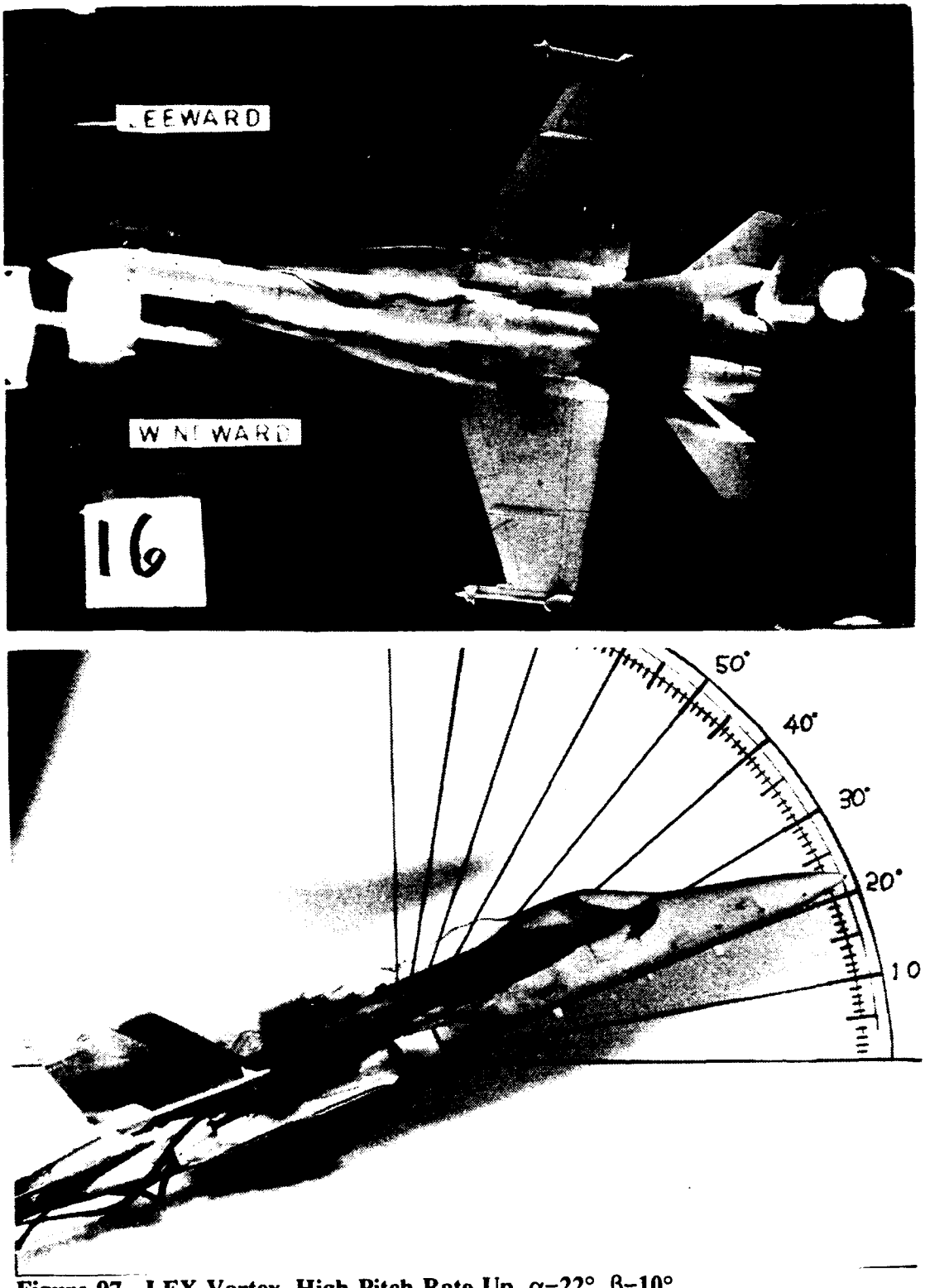

Figure 97. LEX Vortex, High Pitch Rate Up, α=22°, β=10°

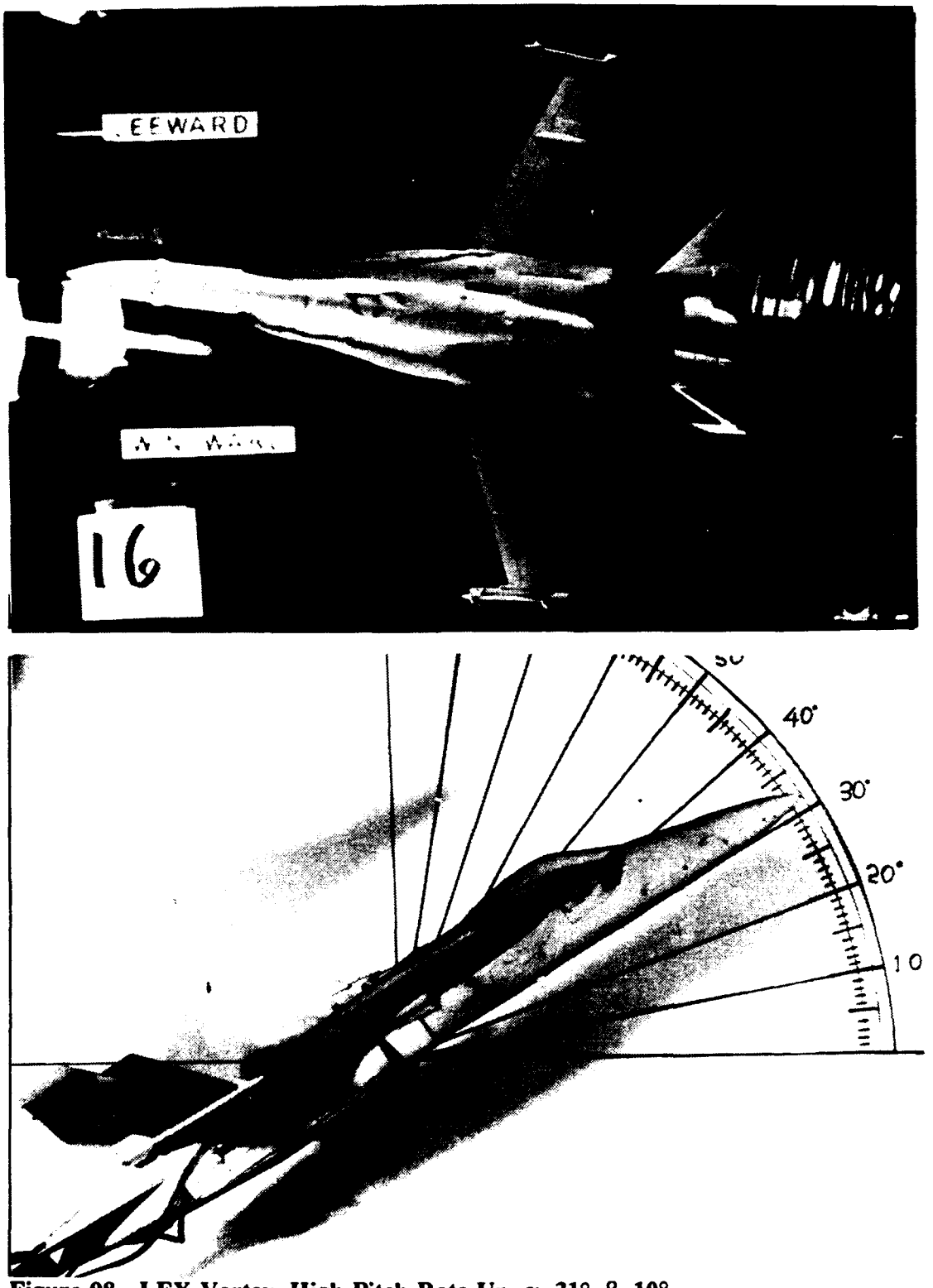

Figure 98. LEX Vortex, High Pitch Rate Up, α=31°, β=10°

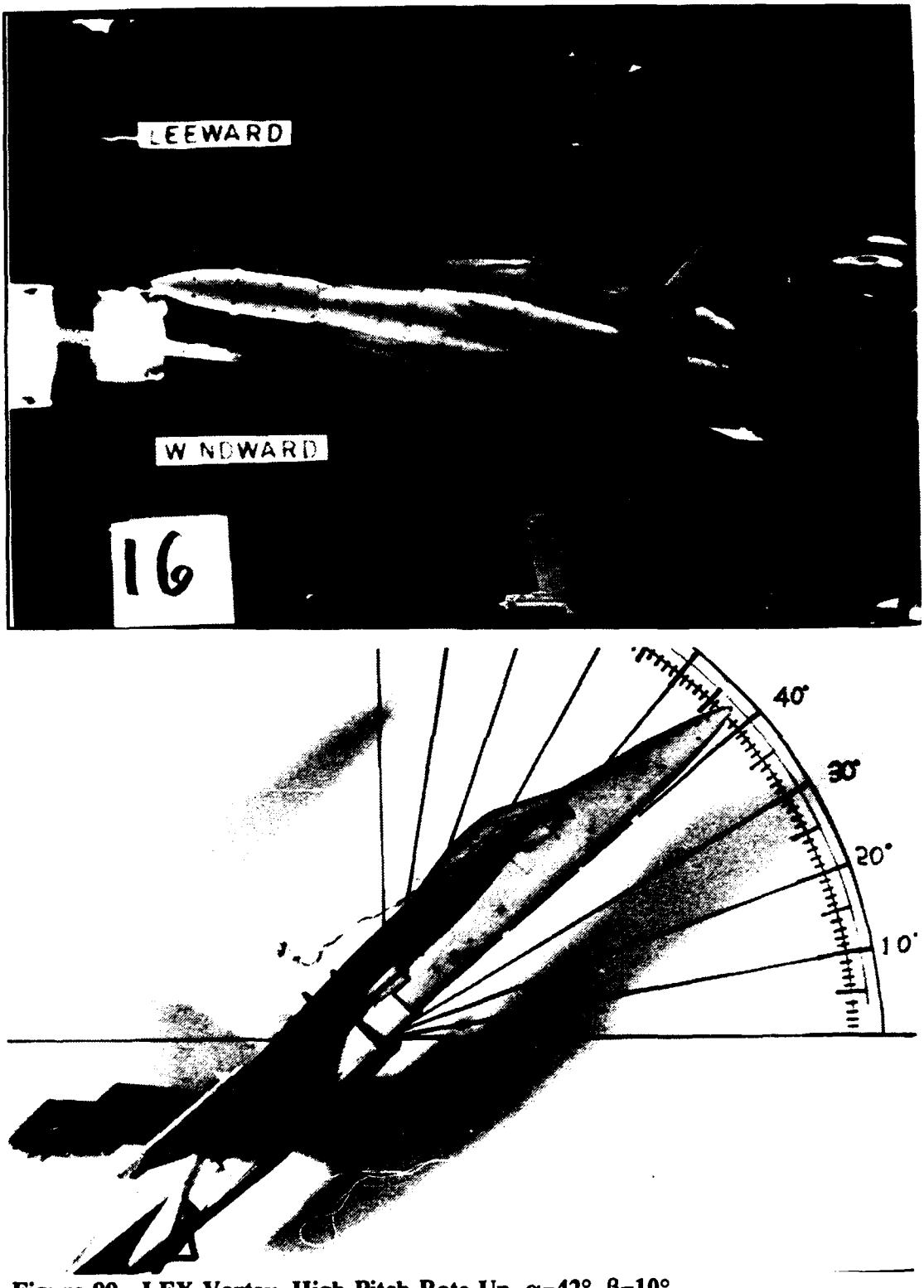

Figure 99. LEX Vortex, High Pitch Rate Up, α=42°, β=10°

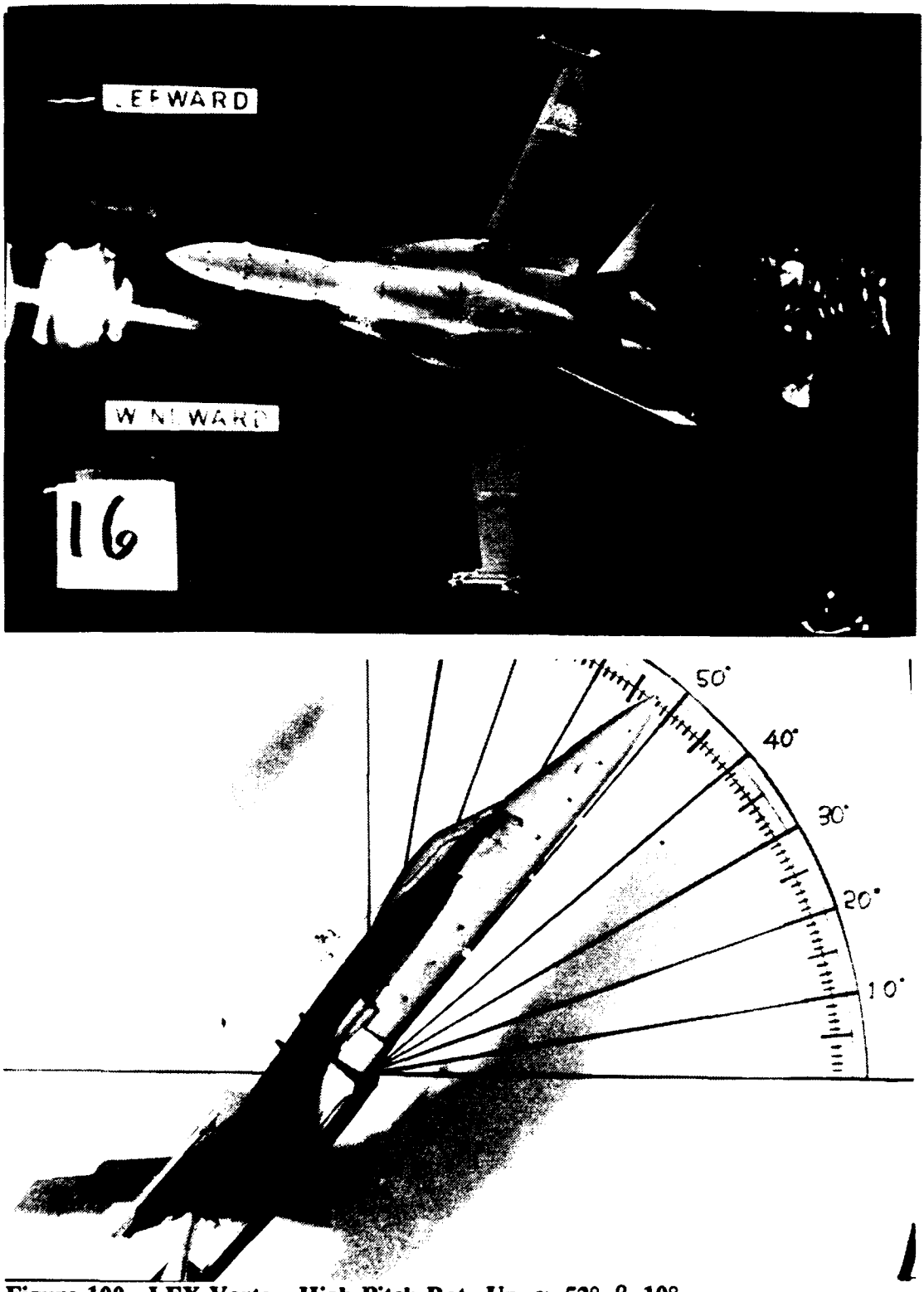

Figure 100. LEX Vortex, High Pitch Rate Up, α=52°, β=10°

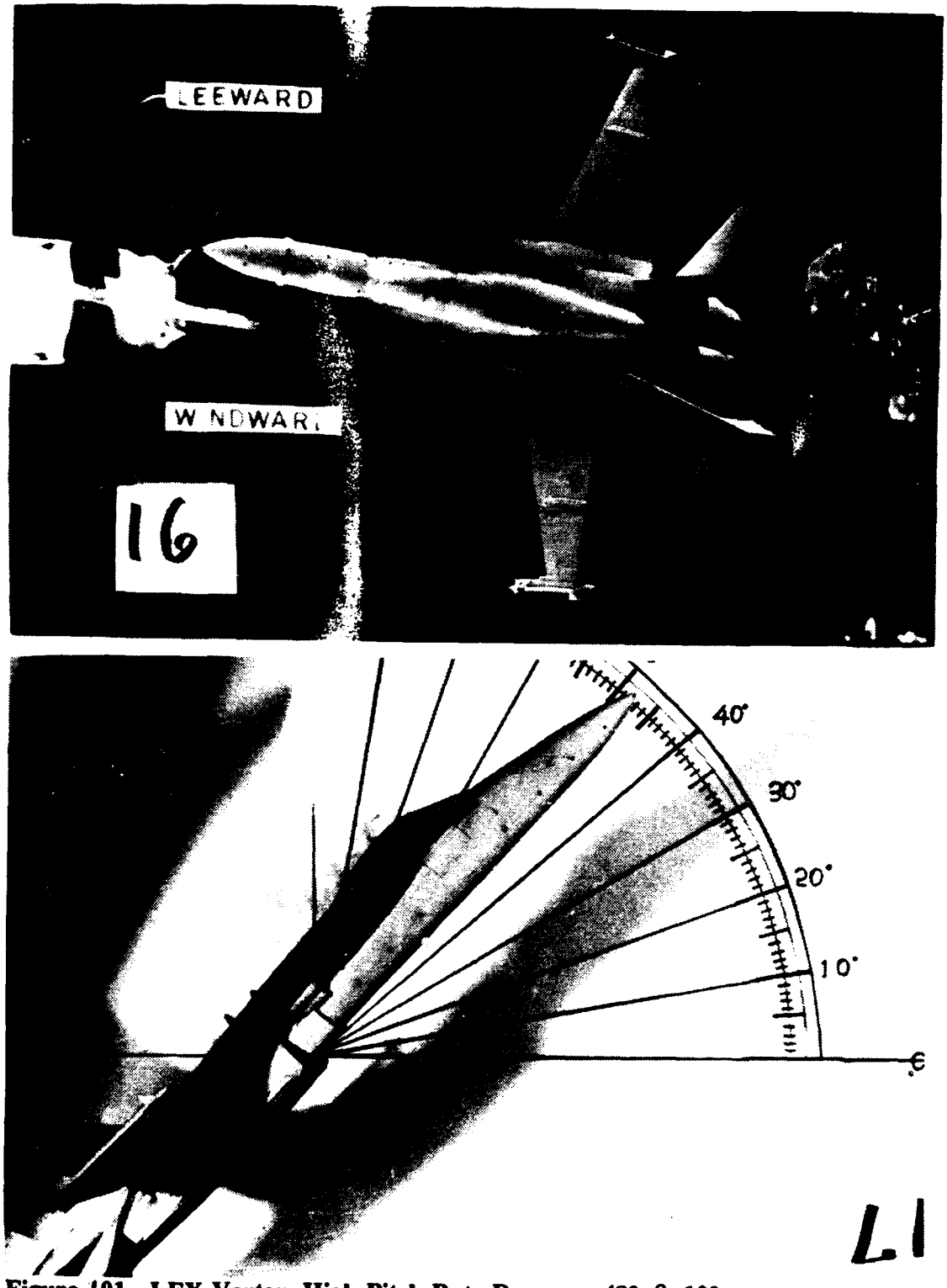

Figure 101. LEX Vortex, High Pitch Rate Down, α=48°, β=10°

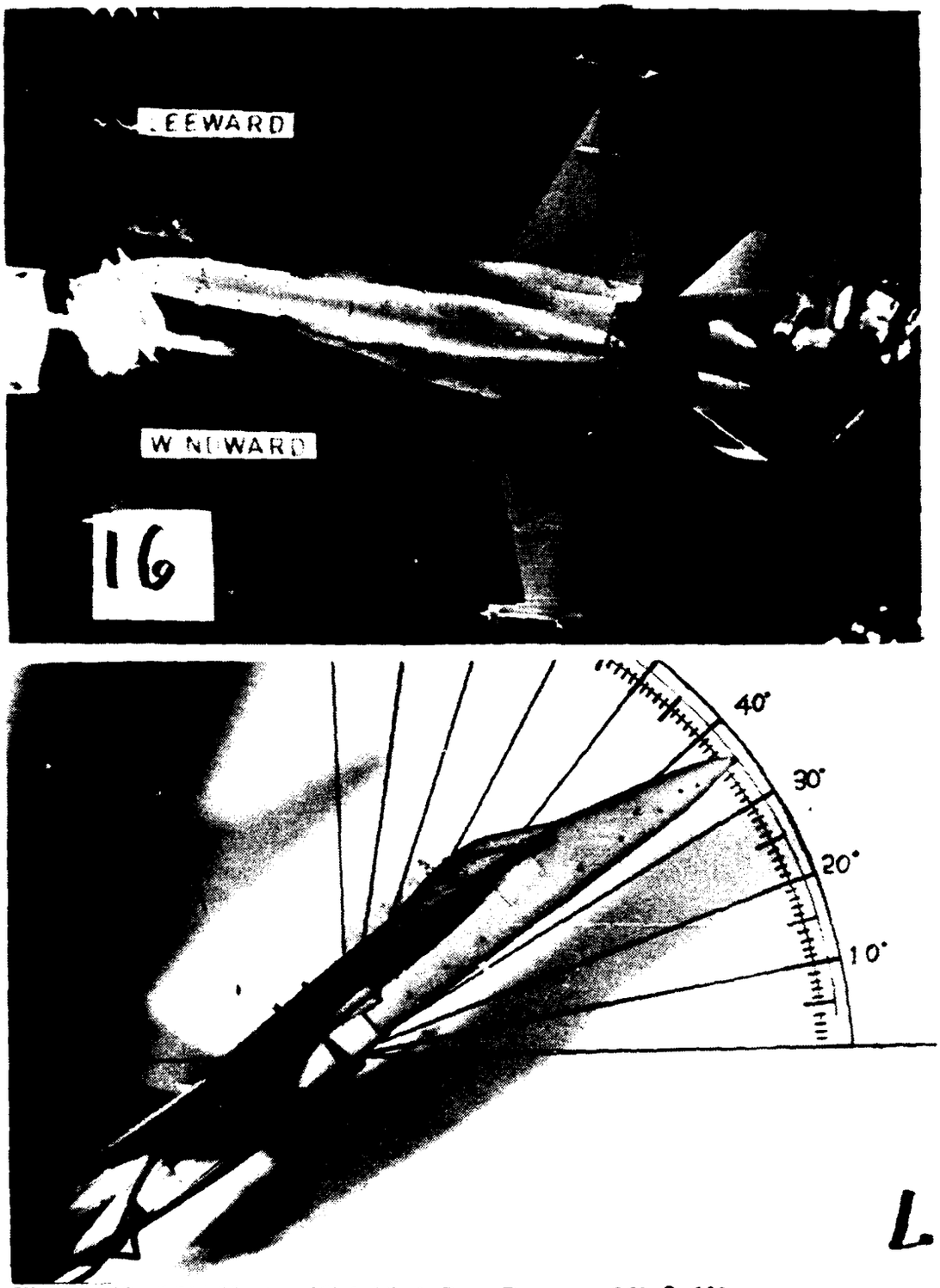

Figure 102. LEX Vortex, High Pitch Rate Down, α=36°, β=10°

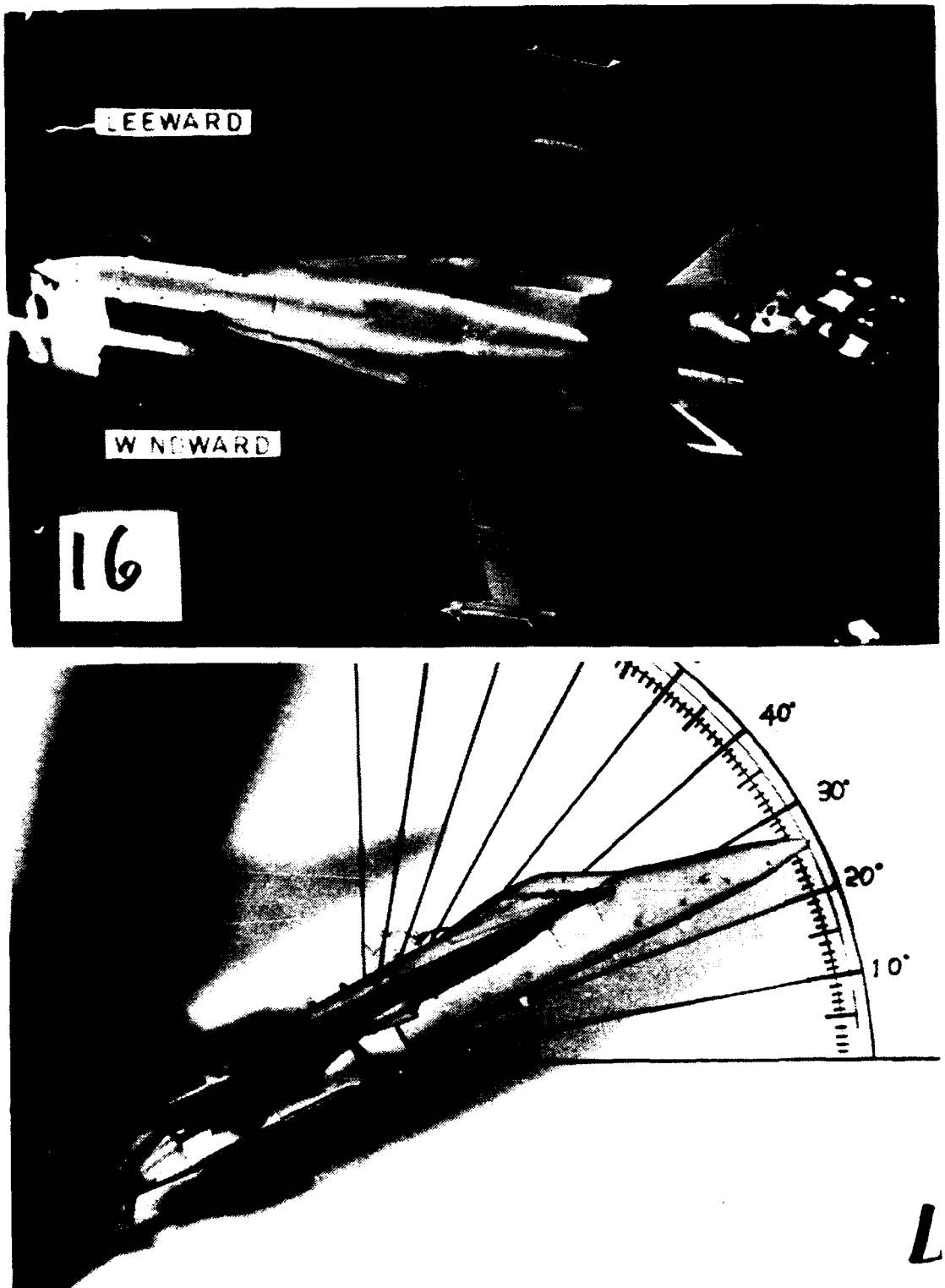

Figure 103. LEX Vortex, High Pitch Rate Down, α=26°, β=10°

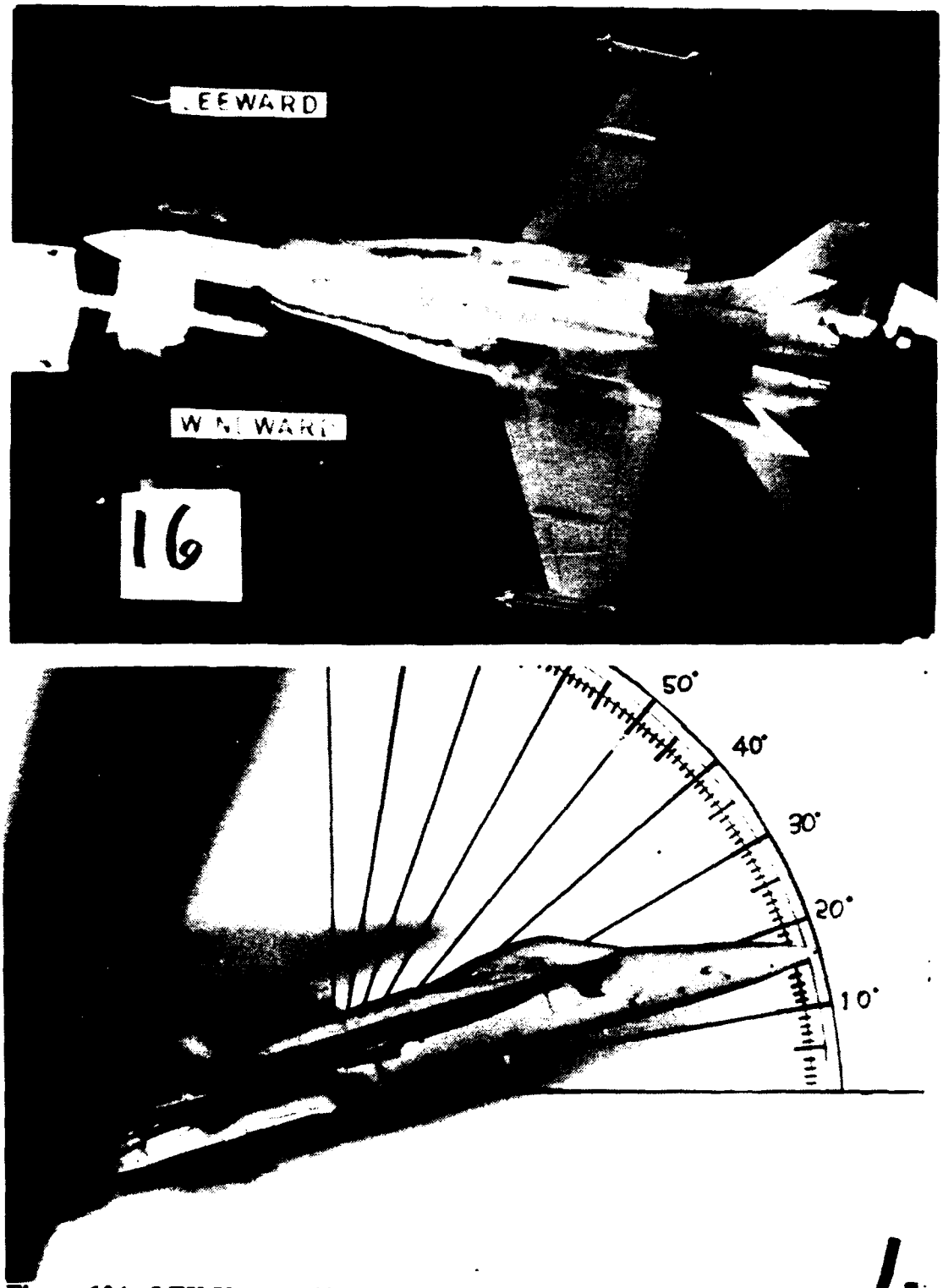

Figure 104. LEX Vortex, High Pitch Rate Down, α=16°, β=10°

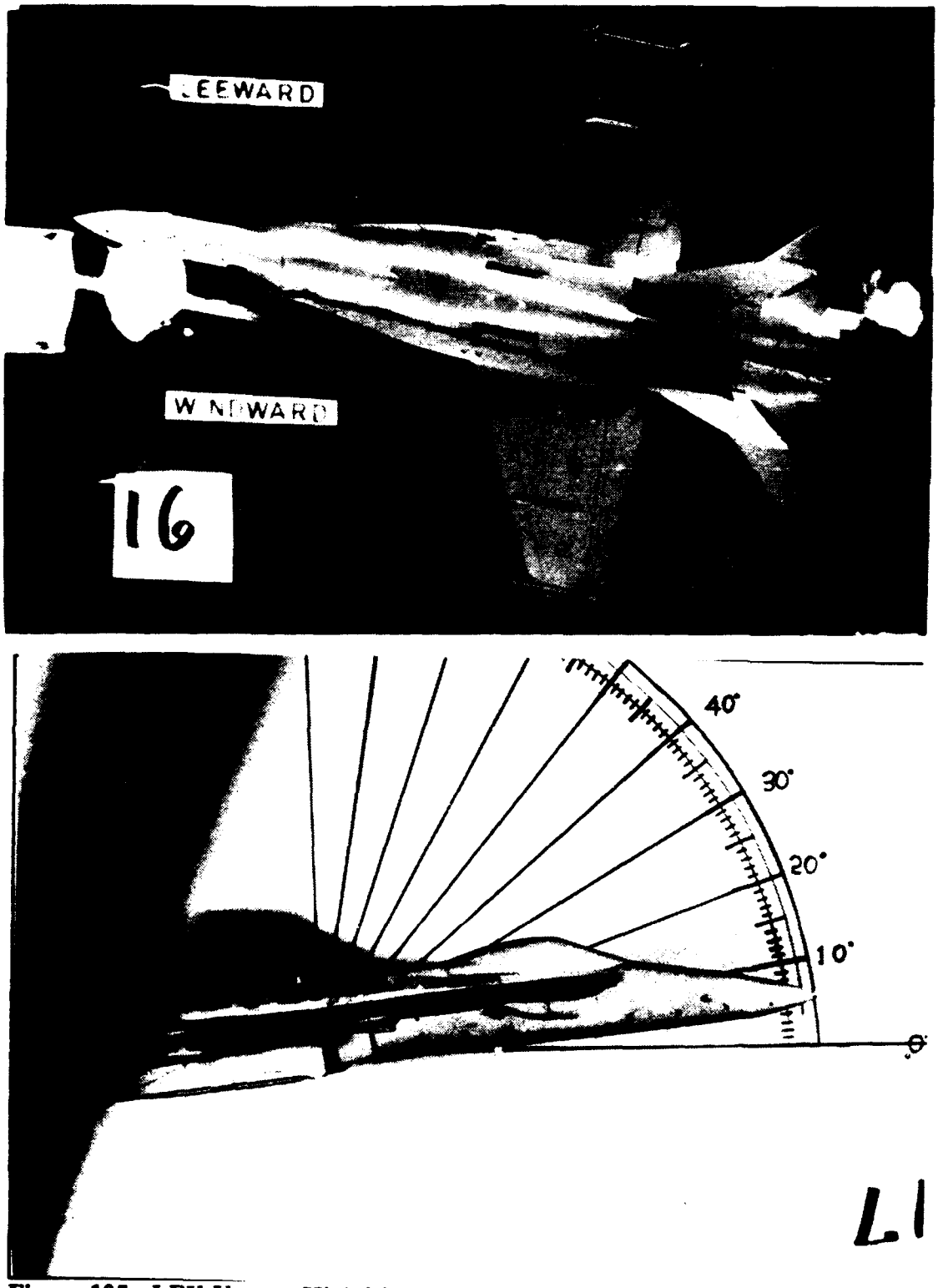

Figure 105. LEX Vortex, High Pitch Rate Down, α=5°, β=10°

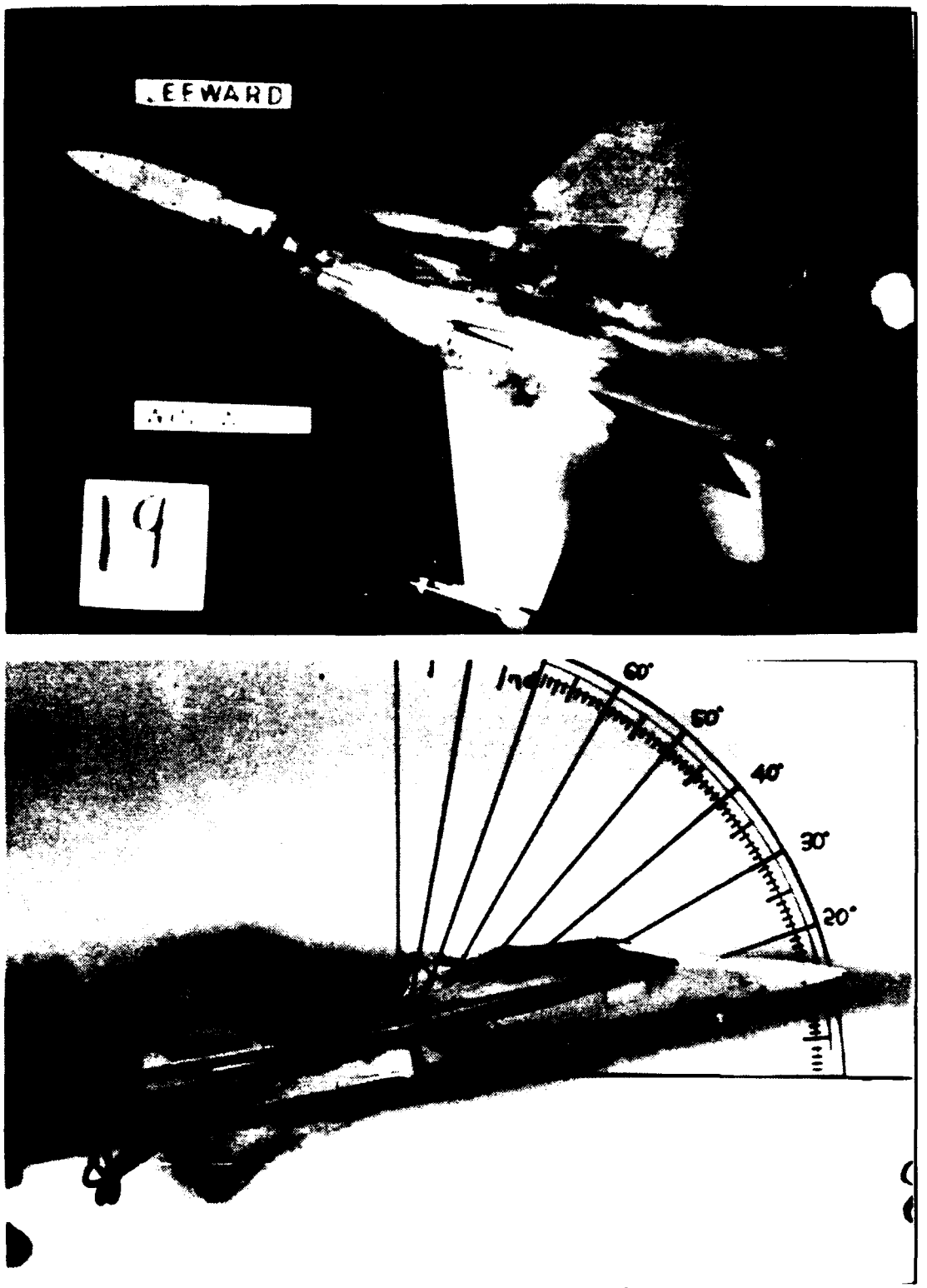

Figure 106. LEX Vortex, High Pitch Rate Up, α=12°, β=20°

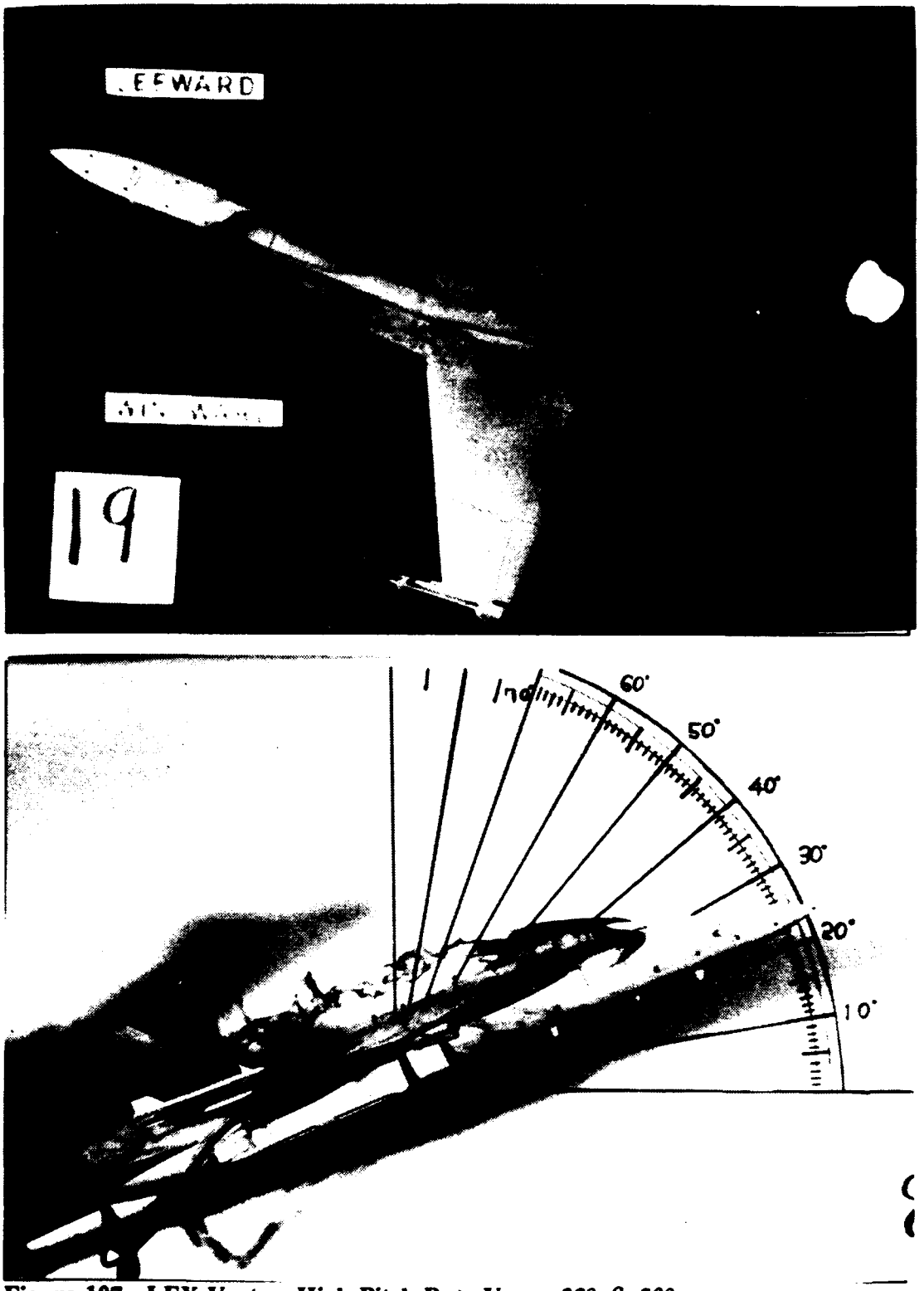

Figure 107. LEX Vortex, High Pitch Rate Up, α=23°, β=20°

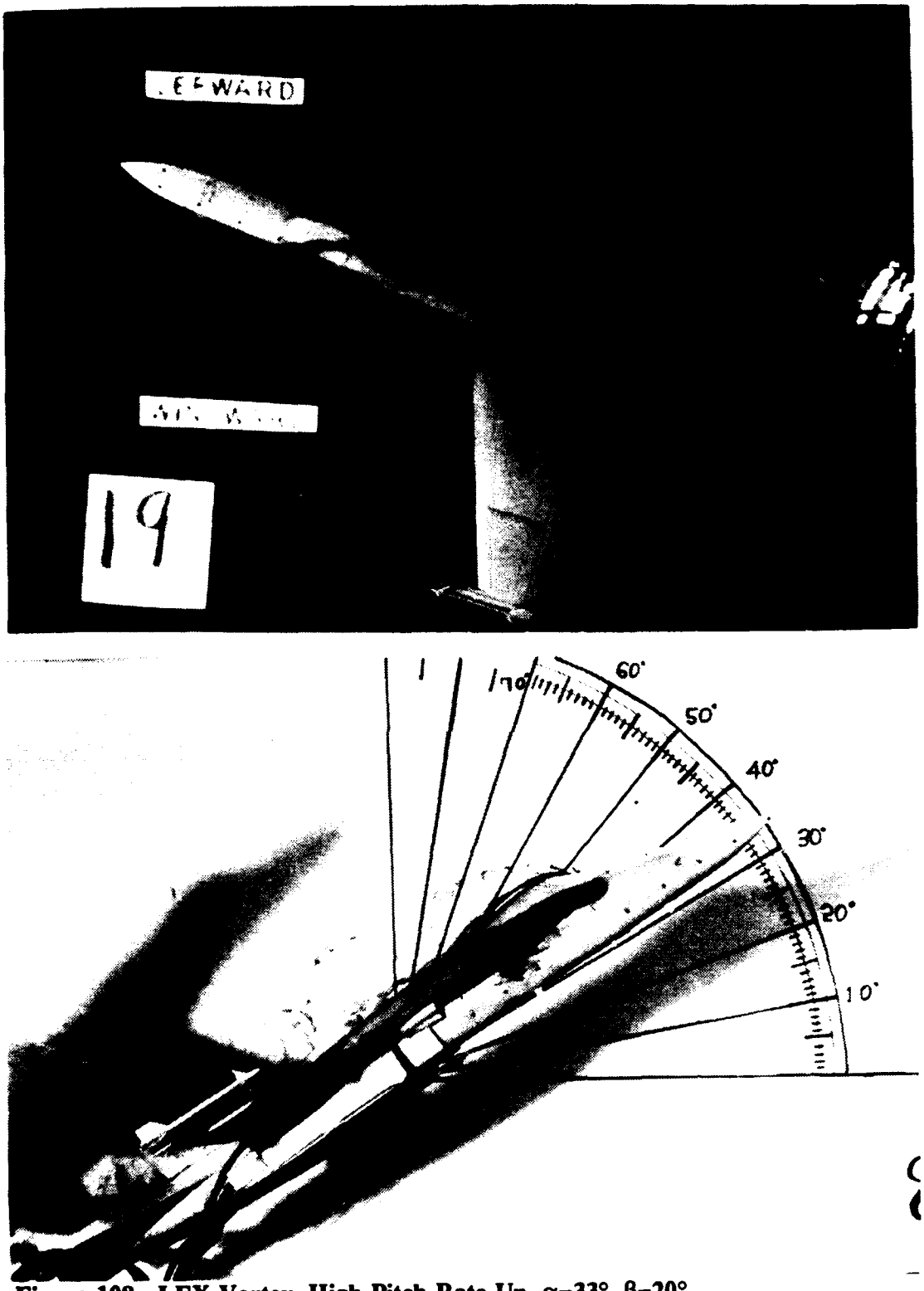

Figure 108. LEX Vortex, High Pitch Rate Up, α=33°, β=20°

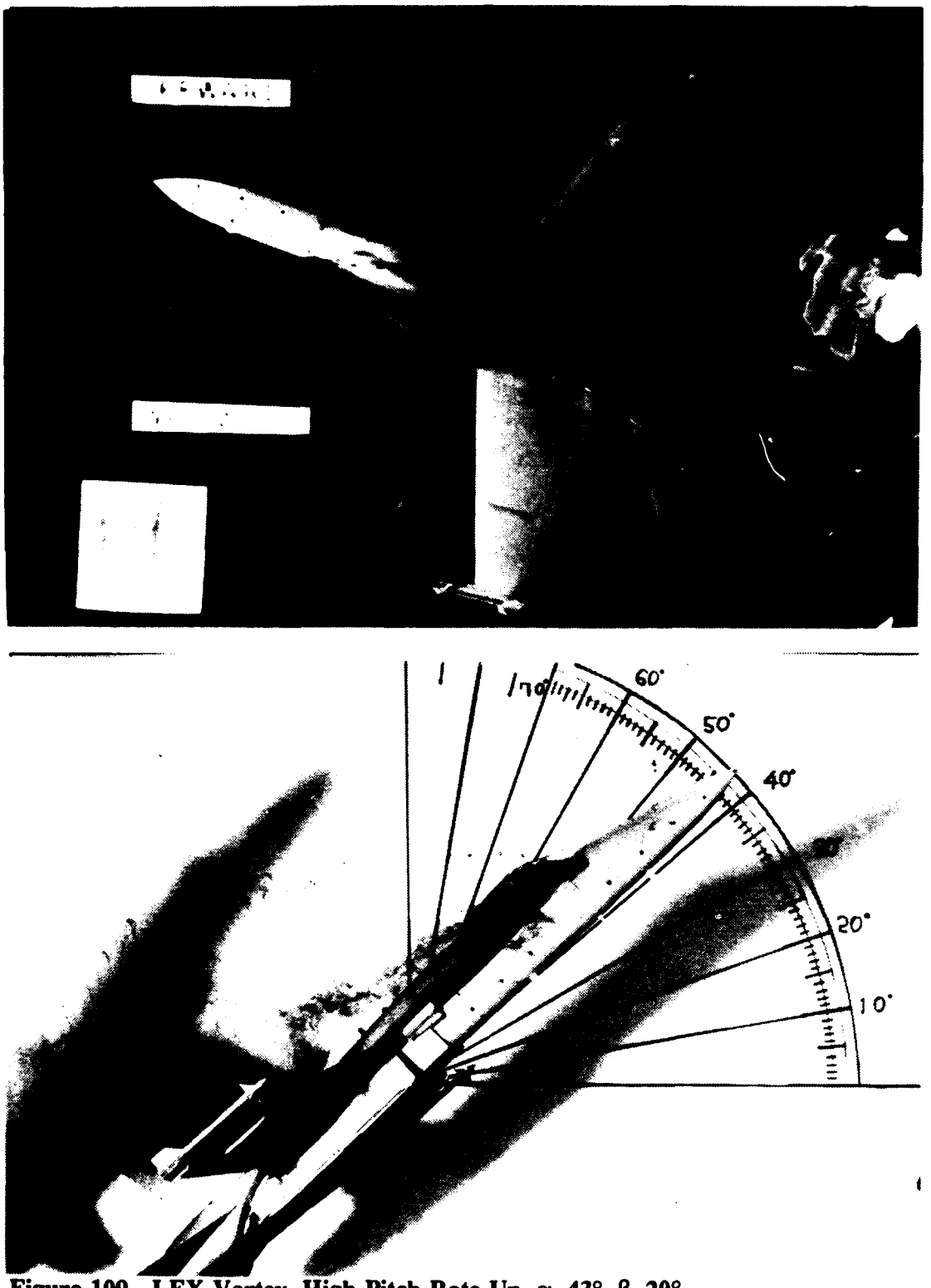

Figure 109. LEX Vortex, High Pitch Rate Up, α=43°, β=20°

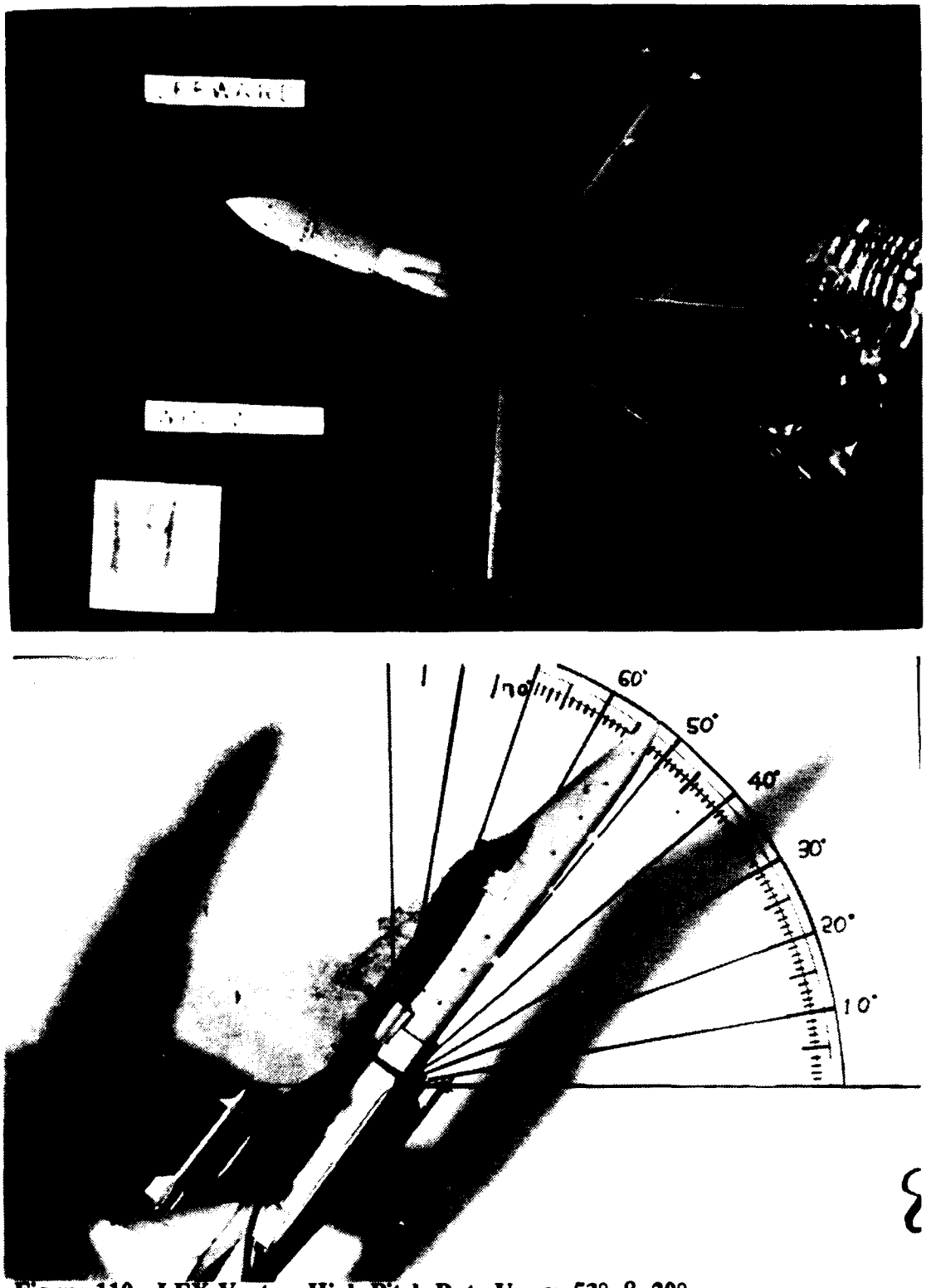

Figure 110. LEX Vortex, High Pitch Rate Up, α=53°, β=20°

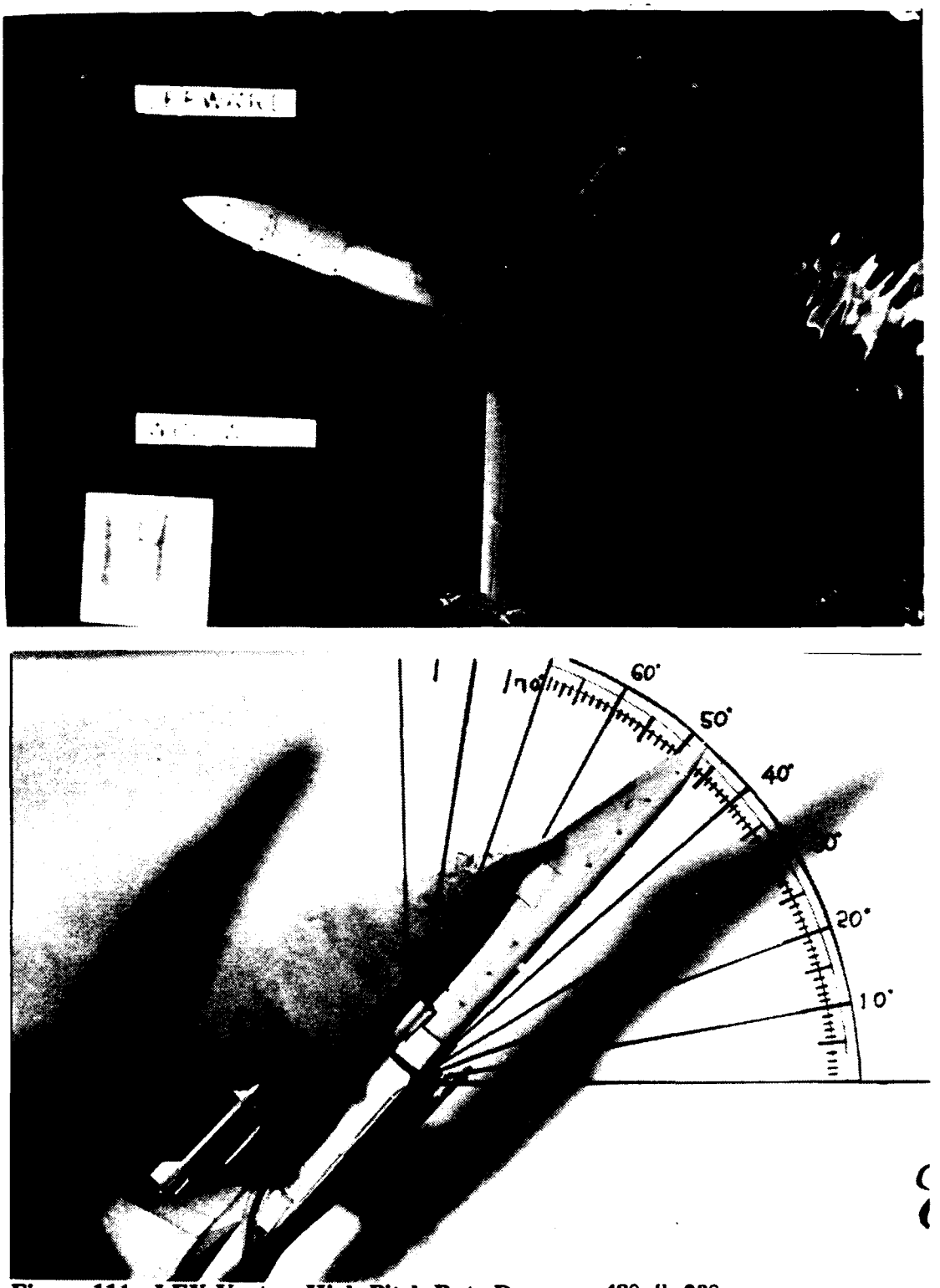

Figure 111. LEX Vortex, High Pitch Rate Down, α=48°, β=20°

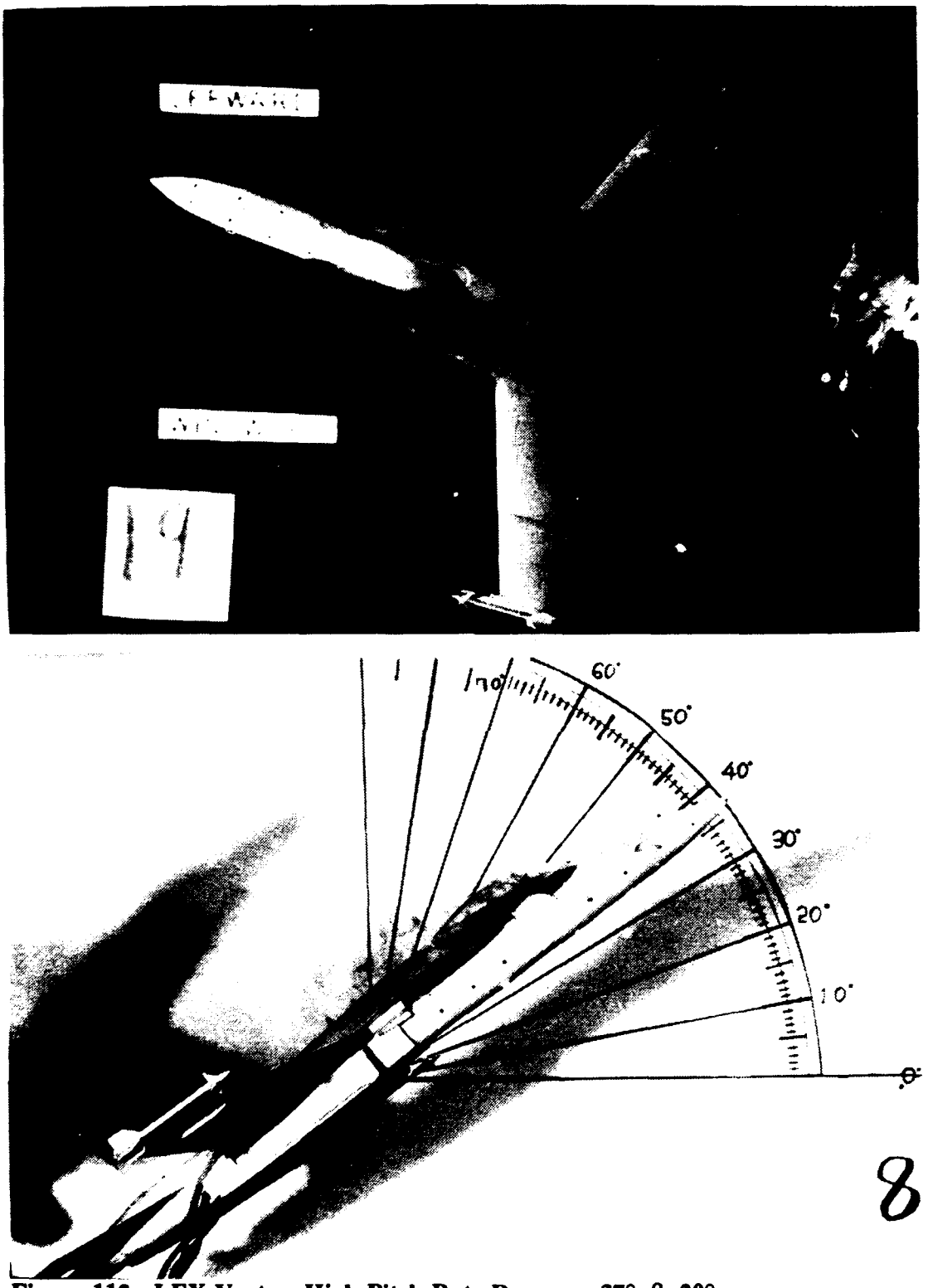

Figure 112. LEX Vortex, High Pitch Rate Down, α=37°, β=20°

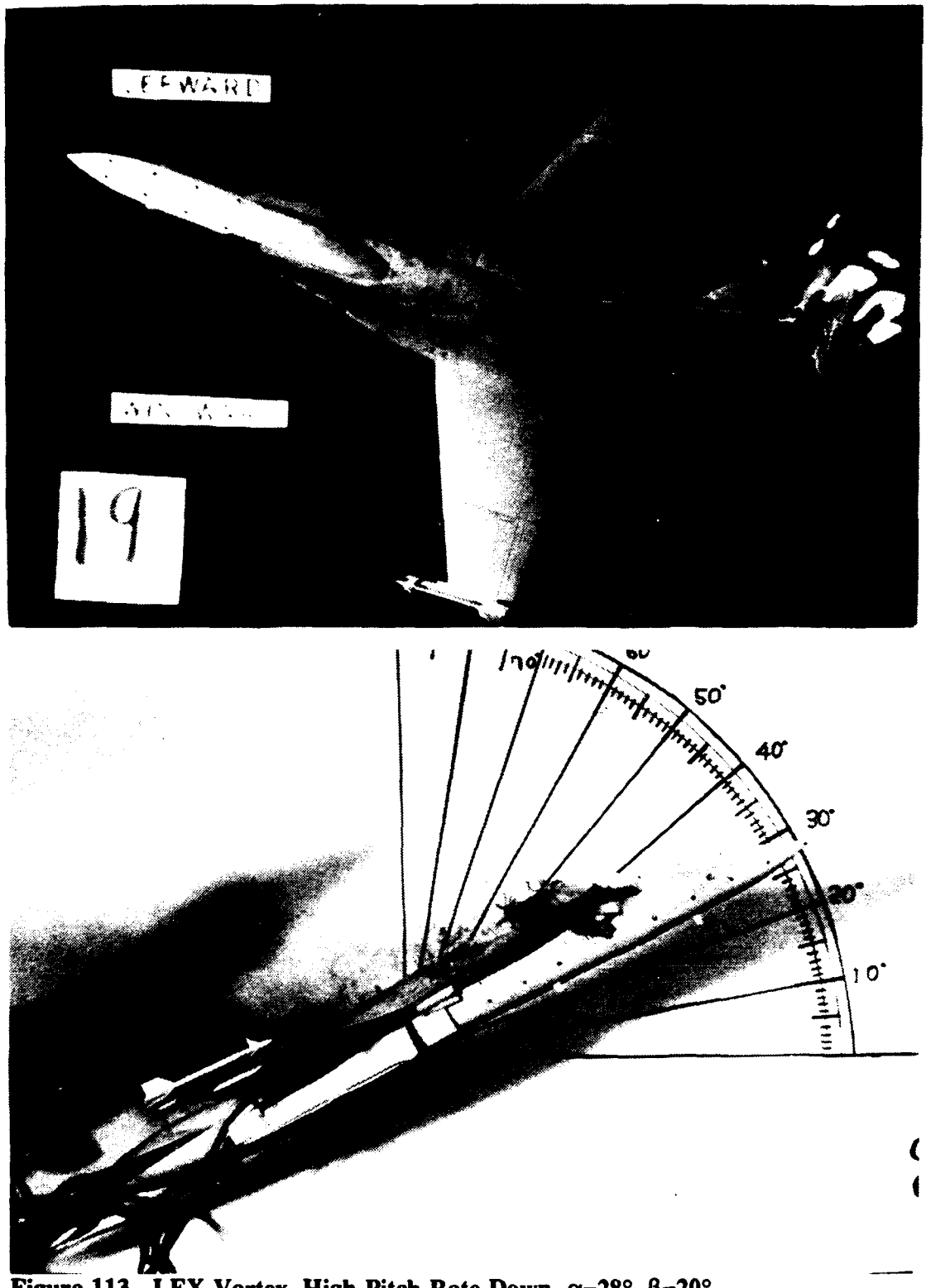

Figure 113. LEX Vortex, High Pitch Rate Down, α=28°, β=20°

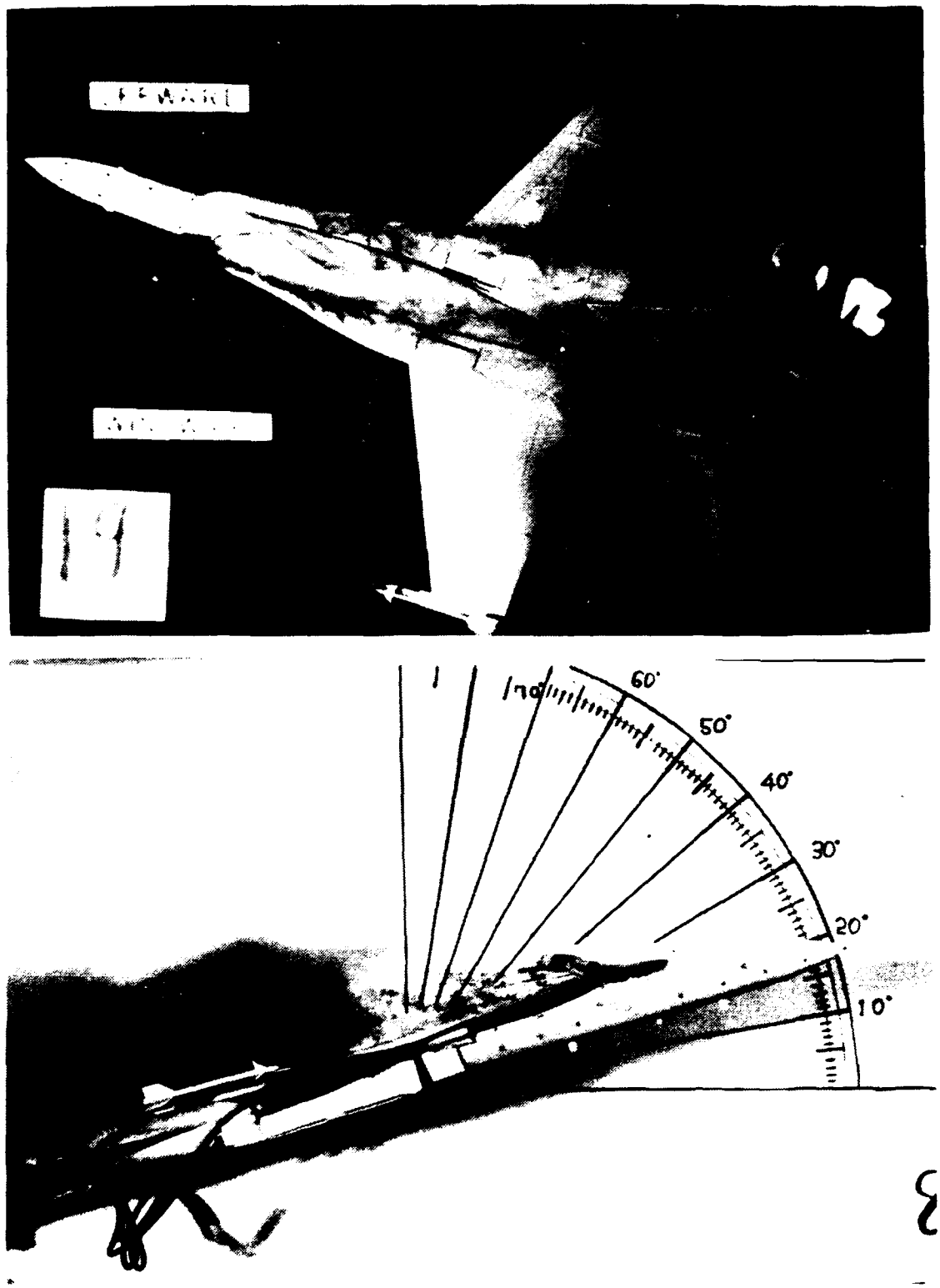

Figure 114. LEX Vortex, High Pitch Rate Down, α=18°, β=20°

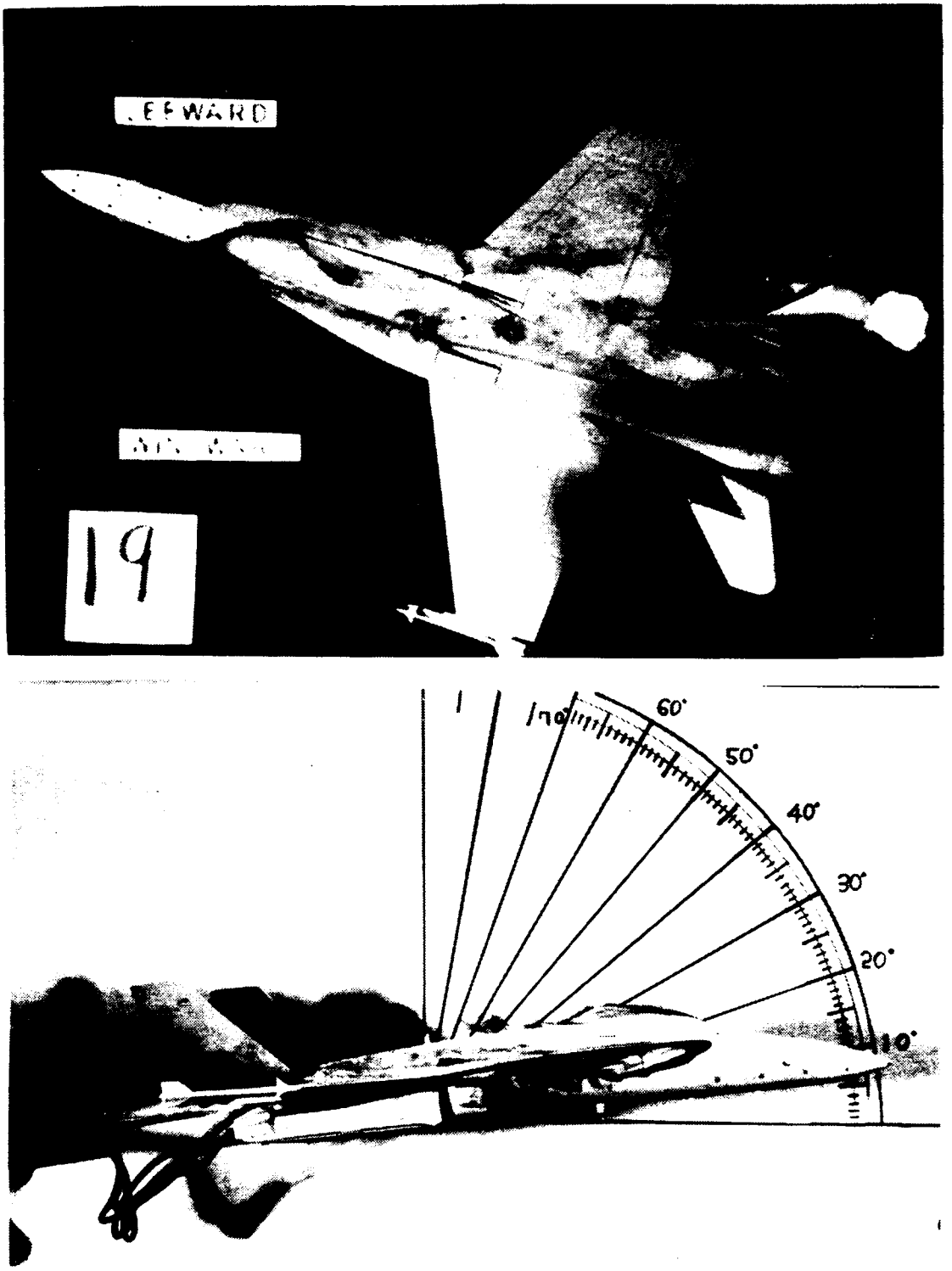

Figure 115. LEX Vortex, High Pitch Rate Down, α=8°, β=20°

APPENDIX B. EXPERIMENTAL RESULTS (GRAPHS)

FIGURES 116 THROUGH 121

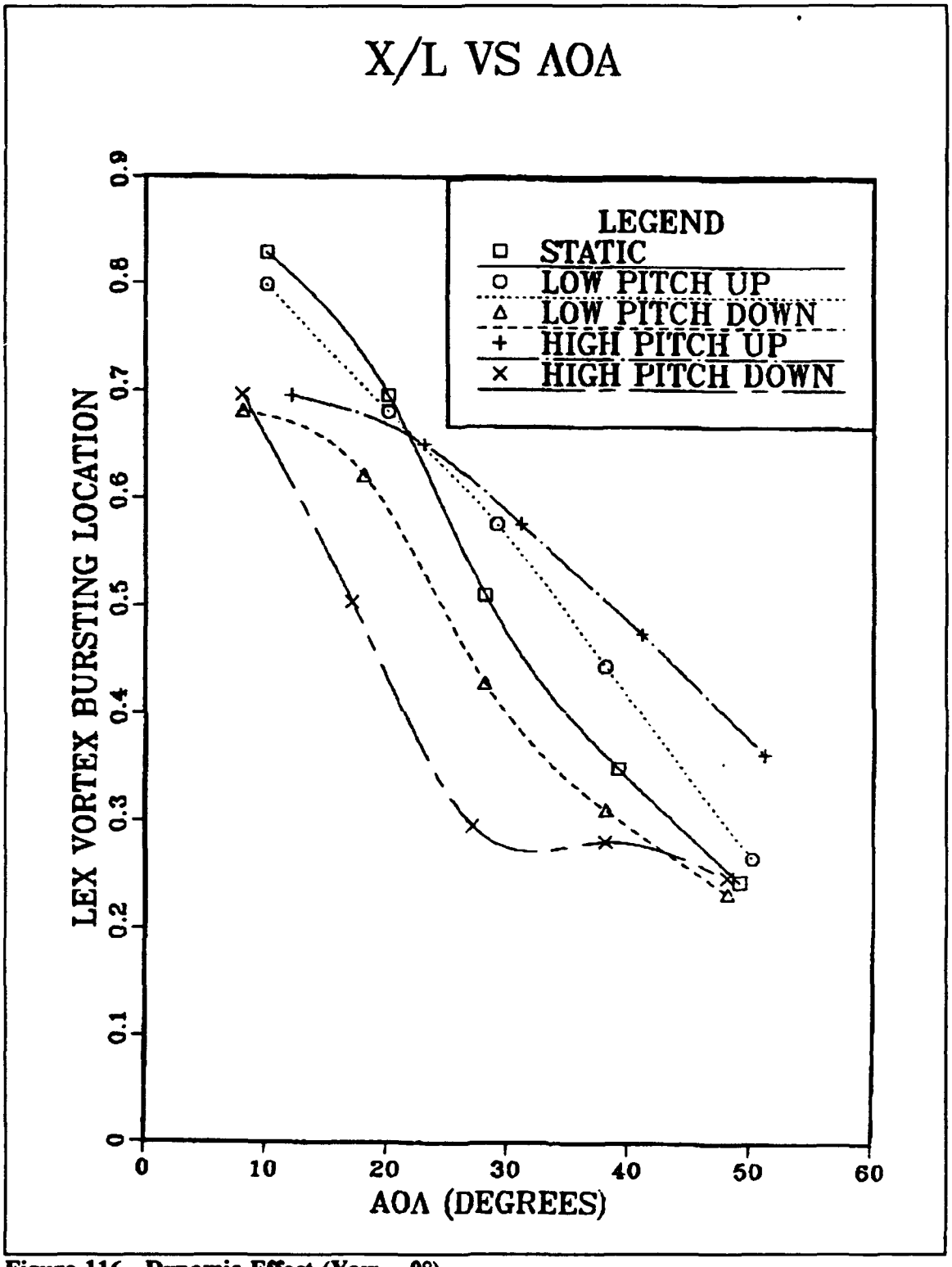

Figure 116. Dynamic Effect (Yaw = 0°)

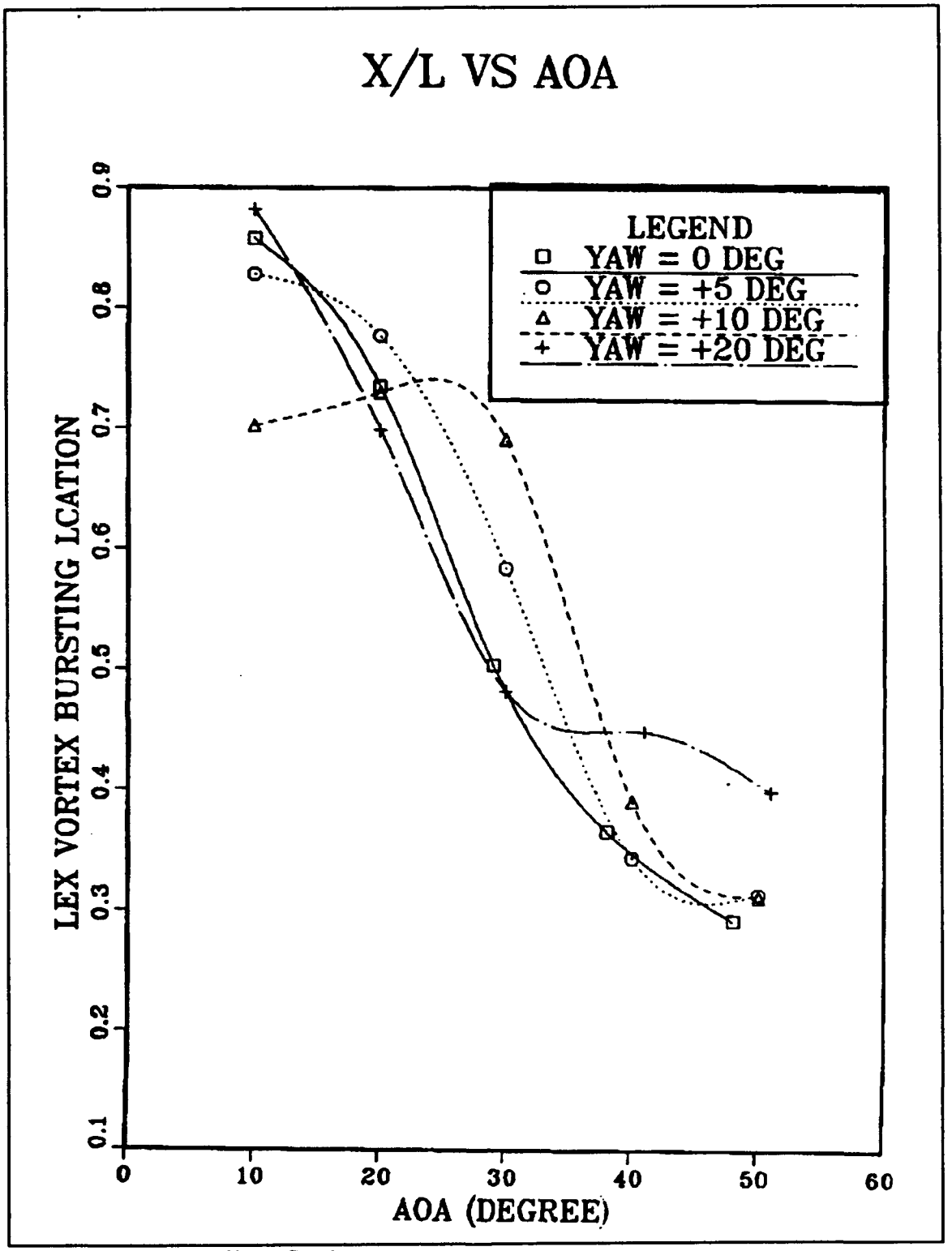

Figure 117. Yaw Effect (Static)

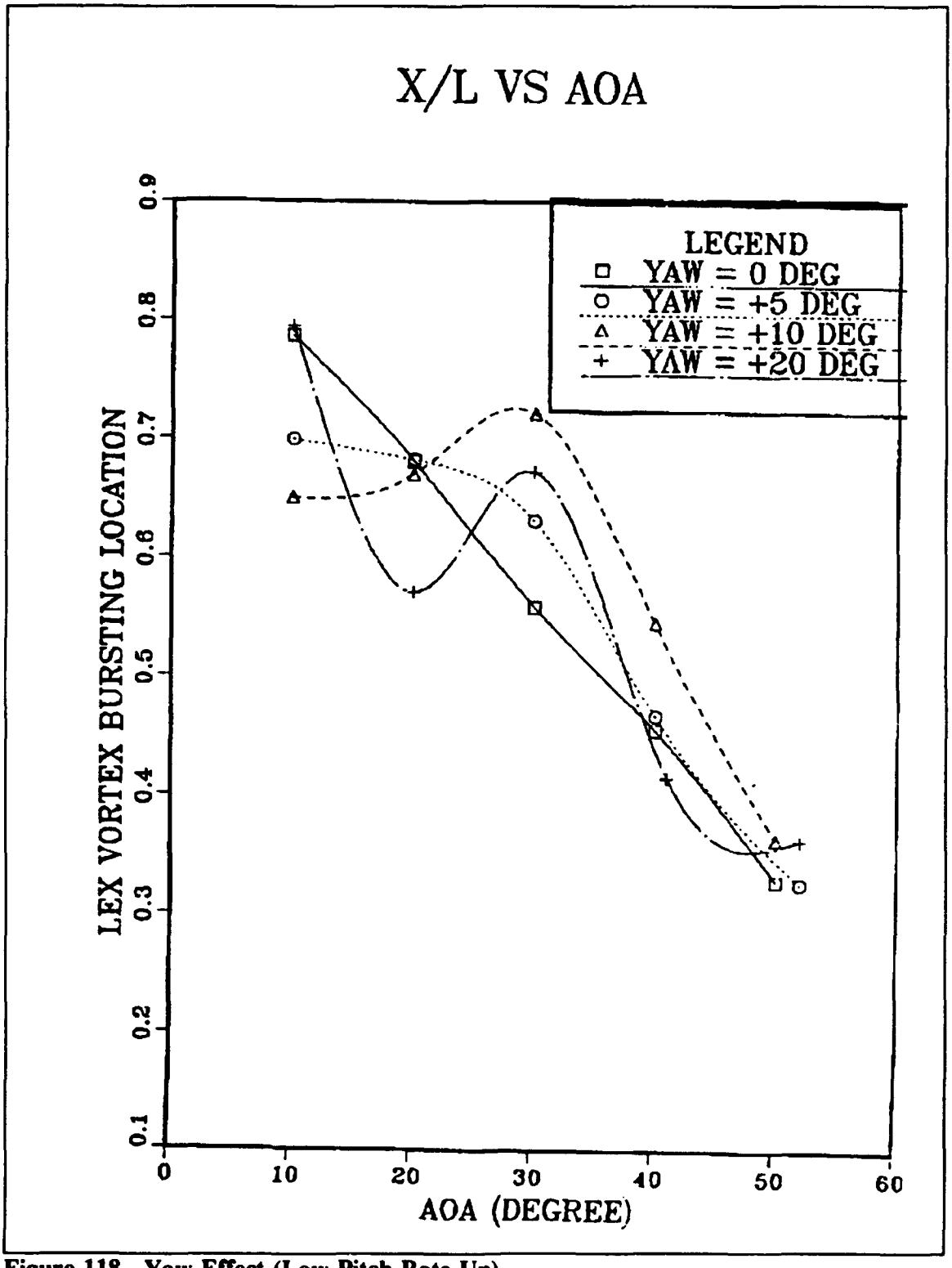

Figure 118. Yaw Effect (Low Pitch Rate Up)

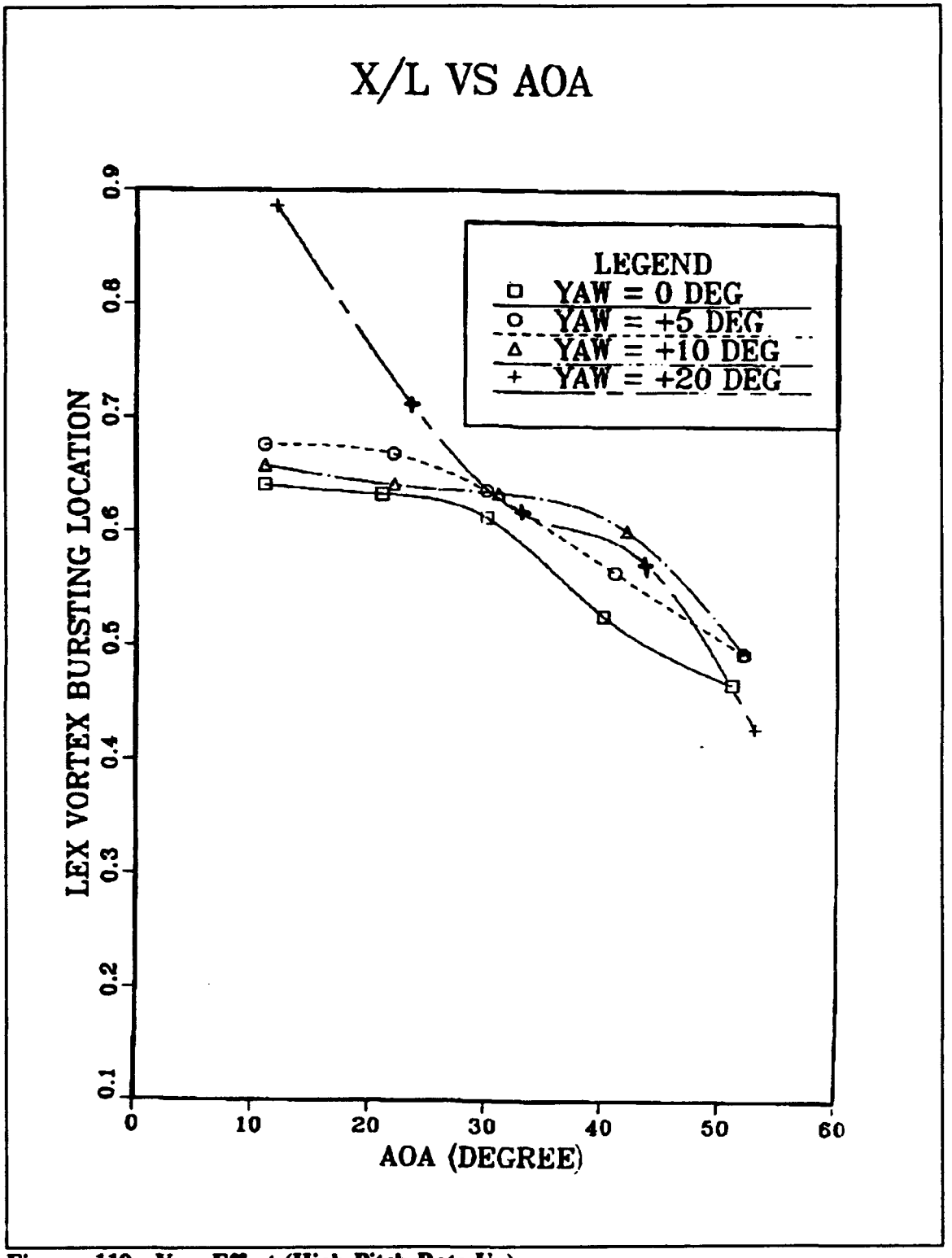

Figure 119. Yaw Effect (High Pitch Rate Up)

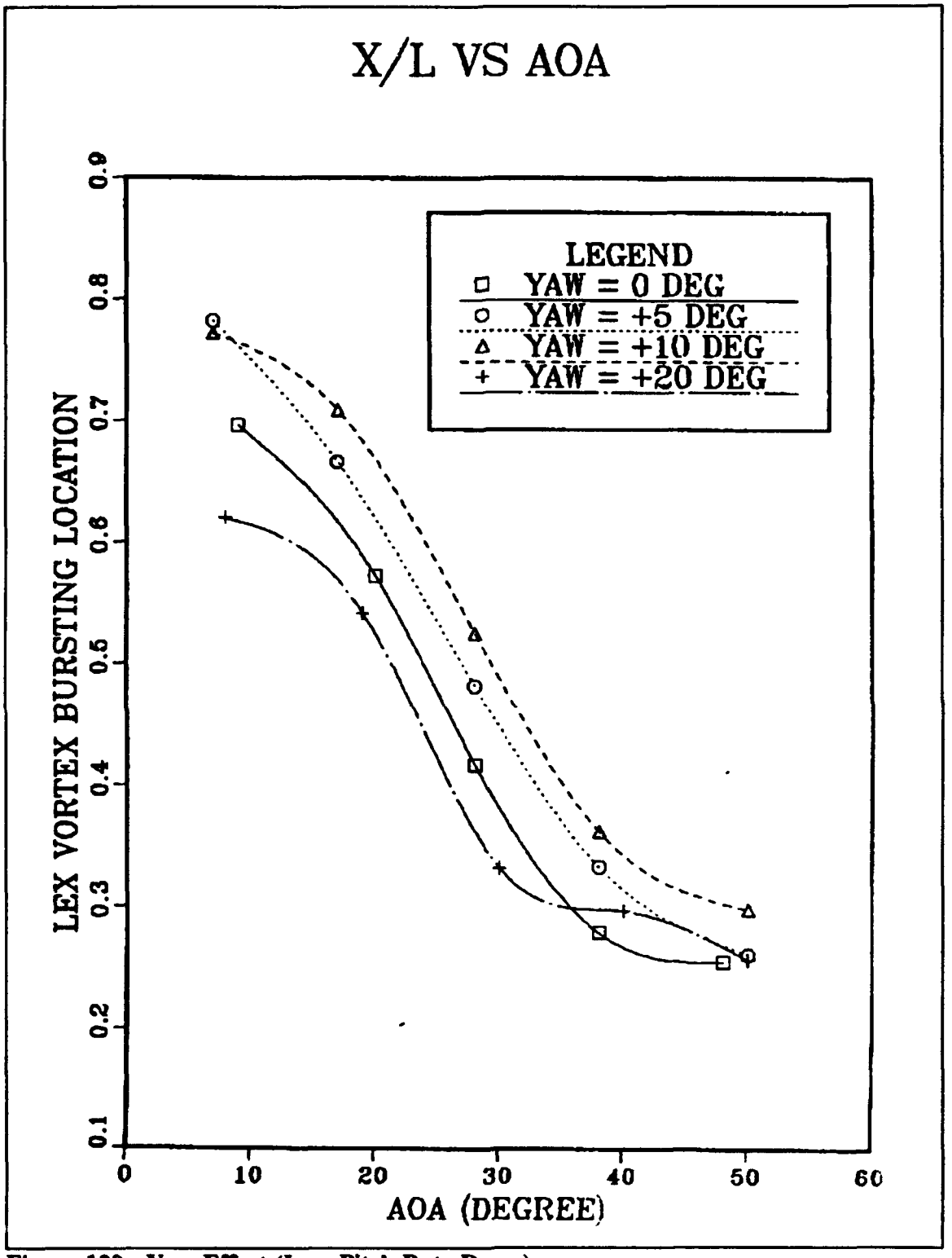

Figure 120. Yaw Effect (Low Pitch Rate Down)

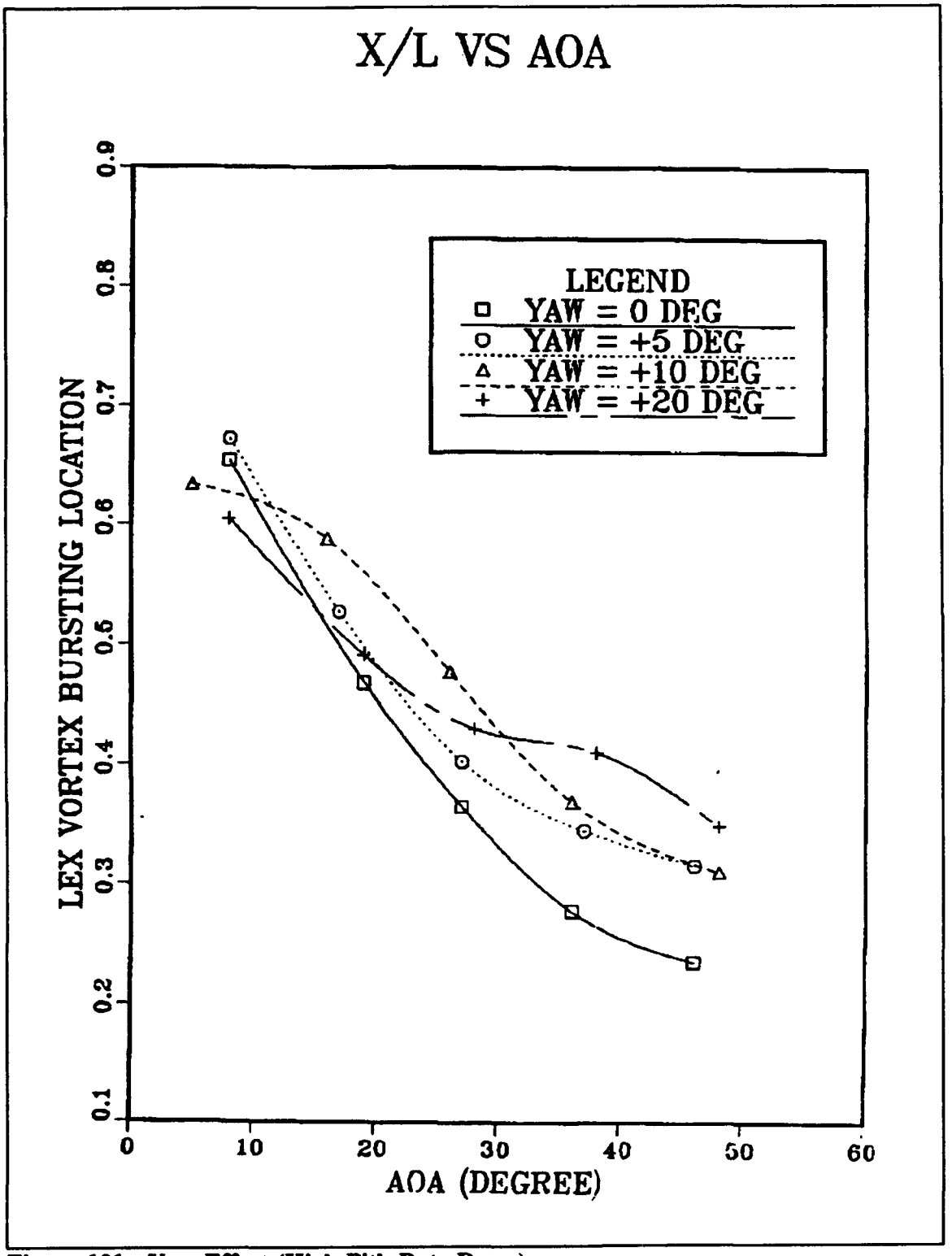

Figure 121. Yaw Effect (High Pith Rate Down)

INITIAL DISTRIBUTION LIST

		No. Copies
1.	Defense Technical Information Center Cameron Station Alexandria, VA 22304-6145	2
2.	Library, Code 52 Naval Postgraduate School Monterey, CA 93943-5002	2
3.	S.K. Hebbar, Code AA/Hb Department of Aeronautics & Astronautics Naval Postgraduate School Monterey, CA 93943-5002	9
4.	M.F. Platzer,Code AA/PL Department of Aeronautics & Astronautics Naval Postgraduate School Monterey, CA 93943-5002	2
5.	W.R. Wood, Chairman, AA Department of Aeronautics & Astronautics Naval Postgraduate School Monterey, CA 93943-5002	1
6.	LT O.V. Cavazos 2855 Arcola Avenue San Diego, CA 92117	2
7.	Mr. B. Neuman Aircraft Division, Code AIR-931 Naval Air Systems Command Washington, DC 20361-9320	1
8.	Mr. D. Findlay Naval Air Development Center Street Road Warminster, PA 18974-5000	1